1-1-1990

3-D Beamspace ML Based Bearing Estimator Incorporating Frequency Diversity and Interference Cancellation

Ta-Sung Lee
Purdue University

Michael D. Zoltowski
Purdue University

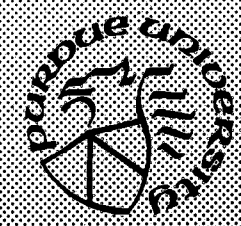

A 3-D Beamspace ML Based Bearing Estimator Incorporating Frequency Diversity and Interference Cancellation

Ta-Sung Lee
Michael D. Zoltowski

TR-EE 90-6
January, 1990

School of Electrical Engineering
Purdue University
West Lafayette, Indiana 47907

prepared for the National Science Foundation under contract number ECS-8707681

A 3-D BEAMSPACE ML BASED BEARING ESTIMATOR INCORPORATING FREQUENCY DIVERSITY AND INTERFERENCE CANCELLATION

prepared for the National Science Foundation

under contract number ECS-8707681

Ta-Sung Lee

and

Michael D. Zoltowski

School of Electrical Engineering

Purdue University

West Lafayette, IN 47907

TR-EE-90-6

January, 1990

TABLE OF CONTENTS

Page

Page

LIST OF TABLES

Table Page

LIST OF FIGURES

Figure Page

Appendix
Figure

ABSTRACT

The problem of low-angle radar tracking utilizing an array of antennas is considered. In the low-angle environment, echoes return from a low flying target via a specular path as well as a direct path. The problem is compounded by the fact that the two signals arrive within a beamwidth of each other and are usually fully correlated, or coherent. In addition, the SNR at each antenna element is typically low and only a small number of data samples, or snapshots, is available for processing due to the rapid movement of the target. Theoretical studies indicates that the Maximum Likelihood (ML) method is the only reliable estimation procedure in this type of scenario. However, the classical ML estimator involves a multi-dimensional search over a multi-modal surface and is consequently computationally burdensome. In order to facilitate real time processing, we here propose the idea of beamspace domain processing in which the element space snapshot vectors are first operated on by a reduced Butler matrix composed of three orthogonal beamforming weight vectors facilitating a simple, closed-form Beamspace Domain ML (BDML) estimator for the direct and specular path angles. The computational simplicity of the method arises from the fact that the respective beams associated with the three columns of the reduced Butler matrix have all but three nulls in common. The performance of the BDML estimator is enhanced by incorporating the estimation of the complex reflection coefficient and the bisector angle, respectively, for the symmetric and nonsymmetric multipath cases. To minimize the probability of track breaking, the use of frequency diversity is incorporated. The concept of coherent signal subspace processing is invoked as a means for retaining the computational simplicity of single frequency operation. With proper selection of the auxiliary frequencies, it is shown that perfect focusing may be achieved without iterating. In order to combat the effects of strong interfering sources, a novel scheme is presented for adaptively forming the three beams which retains the feature of common nulls.

CHAPTER 1
INTRODUCTION

1.1 Motivations for Beamspace Domain Processing

The idea of extracting information about a "scene" of targets or radiating sources from the data outputted from an array of sensors by operating in the beamspace domain as opposed to element space has recently caught the interest of a number of researchers in the field of array signal processing [BUCK88], [XU88], [VAN88], [FORS87], [GABR88]. In element space, the data is taken to be the "raw" snapshot vectors containing a simultaneous sampling of all the array element outputs at a particular instant in time. In the case of beamspace domain processing, the "raw" snapshot vectors are first operated on by a matrix beamformer producing a beamspace snapshot vector typically of lower dimensionality. There are a number of advantages to working in the beamspace domain. First, the lower dimensionality of the beamspace domain snapshot vector serves to reduce the computational burden. Second, as each component of the beamspace domain snapshot vector is formed as the weighted sum of a large number of array element outputs, it is often adequate to assume Gaussian statistics in the beamspace domain. In the case of Maximum Likelihood (ML) based estimation, the Gaussian assumption leads to a tractable least squares problem. Third, the process of beamforming serves to filter out undesired sources such as clutter and jammers. Finally, the "spatial" white noise assumption which is typically invoked but not very often the case in practice, may indeed hold to a good approximation in beamspace. The pertinent assumption here is that the spatial passband associated with the matrix beamformer is narrow enough such that the spatial distribution of the noise over the passband is essentially flat. These advantages of beamspace domain processing over element space processing have lead to the development of beamspace domain versions of the Minimum Variance algorithm. For the narrowband case we have the work of Byrne and Steele [BYRN87] while for the wideband case we have the work of Gabriel [GABR88]. Beamspace domain versions of MUSIC [SCHM79] have also been developed. For the narrowband case, we have the work of Forster and

Vezzosi [FORS87], Mayhan and Niro [MAYH87], and Van Veen [VAN88]. For the wideband case, we have the work of Buckley and Xu [BUCK88], [XU88] who have also developed beamspace domain, wideband versions of other spatial spectral estimators such as Minimum Variance, BASS-ALE, etc. We here develop a beamspace domain based Maximum Likelihood estimation scheme for the low angle radar tracking problem.

1.2 Overview of ML Estimation for Low Angle Radar Tracking

The low angle radar tracking problem has been well studied in the literature [KESL80], [HAYK83], [HAYK84], [DAVI76], [GABR84], [CANT81], [MAYH87], [BALL87], [KEZY88], [KSIE68], [BART74], [WHIT74], [SKOL80], [ZOLT88a], [ZOLT89b-d]. Barton provided a model for the scenario in [BART74]. The goal is to track a target flying at a low altitude, in relative terms, over a fairly smooth reflecting surface such as a calm sea, for example. The problem is complicated by the fact that the angular separation between the echoes returning from the target via the specular path and those arriving via the direct path is typically a fraction of a beamwidth. The classical monopulse bearing estimation technique breaks down under these conditions as it assumes a single target within the mainlobe width of the sum beam [GABR84]. As a consequence, a number of alternative estimation techniques have been proposed, each theoretically capable of resolving two targets angularly separated by less than a beamwidth. Note that the low-angle radar tracking scenario may be viewed as a two target problem; one of the targets is "real" while the other is simply its multipath "reflection". In particular, a number of Maximum Likelihood (ML) based estimation schemes have been developed and proposed [KESL80], [HAYK83], [HAYK84], [HAKY85], [DAVI76], [CANT81], [MAYH87], [BALL87], [KEZY88], [KSIE68], [WHIT74]. The ML estimator is particularly attractive in light of its theoretical ability to handle the single snapshot case, as the term monopulse implies, and 100% correlation between the direct and specular path signals. In these two extreme situations, most Direction-of-Arrival (DOA) finding techniques suffer severe degradation or may even totally break down [BRES86]. The various ML based estimation schemes proposed may be classified under two major categories: those which operate in element space and those which operate in beamspace. Some early treatment of the element space based ML estimator can be found in the pioneering work of Ksienski and McGhee [KSIE68] and that of White [WHIT74]. More recent work on the element space based ML

estimator can be found in the papers of Haykin [HAYK85] and Ballance and Jaffer [BALL87]. One of the major drawbacks of the element space based ML estimator is the attendant computational complexity. In the case of K targets, the element space based likelihood function is a K-dimensional, multi-modal surface. A major contribution in this regard was a computationally efficient algorithmic formulation of the element space based ML estimator for multiple targets proposed by Bresler and Macovski [BRES86] referred to as the Iterative Quadratic Maximum Likelihood (IQML) algorithm. Ziskand and Wax [ZISK88] have also developed a computationally efficient implementation of the element space based ML estimator based on alternating projections. However, even in the simple case of two targets, neither of these formulations leads to a simple, closed-form expression for the ML estimates of the two respective target angles, except in the case of a three element array. The greatest attribute of the monopulse bearing estimation technique, and the reason for its widespread use in radar systems, is that even in the case of a large phased array, the angle of the target is found via a simple computation involving the ratio of the difference beam to the sum beam [GABR84], [SKOL80]. In [DAVI76], Davis et. al. show that the monopulse bearing estimation technique is, in fact, the ML estimator of the target angle given as data the sum and difference beams formed from the array element outputs. That is, it is a beamspace domain based ML estimator in which M-dimensional element space, where M is the number of elements in the array, is transformed into a 2-D beamspace. This insight has lead to an investigation of the use of three beams, i. e., a beamspace domain based ML estimator in which M-dim. element space is transformed into a 3-D beamspace, for the case of two targets angularly separated by less than a beamwidth.

One such 3-D beamspace domain based ML estimator is that proposed by Cantrell et. al. [CANT81]. In this technique, the transformation from element space to 3-D beamspace is achieved by applying the same beamforming weight vector to each of three identical, non-overlapping subarrays. A benefit of working with non-overlapping subarrays is that if the noise is independent at the element level, it will also be independent at the beamspace ports. Another interesting aspect of Cantrell et. al.'s subarray based prescription for converting from element space to beamspace is that the Vandermonde structure of the element space manifold, achieved with a uniformly-spaced array of identical sensors, is retained by the beamspace manifold vector. It is due to this phenomenon that Cantrell. et al. are able to formulate the BDML estimates of the direct and specular path arrival angles, given as data the

three subarray outputs formed from a single snapshot, in terms of the roots of a quadratic equation corresponding to a simple, closed-form estimation scheme. However, a major shortcoming of their method is that the "spatial passband" achieved by such a matrix beamforming scheme is that associated with the subarray which is approximately three times as large as that achievable by applying three different beamforming weight vectors to all of the array element outputs as proposed by Kesler and and Haykin [KESL80], [HAYK83], [HAYK84]. The importance of this observation has to do with the fact that although we may be only interested in two targets located in the general vicinity of broadside, there will undoubtedly be clutter and possibly interfering sources in the field of view of the array. In light of this, it is best to keep the width of the "spatial passband" about broadside as small as possible.

The low-angle radar tracking scheme formulated by Kesler and Haykin is referred to as the least squares adaptive antenna (LSAA) algorithm and is only applicable in the case of symmetric multipath. The conditions for which it is valid to invoke the symmetric multipath model are described in Section 2.3. The LSAA algorithm works in the following manner. Three beams are formed by processing the entire set of array signals with three different sets of weights producing a reference beam pointed to broadside and two auxiliary beams symmetrically positioned about broadside. The scenario is depicted in Figure 1.1. An error criterion is set up as the difference between the reference beam output and the sum of the two auxiliary beam outputs weighted by a scalar w. The optimum weight w which minimizes the mean-square value of this error criterion may be computed via a closed-form expression. The corresponding estimate of the direct path angle is then subsequently determined via the use of a calibration curve [HAYK85]. Although this technique appears to be somewhat ad-hoc, in Section 2.3 we show that under certain conditions it very nearly corresponds to the beamspace domain ML estimator. However, in general, the procedure does not yield the ML estimate primarily due to the fact that it does not account for the correlation between the noise at the beamspace ports. In general, the noise between the three beamspace ports is correlated even if the noise in element space is "spatially white". In addition, in Section 2.3 we show that the use of the calibration curve, which essentially involves a 1-D search, may be avoided if a Butler matrix beamformer is employed. In this case, the beamspace domain ML estimate of the direct path angle may be computed via a simple, closed-form expression similar to the monopulse expression for a single target.

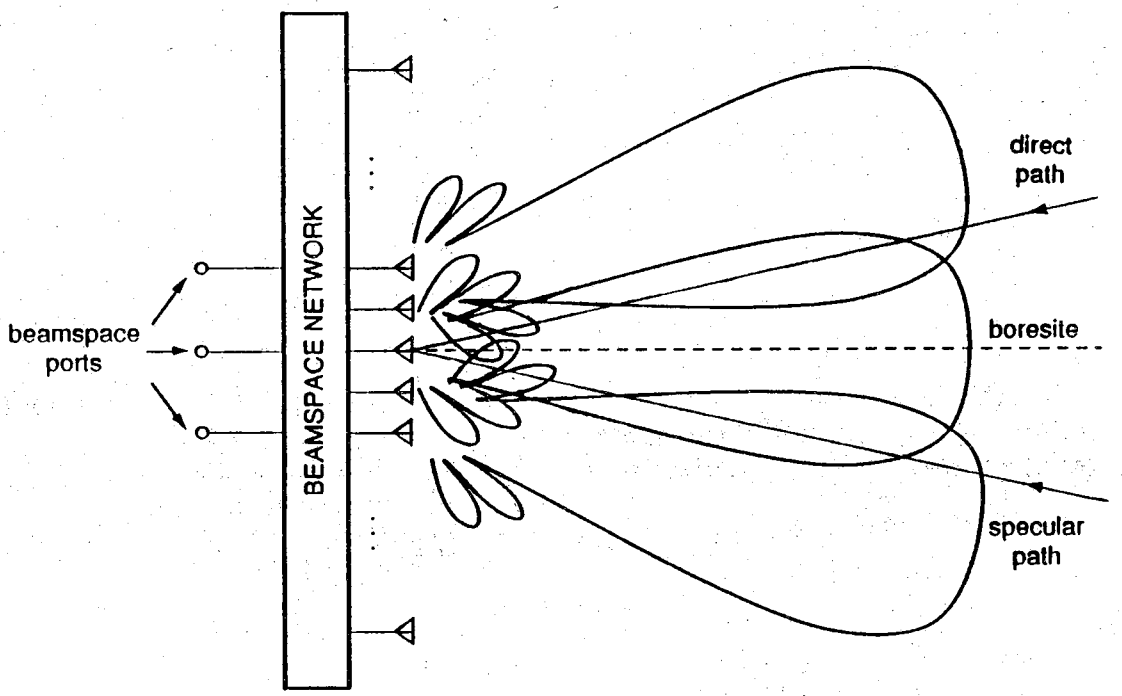

Figure 1.1 Polar depiction of the respective array patterns associated with the reference, upper, and lower beamforming weight vectors superimposed upon an illustration of the corresponding transformation from element space to 3x1 beamspace. The relative orientation of the direct and specular path rays is depicted as well.

1.3 Introduction to BDML Estimation Scheme

We will derive the beamspace domain Maximum Likelihood (BDML) estimator of the direct and specular path angles in a multipath scenario when the three beams are formed in a symmetrical fashion about broadside in the manner suggested by Haykin and Kesler. For the case of symmetric mutipath, Three different algorithmic implementations of the BDML estimator are presented. The development of one is motivated by the auxiliary beam subtraction and calibration curve procedure of Haykin described above. In effect, we make the necessary changes to Haykin's scheme in accordance with the above arguments, in order to put it on a Maximum Likelihood foundation. The two other procedures developed also follow directly from Maximum Likelihood considerations. In the one procedure the symmetry of the multipath is *explicity* exploited while in the other it is *implicitly* exploited. Although the "explicit" procedure is the more computationally simplistic of the two, the "implicit" procedure provides great insight into the performance of the estimator in the case where the multipath is "coherent" or 100% correlated with the direct path signal. Specifically, the development of the "implicit" procedure gives rise to the execution of a single forward-backward average on the 3x3 beamspace correlation matrix. Note that, in contrast to Cantrell's three subarray method, the beamspace manifold vector achieved by processing the entire set of array signals with three different sets of weights according to Haykin's scheme is real-valued and does not exhibit the Vandermonde structure. Hence, the applicability of forward-backward averaging, as it is applied in element space, is not apparent. Indeed, the effect of the forward-backward average in beamspace is quite different from the effect of forward-backward averaging in element space, as will be demonstrated in Section 2.3, and is only applicable in the case of symmetric multipath. With the BDML scheme for symmetric multipath established, we consider the special case of a Butler matrix beamformer which facilitates a simple, closed-form expression for the estimator.

The development of the BDML method for the nonsymmetric multipath case is a simple extension of that for the symmetric case. It is shown that if a Butler Matrix beamformer is employed, the BDML angle estimates may be simply determined from the roots of a judiciously constructed quadratic equation. This is a significant contribution due to the fact that the 3x1 beamspace manifold vector does not exhibit the Vandermonde structure in contrast to the situation with Cantrell's three subarray method as discussed

previously. The ability to nevertheless formulate the estimates in terms of the roots of a quadratic equation arises from the fact that the respective array patterns associated with each of three columns of the Butler beamforming matrix have M-3 nulls in common (M is the number of elements). The appropriate development exploiting this property may be found in Appendix B.

The analysis of the performance of the BDML estimator for both the symmetric and nonsymmetric cases under coherent multipath conditions is presented. We show that the BDML Method for nonsymmetric case can handle coherent multipath so long as the direct and specular path signals are not perfectly in-phase or perfectly 180° out-of-phase at the center element of the array. This is in contrast to MUSIC which, without pre-processing in the form of spatial smoothing or forward-backward averaging [SHAN85a], [WILL88], [EVAN82] breaks down in a coherent multipath scenario for any value of the phase difference. For the symmetric multipath case, it is shown that the only conditions for which breakdown occurs is the extreme case where the direct and specular path signals arrive 180° out-of-phase at the center element of the array and the magnitude of the reflection coefficient is exactly equal to unity. Under such conditions, the two signals cancel each other out entirely at the center element and very nearly cancel each other out at all other elements of the array, depending on how large the array is and how closely-spaced in angle the two signals are. The correctness of the analysis is verified by computing the corresponding Cramer-Rao Lower Bounds (CRLB) for unbiased estimates.

1.4 Generalized Butler Beamformers and BDML Estimators

The ability to formulate the BDML estimates in terms of the roots of a quadratic equation arises from the fact that the respective array patterns associated with each of three columns of the Mx3 Butler beamforming matrix have M-3 nulls in common (M is the number of elements), the locations of which are known regardless of the parameters chosen. The property of M-3 common nulls thus manifests itself as a-priori knowledge for the BDML estimation problem. Motivated by the equivalence between the multiplication of polynomials and the convolution of sequences, it is possible to factorize the Butler beamforming matrix as a product of an Mx3 banded, Toeplitz matrix with another 3x3 matrix. The Mx3 Toeplitz matrix thus obtained corresponds to those common nulls and the 3x3 matrix is related to the remaining

uncommon nulls. One important aspect of the above mentioned factorization is that it allows one to generalize the Butler beamformer by simply replacing the two matrix factors with other judiciously constructed matrices such that the resulting weight vectors have M-3 nulls in common.

The factorization of the Butler matrix beamformer motivates an alternative way of formulating the BDML estimation problem. The Toeplitz structure of the Mx3 matrix associated with the common nulls indicates that Butler beamforming is accomplished first by forming beams from the outputs of three identical, adjacent, overlapping subarray, each one having all but one element in common with the adjacent one. The 3x3 matrix associated with the uncommon nulls serves to transform the resulting 3x1 output vector into a 3x1 real beamspace manifold vector. An interesting aspect of the overlapping subarray based beamforming is that the Vandermonde structure of the element space manifold vector, achieved with a linear uniformly-spaced array of identical sensors, is retained by the beamforming output vector. As a consequence, the Mx3 banded, Toeplitz "common null" matrix, viewed as a beamforming matrix itself, provides an alternative approach to formulating the BDML estimator as that associated with the roots of a quadratic equation. In this case, the BDML estimates for the symmetric (nonsymmetric) case are determined via a 3x3 real (complex) generalized eigenvalue decomposition as opposed to the BDML estimator employing the regular reduced Butler beamformer which requires only a 3x3 real eigenvalue decomposition.

1.5 Auxiliary Procedures for BDML Method

If the surface of reflection is fairly smooth, i. e., the sea is relatively calm, and the target is not moving too fast in relative terms, the specular specular multipath signal is merely a time-delayed, amplitude-attenuated replica of the direct path signal over multiple looks, i. e., multiple snapshots. This condition is referred to as coherent multipath. In this case, the two signals are related by a complex scalar multiple, called the reflection coefficient. The fact that the reflection coefficient is constant over the observation interval changes the complexion of the ML formulation of the problem of estimating the direct path angle. Indeed, it represents a-priori information about a coherent multipath scenario which needs to be incorporated into the ML estimation scheme. Ballance and Jaffer [BALL87] found that at the expense of increased computation, exploitation of the coherence gives rise to an element space based ML estimator exhibiting increased performance over that achieved with

the ML estimator in element space which does not account for the reflection coefficient. As we shall see, this is the case in beamspace as well. In Section 4.2, an iterative algorithm is presented for simultaneously estimating the direct path angle and the complex reflection coefficient in the case of symmetric multipath.

A contradictory phenomenon observed by many researchers in the field of low-angle radar tracking is that for the nonsymmetric coherent multipath case, ML based estimators yield almost as bad a result for the 0° in-phase case as for the 180° out-of-phase case, where the phase is measured at the center of the array. In fact, Cantrell et. al. [CANT81] argue that an estimator which exhibits significantly better performance than the ML estimators in the 0° case must be biased. In fact, some beamspace domain ML estimation procedures will even totally break down under 0° and 180° phase difference conditions. However, the problem with the 0° phase difference does not show up for the case of symmetric multipath and more interestingly, the 0° case gives rise to the best performance. In light of these observations, it is desirable to develop a procedure which would convert convert a nonsymmetric problem to a symmetric one. In Section 4.3, we propose an ad-hoc scheme to accomplish this based on certain distinctive properties of the beamspace correlation matrix in the case of symmetric multipath. In particular, we will be concerned with the three-beam based BDML method wherein the conversion from nonsymmetric to symmetric multipath is simply some secondary steering, or fine tuning, of the three beams so that the pointing angle of the center beam is the bisector angle of the two paths.

The idea of employing frequency diversity to combat the signal cancellation problems occurring in low-angle radar tracking has been proposed by several researchers including Skolnik [SKOL80] and Kezys [KEZY88]. The idea is to have the radar transmitter emit multiple narrowband signals spaced in frequency with the frequency spacings judiciously chosen so that the phase difference occurring at the center of the array at each transmission frequency is significantly different from frequency bin to frequency bin. In Section 4.4, we invoke the coherent signal subspace concept, developed by Wang and Kaveh in their extension of the MUSIC algorithm for wideband sources [WANG85], [HUNG88] as a means for retaining the computational simplicity of the BDML estimation schemes while still incorporating in a coherent manner the additional data provided by the use of the auxiliary frequencies. In the application of coherent signal subspace processing here, focusing matrices serve to coherently combine the signal or target energy at each

frequency while, at the same time, the noise energy in the different frequency bands is combined in an incoherent fashion. By proceeding in this fashion, we find that the only growth in computation with respect to single frequency operation is the computation and implementation of the focusing matrices. This claim is tempered somewhat by the fact that the focusing matrices are not known a-priori giving rise to an iterative procedure and, hence, additional computation. Along these lines, it is also it is also shown in Section 4.4 that if one is able and willing to work a restricted set of "special" frequency values, perfect "focusing" may be achieved at the outset, i. e. without iterating, such that the computational complexity may be reduced to that associated with single frequency operation! The "special" frequencies are those satisfying $f_i = \frac{M}{M_i} f_0$ where M_i is an integer less than M, the total number of array elements, and f_0 is some reference frequency which is typically chosen to be that frequency for which the elements are spaced by a half-wavelength, although it doesn't have to be. It turns out that if spatial smoothing is performed in a judicious manner at each auxiliary frequency satisfying this relationship, the beamspace domain based focusing matrices necessary for coherently combining the signal information contained at each frequency are each a known scalar multiple of the identity matrix. As a final note, we note that the use of coherent signal subspace processing in conjunction with frequency diversity in the manner described above once again illustrates the dramatic computational advantage of working in beamspace: in element space the focusing matrices are MxM and complex whereas in beamspace they are 3x3 and real, regardless of the number of elements.

1.6 Adaptive Interference Cancellation

Although we here only concern ourselves with the estimation of the angles of two signals arriving in the vicinity of broadside, we are not presupposing that these are the only signals impinging upon the array. There may, in fact, be echo returns from clutter and other targets as well. What we are here assuming is that the sidelobes of the array pattern associated with each of the three beamforming weight vectors are low enough such that the contributions of those sources not located within a few beamwidths of broadside may be regarded as negligible. In the case of strong interferers, it is necessary to employ adaptively formed reference, upper, and lower auxiliary in much the same way that adaptively formed sum and difference beams may be

employed in monopulse radar tracking in the manner proposed by Davis et. al.in [DAVI76] and Gabriel in [GABR84]. Synthesis techniques for determining weights which result in a desired pattern response have been proposed by Capon [CAPO69], Griffiths et. al. [GRIF87], and Frost [FROS76]. These methods involved defining a performance criterion such as maximum output SINR, minimum mean-square error (MMSE), or minimum variance (MV), and then finding the weight vector resulting in an optimization of the criterion. The pattern nulls are formed in the direction of strong interfering sources and sidelobe patterns are adjusted accordingly to provide the best performance against noise in an interference environment. Motivated by the relationship between the three columns of the Butler matrix beamformer analyzed within, a novel procedure is desired wherein the upper, center, and lower beamforming weight vectors are constructed with adaptively steered nulls in the direction of interfering sources in such a fashion so as to nevertheless achieve a simple, closed-form expression for the BDML estimates of the direct and specular path angles.

In this thesis, we propose several modified performance criteria for constructing the optimum beamforming matrix, or three beamforming weight vectors, such that prescribed nulls are formed to cancel the interferences and M-3 common nulls are formed for each of the three beams. Our development is based on the linearly constrained minimum variance (MV) criterion, the least squares (LS) criterion, and the factorization property associated with the Butler matrix beamformer. The optimum beamformer obtained with the MV criterion minimizes the expected output noise power from the three beam ports while producing unit gain in the desired directions of look. The LS-based criterion leads to a matrix beamformer whose three columns form a set of mutually orthogonal vectors. The optimality is defined in terms of a least squares fit to the Butler beamforming matrix. In order to retain real-valued beamspace manifold vectors for the BDML methods, an additional constraint is imposed to ensure complex conjugate symmetry of the three weight vectors.

1.7 Outline of the Thesis

The thesis is organized as follows. Chapter 2 develops the beamspace domain maximum likelihood (BDML) estimator for both the symmetric and nonsymmetric multipath scenarios when the three beams are formed symmetrically about the broadside. A simple close-form expression for the BDML estimator is derived for the case of the reduced Butler matrix

beamformer. A performance analysis as the theoretical CRLB of the BDML estimator for both the symmetric and nonsymmetric cases under coherent multipath conditions is discussed. Simulation results illustrating the performance of the BDML estimator for various combinations of signal parameters are presented.

Chapter 3 deals with the structural analysis and generalization of the Butler matrix beamformer. By exploiting the relationship between polynomials and sequences, we convert the beamforming problem considered herein into that associated with some judiciously constructed matrices and based on that, we develop a new class of BDML estimators and derive a parametric representation for the beamspace manifold vectors.

In Chapter 4, three auxiliary procedures for improving the BDML estimator under coherent multipath scenario are investigated. First, an iterative algorithm is presented to simultaneously estimate the beamspace manifold vector of the direct path signal and the complex reflection coefficient. Performance improvement is achieved as the a-priori information about signal coherence is incorporated. It is shown that with Butler beamformer, the computational load is simply that associated with the solution of a quartic equation. Second, an ad-hoc scheme is developed for converting a nonsymmetric problem to a symmetric one. The idea was motivated by the fact that the BDML estimator for nonsymmetric case breaks down for 0° and 180° phase differences while the BDML estimator for symmetric case can handle any phase difference with 0° giving rise to the best performance. The conversion is a two-stage procedure: the bisector angle of the direct and specular paths is first estimated, followed by a secondary steering of the three beams. Significant simplifications can be achieved again with the use of a Butler beamformer. Finally, frequency diversity is incorporated in order to alleviate the rank deficiency and signal cancellation problems occurred at 0° and 180° phase differences. We first invoke the coherent signal subspace concept as a means for retaining the simplicity of the BDML schemes. It is then shown that significant reduction of computational load is achieved if the frequencies used belong to a restricted set of values. Simulation results for each of the above three schemes are presented.

Chapter 5 presents three novel adaptive beamforming techniques to effectively combat the interference and clutter problem often occurring in practice. The optimum weight vectors are determined via the minimum noise power and mutual orthogonality criteria. The idea is to adaptively form the center, upper, and lower beams in a fashion so as to achieve a simple closed-

form expression for the BDML estimator. Computer simulations are conducted to demonstrate the efficacy of the new beamforming schemes.

Chapter 6 concludes the thesis by commenting on the results of these studies and discussing possible future research topics.

CHAPTER 2
BEAMSPACE DOMAIN ML ESTIMATION FOR SPECULAR MULTIPATH

2.1 Introduction

One of the primary motivating factors for the early development of phased arrays was the prospect of "beamforming" to achieve very high gains in signal-to-noise ratio (SNR) at the beamformer output relative to the SNR at each sensor element. The idea, of course, is to coherently combine, or add up in phase, the desired signal at each of the array sensors by judicious weighting of the various array signals. A simple calculation shows that if the noise at each of the sensors is independent and of equal power, the gain in SNR achieved by compensating for the linear phase shift on the desired signal across the array, due to the different lengths traveled from the source to each sensor, is equal to the number of sensors in the array, a number which can be made quit large. It was subsequently found that classical beamforming was quite robust in that the SNR gain exhibited a graceful falloff from this optimal value when the phase compensation was mismatched for whatever reason. However, this robustness of classical beamforming manifests itself in terms of poor resolution when two closely-spaced signals impinge upon the array. In simple terms, a nearby interfering source, within a fraction of a beamwidth of the desired source, will pass through the beamformer with an SNR gain nearly equal to that for the desired source. This aspect of classical beamforming has implications with regard to the dual problem of estimating the respective bearings of two closely-spaced sources. The poor resolution of classical beamforming based direction finding ultimately lead to the development of numerous parametric-based estimation algorithms capable of sub-beamwidth resolution. Among these algorithms, the ones which stand out in terms of versatility and performance are the popular MUSIC algorithm [SCHM79] and the statistically based Maximum Likelihood (ML) algorithm [WHIT74]. Although both of these algorithms have indeed demonstrated superior performance, particularly with respect to classical Fourier-based direction finding, they nonetheless have limitations in terms of a significant degradation

in the sub-beamwidth resolution capability when the SNR of the received signal is very low. The primary application of interest herein is the low-angle radar tracking problem [BART74] wherein two signals, the direct and specular path signals, arrive near broadside to the array within a beamwidth of each other. The SNR associated with either signal at any given sensor is typically low compared to other scenarios. In addition, the number of snapshots available for tracking updating is usually very small, sometimes only one is available. To adequately deal with this problem, we propose the idea of applying either ML or MUSIC in so-called beamspace for the purpose of advantageously exploiting the poor resolution of classical beamforming to convert the element space data vectors to beamspace data vectors having a higher SNR and a lower dimensionality.

In this thesis, we will be primarily interested in the two-ray multipath scenario encountered in low-angle radar tracking and concern ourselves specifically with the problem of estimating the arrival angle of the direct path signal, the actual bearing of the target, when both the direct and specular path signals arrive near broadside to a linear array of antennas within a beamwidth of each other. We will here assume that the antenna elements comprising the array are identical and uniformly-spaced by a half-wavelength; the half-wavelength spacing avoids the infamous grating lobe problem. We further assume the number of antennas to be odd such that $M=2L+1$. A slight modification to each of the results developed within is required if M is even. For brevity, however, we do not include the appropriate modifications for M even. We will also assume that the target is in the far field of the array such that the returning echoes may be modeled as planewaves. Finally, we will also invoke the narrowband signal model.

We begin this chapter by briefly introducing fundamental array principles and aspects of conventional beamforming in Section 2.2. In particular, an analysis of beamforming SNR gain with respect to various weighting schemes is presented. With the knowledge of the array signal model and the concept of beamforming intact, we proceed to develop the ML estimator for the direct path angle. Section 2.3 will be exclusively concerned with the symmetric multipath problem wherein the angle of the specular path signal, with respect to broadside, is merely the negative of the angle of the direct path signal. Specifically, three different algorithmic implementations of the beamspace domain ML (BDML) estimator are presented. It is shown that if a Butler matrix beamformer is employed, the BDML estimate may be simply determined via a quadratic equation, leading to significant reduction in

computational complexity. Section 2.4 develops the BDML estimator for the non-symmetric multipath case, which is a straightforward extension of the estimation for the symmetric multipath case. In Section 2.5, a rigorous performance analysis for both the symmetric and nonsymmetric BDML estimators is presented. The results are shown to agree with the behavior of the theoretical Cramer-Rao Lower Bound (CRLB) discussed in Section 2.6. Finally, simulation results are presented in Section 2.7 to demonstrate the performance of the beam space domain ML estimators under various combinations of signal parameters.

2.2 Array Principles and Conventional Beamforming

In this section, we briefly review the narrowband array signal model which underscores the concept of using an array to achieve a gain in SNR. To this end, consider a single planewave impinging upon a uniformly-spaced linear array of M=2L+1 identical sensors at an angle θ_o with respect to broadside. The geometry of this scenario is illustrated in Figure 2.1. Let f_c denote the center of the frequency band of width B which the signal occupies; $\lambda_c=c/f_c$, where c is the speed of light, is the associated wavelength. Further, let $\mathscr{L}$ denote the length of the array. If this collection of array and signal parameters satisfies $(B/f_c)(\mathscr{L}/\lambda_c)\sin(\theta_o) \ll 1$, the narrowband array signal model may be invoked. Under these conditions, the element space snapshot vector, denoted as $\mathbf{x}(n)$, composed of the of the complex envelopes, $x_i(n)$, $i=-L,\ldots,-1,0,1,\ldots,L$, sensed sensed at each of the M=2L+1 array elements at the n-th snapshot may be expressed as

$$\mathbf{x}(n) = c_o(n)\mathbf{a}(u_o) + \mathbf{n}(n) \tag{2.1}$$

where $c_o(n)$ is the complex amplitude of the signal obtained at the n-th snapshot, the phase of which is that measured at the center of the array (the element indexed 0) such that

$$\mathbf{a}(u_o) = \left[e^{-j\pi Lu_o}, \cdots, e^{-j\pi u_o}, 1, e^{j\pi u_o}, \cdots, e^{j\pi Lu_o}\right]^T \tag{2.2}$$

accounts for the (uniform) linear phase variation across the array. The quantity $u_o=\sin(\theta_o)$ is the so-called reduced angle [STEI76] associated with θ_o. We will throughout work with the reduced angle $u=\sin(\theta)$. There is a one-to-one correspondence between u and θ over the angular interval $-90^\circ \le \theta \le 90^\circ$, corresponding to the so-called visible region [STEI76]. We will therefore concentrate on estimating u from which θ may be recovered via the

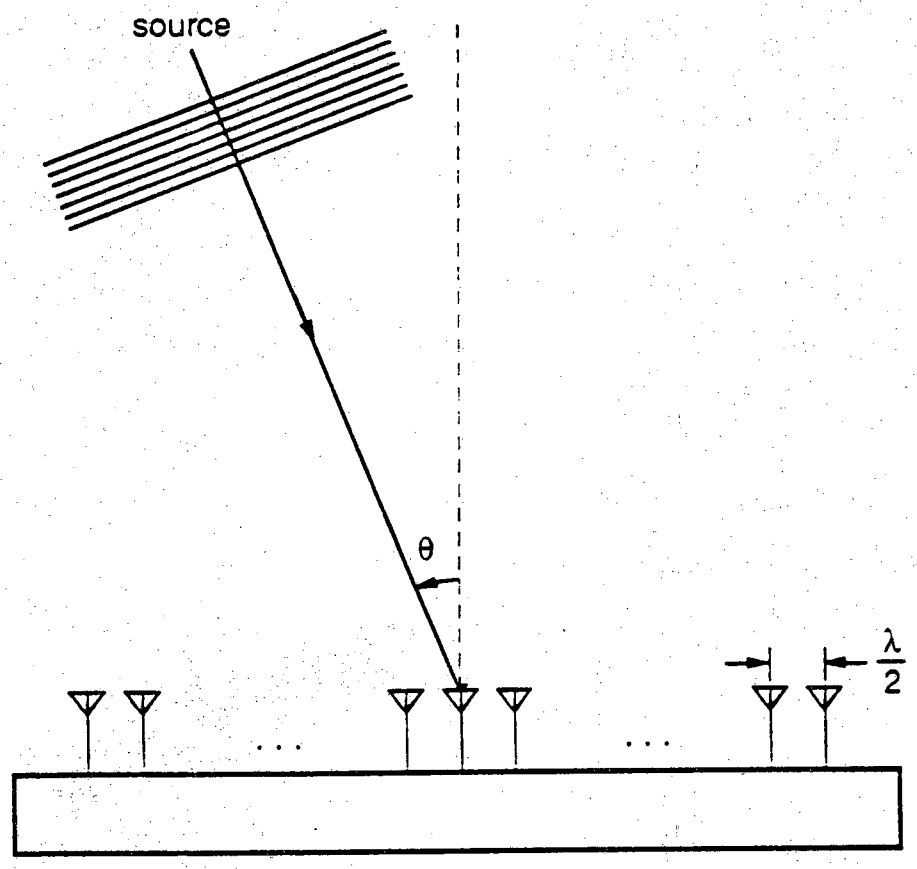

Figure 2.1 Geometry of a uniformly-spaced linear array with a single planewave source arriving from angle θ with respect to broadside.

inverse sine transformation without ambiguity. Finishing the definition of the quantities in (2.1), the elements of $\mathbf{n}(n)$, denoted $\nu_i(n)$, i=-L,...,-1,0,1,...,L, constitute the additive noise present at each sensor at the n-th snapshot.

The most noteworthy aspect of the narrowband array signal model is that the complex envelope of the signal is temporally coincident across the array; this is signified by the fact that $c_o(n)$ in (2.1) is a scalar quantity. This makes the job of coherently combining, or adding up in phase, the desired signal at each of the antenna elements a simple task of judiciously weighting and summing the various array signals. A simple calculation shows that if the noise at each of the antennas is independent and of equal power, equal to σ_n^2, say, the gain in SNR achieved by compensating for the linear phase shift on the desired signal across the array is equal to the number of elements in the array. The appropriate argument is as follows. The SNR at the i-th element, i=-L,...,-1,0,1,...,L, is given by

$$SNR_i = \frac{|e^{j\pi i u_o} c_o(n)|^2}{E\{|\nu_i(n)|^2\}} = \frac{|c_o(n)|^2}{\sigma_n^2} \tag{2.3}$$

which is the same for each antenna element. We are here assuming that the additive noise at each of the antenna elements is primarily receiver generated. We will discuss practical "noisy" sources such as clutter and interferences at a later point. In the case of receiver generated noise, we make the assumption that the additive noise at each element is independent and of the same power equal σ_n^2, i. e., the noise is "spatially white". Let us consider forming a beam with the weight vector $\mathbf{w}$ with elements w_i^*, i=-L,...,-1,0,1,...,L, according to

$$b(n) = \mathbf{w}^H\mathbf{x}(n) = [\mathbf{w}^H\mathbf{a}(u_o)]c_o(n) + \mathbf{w}^H\mathbf{n}(n) \tag{2.4}$$

Note that b(n) is simply a number, i. e., a scalar quantity. Under the same definition as that for the element level, we find that the new SNR associated with the beamspace element is [STEI76]

$$SNR_b = \frac{|[\mathbf{w}^H\mathbf{a}(u_o)]c_o(n)|^2}{E\{|\mathbf{w}^H\mathbf{n}(n)|^2\}} = \frac{|\mathbf{w}^H\mathbf{a}(u_o)|^2}{\mathbf{w}^H\mathbf{w}} SNR_i \tag{2.5}$$

where we have used the fact that $E\{\mathbf{n}(n)\mathbf{n}^H(n)\} = \sigma_n^2\mathbf{I}$. Thus, the quantity

$$SNRG(u_o) = \frac{|\mathbf{w}^H\mathbf{a}(u_o)|^2}{|\mathbf{w}|^2} = \frac{\mathbf{w}^H\mathbf{a}(u_o)\mathbf{a}^H(u_o)\mathbf{w}}{\mathbf{w}^H\mathbf{w}} \tag{2.6}$$

represents the SNR gain achieved by beamforming. As (2.6) is a ratio of two simple quadratic forms, it is easily proven that it is maximized when $\mathbf{w} = \alpha\mathbf{a}(u_o)$, where α is arbitrary, which corresponds to classical beamforming

with Fourier-based phasing and rectangular weighting. Substitution of this weight into (2.6) indicates that the maximum SNR gain is M, the number of array elements. The significance of (2.6) for our purposes here is best understood by considering $u_o=\sin(\theta_o)$ to be variable such that (2.6) represents the SNR gain achieved by beamforming with the particular set of weights comprising $\mathbf{w}$ as a function of the signal angle u_o. If we drop the subscript o, we arrive at the not too surprising result that the gain pattern is proportional to the array power factor $|\mathbf{w}^H\mathbf{a}(u)|^2$. However, the constant of proportionality, the reciprocal of $|\mathbf{w}|^2$, is critically important when comparing the SNR gain performance of various weighting schemes. We demonstrate this point in the example to follow.

We illustrate the utility of the preceding development for operating in the beamspace domain with an example. Consider forming a beam to broadside with rectangular weighting such that $\mathbf{w} = \mathbf{a}(o) = \mathbf{1}$, where $\mathbf{1}$ is an Mx1 vector comprised of all ones. Substitution into (2.6) leads to the array gain pattern

$$\mathrm{SNRG}(u) = \frac{|\mathbf{1}^T\mathbf{a}(u_j)|^2}{|\mathbf{1}|^2} = \frac{1}{M}\left\{\frac{\sin(M\pi u/2)}{\sin(\pi u/2)}\right\}^2 \qquad (2.7)$$

which exhibits the maximum gain of M at u=0 (θ=90°, broadside). Of course, signals arriving slightly off broadside appear at the beamformer output with a significant amount of gain as well. In fact, for $|u| < .88/M$, corresponding to the 3dB beamwidth, $M/2 < \mathrm{SNRG}(u) < M$ which can be quite large if M is large. This is indeed a manifestation of a well known characteristic of classical beamforming: poor resolution. The goal here is to exploit this shortcoming of classical beamforming and at the same time reduce computation and we will do so shortly. First, we would like to point out the significance of the denominator in (2.6). For this purpose, consider forming a beam to broadside with a triangular taper defined by $w_i = L+1-|i|$, i=-L,...,-1,0,1,...,L. In general, the SNR gain achieved with a real set of weights w_i for a signal arriving at broadside is given by $(\sum_{i=-L}^{L} w_i)^2 / (\sum_{i=-L}^{L} w_i^2)$, which is approximately equal to .75M for triangular weighting when L>2 (M=2L+1). The point is that in addition to the classical observation that triangular weighting gives rise to a mainbeam of twice the width of that obtained with rectangular weighting but with much reduced sidelobes, it is also gives rise to a max SNR gain which is only three-fourths that achieved with rectangular weighting. A 3dB beamwidth calculation for the case of triangular tapering [STEI76] finds that $3M/8 < \mathrm{SNRG}(u) < 3M/4$ for $|u| < 1.27/M$.

2.3 BDML Estimator for Symmetric Multipath

The symmetric two-ray multipath model holds to a good approximation if (a) the target is at a great distance from the array site such that the direct and specular path rays are approximately parallel, and (b) the array is mounted orthogonally to the surface of reflection for the multipath. This scenario is depicted in Figure 2.2. We point out, however, that in some cases, calibration may be necessary in order to compensate for the distortion due to atmospheric refraction and the curvature of the earth.

2.3.1 Composition of Data Snapshot Vectors

Under the narrowband assumption described in the preceding section, the n-th element space snapshot vector, $\mathbf{x}(n)$, for the symmetric multipath scenario may be written as [HAYK84], [BART74]

$$\mathbf{x}(n) = c_1(n)\mathbf{a}(u_o) + c_2(n)\mathbf{a}(-u_o) + \mathbf{n}(n) \qquad n = 1,...,N$$

$$= \left[\mathbf{a}(u_o) \vdots \mathbf{a}(-u_o)\right]\begin{bmatrix} c_1(n) \\ c_2(n) \end{bmatrix} + \mathbf{n}(n) = \mathbf{A}\mathbf{c}(n) + \mathbf{n}(n) \tag{2.8}$$

The description of the various terms in (2.8) are as follows. First, $u_o = \sin(\theta_o)$ where θ_o is the angle of the direct path signal with respect to broadside. $c_1(n)$ is the sample value of the complex envelope of the direct path echo at the n-th snapshot. The phase angle of $c_1(n)$ is that measured at the center of the array (the antenna element indexed 0) such that

$$\mathbf{a}(u) = \left[e^{-j\pi Lu}, \cdots, e^{-2j\pi u}, e^{-j\pi u}, 1, e^{j\pi u}, e^{2j\pi u}, \cdots, e^{j\pi Lu}\right]^T \tag{2.9}$$

with $u = u_o$ accounts for the (uniform) linear phase variation across the array due to the planewave assumption. $c_2(n)$ is defined similarly with regard to the specular path signal. Again, the elements of $\mathbf{n}(n)$, denoted $\nu_i(n)$, i=-L,...,-1,0,1,...,L, constitute the additive noise present at each antenna output at the n-th snapshot.

Following the lead of Haykin [HAYK83], [HAYK84], [HAYK85], [KESL80], we form three beams by operating on all of the array elements with three different sets of weights. Figuratively speaking, we form two "auxiliary" beams symmetrically pointed above and below the horizon at $u = u_B$ and $u = -u_B$, respectively, and a "reference" beam pointed directly along the horizon at $u = 0$ (broadside). u_B then represents a design parameter which

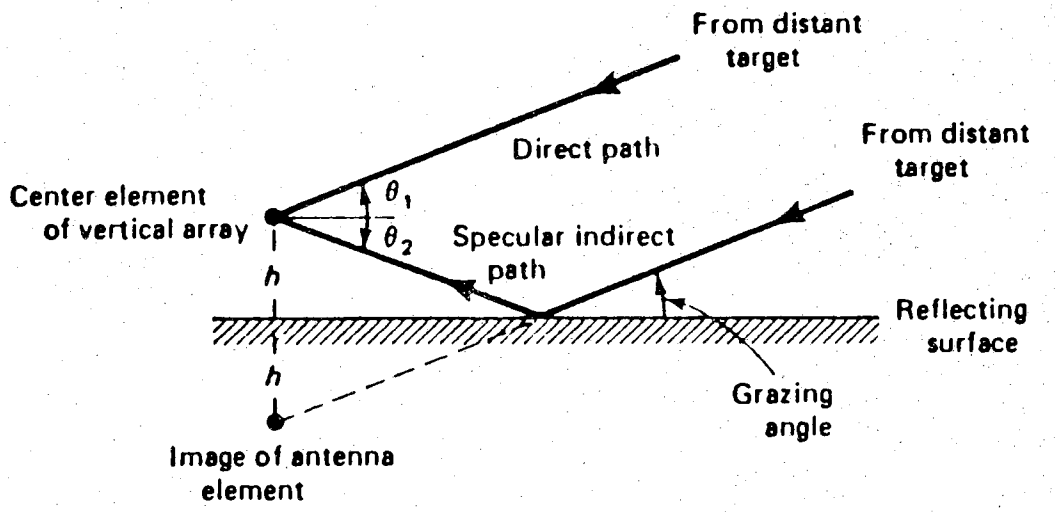

Figure 2.2 Geometry of symmetric specular multipath. The grazing angle is equal to $\theta_1 = \theta_2$

must be determined a-priori. The approach of forming three beams may be simply viewed as an extension of monopulse radar tracking wherein two beams are formed in the angular vicinity of a single target to accurately estimate its bearing. A natural generalization is to form three beams in the vicinity of two closely-spaced targets. Mathematically, the formation of three beams may be represented as a transformation from M-dim. element space to a 3-D beamspace as described by

$$\mathbf{x}_B(n) = \mathbf{S}^H\mathbf{x}(n) \qquad \text{where:} \quad \mathbf{S} = \left[\mathbf{s}(u_B) \vdots \mathbf{s}(0) \vdots \mathbf{s}(-u_B)\right] \tag{2.10}$$

The Mx3 matrix $\mathbf{S}$ is referred to as the beamforming matrix. The three columns of $\mathbf{S}$ are referred to as beamforming or "steering" vectors and are described below.

$$\mathbf{s}(u_B) = \mathbf{D}_a\mathbf{a}(u_B) \;\; ; \;\; \mathbf{s}(0) = \mathbf{D}_r\mathbf{a}(0) \;\; ; \;\; \mathbf{s}(-u_B) = \mathbf{D}_a\mathbf{a}(-u_B) \tag{2.11}$$

where $\mathbf{D}_a = \text{diag}\{a_L, \cdots, a_1, a_0, a_1, \cdots, a_L\}$ and $\mathbf{D}_r = \text{diag}\{r_L, \cdots, r_1, r_0, r_1, \cdots, r_L\}$ are real, diagonal MxM matrices with elements symmetric about the central diagonal element. The a_i, i =0,1,...,L, serve to shape each of the two the auxiliary beams while the r_i, i =0,1,...,L, serve to shape the reference beam such that, in contrast to Haykin's LSAA method, we do not here require that the tapering for the reference beam be the same as that for the two auxiliary beams. Note that a_i and r_i, i=0,1,...,L, represent design parameters which must be determined a-priori.

From its definition in (2.9), we may deduce the following properties of the element space manifold vector $\mathbf{a}(u)$:

$$\text{(a)} \;\; \mathbf{a}^*(u) = \mathbf{a}(-u); \quad \text{(b)} \;\; \tilde{\mathbf{I}}_M\mathbf{a}(u) = \mathbf{a}^*(u); \quad \text{(c)} \;\; \tilde{\mathbf{I}}_M\mathbf{a}(u) = \mathbf{a}(-u) \tag{2.12}$$

where $\tilde{\mathbf{I}}_n$ is an nxn reverse permutation matrix defined as follows

$$\tilde{\mathbf{I}} = \begin{bmatrix} 0 & 0 & & & 1 \\ 0 & 0 & & \cdot & 0 \\ \vdots & \vdots & \cdot & & \vdots \\ 0 & 1 & \cdot & & 0 \\ 1 & 0 & & & 0 \end{bmatrix} \tag{2.13}$$

Note that $\tilde{\mathbf{I}}$ satisfies $\tilde{\mathbf{I}}^T = \tilde{\mathbf{I}}$ and $\tilde{\mathbf{I}}\,\tilde{\mathbf{I}} = \mathbf{I}$ which indicates that it is is a unitary matrix equal to its own transpose. (2.12b) is a mathematical statement that $\mathbf{a}(u)$ is conjugate centro-symmetric for all u. From the two properties of $\mathbf{a}(u)$ described in (2.12) and the symmetric nature of the tapering, we deduce the following properties of $\mathbf{S}$.

$$\text{(a) } \mathbf{S}\tilde{\mathbf{I}}_3 = \mathbf{S}^*; \quad \text{(b) } \tilde{\mathbf{I}}_M\mathbf{S} = \mathbf{S}^*; \quad \text{(c) } \tilde{\mathbf{I}}_M\mathbf{S}\tilde{\mathbf{I}}_3 = \mathbf{S} \tag{2.14}$$

The properties of the beamforming matrix $\mathbf{S}$ described by (2.14) will be invoked at various points in our development.

Invoking the above notation and definitions, we may express the composition of the 3x1 beamspace domain snapshot vector, $\mathbf{x}_B(n)$, in a format similar to that in (2.8) for $\mathbf{x}(n)$, the element space snapshot vector,

$$\mathbf{x}_B(n)=\Big[\mathbf{b}(u_o)\vdots\mathbf{b}(-u_o)\Big]\mathbf{c}(n) + \mathbf{n}_B(n)=\mathbf{B}\mathbf{c}(n) + \mathbf{n}_B(n) \tag{2.15}$$

where $\mathbf{n}_B(n) = \mathbf{S}^H\mathbf{n}(n)$, $\mathbf{b}(u) = \mathbf{S}^H\mathbf{a}(u)$, referred to as the beamspace manifold vector, and $\mathbf{B} = \mathbf{S}^H\mathbf{A} = [\mathbf{b}(u_o) \vdots \mathbf{b}(-u_o)]$. As a consequence of the property of S described by (2.14b) and that of $\mathbf{a}(u)$ described by (2.12b), we have

$$\mathbf{b}(u) = \mathbf{S}^H\mathbf{a}(u) = \mathbf{S}^H\tilde{\mathbf{I}}_M\tilde{\mathbf{I}}_M\mathbf{a}(u) = \mathbf{S}^T\mathbf{a}^*(u) = \mathbf{b}^*(u) \tag{2.16}$$

which indicates that $\mathbf{b}(u)$ is a real-valued 3x1 vector for all u. Hence, $\mathbf{B}$ in (2.15) is real. Note that from (2.15) and (2.16), we may deduce the following relationship between $\mathbf{b}(u_o)$ and $\mathbf{b}(-u_o)$ which will be highly instrumental in our development of the BDML estimator of u_o:

$$\mathbf{b}(-u_o) = \tilde{\mathbf{I}}_3\ \mathbf{b}(u_o) \tag{2.17}$$

where $\tilde{\mathbf{I}}_3$ is the reverse permutation matrix of order 3 defined by (2.13). This property of $\mathbf{b}(u)$ mimics that property of $\mathbf{a}(u)$ described by (2.12c). However, in contrast to $\mathbf{a}(u)$, $\mathbf{b}(u) = \mathbf{S}^H\mathbf{a}(u)$ is composed of purely real elements, does not exhibit centro-symmetry, and does not possess the Vandermonde structure. As an example of a beamspace manifold vector, consider the case of rectangular weighting, i. e., no tapering, for all three beams. In this case, i. e., $\mathbf{D}_a = \mathbf{D}_r = \mathbf{I}$ such that $\mathbf{S} = [\mathbf{a}(u_B) \vdots \mathbf{a}(0) \vdots \mathbf{a}(-u_B)]$. The components of $\mathbf{b}(u)$ are simply the respective array patterns associated with each of the weight vectors, $\mathbf{a}(u_B)$, $\mathbf{a}(0)$ and $\mathbf{a}(-u_B)$. The array pattern associated with the reference beam, denoted $G_r(u)$, is that produced by the weight vector $\mathbf{a}(0)$, a vector composed of all ones. $G_r(u)$ is thus simply the following familiar array pattern:

$$G(u) = \mathbf{a}^H(0)\mathbf{a}(u) = \sum_{i=-L}^{L} e^{j\pi iu} = \frac{\sin(\frac{M}{2}\pi u)}{\sin(\frac{\pi}{2}u)} \tag{2.18}$$

The array patterns associated with the upper and lower auxiliary beams are simply this pattern shifted to the right and left, respectively, by the amount

u_B, i. e., $\mathbf{a}^H(u_B)\mathbf{a}(u) = G(u - u_B)$ and $\mathbf{a}^H(-u_B)\mathbf{a}(u) = G(u + u_B)$. Thus, the beamspace manifold vector with $\mathbf{S} \doteq [\mathbf{a}(u_B) : \mathbf{a}(0) : \mathbf{a}(-u_B)]$ is of the following form:

$$\mathbf{b}(u) = \left[\frac{\sin(\frac{M}{2}\pi(u-u_B))}{\sin(\frac{\pi}{2}(u-u_B))}, \frac{\sin(\frac{M}{2}\pi u)}{\sin(\frac{\pi}{2}u)}, \frac{\sin(\frac{M}{2}\pi(u+u_B))}{\sin(\frac{\pi}{2}(u+u_B))} \right]^T \tag{2.19}$$

Note that the noise terms in the beamspace snapshot vector are, in general, correlated even if the noise terms in the element space snapshot vector are independent. If we assume spatially white noise at the element level such that $E[\mathbf{n}(n)\mathbf{n}^H(n)]=\sigma_n^2\mathbf{I}$, the covariance matrix of the noise in beamspace, denoted $\mathbf{R}_{nn}^{bb}$, simplifies as follows.

$$\mathbf{R}_{nn}^{bb}=E\{\mathbf{n}_B(n)\mathbf{n}_B^H(n)\}=\mathbf{S}^H E\{\mathbf{n}(n)\mathbf{n}^H(n)\}\mathbf{S}=\sigma_n^2\mathbf{S}^H\mathbf{S} \tag{2.20}$$

Let $\mathbf{Q} = \mathbf{S}^H\mathbf{S}$. Invoking the properties of $\mathbf{S}$ described by (2.7), we deduce the following properties of $\mathbf{Q}$:

$$\begin{aligned} &\text{(a)} \quad \tilde{\mathbf{I}}_3\mathbf{Q}\tilde{\mathbf{I}}_3 = \tilde{\mathbf{I}}_3\mathbf{S}^H\tilde{\mathbf{I}}_M\tilde{\mathbf{I}}_M\mathbf{S}\tilde{\mathbf{I}}_3 = \mathbf{S}^H\mathbf{S} = \mathbf{Q} \ ; \\ &\text{(b)} \quad \mathbf{Q}^* = \mathbf{S}^T\mathbf{S}^* = \tilde{\mathbf{I}}_3\mathbf{S}^H\mathbf{S}\tilde{\mathbf{I}}_3 = \tilde{\mathbf{I}}_3\mathbf{Q}\tilde{\mathbf{I}}_3 = \mathbf{Q} \end{aligned} \tag{2.21}$$

where we have used the fact that $\tilde{\mathbf{I}}_M\tilde{\mathbf{I}}_M = \mathbf{I}$. These results indicate that $\mathbf{Q} = \mathbf{S}^H\mathbf{S}$ is real, symmetric, and per-symmetric (symmetric about the anti-diagonal). Finally, we note that $\mathbf{Q}$ is diagonal if and only if the three beamforming vectors $\mathbf{s}(u_B)$, $\mathbf{s}(0)$ and $\mathbf{s}(-u_B)$ are mutually orthogonal. This special case will lead to certain simplifications as will be seen shortly.

2.3.2 Development of Beamspace Domain ML Estimator

With this structural analysis of the beamspace snapshot vector, $\mathbf{x}_B(n)$, as a backdrop, we briefly develop the the Maximum Likelihood (ML) estimator of u_o given as data the beamspace snapshot vectors: $\mathbf{x}_B(n)$, n=1,...,N. It should be kept in mind that this ML estimator will yield different estimates than those obtained from the ML estimator working with the raw data, i. e., the element space snapshot vectors.

If the number of antenna elements, M, is large, each of the three components of the 3x1 beamspace noise vector $\mathbf{n}_B(n)$ is a weighted sum of a large number of random noise variates. Assuming the noise to be independent from element to element, it is therefore reasonable to invoke the Central Limit

Theorem and thus approximate the noise in beamspace as being Gaussian distributed. Thus, assuming the beamspace domain noise to be Gaussian and the sequences $c_1(n)$ and $c_2(n)$, $n=1,...,N$, to be unknown but deterministic, the Likelihood function is given by:

$$\prod_{n=1}^{N} \pi^{-M} |\mathbf{R}_{nn}^{bb}|^{-1} \exp\{-[\mathbf{x}_B(n)-\mathbf{B}\mathbf{c}(n)]^H \mathbf{R}_{nn}^{bb\,-1} [\mathbf{x}_B(n)-\mathbf{B}\mathbf{c}(n)]\} \qquad (2.22)$$

Proceeding in the typical fashion by taking the natural logarithm of the likelihood function and throwing out those terms which do not depend on $\mathbf{B}$, we arrive at the following optimization problem

$$\underset{u_o, \mathbf{c}(1),...,\mathbf{c}(N)}{\text{Minimize}} \quad \sum_{n=1}^{N} ||\mathbf{x}_B(n) - \mathbf{B}\,\mathbf{c}(n)||_{\mathbf{Q}}^2 \qquad (2.23)$$

where the norm is defined such that $||\mathbf{y}||_{\mathbf{Q}}^2 = \mathbf{y}^H \mathbf{Q}^{-1} \mathbf{y}$ and $\mathbf{Q}=\mathbf{S}^H\mathbf{S}$ as defined previously. It is well known [8] that in the estimation of u_o, the problem is separable such that we may proceed by substituting in for $\mathbf{c}(n)$, $n=1,...,N$, the respective least square error solution $\mathbf{c}_{LS}(n)=[\mathbf{B}^T\mathbf{Q}^{-1}\mathbf{B}]^{-1}\mathbf{B}^T\mathbf{Q}^{-1}\mathbf{x}_B(n)$, $n=1,...,N$. Substitution of $\mathbf{c}_{LS}(n)$ into (2.23) yields, after some manipulation, the following objective function to be minimized over u_o only:

$$\underset{u_o}{\text{Minimize}} \quad \sum_{n=1}^{N} \mathbf{x}_B^H(n)\mathbf{Q}^{-1/2}\, \mathbf{P}_{\mathbf{B}_w}^{\perp}(u_o)\, \mathbf{Q}^{-1/2}\mathbf{x}_B(n) \qquad (2.24)$$

where $\mathbf{P}_{\mathbf{B}_w}^{\perp}(u_o) = \mathbf{I} - \mathbf{Q}^{-1/2}\,\mathbf{B}[\mathbf{B}^T\mathbf{Q}^{-1}\mathbf{B}]^{-1}\mathbf{B}^T\mathbf{Q}^{-1/2}$ is a projection operator onto the orthogonal complement of the span of $\mathbf{Q}^{-1/2}\mathbf{b}(u_o)$ and $\mathbf{Q}^{-1/2}\mathbf{b}(-u_o)$, the "whitened" columns of $\mathbf{B}$. With the estimator formulated in this fashion, the ML estimate is obtained by varying u_o, and, hence, $\mathbf{P}_{\mathbf{B}_w}^{\perp}(u_o)$, in accordance with some numerical search technique until the minimum of the objective function in (2.24) is reached. For the purpose of developing a much simpler means for finding the optimum value of u_o, we here convert the optimization problem in (2.24) to an equivalent one motivated by the IQML algorithm formulated by Bresler for ML based direction of arrival estimation in element space [8]. We briefly sketch the appropriate development.

The orthogonal complement of the span of $\mathbf{Q}^{-1/2}\mathbf{b}(u_o)$ and $\mathbf{Q}^{-1/2}\mathbf{b}(-u_o)$ is, of course, a 1-D space such that $\mathbf{P}_{\mathbf{B}_w}^{\perp}(u_o)$ may be expressed in the form $\frac{1}{||\mathbf{d}||^2}\mathbf{d}\mathbf{d}^H$ where $\mathbf{d}$ is orthogonal to both $\mathbf{Q}^{-1/2}\mathbf{b}(u_o)$ and $\mathbf{Q}^{-1/2}\mathbf{b}(-u_o)$. Alternatively, if we let $\mathbf{d} = \mathbf{Q}^{1/2}\,\mathbf{v}$, $\mathbf{P}_{\mathbf{B}_w}^{\perp}(u_o)$ may be expressed in the form

$\frac{\mathbf{Q}^{1/2}\mathbf{v}\,\mathbf{v}^H\mathbf{Q}^{1/2}}{\mathbf{v}^H\,\mathbf{Q}\,\mathbf{v}}$ where $\mathbf{v}$ is orthogonal to $\mathbf{b}(u_o)$ and $\mathbf{b}(-u_o)$. Substitution of this expression for $\mathbf{P}^{\perp}_{\mathbf{B}_u}(u_o)$ into (2.24) yields the following alternative expression for the objective function in terms of $\mathbf{v}$:

$$\frac{\sum_{n=1}^{N} \mathbf{x}_B^H(n)\,\mathbf{v}\,\mathbf{v}^H\,\mathbf{x}_B(n)}{\mathbf{v}^H\,\mathbf{Q}\,\mathbf{v}} = N\,\frac{\mathbf{v}^H\,\hat{\mathbf{R}}_{bb}\,\mathbf{v}}{\mathbf{v}^H\,\mathbf{Q}\,\mathbf{v}} \tag{2.25}$$

where $\hat{\mathbf{R}}_{bb} = \frac{1}{N}\sum_{n=1}^{N} \mathbf{x}_B(n)\,\mathbf{x}_B^H(n)$ is the sample correlation matrix formed in beamspace. Now, for the expression in (2.25) to be equivalent to the objective function in (2.17), $\mathbf{v}$ must be orthogonal to both $\mathbf{b}(u_o)$ and $\mathbf{b}(-u_o)$, as pointed out previously. We make two relevant observations. First, $\mathbf{b}(u_o)$ is a real-valued 3x1 vector as is $\mathbf{b}(-u_o)$. Thus, without loss of generality, $\mathbf{v}$ may be taken to be real-valued. Second, $\mathbf{b}(-u_o) = \tilde{\mathbf{I}}_3\,\mathbf{b}(u_o)$, as indicated in (2.17), giving rise to the following observation:

$$\begin{aligned}\mathbf{v}^T[\mathbf{b}(u_o) \vdots \mathbf{b}(-u_o)] &= \mathbf{v}^T[\mathbf{b}(u_o) \vdots \tilde{\mathbf{I}}_3\mathbf{b}(u_o)] \\ &= \mathbf{v}^T\tilde{\mathbf{I}}_3\,[\,\tilde{\mathbf{I}}_3\mathbf{b}(u_o) \vdots \mathbf{b}(u_o)\,] = 0\end{aligned} \tag{2.26}$$

From this observation we may deduce that $\tilde{\mathbf{I}}_3\mathbf{v} = \mathbf{v}$, i. e., that $\mathbf{v}$ must be centro-symmetric. Taking account these restrictions on $\mathbf{v}$, we formulate the following optimization equivalent to that described by (2.24):

$$\underset{\mathbf{v}}{\text{Minimize}} \quad \frac{\mathbf{v}^T\,\text{Re}\{\hat{\mathbf{R}}_{bb}\}\,\mathbf{v}}{\mathbf{v}^T\,\mathbf{Q}\,\mathbf{v}} \tag{2.27}$$

$$\text{subject to:} \quad \tilde{\mathbf{I}}_3\mathbf{v} = \mathbf{v}$$

Recall that $\mathbf{Q}=\mathbf{S}^H\mathbf{S}$ is real as proved in (2.21). With the solution $\mathbf{v}$ to this optimization problem, one may determine the corresponding value of u_o which solves the optimization problem in (2.24), the BDML estimate of u_o, as the solution to $\mathbf{v}^T\mathbf{b}(u_o) = 0$. Since $\mathbf{b}(u) = \mathbf{S}^H\mathbf{a}(u)$, one may also determine u_o as the solution to $\mathbf{v}^T\mathbf{S}^H\mathbf{a}(u_o) = 0$. Note that in light of the centro-symmetry constraint, the optimum $\mathbf{v}$ has only two distinct elements. Also, note that the objective function in (2.27) is invariant to a scale change in $\mathbf{v}$ such that we may fix one of its elements equal to one, for example. The point is that the optimization problem described by (2.27) is, in fact, a single parameter optimization problem as is the original optimization problem described by (2.24).

We now present three methods for determining the optimum $\mathbf{v}$ satisfying (2.27) and the corresponding u_o which serves as the Beamspace Domain ML (BDML) estimate of the direct path angle. The three methods should, in theory, provide the same numerical value for the BDML estimate of u_o; the difference lies in their computational requirements. As a final observation at this point, note that the beamspace correlation matrix, $\mathbf{R}_{bb}$ is related to the element space correlation matrix, $\hat{\mathbf{R}}_{xx} = \frac{1}{N} \sum_{n=1}^{N} \mathbf{x}(n)\, \mathbf{x}^H(n)$ according to

$$\hat{\mathbf{R}}_{bb} = \frac{1}{N} \sum_{n=1}^{N} \mathbf{x}_B(n)\, \mathbf{x}_B^H(n) = \mathbf{S}^H\, \hat{\mathbf{R}}_{xx}\, \mathbf{S} \tag{2.28}$$

Method I: Explicit Exploitation of Centro-Symmetry. Since $\mathbf{v}$ is centro-symmetric, we may express it as $\mathbf{v} = [v_1 \;\; v_o \;\; v_1]^T$, where v_o and v_1 are real. To account for the centro-symmetry constraint, define

$$\mathbf{S}' = \Big[\mathbf{s}(0) \;\vdots\; \mathbf{s}(u_B) + \mathbf{s}(-u_B)\Big] \quad \text{and} \quad \mathbf{v}' = [v_o \;\; v_1]^T \tag{2.29}$$

such that $\mathbf{Sv} = \mathbf{S}'\mathbf{v}'$. Note that in contrast to $\mathbf{S}$, which is Mx3 as defined in (2.10), the Mx2 matrix $\mathbf{S}'$ is **real** due to the fact that $\mathbf{s}(-u_B) = \mathbf{s}^*(u_B)$. Substituting $\mathbf{S}'\mathbf{v}'$ for $\mathbf{Sv}$ in (2.27) allows us to express the constrained optimization problem in (2.27) as an unconstrained one in the following fashion:

$$\underset{\mathbf{v}'}{\text{Minimize}} \quad \frac{\mathbf{v}'^T\, \mathbf{S}'^T \text{Re}\{\hat{\mathbf{R}}_{xx}\} \mathbf{S}'\, \mathbf{v}'}{\mathbf{v}'^T\, \mathbf{S}'^T \mathbf{S}'\, \mathbf{v}} \tag{2.30}$$

where we have exploited the fact that $\mathbf{S}'$ is real. The solution to (2.30), of course, is such that $\mathbf{v}'$ is that generalized eigenvector (GEVEC) of the 2x2 real, symmetric pencil $\{\mathbf{S}'^T \text{Re}\{\hat{\mathbf{R}}_{xx}\}\mathbf{S}' \;,\; \mathbf{S}'^T\mathbf{S}'\}$ associated with the smaller of the two generalized eigenvalues (GEV's). Given this $\mathbf{v}'$, u_o may be estimated as that root of $G_e(u) = \mathbf{e}^T\mathbf{a}(u)$, where $\mathbf{e} = \mathbf{S}'\mathbf{v}'$, in the vicinity of $u=0$. Note that the two columns of $\mathbf{S}'$ are real and centro-symmetric such that $\mathbf{e} = \mathbf{S}'\mathbf{v}'$ is real and centro-symmetric as well. Hence, $\mathbf{e} = \mathbf{S}'\mathbf{v}' = \Big[e_L \;\cdots\; e_1 \; e_0 \; e_1 \;\cdots\; e_L\Big]^T$ such that

$$G_e(u) = \mathbf{e}^T\mathbf{a}(u) = \sum_{i=-L}^{L} e_i\, e^{j\pi i u} \;=\; e_o + 2 \sum_{i=1}^{L} e_i \cos(\pi i u) \tag{2.31}$$

Note that $G_e(u)$ may be viewed as an array pattern associated with the weight vector $\mathbf{e} = \mathbf{S}'\mathbf{v}'$. In any case, $G_e(u)$ is a real and even function of u and exhibits a local maximum at $u=0$. The BDML estimate of u_o is then that

angle at which the first null of the array pattern $G_e(u)$ occurs, i. e., that null closest to $u=0$. One may employ a Newton-Raphson search, for example, in order to locate this null. In the case of tracking, the search should be started at the most recent estimate of u_o. As a practical note, it is recommended that the search be terminated and a failure be registered if the value $u = u_B + \frac{1}{M}$ is exceeded before a null is located. $u_B + \frac{1}{M}$ is approximately the location of the first null on the upper side of the mainlobe of the array pattern associated with the upper auxiliary beam. A summary of BDML method I is delineated below.

Algorithmic Summary of BDML Method I

(1.) With $\mathbf{S}' = \left[\mathbf{s}(0) \;\vdots\; \mathbf{s}(u_B) + \mathbf{s}(-u_B)\right]$ and $\hat{\mathbf{R}}_{xx} = \frac{1}{N}\sum_{n=1}^{N} \mathbf{x}(n)\,\mathbf{x}^H(n)$, compute $\mathbf{v}'$ as "smallest" GEVEC of 2x2 pencil $\{\mathbf{S}'^T \mathrm{Re}\{\hat{\mathbf{R}}_{xx}\}\mathbf{S}', \mathbf{S}'^T\mathbf{S}'\}$.

(2.) With $\mathbf{S}'\mathbf{v}' = \left[e_L \;\cdots\; e_1\; e_0\; e_1 \;\cdots\; e_L\right]^T$, form $G_e(u) = e_o + 2\sum_{i=1}^{L} e_i \cos(\pi i u)$

(3.) u_o is estimated as the first null of $G_e(u)$ occurring within the interval $(0, u_B + \frac{1}{M})$.

Method II: Implicit Exploitation of Centro-Symmetry. As an alternative to the previous means of accounting for the centro-symmetric constraint on $\mathbf{v}$, consider that if, in fact, $\tilde{\mathbf{I}}_3\mathbf{v} = \mathbf{v}$, then $(\tilde{\mathbf{I}}_3\mathbf{v})^T \mathrm{Re}\{\hat{\mathbf{R}}_{bb}\}\tilde{\mathbf{I}}_3\mathbf{v} = \mathbf{v}^T \mathrm{Re}\{\hat{\mathbf{R}}_{bb}\}\mathbf{v}$. Likewise, $(\tilde{\mathbf{I}}_3\mathbf{v})^T\mathbf{Q}\tilde{\mathbf{I}}_3\mathbf{v} = \mathbf{v}^T\mathbf{Q}\mathbf{v}$. Hence, we may express the objective function in (2.27) in the following alternative fashion.

$$\underset{\mathbf{v}}{\text{Minimize}} \;\; \frac{\frac{1}{2}\,\mathbf{v}^T[\mathrm{Re}\{\hat{\mathbf{R}}_{bb}\} + \tilde{\mathbf{I}}_3\mathrm{Re}\{\hat{\mathbf{R}}_{bb}\}\tilde{\mathbf{I}}_3]\mathbf{v}}{\frac{1}{2}\,\mathbf{v}^T[\mathbf{Q} + \tilde{\mathbf{I}}_3\mathbf{Q}\tilde{\mathbf{I}}_3]\mathbf{v}} = \frac{\mathbf{v}^T\mathrm{Re}\{\hat{\mathbf{R}}_{bb}^{fb}\}\mathbf{v}}{\mathbf{v}^T\mathbf{Q}\mathbf{v}} \qquad (2.32)$$

$$\text{subject to:} \quad \tilde{\mathbf{I}}_3\mathbf{v} = \mathbf{v}$$

where we have exploited the properties of $\mathbf{Q} = \mathbf{S}^H\mathbf{S}$ described by (2.21) and where

$$\hat{\mathbf{R}}_{bb}^{fb} = \frac{1}{2}\left\{\hat{\mathbf{R}}_{bb} + \tilde{\mathbf{I}}_3\hat{\mathbf{R}}_{bb}\tilde{\mathbf{I}}_3\right\} \tag{2.33}$$

may be interpreted as the forward-backward averaged beamspace correlation matrix [SHAN85], [EVAN82], [WILL88]. It is easy to show that $\tilde{\mathbf{I}}_3 \mathrm{Re}\{\hat{\mathbf{R}}_{bb}^{fb}\}\tilde{\mathbf{I}}_3 = \mathrm{Re}\{\hat{\mathbf{R}}_{bb}^{fb}\}$ which when combined with the fact that $\mathrm{Re}\{\hat{\mathbf{R}}_{bb}^{fb}\}$ is symmetric indicates that it is per-symmetric, i. e., symmetric about the anti-diagonal, as well. In Appendix A, we prove that two of the three GEVEC's of the pencil $\{\mathrm{Re}\{\hat{\mathbf{R}}_{bb}^{fb}\}, \mathbf{Q}\}$ exhibit centro-symmetry while the third exhibits centro-anti-symmetry. An nx1 vector, $\mathbf{x}$, exhibits centro-anti-symmetry if $\tilde{\mathbf{I}}_n\mathbf{x} = -\mathbf{x}$. In the case of n odd, this implies that the center element of $\mathbf{x}$ is zero. These observations combined with the fact that the centro-anti-symmetric GEVEC spans a space orthogonal to the space spanned by the two centro-symmetric GEVEC's produces the final result that the solution to the constrained optimization problem described by (2.32) is such that the minimizing $\mathbf{v}$ is that centro-symmetric (CS-) GEVEC of the 3x3 real pencil $\{\mathrm{Re}\{\hat{\mathbf{R}}_{bb}^{fb}\}, \mathbf{Q}\}$ associated with the smaller GEV.

With this particular $\mathbf{v}$, u_o may be determined as in the previous method as the solution to $\mathbf{e}^T\mathbf{a}(u_o) = 0$ where $\mathbf{e} = \mathbf{S}\mathbf{v}$. In light of the Vandermonde structure of $\mathbf{a}(u_o)$, as illustrated by substituting $\lambda = e^{j\pi u_o}$ in (2.9) yielding $\mathbf{a}(u_o) = \left[\lambda^{-L}, \cdots, \lambda^{-2}, \lambda^{-1}, 1, \lambda, \lambda^2, \cdots, \lambda^L\right]$, we may alternatively find $z_o = e^{j\pi u_o}$ as a root of the polynomial $e(z) = \sum_{i=0}^{M-1} e_i z^i$, where e_i, i=1,...,M-1, is the i-th element of $\mathbf{e} = \mathbf{S}\mathbf{v}$, i. e., $\mathbf{e} = \mathbf{S}\mathbf{v} = \left[e_0, e_1, e_2, \cdots, e_{M-1}\right]^T$. u_o may then be extracted from z_o in the obvious manner. Note that $\mathbf{e}$ is real and centro-symmetric as before; the centro-symmetry follows from the following argument: $\tilde{\mathbf{I}}_M\mathbf{e} = \tilde{\mathbf{I}}_M\mathbf{S}\tilde{\mathbf{I}}_3\tilde{\mathbf{I}}_3\mathbf{v} = \mathbf{S}\mathbf{v} = \mathbf{e}$. As a consequence, it is easy to show that if z_i is a root of e(z), then z_i^*, $\frac{1}{z_i}$, and $\frac{1}{z_i^*}$ are roots as well. A summary of BDML method II is delineated below.

Algorithmic Summary of BDML Method II

(1.) With $\mathbf{S} = \left[\mathbf{s}(u_B) : \mathbf{s}(0) : \mathbf{s}(-u_B)\right]$ & $\hat{\mathbf{R}}_{xx} = \frac{1}{N}\sum_{n=1}^{N}\mathbf{x}(n)\,\mathbf{x}^H(n)$, form $\hat{\mathbf{R}}_{bb} = \mathbf{S}^H\hat{\mathbf{R}}_{xx}\mathbf{S}$.

(2.) With $\hat{\mathbf{R}}_{bb}^{fb} = \frac{1}{2}\left\{\hat{\mathbf{R}}_{bb} + \tilde{\mathbf{I}}_3\hat{\mathbf{R}}_{bb}\tilde{\mathbf{I}}_3\right\}$, compute $\mathbf{v}$ as CS-GEVEC of 3x3 pencil $\{\mathrm{Re}\{\hat{\mathbf{R}}_{bb}^{fb}\}, \mathbf{S}^H\mathbf{S}\}$ assoc. with smaller GEV.

(3.) With $\mathbf{Sv} = \left[e_0\ ,\ e_1\ ,\ e_2\ ,\ \cdots\ ,\ e_{M-1}\right]^T$, form $e(z) = \sum_{i=0}^{M-1} e_i\ z^i$

(4.) $z_o = e^{j\pi u_o}$ is estimated as that root of $e(z)$ in the vicinity of $z=1$; $u_o = \frac{1}{j\pi}\ln\{z_o\}$.

Method III: Auxiliary Beam Subtraction and Calibration Curve. We can arrive at an algorithm somewhat similar in form to the LSAA algorithm of Haykin [HAYK83], [HAYK84] if we express $\mathbf{v}$ as $\mathbf{v} = [-w_o\ ,\ 1\ ,\ -w_o]^T$. Here we have normalized $\mathbf{v}$ such that its center element is equal to one, i. e., $v_o=1$. Such a normalization appears feasible since the objective function in (2.27) is invariant to a scale change on $\mathbf{v}$.

As in the development of Method I we may express $\mathbf{Sv}$ as $\mathbf{S'v'}$ where $\mathbf{S'} = \left[\mathbf{s}(0)\ :\ \mathbf{s}(u_B) + \mathbf{s}(-u_B)\right]$ and $\mathbf{v'} = [1\ ,\ -w_o]^T$. Substituting $\mathbf{v'} = [1\ ,\ -w_o]^T$ in (2.23), we find that the resulting objective function to be minimized with respect to w_o may be expressed as a ratio of two quadratic functions of w_o in the following manner

$$\underset{w_o}{\text{Minimize}} \quad \frac{r_{11} - 2r_{21}w_o + r_{22}w_o^2}{s_{11} - 2s_{21}w_o + s_{22}w_o^2} \tag{2.34}$$

where r_{ij} and s_{ij}, i,j=1,2, are the i,j-th elements the 2x2 real, symmetric matrices $\mathbf{S'}^T\mathrm{Re}\{\hat{\mathbf{R}}_{xx}\}\mathbf{S'}$ and $\mathbf{S'}^T\mathbf{S'}$, respectively. Differentiating with respect to w_o and equating to zero leads us to find that solution of the quadratic equation $(r_{22}s_{21} - r_{21}s_{22})\ w_o^2 + (r_{11}s_{22} - r_{22}s_{11})\ w_o + (r_{21}s_{11} - r_{11}s_{21}) = 0$ for which the objective function in (2.34) is smaller.

At this point, we remark that in contrast to the above procedure, Haykin's LSAA algorithm finds the optimum weight w_o as that value which minimizes the quadratic function $\mathbf{v'}^T\mathbf{S'}^T\hat{\mathbf{R}}_{xx}\mathbf{S'v'} = \{\mathbf{s}(0) - w_o[\mathbf{s}(u_B) + \mathbf{s}(-u_B)]\}^T\ \hat{\mathbf{R}}_{xx}\{\mathbf{s}(0) - w_o[\mathbf{s}(u_B) + \mathbf{s}(-u_B)]\}$. This quadratic polynomial is similar to the numerator of the objective function in (2.34) with the exception that $\mathrm{Re}\{\hat{\mathbf{R}}_{xx}\}$ is replaced by $\hat{\mathbf{R}}_{xx}$. An immediate consequence of this observation is that the w_o obtained from Haykin's procedure is not guaranteed to be real as it should be. More importantly, however, the fact

that only the numerator is involved in Haykin's method is a manifestation of the fact that the method does not account for the correlation between the noise at the beamspace ports. Recall that, in general, the noise between beamspace ports is correlated even if the noise in element space is "spatially white". As a consequence of these observations, the LSAA algorithm only corresponds to the beamspace domain based Maximum Likelihood (BDML) method if $\hat{\mathbf{R}}_{xx}$ satisfies $\tilde{\mathbf{I}}_M \hat{\mathbf{R}}_{xx} \tilde{\mathbf{I}}_M = \hat{\mathbf{R}}_{xx}^*$ and the columns of $\mathbf{S}$ are orthogonal.

After the optimum w_o is determined, we may once again invoke the relationship $\mathbf{v}^T \mathbf{S}^H \mathbf{a}(u_o) = 0$ to determine the corresponding u_o. As $\mathbf{Sv} = \mathbf{S'v'} = \mathbf{s}(0) - w_o[\mathbf{s}(u_B) + \mathbf{s}(-u_B)]$, this translates into a statement that u_o may be determined from w_o as the solution to the equation $\{\mathbf{s}(0) - w_o[\mathbf{s}(u_B) + \mathbf{s}(-u_B)]\}^T \mathbf{a}(u_o) = 0$. Motivated by the calibration curve of Haykin, consider solving this equation for w_o. Denoting the solution as w_{cal}, we have:

$$w_{cal} = \frac{\mathbf{s}^T(0)\, \mathbf{a}(u_o)}{[\mathbf{s}(u_B) + \mathbf{s}(-u_B)]^T\, \mathbf{a}(u_o)} \tag{2.35}$$

Consider plotting w_{cal} as a function of u_o; all the quantities on the right hand side of (2.35) are known except for u_o. The result may be thought of as a calibration curve which may be discretized and stored in memory on a computer. With the optimum w_o estimated via the procedure outlined previously, the corresponding value of u_o may be simply gleaned from the calibration curve. Note that this calibration curve is identical to that constructed by Haykin [HAYK84] for the LSAA algorithm. However, in contrast to the present procedure, Haykin generated his calibration curve by examining the effect of letting the SNR go to infinity in his least squares error criterion. This is similar to the case here as the calibration curve was generated assuming the ideal value of w_o, that value which would be obtained if the SNR was infinite corresponding to either no noise or infinite signal power. A summary of method III is delineated below.

Algorithmic Summary of BDML Method III

(1.) With $\mathbf{S'} = \left[\mathbf{s}(0) \;\vdots\; \mathbf{s}(u_B) + \mathbf{s}(-u_B)\right]$ and $\hat{\mathbf{R}}_{xx} = \frac{1}{N} \sum_{n=1}^{N} \mathbf{x}(n)\, \mathbf{x}^H(n)$, form

$$\mathbf{S}'^{T}\mathrm{Re}\{\hat{\mathbf{R}}_{xx}\}\mathbf{S}' = \begin{bmatrix} r_{11} & r_{21} \\ r_{21} & r_{22} \end{bmatrix} \quad ; \quad \mathbf{S}'^{T}\mathbf{S}' = \begin{bmatrix} s_{11} & s_{21} \\ s_{21} & s_{22} \end{bmatrix}$$

(2.) With the elements of the 2x2 matrices formed in (1.), form the following 2nd order polynomial and compute its two roots:

$$(r_{22}s_{21} - r_{21}s_{22})\, w_o^2 + (r_{11}s_{22} - r_{22}s_{11})\, w_o + (r_{21}s_{11} - r_{11}s_{21}) = 0$$

(3.) With $\mathbf{v}' = \begin{bmatrix} 1 \\ -w_o \end{bmatrix}$, select value of w_o from (2) minimizing $\dfrac{\mathbf{v}'^{T}\,\mathbf{S}'^{T}\mathrm{Re}\{\hat{\mathbf{R}}_{xx}\}\mathbf{S}'\,\mathbf{v}'}{\mathbf{v}'^{T}\,\mathbf{S}'^{T}\mathbf{S}'\,\mathbf{v}}$.

(4.) Locate value of u_o on calibration curve corresponding to minimizing w_o from (3.).

2.3.3 Simplifications for Butler Matrix Beamformer

The last step in each of the three BDML methods outlined previously may be formulated as finding $z_o = e^{j\pi u_o}$ as a root of a polynomial of order M-1. In light of the practical consideration that the signals arrive near broadside to the array, we may restrict our search to finding that root "closest" to z=1 on the unit circle. Although root finding algorithms which allow one to restrict the search for roots to some specified region in the complex plane do exist, the root finding problem may be greatly simplified if a Butler Beamforming Matrix is employed. In this case, we select unity magnitude weighting, i. e., no tapering such that $\mathbf{D}_a = \mathbf{D}_r = \mathbf{I}$ in (2.11), and u_B as the location of the first null of the reference beam pattern which, in this case, is described by (2.18). The first null of the reference beam is, in fact, located at $u = 2/M$; hence, $u_B = 2/M$. The beamforming matrix in this case is then

$$\mathbf{S} = \left[\mathbf{a}(2/M) \vdots \mathbf{a}(0) \vdots \mathbf{a}(-2/M)\right] \tag{2.36}$$

which when invoking the definition of $\mathbf{a}(u)$ in (2.9) may be seen to correspond to a Mx3 Butler Matrix Beamformer [GABR84], [BUCK88], [FORS87]. The respective three beams for the case of M=15 are plotted in Figure 2.3. Note that the respective peaks of the mainlobes associated with the upper and lower auxiliary beams are located at the nulls of the reference beam occurring at $u = 2/M$ and $u = -2/M$, respectively. This is a manifestation of the fact that the 3 columns of the Butler Matrix Beamformer in (2.36) are orthogonal. This

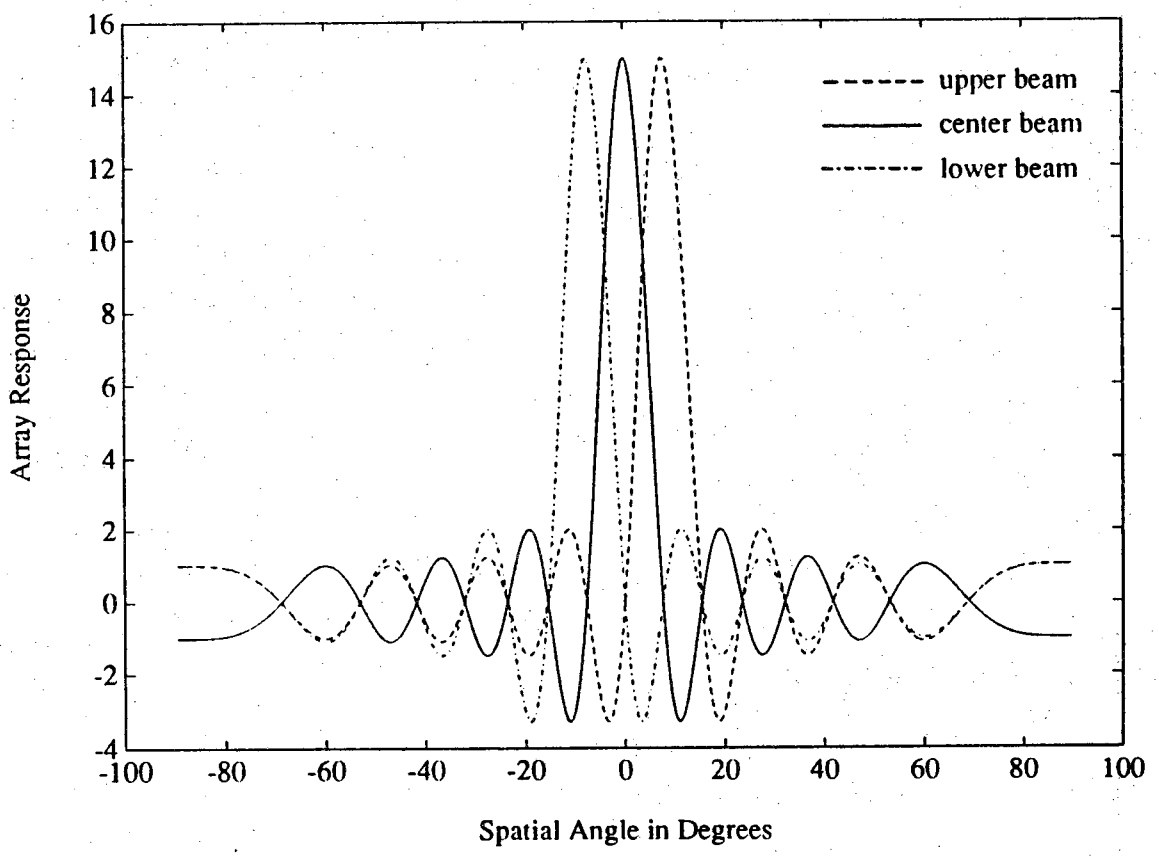

Figure 2.3 Plot of the respective array patterns associated with the three columns of a 15x3 Butler matrix beamformer for the case of a 15 element uniformly- spaced linear array. The array patterns have 12 nulls in common.

also implies that if the noise is uncorrelated in element space, it will be so in beamspace as well, i. e., "spatial whiteness" of the noise is preserved with the Butler Matrix Beamformer. However, a more important observation is that the three beam patterns have M-3 nulls in common. This fact may be exploited to reduce the computation involved in the final step of each of the three BDML methods as discussed above. The appropriate development is as follows.

Define the Vandermonde vector $\mathbf{z}$ as follows:

$$\mathbf{z} = [1 \;\; z \;\; z^2 \;\; z^3 \;\; ..... \;\; z^{M-1}]^T \tag{2.37}$$

The inner product of any Mx1 vector with the Vandermonde vector $\mathbf{z}$ is then a polynomial of order M-1. Recall, that for the sake of simplicity, we have assumed throughout that M is odd. The final step in each of the three BDML methods outlined previously may be formulated as finding the roots of the (M-1)-th order polynomial $e(z)=(\mathbf{Sv})^T\mathbf{z}$, where $\mathbf{v} = [v_1 \;, v_0 \;, v_1]^T$. More specifically, we seek a pair of complex conjugate roots of the (M-1)-th order polynomial $(\mathbf{Sv})^T\mathbf{z}$ in the vicinity of $z=1$ on the unit circle: the direct and specular path signals arrive within a beamwidth of broadside. The full development may be found in Appendix B but the fact that the respective array patterns associated with each of the beamforming weight vectors $\mathbf{a}(2/M)$, $\mathbf{a}(0)$, and $\mathbf{a}(-2/M)$ have M-3 nulls in common is a manifestation of the fact that the respective polynomials $\mathbf{a}^H(2/M)\mathbf{z}$, $\mathbf{a}^H(0)\mathbf{z}$, and $\mathbf{a}^H(-2/M)\mathbf{z}$ have M-3 roots in common equal to $z = e^{j\frac{2\pi m}{M}}$, m=2,...,M-2. The importance of this observation becomes apparent when we view the (M-1)-th order polynomial $e(z)= (\mathbf{Sv})^H\mathbf{z}$ as a linear combination of these three polynomials as follows

$$e(z) = (\mathbf{Sv})^H\mathbf{z} = v_1 \, \mathbf{a}^H(2/M)\mathbf{z} + v_0 \, \mathbf{a}^H(0)\mathbf{z} + v_1\mathbf{a}^H(-2/M)\mathbf{z} \tag{2.38}$$

Since any root common to all three polynomials is a root of any linear combination of the three polynomials, it follows that regardless of the values of v_0 and v_1, M-3 roots of the polynomial $(\mathbf{Sv})^T\mathbf{z}$ occur at $z = e^{j\frac{2\pi m}{M}}$, m=2,...,M-2. This statement involves no approximation whatsoever. Thus, the roots of interest are those of a quadratic equation obtained via the following polynomial division:

$$q(z) = q_0 + q_1 z + q_2 z^2 = \frac{(Sv)^T z}{\prod_{m=2}^{M-2} (z - e^{j\frac{2\pi m}{M}})} \tag{2.39}$$

The details of this polynomial division may be found in Appendix B where it is shown that the coefficients of q(z) are as follows:

$$q_0 = v_0 - 2v_1\cos(\frac{\pi}{M}) = q_2 \;\; ; \;\; q_1 = 4v_1\cos(\frac{\pi}{M}) - 2v_0\cos(\frac{2\pi}{M}) \tag{2.40}$$

Letting $\mathbf{q} = [q_0 \; , \; q_1 \; , \; q_2]^T$, we note that $\mathbf{q}$ is real and centro-symmetric, i. e., $q_0 = q_2$, such that $q(z) = q_1 z + q_0(1 + z^2)$. As a consequence, the two roots of the polynomial $q(z)=\mathbf{q}^T\mathbf{z}$ either form a complex conjugate pair with both roots lying on the unit circle **or** are real with one the reciprocal of the other. The latter situation may be interpreted as a case where the direct and specular path signals are not resolved.

It will be easier for us to work with a normalized version of q(z) obtained by dividing the coefficients above by $q_0 = q_2$ giving rise to the polynomial $1 + \alpha z + z^2$ where

$$\alpha = \frac{4v_1\cos(\frac{\pi}{M}) - 2v_0\cos(\frac{2\pi}{M})}{v_0 - 2v_1\cos(\frac{\pi}{M})} \tag{2.41}$$

The two roots of a polynomial of the form $1 + \alpha z + z^2$, where α is real, are located on the unit circle if and only if $|\alpha|<2$ in which case the two roots are given by

$$\hat{z}_0 = -\frac{\alpha}{2} + j\frac{1}{2}\sqrt{4 - \alpha^2} \qquad \hat{z}_0^* = -\frac{\alpha}{2} - j\frac{1}{2}\sqrt{4 - \alpha^2} \tag{2.42}$$

It is easy to show that these two roots do indeed have unity magnitude. As a practical matter, the roots should be located in the vicinity of $z=1$. We thus further restrict α to be strictly non-positive such that $-2 < \alpha < 0$. With α given by (2.41) and $\mathbf{v}$ normalized such that v_o is non-negative, it is easily shown that this constraint is satisfied as long as v_o and v_1 satisfy the inequality $v_o > 2v_1\cos(\frac{\pi}{M})$. From observations gleaned from numerous simulations, we recommend that this condition be used as a flag for determining whether the signals have been resolved or not. That is, it is recommended that the condition $v_o < 2v_1\cos(\frac{\pi}{M})$ be taken as a flag that the

algorithm has failed to resolve the two signals.

The value of $\hat{z}_o$ given by (2.42) with α given by (2.41) is the ML estimate of $z_o = e^{j\pi u_o}$. In order to obtain the ML estimate of u_o, we must compute the argument or phase angle of $\hat{z}_o$. With $\hat{z}_o$ given by (2.42), the phase angle is given by $\hat{\arg}(z_o) = \tan^{-1}\left\{\frac{\sqrt{4-\alpha^2}}{-\alpha}\right\}$ with α given by (2.34). Trivial manipulation yields the following expression for the ML estimate of u_0:

$$\hat{u}_o = \frac{1}{\pi}\tan^{-1}\left\{\left[\left\{\frac{v_o - 2v_1\cos(\frac{\pi}{M})}{v_0\cos(\frac{2\pi}{M}) - 2v_1\cos(\frac{\pi}{M})}\right\}^2 - 1\right]^{\frac{1}{2}}\right\} \qquad (2.43)$$

As a check on the correctness of this formula, consider the case $u_o = u_B = 2/M$, i. e., the angle of the direct path is exactly equal to the location of the peak of the mainlobe associated with the upper auxiliary beam, which corresponds to a null in the reference beam. Substituting $u_B = 2/M$ into (2.19) and evaluating at $u = 2/M$ and $u=-2/M$, we find that the beamspace manifold vectors for the direct and specular path arrivals are $\mathbf{b}(u_o) = [M\ ,\ 0\ ,\ 0]^T$ and $\mathbf{b}(-u_o) = [0\ ,\ 0\ ,\ M]^T$, respectively. The vector $\mathbf{v}$ of unit length orthogonal to both of these vectors is $\mathbf{v} = [0\ ,\ 1\ ,\ 0]^T$. The reader may verify that substitution of $v_0 = 1$ and $v_1 = 0$ into (2.43) does indeed provide the correct value $u_o = 2/M$. Another test case of interest is that of $u_o = 0$ which corresponds to a single signal arriving directly broadside to the array. In this case, the beamspace manifold vector according to (2.19) is $\mathbf{b}(0) = [0\ ,\ M\ ,\ 0]^T$. The appropriate centro-symmetric $\mathbf{v}$ vector for this case is: $\mathbf{v} = [1/\sqrt{2}\ ,\ 0\ ,\ 1/\sqrt{2}]^T$. The reader may easily verify that substitution of the values $v_0 = 0$ and $v_1 = 1/\sqrt{2}$ into (2.43) does indeed produce the correct value $\hat{u}_o = 0$. Note that BDML Method III outlined previously, based on Haykin's LSAA algorithm, forces v_0 to be equal to one and thus breaks down in this test case. From this observation, we deduce that as the direct path angle u_o becomes smaller and smaller approaching $u = 0$ corresponding to broadside, the middle component of $\mathbf{v}$, v_o, becomes smaller and smaller approaching zero as well, regardless of how $\mathbf{v}$ is normalized. A practical implication of this observation, therefore, is that BDML Method III, and hence the LSAA algorithm of Haykin, may exhibit numerical difficulties such as high sensitivity to round-off errors, for example, when the direct and specular path

angles are only a couple of tenths of a beamwidth away from broadside. In terms of the calibration curve, we note that with $u_B = 2/M$ and no tapering, the denominator in the expression on the right hand side of (2.35) is zero when $u_o = 0$. This implication is that for Butler matrix beamforming the calibration curve defined by (2.35) tends to infinity as u_o approaches zero making it difficult to discretize and store the curve for small values of u.

In closing, we present the appropriate version of BDML Method II when the Butler Matrix Beamformer in (2.36) is employed which incorporates the simplification developed above. The summary is as follows.

Algorithmic Summary of BDML Method II
With Butler Beamformer

(1.) With $\mathbf{S}=\left[\mathbf{a}(2/M):\mathbf{a}(0):\mathbf{a}(-2/M)\right]$ & $\hat{\mathbf{R}}_{xx}=\frac{1}{N}\sum_{n=1}^{N}\mathbf{x}(n)\mathbf{x}^H(n)$, form $\hat{\mathbf{R}}_{bb}=\mathbf{S}^H\hat{\mathbf{R}}_{xx}\mathbf{S}$.

(2.) Compute $\mathbf{v} = [v_1 , v_0 , v_1]^T$ as that CS-EVEC of $\mathrm{Re}\{\hat{\mathbf{R}}_{bb}^{fb}\} = \frac{1}{2}\mathrm{Re}\left\{\hat{\mathbf{R}}_{bb} + \tilde{\mathbf{I}}_3\hat{\mathbf{R}}_{bb}\tilde{\mathbf{I}}_3\right\}$ associated with the smaller EV.

(3.) With v from (2.) normalized such that $v_o \geq 0$, if $v_o < 2v_1\cos(\frac{\pi}{M})$, signals not resolved.

(4.) Otherwise: With v_0 and v_1 determined in (2.), estimate u_o according to:

$$\hat{u}_o = \frac{1}{\pi}\tan^{-1}\left\{\left[\left\{\frac{v_o - 2v_1\cos(\frac{\pi}{M})}{v_0\cos(\frac{2\pi}{M}) - 2v_1\cos(\frac{\pi}{M})}\right\}^2 - 1\right]^{\frac{1}{2}}\right\}$$

Note that inherent in step 2 is the fact that in the case of the Butler Matrix Beamformer $\mathbf{Q} = \mathbf{S}^H\mathbf{S} = M\mathbf{I}$. We also point out that $\mathrm{Re}\{\hat{\mathbf{R}}_{bb}^{fb}\}$ in step (2.) is both symmetric and per-symmetric. As a consequence, out of its nine elements, only three are distinct making its eigenvalue decomposition a fairly trivial task. These advantages combined with the avoidance of the task of finding a root of a (M-1)-th order polynomial illustrates the dramatic reduction in computation achieved by working with the Butler beamforming matrix S defined by (2.36).

2.4 BDML Method for Nonsymmetric Multipath

In this section, we consider the case where the multipath is not symmetric about broadside or $u = 0$. The composition of the element space snapshot vector and the corresponding beamspace snapshot vector are described by (2.8) and (2.15), respectively, with u_o replaced by u_1 and $-u_o$ replaced by u_2. We seek the ML estimator of u_1 and that of u_2 given as data N snapshot vectors in 3-D beamspace. Similar to the development for symmetric multipath which lead one from the description of the joint density of the beamspace snapshot vectors in (2.22) to the "equivalent" optimization problem over $\mathbf{v}$ in (2.27), we find that we may formulate the desired BDML estimation scheme as finding a 3x1 real-valued vector $\mathbf{v}$, related to u_1 and u_2 according to

$$\mathbf{v}^T\mathbf{b}(u_1) = 0 \qquad \mathbf{v}^T\mathbf{b}(u_2) = 0, \tag{2.44}$$

as the solution to the following optimization problem

$$\underset{\mathbf{v}}{\text{Minimize}} \quad \frac{\mathbf{v}^T\, \text{Re}\{\hat{\mathbf{R}}_{bb}\}\, \mathbf{v}}{\mathbf{v}^T\, \mathbf{Q}\, \mathbf{v}} = \frac{\mathbf{v}^T\, \text{Re}\{\mathbf{S}^H\hat{\mathbf{R}}_{xx}\mathbf{S}\}\, \mathbf{v}}{\mathbf{v}^T\, \mathbf{S}^H\mathbf{S}\, \mathbf{v}} \tag{2.45}$$

Note that although the centro-symmetric constraint on $\mathbf{v}$ is not applicable in the nonsymmetric case, the restriction that $\mathbf{v}$ is real, which follows from (2.44), is applicable. From (2.45), the optimizing $\mathbf{v}$ is that GEVEC of the 3x3 real pencil $\{\text{Re}\{\hat{\mathbf{R}}_{bb}\}\,,\ \mathbf{S}^H\mathbf{S}\}$ associated with the smallest GEV. With this $\mathbf{v}$, the BDML estimates of u_1 and u_2 are obtained as the two roots to the nonlinear equation $\mathbf{v}^T\mathbf{b}(u) = \mathbf{v}^T\mathbf{S}^H\mathbf{a}(u) = 0$ in the general vicinity of $u=0$ (within plus or minus a beamwidth from broadside.) This corresponds to locating two nulls of the array pattern $\mathbf{e}^H\mathbf{a}(u)$, where the weight vector $\mathbf{e}$ is equal to $\mathbf{Sv}$. This "double null tracker" type of estimation procedure has arisen in various element space based approaches to both the symmetric and nonsymmetric multipath problems proposed in the literature [CANT81], [MAYH87], [BALL87], [KSIE68], [WHIT74]. As a consequence of the uniform spacing of the antenna elements, the search for u_1 and u_2 may be formulated in terms of finding $z_1 = e^{j\pi u_1}$ and $z_2 = e^{j\pi u_2}$ as the two roots of the (M-1)-th order polynomial $\mathbf{e}^H\mathbf{z}$ in the vicinity of $z=1$. As in the case of symmetric multipath, the root finding problem may be greatly reduced if the Butler matrix beamformer in (2.36) is employed. In this case, we divide out of the (M-1)-th order polynomial $e(z) = (\mathbf{Sv})^H\mathbf{z} = v_1\, \mathbf{a}^H(2/M)\mathbf{z} + v_2\, \mathbf{a}^H(0)\mathbf{z} + v_3\mathbf{a}^H(-2/M)\mathbf{z}$ each of the M-3 roots, $z = e^{j\frac{2\pi m}{M}}$, $m=2,\ldots,M-2$, common to each of the three polynomials

$\mathbf{a}^H(2/M)\mathbf{z}$, $\mathbf{a}^H(0)\mathbf{z}$, and $\mathbf{a}^H(-2/M)\mathbf{z}$ individually. The appropriate development is found in Appendix B where it is shown that the two roots of interest are those of a second-order polynomial $q(z)=q_0 + q_1 z + q_2 z^2$ where

$$q_0 = -v_1 e^{-j\frac{\pi}{M}} + v_2 - v_3 e^{j\frac{\pi}{M}} = q_2^*$$

$$q_1 = 2(v_1 + v_3)\cos(\frac{\pi}{M}) - 2v_2\cos(\frac{2\pi}{M}) \tag{2.46}$$

Consider the normalized version of $q(z)$, denoted $q_n(z)$, obtained by dividing each of the coefficients by q_1, which is observed to be real:

$$q_n(z) = \frac{q_o}{q_1} + z + \frac{q_o^*}{q_1} z^2 = 0 \tag{2.47}$$

q_o and q_1 are given by (2.46). $q_n(z)$, of course, has the same roots as $q(z)$. The two roots of a quadratic polynomial of the form $\alpha + z + \alpha^* z^2$, where in our case $\alpha = \frac{q_o}{q_1}$, are given by $\hat{z}_{1,2} = \frac{-1 \pm \sqrt{1 - 4|\alpha|^2}}{2\alpha}$. It is easily shown that both of the roots have unity magnitude, i. e., lie on the unit circle, if $|\alpha| > \frac{1}{2}$. We also note that classical algebra dictates that the product of the two roots of $q(z)$ must be equal to $\frac{q_o}{q_2} = \frac{q_o}{q_o^*}$, which is observed to have unity magnitude. From this we deduce that the magnitude of one root must be equal to the reciprocal of the magnitude of the other root. This condition is, of course, satisfied if both of the roots lie on the unit circle as is the case when $|\alpha| > \frac{1}{2}$. From these observations as well as from observations gleaned from the simulation results, we recommend that the condition $|\alpha| < \frac{1}{2}$ be taken as a flag that the algorithm has failed to resolve the two signals.

For the sake of brevity, we here summarize the BDML Method for a nonsymmetric multipath scenario only for the case where the Butler Matrix beamformer is employed. The steps are delineated below.

BDML Method for Nonsymmetric Multipath
with Butler Matrix Beamformer

(1.) With $\mathbf{S} = \left[\mathbf{a}(2/M) \vdots \mathbf{a}(0) \vdots \mathbf{a}(-2/M)\right]$ and $\hat{\mathbf{R}}_{xx} = \frac{1}{N}\sum_{n=1}^{N} \mathbf{x}(n)\mathbf{x}^H(n)$, form

$\hat{\mathbf{R}}_{bb} = \mathbf{S}^H \hat{\mathbf{R}}_{xx} \mathbf{S}$.

(2.) Compute $\mathbf{v} = [v_1 , v_2 , v_3]^T$ as EVEC of 3x3 matrix $\mathrm{Re}\{\hat{\mathbf{R}}_{bb}\}$ assoc. with smallest EV.

(3.) With v_i, i=1,2,3, from (2.), form $q(z) = q_0 + q_1 z + q_0^* z^2$ where:

$$q_0 = -v_1 e^{-j\frac{\pi}{M}} + v_2 - v_3 e^{j\frac{\pi}{M}} \; ; \; q_1 = 2(v_1+v_3)\cos(\frac{\pi}{M}) - 2v_2\cos(\frac{2\pi}{M})$$

(4.) Let $\alpha = \frac{q_0}{q_1}$. If $|\alpha| < \frac{1}{2}$, multipath signals not resolved. Otherwise:

(5.) $$\hat{z}_1 = \frac{-1 + j\sqrt{4|\alpha|^2 - 1}}{2\alpha} \Rightarrow \hat{u}_1 = \frac{1}{j\pi}\ln\{\hat{z}_1\}$$

$$\hat{z}_2 = \frac{-1 - j\sqrt{4|\alpha|^2 - 1}}{2\alpha} \Rightarrow \hat{u}_2 = \frac{1}{j\pi}\ln\{\hat{z}_2\}$$

2.5 Performance Analysis of BDML in Coherent Multipath Scenario

If the surface of reflection is fairly smooth, i. e., the sea is relatively calm, and the target is not moving too fast in relative terms, the specular multipath signal is merely a time-delayed, amplitude-attenuated replica of the direct path signal over multiple looks, i. e., over multiple snapshots. Due to the sinusoidal nature of the returning signals, the time-delay translates into a phase-shift such that $c_2(n) = \rho e^{j\Delta\Psi} c_1(n)$, n=1,...,N, where $c_1(n)$ is the direct path complex signal, $c_2(n)$ is the specular path complex signal, ρ is the magnitude of the surface reflection coefficient, $\rho<1$, and $\Delta\Psi$ is the phase difference between the two signals occurring at the center of the array. Again assuming spatially white noise and that the signal is uncorrelated with the noise, the expected value of the element space correlation matrix has the following form

$$\mathbf{R}_{xx} = E\{\mathbf{x}(n)\,\mathbf{x}^H(n)\} = \mathbf{A}\mathbf{R}_{ss}\mathbf{A}^H + \sigma_n^2\mathbf{I} \qquad (2.48)$$

where $\mathbf{A} = \left[\mathbf{a}(u_o) : \mathbf{a}(-u_o)\right]$ for symmetric multipath and $\mathbf{A} = \left[\mathbf{a}(u_1) : \mathbf{a}(u_2)\right]$ for nonsymmetric multipath. The 2x2 matrix $\mathbf{R}_{ss}$ in (2.48) is referred to as the source covariance matrix and, under the coherent multipath condition stated, can be expressed in the following manner

$$\mathbf{R}_{ss} = \mathrm{E}\left\{ \begin{bmatrix} c_1(n) \\ c_2(n) \end{bmatrix} \begin{bmatrix} c_1(n) \\ c_2(n) \end{bmatrix}^H \right\} = \begin{bmatrix} \sigma_1^2 & \rho e^{-j\Delta\Psi}\sigma_1^2 \\ \rho e^{j\Delta\Psi}\sigma_1^2 & \rho^2\sigma_1^2 \end{bmatrix}$$

$$= \sigma_1^2 \begin{bmatrix} 1 \\ \rho e^{j\Delta\Psi} \end{bmatrix} [1 \ , \ \rho e^{-j\Delta\Psi}] \tag{2.49}$$

where $\sigma_1^2 = \mathrm{E}\{ | c_1(n) |^2 \}$. Note that $\mathbf{R}_{ss}$ is of rank 1 regardless of the values of ρ and $\Delta\Psi$. With $\mathbf{R}_{xx}$ given by (2.48), the beamspace correlation matrix takes on a similar form

$$\mathbf{R}_{bb} = \mathbf{S}^H\mathbf{R}_{xx}\mathbf{S} = \mathbf{B}\mathbf{R}_{ss}\mathbf{B}^T + \sigma_n^2\mathbf{Q} \tag{2.50}$$

where $\mathbf{B} = \left[\mathbf{b}(u_o) \vdots \mathbf{b}(-u_o)\right]$ for symmetric multipath and $\mathbf{B} = \left[\mathbf{b}(u_1) \vdots \mathbf{b}(u_2)\right]$ for nonsymmetric multipath; $\mathbf{R}_{ss}$ is given by (2.49). Now, consider the form of the beamspace correlation matrix in (2.50) employed in both the BDML Method II for symmetric multipath and the BDML Method for nonsymmetric multipath outlined above as well. We deal with the nonsymmetric case first.

The BDML Method for nonsymmetric multipath dictates that we take $\mathbf{v}$ as that GEVEC of the 3x3 real pencil $\{\mathrm{Re}\{\mathbf{R}_{bb}\}, \mathbf{Q}\}$ associated with the smallest GEV. Since $\mathbf{B}$ in (4.3) is real, we have that $\mathrm{Re}\{\mathbf{R}_{bb}\} = \mathbf{B}\mathrm{Re}\{\mathbf{R}_{ss}\}\mathbf{B}^T + \sigma_n^2\mathbf{Q}$ where the real part of $\mathbf{R}_{ss}$ in (2.49) is given by

$$\mathrm{Re}\{\mathbf{R}_{ss}\} = \sigma_1^2 \begin{bmatrix} 1 & \rho\cos(\Delta\Psi) \\ \rho\cos(\Delta\Psi) & \rho^2 \end{bmatrix} \tag{2.51}$$

Invoking observations made in the formulation of the MUSIC algorithm [22], it is easy to show that as long as $\mathrm{Re}\{\mathbf{R}_{ss}\}$ is of rank two, the "smallest" GEVEC of the pencil $\{\mathrm{Re}\{\hat{\mathbf{R}}_{bb}\}, \mathbf{Q}\}$ is, in fact, orthogonal to both $\mathbf{b}(u_1)$ and $\mathbf{b}(u_2)$ indicating that the BDML estimation scheme produces the true values of u_1 and u_2 in the asymptotic case. This property follows from the fact that when $\mathrm{Re}\{\mathbf{R}_{ss}\}$ is of rank 2, range $\{\mathbf{B}\mathrm{Re}\{\mathbf{R}_{ss}\}\mathbf{B}^T\}$ = range$\{\mathbf{B}\}$ = span$\{\mathbf{b}(u_1), \mathbf{b}(u_2)\}$. Now, observing (2.51), $\mathrm{Re}\{\mathbf{R}_{ss}\}$ is of full rank equal to 2 despite the coherent nature of the multipath so long as $\Delta\Psi$ does not equal to either 0° or 180°. In these two cases, $\mathrm{Re}\{\mathbf{R}_{ss}\}$ is of rank 1 such that range $\{\mathbf{B}\mathrm{Re}\{\mathbf{R}_{ss}\}\mathbf{B}^T\}$ = span$\{\mathbf{b}(u_1) \pm \rho\mathbf{b}(u_2)\}$, where "+" is for the $\Delta\Psi = 0^\circ$ case and "−" is for the $\Delta\Psi = 180^\circ$ case. All we can say in these two cases is that the "smallest" GEVEC of the pencil $\{\mathrm{Re}\{\mathbf{R}_{bb}\}, \mathbf{Q}\}$, $\mathbf{v}$, is orthogonal to the

linear combination $\mathbf{b}(u_1) \pm \rho\mathbf{b}(u_2)$ which does not imply that $\mathbf{v}$ is orthogonal to $\mathbf{b}(u_1)$ and $\mathbf{b}(u_2)$ individually. Thus, the BDML Method can handle coherent multipath so long as the direct and specular path signals are not perfectly in-phase or perfectly 180° out-of-phase at the center element of the array. This is in contrast to MUSIC which, without pre-processing in the form of spatial smoothing or forward-backward averaging [WILL88], breaks down in a coherent multipath scenario for any value of the phase difference, $\Delta\Psi$. This is true even in the case of MUSIC applied in beamspace. Note that, without hindsight, beamspace domain based MUSIC (BD-MUSIC) applied here would have simply computed $\mathbf{v}$ as the "smallest" GEVEC of the pencil $\{\mathbf{R}_{bb}, \mathbf{Q}\}$. It is interesting to note, though, that BDML and BD-MUSIC are equivalent, for the nonsymmetric case, if the transformation to beamspace is performed on the matrix $\hat{\mathbf{R}}_{xx}^{fb} = \frac{1}{2}\{\hat{\mathbf{R}}_{xx} + \tilde{\mathbf{I}}_M \hat{\mathbf{R}}_{xx}^{*} \tilde{\mathbf{I}}_M\}$ as opposed to $\hat{\mathbf{R}}_{xx}$ itself. This claim is substantiated by the following argument:

$$\mathbf{S}^H \hat{\mathbf{R}}_{xx}^{fb} \mathbf{S} = \mathbf{S}^H \frac{1}{2}\{\hat{\mathbf{R}}_{xx} + \tilde{\mathbf{I}}_M \hat{\mathbf{R}}_{xx}^{*} \tilde{\mathbf{I}}_M\}\mathbf{S} = \frac{1}{2}\mathbf{S}^H \hat{\mathbf{R}}_{xx} \mathbf{S} + \frac{1}{2}\mathbf{S}^T \hat{\mathbf{R}}_{xx}^{*} \mathbf{S}^{*}$$

$$= \mathrm{Re}\{\mathbf{S}^H \hat{\mathbf{R}}_{xx} \mathbf{S}\} = \mathrm{Re}\{\hat{\mathbf{R}}_{bb}\} \tag{2.52}$$

where we have employed (2.14b). Use of $\hat{\mathbf{R}}_{xx}^{fb}$ as defined above corresponds to first performing a single forward-backward average in element space [WILL88] before the transformation to beamspace.

We next consider the execution of BDML Method II for symmetric multipath, outlined in Section 2.3, when $\mathbf{R}_{bb}$ is given by (2.50) with $\mathbf{R}_{ss}$, in turn, given by (2.49) corresponding to an ideal coherent multipath scenario. BDML Method II dictates that we take $\mathbf{v}$ as that GEVEC of the 3x3 real pencil $\{\mathrm{Re}\{\hat{\mathbf{R}}_{bb}^{fb}\}, \mathbf{Q}\}$ associated with the smallest GEV, where $\hat{\mathbf{R}}_{bb}^{fb} = \frac{1}{2}\left\{\hat{\mathbf{R}}_{bb} + \tilde{\mathbf{I}}_3 \hat{\mathbf{R}}_{bb} \tilde{\mathbf{I}}_3\right\}$. We have proved in Appendix A that the $\mathbf{v}$ thus obtained is centro-symmetric, $\tilde{\mathbf{I}}_3 \mathbf{v} = \mathbf{v}$, a very important property which will be illustrated shortly. We first analyze the effect of the backward average in beamspace. Recall that the two columns of $\mathbf{B}$ in the symmetric case are related according to $\mathbf{b}(-u_o) = \tilde{\mathbf{I}}_3\, \mathbf{b}(u_o)$ such that $\tilde{\mathbf{I}}_3 \mathbf{B} \tilde{\mathbf{I}}_2 = \mathbf{B}$. This property of $\mathbf{B}$ gives rise to the following interesting result:

$$\mathbf{R}_{bb}^{fb} = \frac{1}{2}\left\{\mathbf{R}_{bb} + \tilde{\mathbf{I}}_3 \mathbf{R}_{bb} \tilde{\mathbf{I}}_3\right\}$$

$$= \frac{1}{2}\left\{\mathbf{B}\mathbf{R}_{ss}\mathbf{B}^T + \tilde{\mathbf{I}}_3\mathbf{B}\tilde{\mathbf{I}}_2\tilde{\mathbf{I}}_2\mathbf{R}_{ss}\tilde{\mathbf{I}}_2\tilde{\mathbf{I}}_2\mathbf{B}^T\tilde{\mathbf{I}}_3\right\} + \frac{1}{2}\left\{\mathbf{Q} + \tilde{\mathbf{I}}_3\mathbf{Q}\tilde{\mathbf{I}}_3\right\}$$

$$= \mathbf{B}\frac{1}{2}\left\{\mathbf{R}_{ss} + \tilde{\mathbf{I}}_2\mathbf{R}_{ss}\tilde{\mathbf{I}}_2\right\}\mathbf{B}^T + \mathbf{Q} \qquad (2.53)$$

where have invoked (2.21), $\tilde{\mathbf{I}}_2\tilde{\mathbf{I}}_2 = \mathbf{I}$ and the fact that $\mathbf{B}$ is real. Thus, $\mathbf{R}_{bb}^{fb}$ can be expressed in the form $\mathbf{B}\mathbf{R}_{ss}^{fb}\mathbf{B}^T + \sigma_n^2\mathbf{Q}$, where $\mathbf{R}_{ss}^{fb}$ is given by

$$\mathbf{R}_{ss}^{fb} = \frac{1}{2}\left\{\mathbf{R}_{ss} + \tilde{\mathbf{I}}_2\mathbf{R}_{ss}\tilde{\mathbf{I}}_2\right\} = \sigma_1^2\begin{bmatrix} \frac{1+\rho^2}{2} & \rho\cos\Delta\Psi \\ \rho\cos\Delta\Psi & \frac{1+\rho^2}{2} \end{bmatrix} \qquad (2.54)$$

where we have substituted (2.49) for $\mathbf{R}_{ss}$. We note that the elements of $\mathbf{R}_{ss}^{fb}$ are purely real. Combined with the fact that $\mathbf{B}$ and $\mathbf{Q}$ are real, this implies that $\mathbf{R}_{bb}^{fb}$ in (2.53) is real as well. Note, however, that we are only guaranteed that $\hat{\mathbf{R}}_{bb}^{fb}$ is real in the asymptotic case, due to the complex additive noise, such that $\mathbf{v}$ should nevertheless be computed as the GEVEC of the pencil $\{\mathrm{Re}\{\hat{\mathbf{R}}_{bb}^{fb}\}, \mathbf{Q}\}$. Returning to the issue at hand, though, we remark that it is easily proved $\mathbf{R}_{ss}^{fb}$ in (2.54) is of rank 2 such that $\mathrm{range}\{\mathbf{B}\mathbf{R}_{ss}^{fb}\mathbf{B}^T\} = \mathrm{range}\{\mathbf{B}\} = \mathrm{span}\{\mathbf{b}(u_o), \mathbf{b}(-u_o)\}$ even if $\Delta\Psi = 0^\circ$ or $\Delta\Psi = 180^\circ$ so long as ρ is not at the same time equal to unity. That is, the only conditions under which $\mathbf{R}_{ss}^{fb}$ in (2.54) will be of rank 1 is when $\Delta\Psi$ equals either 0° or 180° and, at the same time, ρ is equal to one. Under these conditions, $\mathrm{range}\{\mathbf{B}\mathrm{Re}\{\mathbf{R}_{ss}^{fb}\}\mathbf{B}^T\} = \mathrm{span}\{\mathbf{b}(u_o) \pm \mathbf{b}(-u_o)\}$, where, as before, $+$ is for the $\Delta\Psi = 0^\circ$ case and $-$ is for the $\Delta\Psi = 180^\circ$ case. This is in contrast to the situation with $\mathrm{Re}\{\mathbf{R}_{ss}\}$ which is rank 1 when either $\Delta\Psi = 0^\circ$ or $\Delta\Psi = 180^\circ$ regardless of the value of ρ. As a practical matter, the amplitude of the specular multipath signal will always be less than that of the direct path signal, due to losses incurred at the surface of reflection, such that ρ is strictly less than one. Nevertheless, the BDML Method can, in fact, handle the ideal scenario in which $\Delta\Psi = 0^\circ$ and ρ=1 despite the rank deficiency problem. Its ability to do so is directly attributable to the centro-symmetry of $\mathbf{v}$ which yields the following interesting result:

$$\mathbf{v}^T\{\mathbf{b}(u_o) + \rho_c\mathbf{b}(-u_o)\} = \mathbf{v}^T\{\mathbf{b}(u_o) + \rho_c\tilde{\mathbf{I}}_3\mathbf{b}(u_o)\}$$

$$= (1 + \rho_c)\mathbf{v}^T\mathbf{b}(u_o) = 0 \qquad (2.55)$$

This implies that if $\mathbf{v}$ is orthogonal to the linear combination $\mathbf{b}(u_o) + \rho_c\mathbf{b}(-u_o)$, where $\rho_c = \rho e^{j\Delta\Psi}$, it is also orthogonal to $\mathbf{b}(u_o)$ itself, so long as ρ_c does not equal to -1 corresponding to the case $\Delta\Psi = 180^\circ$ and $\rho = 1$. Specifically, we may deduce from (2.55) that for $\rho_c = 1$, corresponding to the case $\Delta\Psi = 0^\circ$ and $\rho = 1$, the condition $\mathbf{v}^T\{\mathbf{b}(u_o) + \mathbf{b}(-u_o)\} = 0$ implies $\mathbf{v}^T\mathbf{b}(u_o) = 0$ which, in turn, indicates that the BDML estimation scheme will produce the true value of u_o in the asymptotic case under these conditions.

Thus, the only conditions for which the BDML Method breaks down in a symmetric multipath scenario is the extreme case where $\Delta\Psi = 180^\circ$ and ρ=1. Under such conditions, the two signals cancel each other out entirely at the center element and very nearly cancel each other out at all other elements of the array, depending on how large the array is and how closely-spaced in angle the two signals are. One of the ways to deal with the practical situation where the direct and specular path signals arrive at the center element of the array very nearly equal in amplitude and perfectly or very nearly 180° out of phase is to employ frequency diversity. This is the subject of the next section. Note that the use of frequency diversity will also remedy the problem occurring with BDML in the nonsymmetric case when the phase difference between the two signals at the center of the array is 0°. We should point out that the problem with $\Delta\Psi = 0^\circ$ in the nonsymmetric case is not confined to the ML method in beamspace. It is a problem with the element space based Maximum Likelihood method as well as observed by White [WHIT74]. Cantrell et al [CANT81] also encounter the problem in their three subarray based beamspace domain ML method. Cantrell et al, in fact, argue that if an estimator exists which significantly outperforms the ML estimator in the nonsymmetric case when $\Delta\Psi = 0^\circ$, the estimator must be biased.

As a final note with regard to the effect of the single forward-backward average in beamspace illustrated by (2.53), observe that the diagonal elements of the effective source covariance matrix achieved by this process, $\mathbf{R}_{ss}^{fb}$ defined by (2.54), are equal. The forward-backward averaging process, in effect, exploits the inherent symmetry to "redistribute" the combined power equally among the two signals. This has implications with regard to the much observed phenomenon that the ability to resolve two very closely spaced signals (in angle) largely depends on the strength of the weaker source, assuming a moderate signal-to-noise ratio. The single forward- backward

average in beamspace effectively equalizes the strengths of the two signals providing the optimum condition for resolution given all the other relevant parameters fixed such as phase difference, noise power, etc. We note that the forward-backward average in beamspace as defined by (2.53) is only applicable in the case of symmetric multipath.

2.6 Cramer-Rao Lower Bounds for Coherent Multipath Scenario

When the statistical model for an estimation problem is well defined, it is usually possible to derive an explicit expression for the performance bounds associated with the estimator. In particular, we are interested in the performance bounds associated with unbiased estimators. It is well known that the Cramer-Rao Lower Bound (CRLB) [VAN68] provides a lower bound for the covariance matrix of the estimation error of all unbiased estimators. Specifically, if $\hat{\theta}$ is any unbiased estimator of θ based on the observation bold z, then the covariance of the error in the estimator satisfies the following inequality:

$$\mathrm{E}\left\{ (\theta - \hat{\theta})\,(\theta - \hat{\theta})^{\mathrm{T}} \right\} \geq \mathbf{J}^{-1} \tag{2.56}$$

where

$$\mathbf{J} = \mathrm{E}\left\{ \left[\frac{\partial}{\partial \theta} \ln \mathrm{p}(\mathbf{z} \mid \theta) \right] \left[\frac{\partial}{\partial \theta} \ln \mathrm{p}(\mathbf{z} \mid \theta) \right]^{\mathrm{T}} \,\middle|\, \theta \right\} \tag{2.57}$$

and $\mathrm{p}(\mathbf{z} \mid \theta)$ is the conditional density of $\mathbf{z}$ given θ. Equality holds in (2.56) if and only if

$$\frac{\partial}{\partial \theta} \ln \mathrm{p}(\mathbf{z} \mid \theta) = \mathrm{c}(\theta)[\theta - \hat{\theta}] \tag{2.58}$$

where $\mathrm{c}(\theta)$ is a constant depending on θ. The matrix $\mathbf{J}$ is the well known Fisher Information Matrix [VAN68] An interesting relationship between the CRLB and the ML estimators is that if an estimator satisfies the equality in (2.58), it can be formulated as an ML estimator. In other words, if the CRLB can be attained, it can always be done with the ML estimator.

Their are two advantages to working with the CRLB: 1) analytic expressions are usually attainable; 2) it can handle multiple parameters; i. e., it provides bounds for multiple parameters simultaneously. The computation of the CRLB has been a topic of considerable interest in the area of array

signal processing. Schmidt [SCHM79] developed a formula for computing the Fisher Information matrix for the problem of MUSIC DOA estimation. Trunk et. al. [TRUN79b] derived an explicit expression of the Fisher Information matrix for the scenario of low-angle radar tracking and compared it with their ML estimates. Wang and Kaveh [WANG85] presented a simplified expression for the CRLB for wide-band coherent signal subspace DOA estimation. More recent work includes that of Stoica and Nehorai [STOI88], [STOI89] and Ottersten et al [OTTE89]. Stoica and Nehorai considered the asymptotical behavior of both MUSIC and ML DOA estimators and compared their performance with the CRLB they derived. Ottersten et al, on the other hand, concerned themselves exclusively with the total least squares [VAN84] based ESPRIT algorithm. These CRLB's can be classified in two major categories: the stochastic CRLB and the deterministic CRLB. The latter includes those derived by Trunk et al and Stoica and Nehorai. The former includes those of Wang and Kaveh, and Ottersten et al In the derivation of the stochastic CRLB, the emitter signals are assumed to be random with a given distribution, which is usually assumed to be normal. The unknown parameters are the DOA's, the signal covariance matrix, and the noise power. The deterministic CRLB, on the other hand, considers all unknown quantities as desired parameters that remain to be estimated.

The CRLB developed by Stoica and Nehorai is particularly attractive primarily due to its simple, closed-form expression. Under the two-ray multipath conditions and the spatially white Gaussian noise assumption, their CRLB for u_1 and u_2 is given by

$$\mathbf{J}^{-1} = \frac{\sigma_n^2}{2}\left\{\sum_{n=1}^{N} \mathrm{Re}\left[\mathbf{Y}^H(n)\mathbf{A}_d^H(\mathbf{I}_M - \mathbf{A}(\mathbf{A}^H\mathbf{A})^{-1}\mathbf{A}^H)\mathbf{A}_d\mathbf{Y}(n)\right]\right\}^{-1} \tag{2.59}$$

where

$$\mathbf{Y}(n) = \begin{bmatrix} c_1(n) & 0 \\ 0 & c_2(n) \end{bmatrix} \tag{2.60a}$$

$$\mathbf{A}_d = \left[\frac{\partial \mathbf{a}(u_1)}{\partial u_1} \vdots \frac{\partial \mathbf{a}(u_2)}{\partial u_2}\right] \tag{2.60b}$$

$c_1(n)$ and $c_2(n)$, $n = 1,...,N$, are the direct and specular path signals received at the center element of the array at the n-th snapshot, respectively, as defined in Section 2.3, $\mathbf{A}$ is the DOA matrix, and σ_n^2 is the noise power. Trunk et. al. also derived a close-form expression for the Fisher Information matrix,

but restricted themselves to the single snapshot case. For the stochastic CRLB's, Schmidt proposed an explicit way of computing the components of the Fisher Information matrix described as follows

$$\mathrm{E}\left\{\frac{\partial \ln p(\mathbf{z} \mid \theta)}{\partial \theta_i}\frac{\partial \ln p(\mathbf{z} \mid \theta)}{\partial \theta_j}\right\} = \mathrm{tr}\left\{\mathbf{R}_{xx}^{-1}\frac{\partial \mathbf{R}_{xx}}{\partial \theta_i}\mathbf{R}_{xx}^{-1}\frac{\partial \mathbf{R}_{xx}}{\partial \theta_j}\right\} \qquad (2.61)$$

where $\mathbf{R}_{xx} = \mathrm{E}\{\mathbf{x}(n)\mathbf{x}^H(n)\}$ is the array output correlation matrix. The parameters over which θ_i and θ_j range may differ from case to case, depending on the assumptions made. The deterministic CRLB of Stoica and Nehorai can be easily modified for the case of symmetric multipath. The point is that in symmetric case, the DOA matrix $\mathbf{A} = \left[\mathbf{a}(u_o) \vdots \mathbf{a}(-u_o)\right]$ involves only one parameter u_o such that we may replace $\mathbf{A}_d\mathbf{Y}(n)$ in (2.59) by $\frac{\partial \mathbf{a}(u_o)}{\partial u_o}c_1(n) - \frac{\partial \mathbf{a}(-u_o)}{\partial u_o}c_2(n)$.

Ottersten [OTTE89] argue that the deterministic CRLB is more optimistic than the stochastic CRLB, i. e., the former is lower than the latter, which is somewhat intuitively contradictory. Stoica and Nehorai [STOI89] confirmed this statement by showing that the deterministic CRLB cannot be attained asymptotically by the ML estimator with finite number of array elements. As a consequence, the stochastic approach appears to be more appropriate. For the application of BDML method, the deterministic approach is nevertheless recommended since no a-priori information about the distribution of the echoes was incorporated. Recall that the first step involved in the development of the BDML estimator was to substitute into the cost function the least squares solutions for $\mathbf{c}(n)$, $n = 1,...,N$. In addition, in the case of very few snapshots, the difference between the stochastic and deterministic CRLB's is insignificant. In the following simulation studies, therefore, we will adopt the approach of Stoica and Nehorai for computing the CRLB's.

The CRLB derived by Stoica and Nehorai agrees with the analysis presented in the preceding section, as can be seen from the examples illustrated in Figure 2.4. First, the CRLB for symmetric case is strictly increasing as $\Delta\Psi$ increases form 0° to 180°. Second, the CRLB for nonsymmetric case is symmetric about $\Delta\Psi = 90^\circ$ and reaches its maxima at $\Delta\Psi = 0^\circ$ and 180°. Similar observations hold with regard to the CRLB derived by Trunk et. al. [TRUN79b]. This suggests that an estimator for nonsymmetric case that yields low variance at $\Delta\Psi = 0^\circ$ must be biased. The

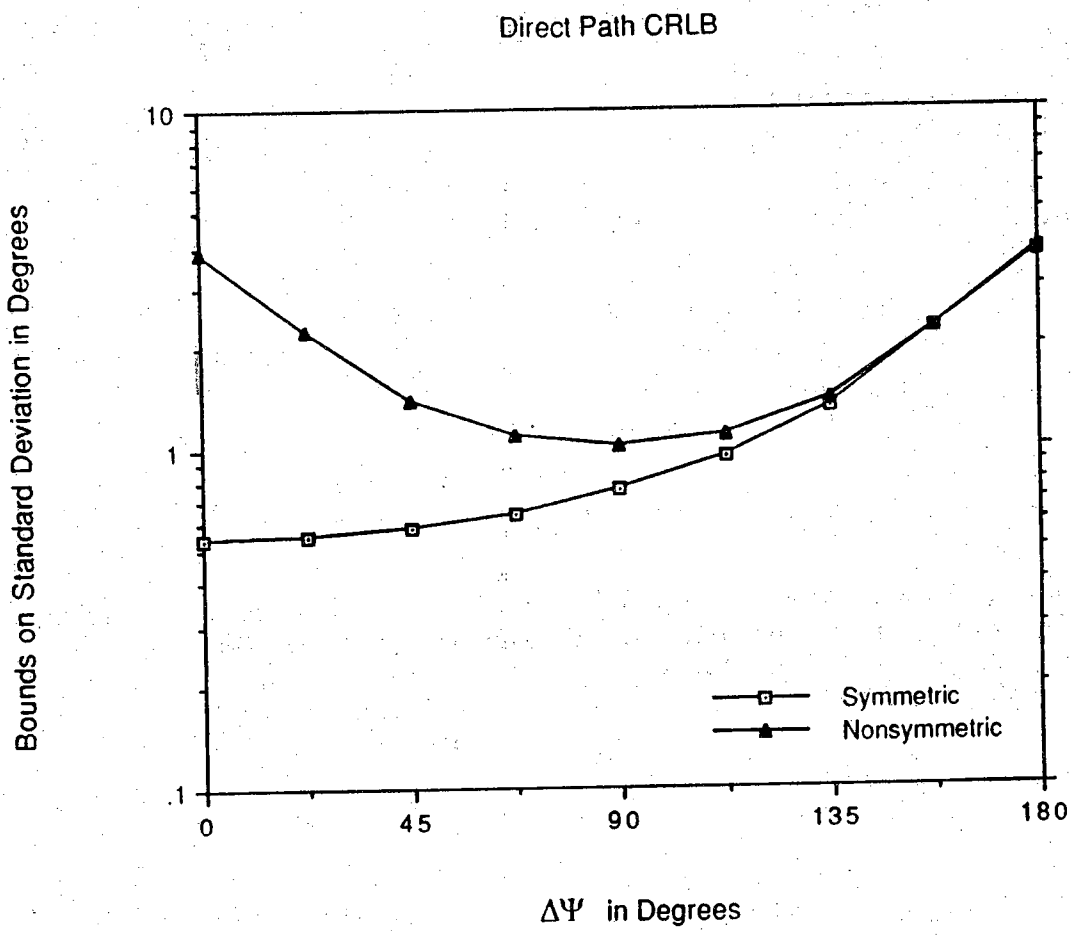

Figure 2.4 Cramer-Rao lower bounds for unbiased estimates of the direct path angle θ_1 for the case of Gaussian additive noise when θ_1=2°, θ_2=–2°, M=15, N=1, ρ=0.9, and SNR=5 dB. Both the symmetric and nonsymmetric cases are shown on the same plot.

problem associated with nonsymmetric multipath at $\Delta\Psi = 0°$ phase difference has remained unsolved for many years. The "improved" three-aperture method proposed by Gorden [GORD83] did not yield a definitive solution. In fact, as will be seen in Section 4.3, the improved three-aperture scheme produces large bias and variance for the specular path angle in an attempt to increase the accuracy for the direct path angle. In light of the good performance of the symmetric BDML estimator at $\Delta\Psi = 0°$, we recommend that a scheme be developed to convert a nonsymmetric problem into a symmetric one. It is interesting to investigate the possibility of breaking the CRLB if the above mentioned conversion can be successfully done. However, it should be kept in mind that the estimator thus developed must exhibit bias at small phase differences and cannot outperform the corresponding BDML estimator for symmetric multipath. A detail discussion will be provided in Section 4.3.

2.7 Computer Simulations

Computer simulations were conducted for the purpose of determining how well the various beamspace domain based ML estimation schemes developed within perform in a simulated low-angle radar tracking scenario. In all test cases, the array employed was linear consisting of M=15 elements uniformly-spaced by a half-wavelength. Echoes from a single target angularly located near broadside returned to the array via a specular path as well as via a direct path. Each execution of the appropriate BDML estimation algorithm was conducted with N=10 snapshots collected over an interval in which the ratio of the amplitudes, ρ, and the phase difference between the direct and specular path signals, $\Delta\Psi$, was constant corresponding to a coherent multipath scenario. A practical value of $\rho = 0.9$ [BART74], [STEI76] was used as the magnitude of the complex reflection coefficient in the model. The transformation to beamspace was accomplished via a Butler Matrix beamformer of the form in (2.36) where $u_B = \frac{2}{M} = .133$. In terms of degrees, this corresponds to upper and lower auxiliary beams pointed at $\theta_B = 7.64°$ and $-\theta_B = -7.64°$, respectively. Finally, the additive noise was modeled to be spatially white and uncorrelated with the received echoes. Again, these parameters and quantities were common to each and every simulation run.

In order to talk about the relative proximity of the direct and specular path signals, a measure of the beamwidth associated with the array is needed. A good approximation to the 3 dB beamwidth is $\frac{2}{15}$rads. $= 7.64°$ which is

half the separation between the first null on either side of the mainlobe of the reference beam when rectangular weighting is employed. In the examples to follow, angle measurements may be periodically cited in units of beamwidths, denoted BW, where one beamwidth is 7.64°.

The first simulation results compare the performance and computational load of BDML Method II for symmetric multipath outlined in Section 2.3 with that of the IQML algorithm of Bresler and Macovski [BRES86], a computationally efficient element space based ML estimation scheme. For each trial run, the target angle was 2° such that the angular separation between the direct and specular path signals was $4/7.64 = .52$ beamwidths. The SNR for the direct path signal was 5 dB at each element. Sample means and sample standard deviations in degrees for both the BDML estimates and the IQML estimates computed from 100 independent trials for seven different values of the phase difference measured at the center of the array as well as the corresponding CRLB's are shown in Table 2.1 and Figure 2.5. For each trial run, the polynomial coefficients gleaned from the IQML algorithm were those obtained after the execution of five iterations. Recall that the IQML algorithm is not a closed form procedure as discussed previously. Comparing results, we note the performance of the two algorithms to be quite comparable. Interestingly enough, for all cases the sample standard deviation of the IQML estimates is smaller than those of the BDML estimates while the difference between the sample mean and the true target angle is smaller for the BDML estimates. In both cases, the sample standard deviation increases as the phase difference $\Delta\Psi$ increases from 0° to 180°. This phenomenon is characteristic of all ML based estimators developed for symmetric multipath [HAYK85], [CANT81], [KSIE68], [WHIT74]. Note that a failure was registered whenever the estimate obtained from either algorithm was equal to 0° corresponding to a situation in which the direct and specular signals are not resolved. In the case of $\Delta\Psi = 180^{\circ}$, 35 failures occurred with the BDML estimator, giving rise to a large bias and standard deviation, while no failures were incurred with the IQML estimator. The fact that the IQML algorithm outperforms the BDML algorithm in the case of $\Delta\Psi = 180^{\circ}$ may be attributed, in part, to the fact that it inherently incorporates some spatial smoothing of the array data. The BDML estimator could be modified to incorporate spatial smoothing prior to the transformation to beamspace but this was not done so here. We also note that the IQML estimator is nevertheless heavily biased in the case of $\Delta\Psi = 180^{\circ}$ such that neither algorithm provides reliable estimates under this condition. As argued

Table 2.1 Comparison of the performance and computational load of the BDML method with that of the IQML method in a symmetric multipath scenario with target angle θ_o=2°, M=15, N=10, SNR=5 dB for direct path, and ρ=0.9. The bottom row indicates the respective approximate number of floating point operations required for each trial run for both methods. $\bar{\theta}$ and $\hat{\sigma}$ represent the sample mean and sample standard deviation in degrees computed from 100 independent trials. The rightmost column shows the corresponding CRLB's for σ.

$\Delta\psi$	BDML			IQML			CRLB
	$\bar{\theta}$	$\hat{\sigma}$	# failures	$\bar{\theta}$	$\hat{\sigma}$	# failures	
0°	2.0014	0.1748	0	2.0694	0.1651	0	0.1689
22.5°	1.9986	0.1816	0	2.0712	0.1693	0	0.1722
45°	1.9942	0.1959	0	2.0789	0.1792	0	0.1825
67.5°	1.9869	0.2213	0	2.0922	0.1995	0	0.2022
90°	1.9744	0.2668	0	2.1237	0.2322	0	0.2365
112.5°	1.9500	0.3573	0	2.1881	0.2883	0	0.2973
135°	1.8816	0.5858	3	2.3511	0.3806	0	0.4171
157.5°	1.7197	1.0355	17	2.8282	0.5176	0	0.7022
180°	3.5874	4.6536	35	3.5909	0.5120	0	1.1774
	5.3×10^4 flops/run			1.2×10^7 flops/run			

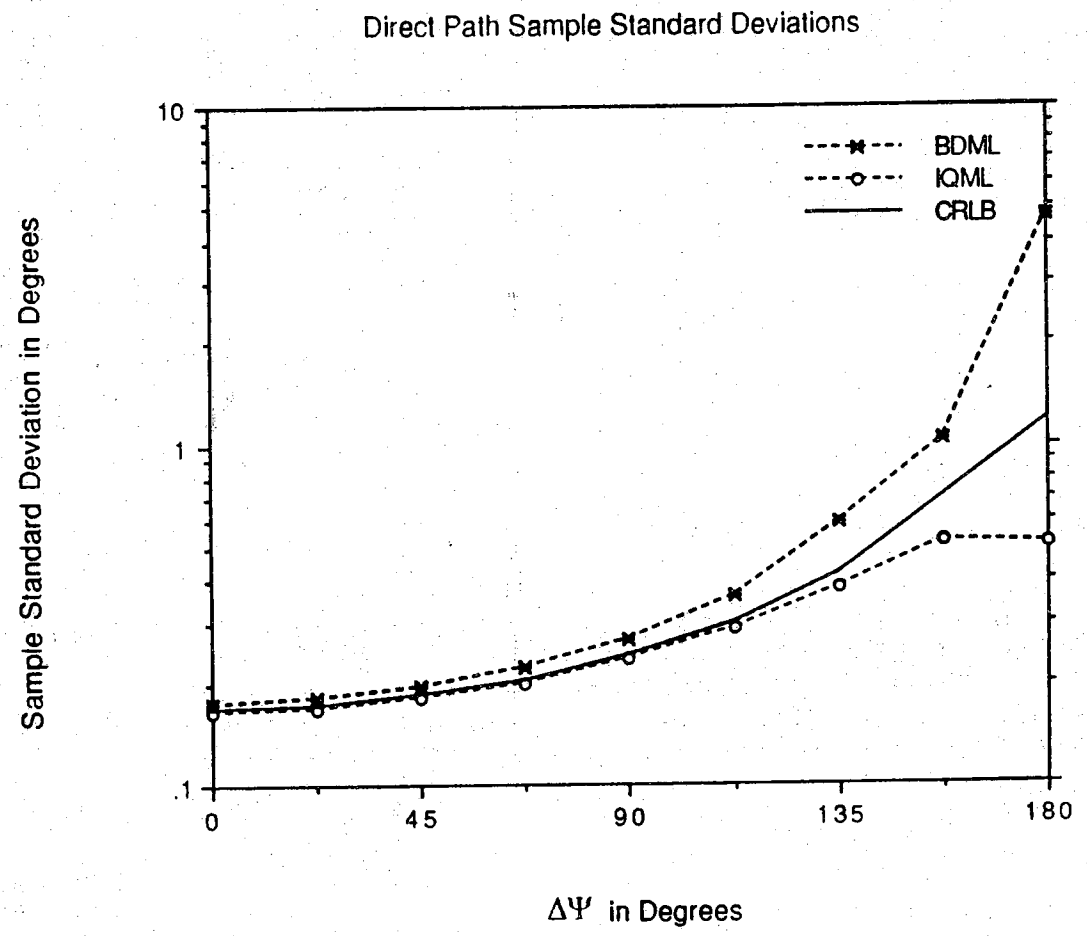

Figure 2.5 Comparison of the performance of the BDML method and that of the IQML method with the theoretical CRLB in a symmetric multipath scenario with target angle θ_o=2°, M=15, N=10, SNR=5 dB for direct path, and ρ=0.9. Sample mean and sample standard deviation were computed from 100 independent trials.

previously, this is due to severe signal cancellation occurring across the array. The BDML estimator does, however, provide reliable estimates as long as $\Delta\Psi$ is not too close to 180°, as does the IQML estimator. Comparing the sample standard deviations associated with both methods with the corresponding CRLB, we find that the BDML estimator approaches the CRLB for small phase differences while the IQML estimator produces standard deviations smaller than the CRLB for all phase differences. The behavior of the IQML estimator here is of no contradiction since it exhibits bias for all phase differences as can be seen from Table 2.1. The drastic reduction in the amount of computation incurred with BDML with respect to that of IQML is indicated by the average number of floating point operations per algorithm execution which is listed in the bottom row of Table 2.1. This number was determined using the PRO-MATLAB software package and did not include the initial computation involved in setting up the data. *We note that the computational load of BDML is three orders of magnitude less than that of IQML!!* We should point out that the disparity between the computational loads of the two algorithms becomes even greater as the number of array elements increases. Except for the initial transformation from element space to beamspace, which effectively involves the computation of 3 values of an M-point DFT, the computational burden of BDML remains essentially the same: a 3x3 eigenvalue decomposition (EVD) and subsequent evaluation of the formula in (2.43). As a final point, we note that if M is large, the required 3 values of the M point DFT may be computed in an efficient manner via the Goertzel algorithm.

The second set of simulation results presented in Tables 2.2 and 2.3 provide an indication as to the performance of the BDML estimator in a coherent symmetric multipath scenario for various combinations of target elevation angle, phase difference, and direct path SNR. For each particular set of parameters, sample means and sample standard deviations were computed from the results of 100 independent trials. Table 2.2 illustrates the trend in estimator performance as the angular separation between the direct and specular path signals increases while the phase difference between the two at the center of the array and the direct path SNR remain constant. In each case, the direct path SNR was 5 dB at each element. The five target elevation angle test cases were 1° , 2° , 3° , 4°, and 5° corresponding to angular separations between the direct and specular path signals of .26 BW, .52 BW, .78 BW, 1.04 BW, and 1.96 BW, respectively. Again, the unit BW is the 3 dB beamwidth equal to 7.64 ° . As before, a failure was registered whenever the

Table 2.2 Performance of the BDML estimator in a symmetric multipath scenario for five different target angles with M=15, N=10, SNR=5 dB for direct path, and ρ=0.9. The 3-dB beamwidth of the quiescent array pattern is approximately 7.6°. $\bar{\theta}$ and $\hat{\sigma}$ denote the sample mean and sample standard deviation in degrees computed from 100 independent trials.

$\Delta\Psi$		$\theta = 1°$	$\theta = 2°$	$\theta = 3°$	$\theta = 4°$	$\theta = 5°$
0°	$\bar{\theta}$	0.9420	2.0014	3.0037	4.0032	5.0028
	$\hat{\sigma}$	0.4120	0.1748	0.1134	0.0884	0.0847
	# failures	9	0	0	0	0
45°	$\bar{\theta}$	0.9151	1.9942	2.9993	3.9998	4.9997
	$\hat{\sigma}$	0.4609	0.1959	0.1280	0.0992	0.0925
	# failures	13	0	0	0	0
90°	$\bar{\theta}$	0.8907	1.9744	2.9892	3.9926	4.9936
	$\hat{\sigma}$	0.5274	0.2668	0.1727	0.1336	0.1226
	# failures	15	0	0	0	0
135°	$\bar{\theta}$	0.8570	1.8816	2.9598	3.9768	4.9848
	$\hat{\sigma}$	0.7411	0.5858	0.3350	0.2561	0.2344
	# failures	33	3	0	0	0
180°	$\bar{\theta}$	3.2218	3.5874	4.2664	4.2603	4.4583
	$\hat{\sigma}$	4.8142	4.6536	5.0073	3.8272	3.6688
	# failures	42	35	28	26	25

Table 2.3 Performance of the BDML estimator in a symmetric multipath scenario for seven different direct path SNR values with target angle θ=1°, M=15, N=10, and ρ=0.9. The 3-dB beamwidth of the quiescent array pattern is approximately 7.6°. $\bar{\theta}$ and $\hat{\sigma}$ denote the sample mean and sample standard deviation in degrees computed from 100 independent trials.

$\Delta\Psi \downarrow$	SNR $\rightarrow$	0 dB	5 dB	10 dB	15 dB	20 dB	25 dB	30 dB
0°	$\bar{\theta}$	0.9210	0.9420	0.9882	1.0007	1.0021	1.0017	1.0011
	$\hat{\sigma}$	0.5959	0.4120	0.2185	0.1126	0.0625	0.0351	0.0197
	# failures	21	9	0	0	0	0	0
45°	$\bar{\theta}$	0.9021	0.9151	0.9776	0.9959	0.9999	1.0006	1.0005
	$\hat{\sigma}$	0.6337	0.4609	0.2379	0.1261	0.0703	0.0396	0.0223
	# failures	24	13	0	0	0	0	0
90°	$\bar{\theta}$	0.8765	0.8907	0.9341	0.9818	0.9940	0.9978	0.9991
	$\hat{\sigma}$	0.7274	0.5274	0.3491	0.1734	0.0945	0.0528	0.0297
	# failures	28	15	4	0	0	0	0
135°	$\bar{\theta}$	0.9358	0.8570	0.8627	0.9177	0.9718	0.9893	0.9953
	$\hat{\sigma}$	0.9676	0.7411	0.5533	0.3684	0.1876	0.1000	0.0555
	#failures	42	33	20	6	0	0	0
180°	$\bar{\theta}$	4.3657	3.2218	1.2696	1.0037	0.8885	0.8593	0.9035
	$\hat{\sigma}$	4.5328	4.8142	1.5713	1.0433	0.7979	0.6050	0.4160
	# failures	32	42	53	43	38	24	9

algorithm produced an estimate equal to 0°. Similar to the trend observed in Table 2.1, we note that the performance of the BDML estimator decreases as the phase difference, $\Delta\Psi$ increases from 0° to 180°. Observe that a large number of failures occurred for each target elevation angle test case when the phase difference was 180°, although the bias and standard deviation of the estimates did decrease somewhat as the angular separation between the two signals increased. However, it may be inferred from these results that under the condition $\Delta\Psi = 180^\circ$ and ρ=.9, the symmetric BDML estimator does not provide reliable estimates when the angular separation between the direct and specular path signals is less than a beamwidth and the SNR is less than 20 dB, thus necessitating the use of frequency diversity. This will be discussed in Section 4.4. Note that the smaller the magnitude of the reflection coefficient, ρ, the lesser the amount of signal cancellation across the array and, hence, degradation in performance.

In contrast to Table 2.2, Table 2.3 illustrates the trend in estimator performance as the direct path SNR is increased while the phase difference and angular separation between the direct and specular path signals remain constant. In each case, the target elevation angle was $\theta = 1^\circ$ corresponding to an angular separation between the direct and specular path signals of .26 BW. We observe that a significant number of failures were incurred in the case of direct path SNR = 0 dB for each value of the phase difference, although the sample mean was not too far off from the true value in all cases except $\Delta\Psi = 180^\circ$. For a fixed phase difference, though, the bias and standard deviation of the estimates did decrease as the direct path SNR was increased as would be expected. Once again, though, the results in Table 2.3 indicate that without spatial smoothing pre-processing or frequency diversity, the symmetric BDML estimator does not provide reliable estimates in the case $\Delta\Psi$=180° unless the direct path SNR is well over 25 dB.

Table 2.4 is similar to Table 2.3 except that the multipath scenario simulated was a nonsymmetric one as opposed to a symmetric one necessitating the use of the BDML estimation scheme outlined in Sect. III. Specifically, Table 2.4 illustrates the trend in the performance of the BDML estimator for the nonsymmetric multipath case as the direct path SNR is increased while the angles of the direct and specular path signals remain fixed at $\theta_1 = 2^\circ$ and $\theta_2 = -1^\circ$, respectively. Note that these test angles correspond to an angular separation of approximately .4 BW. For each particular combination of direct path SNR and phase difference, sample means and sample standard deviations were computed from the results of 100

Table 2.4 Performance of the BDML estimator in a nonsymmetric multipath scenario for seven different direct path SNR values with target angle $\theta_1=2°$, specular path angle $\theta_2=-1°$ M=15, N=10, and ρ=0.9. The 3-dB beamwidth of the quiescent array pattern is approximately 7.6°. $\bar{\theta}$ and $\hat{\sigma}$ denote the sample mean and sample standard deviation in degrees computed from 100 independent trials.

$\Delta\Psi\downarrow$	SNR $\rightarrow$	0 dB	5 dB	10 dB	15 dB	20 dB	25 dB	30 dB
0°	$\bar{\theta}_1$	7.2339	7.1861	6.3242	6.3116	7.1098	7.0075	6.9677
	$\hat{\sigma}_1$	14.2508	14.2476	11.9758	11.9671	14.0673	13.5727	13.3977
	$\bar{\theta}_2$	-8.8693	-8.9785	-9.9942	-10.1247	-9.4200	-9.4229	-9.4253
	$\hat{\sigma}_2$	15.9760	16.0743	18.1285	18.4851	17.5121	17.5264	17.5382
	# failures	1	0	0	0	0	0	0
45°	$\bar{\theta}_1$	5.1689	2.2779	2.0472	2.0095	2.0015	1.9997	1.9995
	$\hat{\sigma}_1$	11.6015	1.1751	0.4196	0.2137	0.1165	0.0648	0.0363
	$\bar{\theta}_2$	-2.5086	-1.2232	-1.0608	-1.0240	-1.0110	-1.0055	-1.0029
	$\hat{\sigma}_2$	5.2645	1.1485	0.5002	0.2576	0.1403	0.0778	0.0435
	# failures	0	0	0	0	0	0	0
90°	$\bar{\theta}_1$	2.1785	1.9945	1.9907	1.9936	1.9962	1.9979	1.9988
	$\hat{\sigma}_1$	1.2995	0.5147	0.2579	0.1416	0.0791	0.0444	0.0249
	$\bar{\theta}_2$	-1.1134	-1.0065	-1.0080	-1.0061	-1.0040	-1.0025	-1.0014
	$\hat{\sigma}_2$	1.3309	0.6200	0.3255	0.1802	0.1008	0.0566	0.0318
	# failures	7	1	0	0	0	0	0
135°	$\bar{\theta}_1$	1.8910	1.8483	1.9163	1.9721	1.9881	1.9944	1.9972
	$\hat{\sigma}_1$	1.1330	0.7311	0.4524	0.2213	0.1212	0.0677	0.0380
	$\bar{\theta}_2$	-0.8360	-0.8537	-0.9280	-0.9809	-0.9937	-0.9977	-0.9991
	$\hat{\sigma}_2$	1.3153	0.8315	0.4940	0.2491	0.1374	0.0769	0.0432
	# failures	29	14	3	0	0	0	0
180°	$\bar{\theta}_1$	5.7741	5.7616	5.2044	5.1602	5.1425	5.1413	5.1406
	$\hat{\sigma}_1$	6.2038	8.1700	4.2438	4.1145	4.0694	4.0449	4.0351
	$\bar{\theta}_2$	-4.0581	-4.0492	-5.0131	-4.9927	-4.9969	-5.0102	-5.0184
	$\hat{\sigma}_2$	6.6271	6.3873	7.1030	6.7137	6.5854	6.5304	6.5069
	# failures	27	28	27	28	28	27	28

independent trials. For the case of direct path SNR = 0 dB, we note that the algorithm performed quite miserably, although the sample means were not too far off from the true values in the cases $\Delta\Psi = 90°$ and $\Delta\Psi = 135°$. A failure was registered whenever the algorithm supplied the same angular value for both estimates. For the cases $\Delta\Psi = 45°$, $\Delta\Psi = 90°$ and $\Delta\Psi = 135°$, we observe that the bias and standard deviation of the estimates decreases as the direct path SNR increases with $\Delta\Psi = 90°$ giving rise to the best performance. In the cases $\Delta\Psi = 0°$ and $\Delta\Psi = 180°$, however, we observe that the nonsymmetric BDML estimator provides totally unreliable estimates regardless of the value of the direct path SNR. This shortcoming of the nonsymmetric BDML estimator is due to a rank deficiency phenomenon occurring with these two phase differences as discussed in Section 2.5. Again, we could remedy the problem somewhat by spatial smoothing prior to the transformation from element space to beamspace. However, in chapter 4, we will present several novel procedures for overcoming this problem.

CHAPTER 3
GENERALIZED BUTLER MATRIX BEAMFORMERS AND BDML ESTIMATORS

3.1 Introduction

At the end of Chapter 2, we showed that significant simplifications in computation for the BDML estimation procedure may be achieved with the use of an Mx3 Butler matrix beamformer. In fact, the BDML angle estimates may be simply determined from the roots of a judiciously constructed quadratic equation. This is a significant contribution due to the fact that the 3x1 beamspace manifold vector does not exhibit the Vandermonde structure in contrast to the situation with Cantrell's three subarray method as discussed previously. The ability to nevertheless formulate the estimates in terms of the roots of a quadratic equation arises from the fact that the respective array beam patterns associated with each of three columns of the Mx3 Butler beamforming matrix have M-3 nulls in common (M is the number of elements), the locations of which are known regardless of the signal and noise parameters. The property of M-3 common nulls may be viewed as a-priori knowledge for the underlying estimation problem.

Due to the Vandermonde structure of the element space manifold vector, it is appropriate to interprete the common nulls associated with the three columns of the Butler beamformer as those common "roots" associated with the three polynomials correspondingly constructed. Motivated by the equivalence between the multiplication of polynomials and the convolution of sequences, it is possible to factorize the Butler beamforming matrix as a product of an Mx3 banded, toeplitz matrix and a 3x3 matrix. The Mx3 toeplitz matrix thus obtained corresponds to the M-3 common nulls while the 3x3 matrix corresponds to the remaining uncommon nulls. An important aspect of this factorization is that it allows one to generalize the Butler beamformer by simply replacing the two matrix factors with other judiciously constructed matrices such that the resulting weight vectors have M-3 nulls in common. Further extensions can be made to the generalized Butler beamformers if we adopt the concept of polynomials and roots. Under such a

premise, the polynomials associated with the three columns of a generalized Butler beamformer need not have all of their roots lie exactly on the unit circle. Consequently, the common and uncommon roots represent two groups of design parameters that must be carefully determined a-priori.

Although the idea of generalized Butler matrix beamforming facilitates substantial reduction in computational complexity, applying it directly to the BDML estimation scheme does not necessarily lead to reliable estimates. As was discussed in the preceding chapter, the performance of the BDML estimators relies heavily on the beamformer employed, especially for the symmetric multipath case. In order to nevertheless exploit the advantages of processing in the beamspace domain, some modifications should be made for the generalized Butler beamformers. First, the beamforming weight vectors should exhibit conjugate centro-symmetry so as to produce a purely real beamspace manifold vector. Second, the lower and upper auxiliary weight vectors should be constructed in such a fashion that they produce mutually reverse beamspace domain manifold vectors when the multipath is symmetric. These two design considerations are crucial in our development of the BDML methods as evidenced by the performance analysis presented in Section 2.5. Combined with the SNR gain consideration, they constitute a new area of beamforming problems. A primary objective of this chapter is to provide a structural description of the common roots property, and develop BDML estimators based on the new generalized Butler beamformers.

The chapter is organized as follows. Section 3.2 describes the structure of the Butler matrix beamformer and its associated factorization property. Section 3.3 develops alternative BDML estimators for both symmetric and nonsymmetric multipath cases based on the generalized Butler beamformers. Specifically, a new processing technique is developed to exploit the Vandermonde structure in beamspace domain obtained with a generalized Butler beamformer. Finally, Section 3.4 develops a parametric representation for the beamspace domain vector and discusses its applications to BDML estimation.

3.2 Factorization of the Butler Beamforming Matrix

In the preceding chapter, we found out that the property possessed by the Mx3 Butler matrix beamformer, i. e., the three beamforming weight vectors have M-3 nulls in common, leads to significant simplifications in computation for the BDML estimation procedure. The main point is that we

were able to convert the original (M-1)-th order polynomial equation necessary for finding the angle estimates into a quadratic equation without loss of information. The procedure involved was in fact a polynomial division in which the (M-3)-th order "common" polynomial was factored out of the (M-1)-th order polynomial mentioned above. The problem is best understood with the aid of polynomial notation. We first introduce the following notation relating vectors, sequences, and polynomials

$$\mathbf{p} = \left[p_o \, , \, p_1 \, , \, \cdots \, , \, p_{N-1}\right]^T \tag{3.1a}$$

$$\{\mathbf{p}\} = \{p_o \, , \, p_1 \, , \, \cdots \, , \, p_{N-1}\} \tag{3.1b}$$

$$p(z) = p_o + p_1 z + \cdots + p_{N-1} z^{N-1} \tag{3.1c}$$

That is, if $\mathbf{p}$ is an Nx1 vector given by (3.1a), then its associated sequence and polynomial representations are given by (3.1b) and (3.1c), respectively. Motivated by the equivalence between the multiplication of polynomials and convolution of sequences, three expressions in accordance with the above notation are as follows

$$p(z) = q(z)r(z) \tag{3.2a}$$

$$\{\mathbf{p}\} = \{\mathbf{q}\} * \{\mathbf{r}\} \tag{3.2b}$$

$$\mathbf{p} = \begin{bmatrix} \mathbf{q} & 0 & & 0 & 0 \\ 0 & \mathbf{q} & & 0 & 0 \\ \vdots & \vdots & \vdots & \vdots & \vdots \\ 0 & 0 & & \mathbf{q} & 0 \\ 0 & 0 & & 0 & \mathbf{q} \end{bmatrix} \mathbf{r} = \begin{bmatrix} \mathbf{r} & 0 & & 0 & 0 \\ 0 & \mathbf{r} & & 0 & 0 \\ \vdots & \vdots & \vdots & \vdots & \vdots \\ 0 & 0 & & \mathbf{r} & 0 \\ 0 & 0 & & 0 & \mathbf{r} \end{bmatrix} \mathbf{q} \tag{3.2c}$$

where "*" denotes sequence linear convolution. To further simplify notations, we denote as $\mathbf{X}$ the banded, toeplitz matrix constructed with the corresponding vector $\mathbf{x}$ in the following fashion

$$\mathbf{X} = \begin{bmatrix} \mathbf{x} & 0 & & 0 & 0 \\ 0 & \mathbf{x} & & 0 & 0 \\ \vdots & \vdots & \vdots & \vdots & \vdots \\ 0 & 0 & & \mathbf{x} & 0 \\ 0 & 0 & & 0 & \mathbf{x} \end{bmatrix} \tag{3.3}$$

The dimension of $\mathbf{X}$ depends upon the order of the polynomial multiplied with $\mathbf{x}(z)$, the polynomial representation of $\mathbf{x}$. In general, if the product is an N-th

order polynomial, then $\mathbf{X}$ must have N+1 rows. With this notation established, the structure of the Mx3 Butler beamforming matrix can be easily analyzed in a few steps.

Let $\mathbf{s}_l$, $\mathbf{s}_c$, and $\mathbf{s}_u$ denote the lower, center, and upper beamforming weight vectors corresponding to the three columns of the Butler beamforming matrix $\mathbf{S}$. The common nulls property of $\mathbf{S}$ suggests the following expressions for the these three weight vectors.

$$\mathbf{s}_l = \begin{bmatrix} \mathbf{h} & 0 & 0 \\ 0 & \mathbf{h} & 0 \\ 0 & 0 & \mathbf{h} \end{bmatrix} \mathbf{e}_l = \mathbf{H}\mathbf{e}_l \tag{3.4a}$$

$$\mathbf{s}_c = \begin{bmatrix} \mathbf{h} & 0 & 0 \\ 0 & \mathbf{h} & 0 \\ 0 & 0 & \mathbf{h} \end{bmatrix} \mathbf{e}_c = \mathbf{H}\mathbf{e}_c \tag{3.4b}$$

$$\mathbf{s}_u = \begin{bmatrix} \mathbf{h} & 0 & 0 \\ 0 & \mathbf{h} & 0 \\ 0 & 0 & \mathbf{h} \end{bmatrix} \mathbf{e}_u = \mathbf{H}\mathbf{e}_u \tag{3.4c}$$

where $\mathbf{h}$ denote the vector representation of the (M-3)-th order "common" polynomial given by

$$h(z) = \alpha \prod_{m=2}^{M-2} (z - e^{j\frac{2\pi m}{M}}) \tag{3.5}$$

and $\mathbf{e}_l$, $\mathbf{e}_c$, and $\mathbf{e}_u$ correspond to the remaining uncommon nulls associated with the lower, center, and upper beams, respectively, in the following fashion

$$\mathbf{e}_l(z) = \alpha_l (z-1)(z - e^{-j\frac{2\pi}{M}}) \tag{3.6a}$$

$$\mathbf{e}_c = \alpha_c (z - e^{-j\frac{2\pi}{M}})(z - e^{j\frac{2\pi}{M}}) \tag{3.6b}$$

$$\mathbf{e}_u = \alpha_u (z-1)(z - e^{j\frac{2\pi}{M}}) \tag{3.6c}$$

Note that α, α_l, α_c, and α_u are complex scalars ensuring that each of the above four polynomials has a set of conjugate centro-symmetric coefficients. Combining (3.4a), (3.4b), and (3.4c) and putting in matrix form, the Mx3 Butler beamforming matrix has the following factorization

$$\mathbf{S} = \mathbf{HE} = \begin{bmatrix} \mathbf{h} & 0 & 0 \\ 0 & \mathbf{h} & 0 \\ 0 & 0 & \mathbf{h} \end{bmatrix} \left[\mathbf{e}_l \vdots \mathbf{e}_c \vdots \mathbf{e}_u \right] \tag{3.7}$$

Note that **S** is Mx3, **H** is Mx3, and **E** is 3x3.

An indication inherent in the above factorization is that the beamforming achieved with the Butler matrix can be considered as a two-stage procedure: 1) transform form M-dimensional element space to 3-dimensional beamspace using **H** matrix; 2) shape the three beams obtained in 1) by the transformation **E**. This operation may be mathematically described by

$$(1)\ \ \mathbf{c}(u) = \mathbf{H}^H \mathbf{a}(u) \tag{3.8a}$$

$$(2)\ \ \mathbf{b}(u) = \mathbf{E}^H \mathbf{c}(u) \tag{3.8b}$$

We here concern ourselves solely with nonsingular **E** matrix, which can be guaranteed by judiciously choosing the uncommon nulls. The advantage to working with nonsingular **E** will become clear in the next section. It is interesting to note that stage 1 produces three beams pointing at the same direction but with a different phase center. A close look at the Toeplitz structure of **H** reveals that they differ by a constant phase displacement corresponding to that occurring between two adjacent array elements. This indicates that the components of $\mathbf{c}(u)$ exhibit Vandermonde structure as described in the following fashion

$$\mathbf{c}(u) = \begin{bmatrix} e^{-j\pi u} \\ 1 \\ e^{j\pi u} \end{bmatrix} G(u) \tag{3.9}$$

where

$$G(u) = \mathbf{h}^H \mathbf{a}_{M-2}(u) \tag{3.10a}$$

$$\mathbf{a}_{M-2}(u) = \left[e^{-j\pi \frac{M-3}{2} u}, \ldots, e^{-2j\pi u}, e^{-j\pi u}, 1, e^{j\pi u}, e^{2j\pi u}, \ldots, e^{j\pi \frac{M-3}{2} u} \right]^T \tag{3.10b}$$

Therefore the beamspace manifold vector constructed with **H** has the same compositional form as the element space manifold vector except for the gain factor $G(u)$ and the reduced dimensionality. This phenomenon that the Vandermonde structure of the element space manifold is retained by the beamspace manifold vector with a banded, Toeplitz beamforming matrix is the basis for why the Mx3 Butler beamformer facilitates simple BDML

computation. Indeed, if we substitute into the orthogonality condition $\mathbf{v}^T\mathbf{b}(u) = 0$ as described in Section 2.3 the alternative expression for $\mathbf{b}(u)$ given by (3.8b) and (3.9), we obtain

$$\mathbf{v}^T\mathbf{b}(u) = \mathbf{v}^T\mathbf{E}^H\mathbf{c}(u) = (\mathbf{E}\mathbf{v})^H\mathbf{c}(u)$$

$$= (g_1 e^{-j\pi u} + g_2 + g_3 e^{j\pi u})\, G(u) = 0 \qquad (3.11)$$

where g_i is the i-th component of $\mathbf{E}\mathbf{v}$. Assuming $G(u) \neq 0$, or u does not belong to one of the M-3 common nulls, (3.11) can be formulated as a quadratic equation as described by

$$g(z) = g_1 + g_1 z + g_2 z^2 = 0 \qquad (3.12)$$

The estimates of u_1 and u_2 can then be determined as two unit roots of $g(z)$. A direct computation verifies that the coefficients of $g(z)$, given according to

$$g_1 = -v_1\, e^{-j\frac{\pi}{M}} + v_2 - v_3\, e^{j\frac{\pi}{M}} \qquad (3.13a)$$

$$g_2 = 2(v_1 + v_3)\cos(\frac{\pi}{M}) - 2v_2\cos(\frac{2\pi}{M}) \qquad (3.13b)$$

$$g_3 = -v_1\, e^{j\frac{\pi}{M}} + v_2 - v_3\, e^{-j\frac{\pi}{M}} \qquad (3.13c)$$

are exactly identical to those given in (2.46).

Of course, the Mx3 Butler matrix beamformer is not the only one possessing the M-3 common nulls property. In fact, any beamforming matrix that can be factorized in a form similar to that described by (3.7) will also lead to simplifications in computation. However, both $\mathbf{H}$ and $\mathbf{E}$ matrices should be judiciously chosen so as to retain high SNR gain in the desired directions and provide sufficient supression for noise and interferences outside the mainlobe region. This is the topic of Chapter 5.

3.3 Generalized Butler Matrix Beamformers

This section discusses a class of generalized Butler matrix beamformers and their associated BDML estimators. In particular, a new approach to the BDML estimation scheme will be developed.

3.3.1 Construction of Beamformers

To begin with, we introduce the following definition:

Definition An Mx3 generalized Butler matrix beamformer $\mathbf{W}_B$ is a matrix exhibiting the following factorization

$$\mathbf{W}_B = \left[\mathbf{w}_1 \vdots \mathbf{w}_2 \vdots \mathbf{w}_3 \right] = \mathbf{CU} \tag{3.14}$$

where $\mathbf{C}$ is an Mx3 banded, toeplitz matrix given by

$$\mathbf{C} = \begin{bmatrix} \mathbf{c} & 0 & 0 \\ 0 & \mathbf{c} & 0 \\ 0 & 0 & \mathbf{c} \end{bmatrix} \tag{3.15}$$

and $\mathbf{U} = [\, \mathbf{u}_1 \vdots \mathbf{u}_2 \vdots \mathbf{u}_3 \,]$ is 3x3. This indicates that the three columns of $\mathbf{W}_B$ are related through $\mathbf{c}$ in terms of polynomials as:

$$\begin{aligned} w_1(z) &= c(z)\, u_1(z) \\ w_2(z) &= c(z)\, u_2(z) \\ w_3(z) &= c(z)\, u_3(z) \end{aligned} \tag{3.16}$$

which implies that the three polynomials $w_1(z)$, $w_2(z)$, and $w_3(z)$ have M-3 roots in common determined by $c(z) = 0$. The generalized Butler matrix beamformers retain the Vandermonde structure in beamspace domain, up to a nonsingular transformation, in exactly the same way the Mx3 Butler beamformer does. In order to apply the generalized Butler beamformers in BDML estimation, it is necessary to account for the following two factors: 1) the weight vectors must produce a purely real beamspace domain manifold vector ; 2) for symmetric multipath, the beamspace domain manifold vectors must satisfy $\mathbf{b}(-u) = \tilde{\mathbf{I}}_3 \mathbf{b}(u)$. We now investigate the sufficient conditions for 1) and 2) individually.

The first constraint is easily accounted for if we make each of the three columns of $\mathbf{W}_B$ conjugate centro-symmetric, i. e.,

$$\tilde{\mathbf{I}}_M \mathbf{w}_1 = \mathbf{w}_1^* \; ; \; \tilde{\mathbf{I}}_M \mathbf{w}_2 = \mathbf{w}_2^* \; ; \; \tilde{\mathbf{I}}_M \mathbf{w}_3 = \mathbf{w}_3^* \tag{3.17}$$

which also implies $\tilde{\mathbf{I}}_M \mathbf{W}_B = \mathbf{W}_B^*$. Due to the conjugate centro-symmetry property of the element space manifold vectors as described by (2.2), it is straightforward to show

$$\mathbf{b}(u) = \mathbf{W}_B^H \mathbf{a}(u) = \mathbf{W}_B^T \tilde{\mathbf{I}}_M \tilde{\mathbf{I}}_M \mathbf{a}^*(u) = \mathbf{W}_B^T \mathbf{a}^*(u) = \mathbf{b}^*(u) \tag{3.18}$$

Therefore, $\mathbf{b}(u)$ is real for all u. The second constraint states that

$$\tilde{\mathbf{I}}_3 \mathbf{W}_B^H \mathbf{a}(-u) = \mathbf{W}_B^H \mathbf{a}(u) \tag{3.19}$$

Incorporating the fact that $\mathbf{a}(-u) = \tilde{\mathbf{I}}_M \mathbf{a}(u)$ and that $\tilde{\mathbf{I}}_M \mathbf{W}_B = \mathbf{W}_B^*$, (3.19) can be written as

$$\tilde{\mathbf{I}}_3 \mathbf{W}_B^H \tilde{\mathbf{I}}_M \tilde{\mathbf{I}}_M \mathbf{a}(-u) = \tilde{\mathbf{I}}_3 \mathbf{W}_B^H \tilde{\mathbf{I}}_M \mathbf{a}(u) = \mathbf{W}_B^H \mathbf{a}(u) \tag{3.20}$$

which is guaranteed by taking $\tilde{\mathbf{I}}_3 \mathbf{W}_B^H \tilde{\mathbf{I}}_M = \mathbf{W}_B^H$. These two constraints on $\mathbf{W}_B$ combined together suggest that the three columns of $\mathbf{W}_B$ should be chosen in the following manner

$$\mathbf{W}_B = \left[\mathbf{w}_1 \vdots \mathbf{w}_o \vdots \tilde{\mathbf{I}}_M \mathbf{w}_1 \right]$$

$$\text{with : } \tilde{\mathbf{I}}_M \mathbf{w}_1 = \mathbf{w}_1^* \ ; \ \tilde{\mathbf{I}}_M \mathbf{w}_o = \mathbf{w}_o = \mathbf{w}_o^* \tag{3.21}$$

The center beamforming weight vector is thus restricted to be purely real. Substitution of (3.21) into (3.14) yields

$$\tilde{\mathbf{I}}_M \mathbf{C} \mathbf{u}_1 = \tilde{\mathbf{I}}_M \mathbf{C} \tilde{\mathbf{I}}_3 \tilde{\mathbf{I}}_3 \mathbf{u}_1 = \mathbf{C}^* \mathbf{u}_1^* \tag{3.22a}$$

$$\tilde{\mathbf{I}}_M \mathbf{C} \mathbf{u}_2 = \tilde{\mathbf{I}}_M \mathbf{C} \tilde{\mathbf{I}}_3 \tilde{\mathbf{I}}_3 \mathbf{u}_2 = \mathbf{C} \mathbf{u}_2 = \mathbf{C}^* \mathbf{u}_2^* \tag{3.22b}$$

$$\tilde{\mathbf{I}}_M \mathbf{C} \mathbf{u}_3 = \tilde{\mathbf{I}}_M \mathbf{C} \tilde{\mathbf{I}}_3 \tilde{\mathbf{I}}_3 \mathbf{u}_3 = \mathbf{C} \mathbf{u}_1 \tag{3.22c}$$

Sufficient conditions for satisfying (3.22) are easily found to be

$$\tilde{\mathbf{I}}_M \mathbf{C} \tilde{\mathbf{I}}_3 = \mathbf{C} = \mathbf{C}^* \tag{3.23a}$$

$$\tilde{\mathbf{I}}_3 \mathbf{u}_1 = \mathbf{u}_1^* = \mathbf{u}_3 \tag{3.23b}$$

$$\tilde{\mathbf{I}}_3 \mathbf{u}_2 = \mathbf{u}_2 = \mathbf{u}_2^* \tag{3.23c}$$

with (3.23a) in turn guaranteed by

$$\tilde{\mathbf{I}}_{M-2} \mathbf{c} = \mathbf{c} = \mathbf{c}^* \tag{3.24}$$

Note that the real quantities involved in the above relations are $\mathbf{c}$, $\mathbf{C}$, $\mathbf{u}_2$, and $\mathbf{w}_o$. (3.21)-(3.23) provide a guideline for constructing generalized Butler matrix beamformers for the BDML estimation schemes developed in Chapter 2. However, we mention that some auxiliary procedures should be performed to account for the SNR gain and sidelobe problems occurred in low-angle radar tracking. For example, we might want to maximize the response of the

beamformer at desired look directions while at the same time rejecting undesired returns from clutter and noise as well. In the case of strong interferences, it is necessary to form adaptive lower, center, and upper beams such that each beam has a null in each interfering direction and the three beams have M-3 nulls in common. The generalized Butler beamformer so constructed may not exhibit the properties described by (3.21)-(3.23). As a result, the BDML estimators may fail to handle 0° phase difference in the case of symmetric multipath. To remedy this difficulty, we propose, in the next subsection, an alternative approach to formulating the BDML problems, utilizing the fact that the Vandermonde structure is retained in beamspace domain via the use of C.

3.3.2 Alternative BDML Methods

A structural means for interpreting the C matrix given by (3.15) is that it can be considered as a beamforming matrix itself with three beams formed from the outputs of three identical, adjacent, overlapping subarrays of size M-2, each subarray having all but one sensor in common with the adjacent one. The weight vector **c**, corresponding to the common roots, is applied to each subarray. This represents a class of element space to beamspace transformations alternative to that proposed by Cantrell et. al. [CANT81]. The main difference between these two methods lies in that Cantrell et. al. developed their ML estimators based on "nonoverlapping" subarrays. We here develop new BDML estimators with the overlapping subarrays approach.

Let $\mathbf{a}_N(u)$ denote the Nx1 array manifold vector associated with angle u as given by

$$\mathbf{a}_N(u) = \left[e^{-j\pi\frac{N-1}{2}u}, \cdots, e^{-2j\pi u}, e^{-j\pi u}, 1, e^{j\pi u}, e^{2j\pi u}, \cdots, e^{j\pi\frac{N-1}{2}u} \right]^T \quad (3.25)$$

The transformation from an Mx1 element space manifold vector to a 3x1 beamspace manifold vector achieved with the Mx3 generalized Butler matrix beamformer $\mathbf{W}_B$ is described by

$$\mathbf{W}_B^H \mathbf{a}_M(u) = \mathbf{U}^H \mathbf{C}^H \mathbf{a}_M(u) = \mathbf{U}^H \mathbf{a}_3(u) G(u) \quad (3.26)$$

where

$$G(u) = \mathbf{c}^H \mathbf{a}_{M-2}(u) \quad (3.27)$$

which leads to the asymptotic beamspace correlation matrix given by

$$\mathbf{R}_{bb} = \mathbf{W}_B^H \left\{ \mathbf{A}\mathbf{R}_{ss}\mathbf{A}^H + \sigma_n^2 \mathbf{I}_3 \right\} \mathbf{W}_B$$

$$= \mathbf{U}^H \mathbf{C}^H \mathbf{A}\mathbf{R}_{ss}\mathbf{A}^H \mathbf{C}\mathbf{U} + \sigma_n^2 \mathbf{U}^H \mathbf{C}^H \mathbf{C}\mathbf{U}$$

$$= \mathbf{U}^H \mathbf{A}_3 \mathbf{R}_{ss}^G \mathbf{A}_3^H \mathbf{U} + \sigma_n^2 \mathbf{U}^H \mathbf{C}^H \mathbf{C}\mathbf{U}$$

$$= \mathbf{U}^H \left\{ \mathbf{A}_3 \mathbf{R}_{ss}^G \mathbf{A}_3^H + \sigma_n^2 \mathbf{C}^H \mathbf{C} \right\} \mathbf{U} = \mathbf{U}^H \mathbf{R}_{cc} \mathbf{U} \tag{3.28}$$

where

$$\mathbf{A}_3 = \left[\mathbf{a}_3(u_1) \vdots \mathbf{a}_3(u_2) \right] \tag{3.29a}$$

$$\mathbf{R}_{ss}^G = \mathbf{G}\mathbf{R}_{ss}\mathbf{G}^H \tag{3.29b}$$

$$\mathbf{G} = \begin{bmatrix} G(u_1) & 0 \\ 0 & G(u_2) \end{bmatrix} \tag{3.29c}$$

and G(u) is defined by (3.27). This states that the beamspace correlation matrix thus constructed has exactly the same compositional structure as the element space correlation matrix except for the multiplicative matrix factor **U**, which is usually chosen to be nonsingular. Under such a condition, $\mathbf{R}_{cc}$ is simply obtained from $\mathbf{R}_{bb}$ via the following relation

$$\mathbf{R}_{cc} = (\mathbf{U}^H)^{-1} \mathbf{R}_{bb} \mathbf{U}^{-1} \tag{3.30}$$

With $\mathbf{R}_{cc}$ constructed, we proceed to develop the corresponding BDML estimators. We first consider the more general nonsymmetric multipath case.

Following the development in Section 2.3 and 2.4, we obtain an optimization problem described by

$$\underset{\mathbf{v}_c}{\text{Minimize}} \quad \frac{\mathbf{v}_c^H \hat{\mathbf{R}}_{cc} \mathbf{v}_c}{\mathbf{v}_c^H \mathbf{P} \mathbf{v}_c} \tag{3.31}$$

where $\hat{\mathbf{R}}_{cc} = (\mathbf{U}^H)^{-1} \hat{\mathbf{R}}_{bb} \mathbf{U}^{-1}$, $\mathbf{P} = \mathbf{C}^H \mathbf{C}$, and $\mathbf{v}_c$ satisfies $\mathbf{v}_c^H \mathbf{a}_3(u_1) = \mathbf{v}_c^H \mathbf{a}_3(u_2) = 0$. If $\mathbf{v}_c = [v_{c1}\ v_{c2}\ v_{c3}]$ is the solution to (3.31), then $e^{j\pi u_1}$ and $e^{j\pi u_2}$ can be estimated as the two roots of the following polynomial equation:

$$v_c(z) = v_{c1} + v_{c2} z + v_{c3} z^2 = 0 \tag{3.32}$$

To account for the fact that the roots must lie on the unit circle, we impose

the constraint $\tilde{I}_3 v_c = v_c^*$ in (3.31), knowing that it is only a necessary condition for $v_c(z)$ to have unit roots. Utilizing the technique described in Section 2.3 for solving the symmetric BDML problem, (3.31) combined with the conjugate centro-symmetry constraint can be written as

$$\underset{v_c}{\text{Minimize}} \quad \frac{v_c^H \hat{R}_{cc} v_c + v_c^T \tilde{I}_3 \hat{R}_{cc} \tilde{I}_3 v_c^*}{v_c^T P v_c + v_c^H \tilde{I}_3 P \tilde{I}_3 v_c^*} \tag{3.33}$$

$$\text{subject to} \quad \tilde{I}_3 v_c = v_c^*$$

Note that $v_c^H \hat{R}_{cc} v_c$ and $v_c^H P v_c$ are real such that (3.33) simplifies to

$$\underset{v_c}{\text{Minimize}} \quad \frac{v_c^H \{\hat{R}_{cc} + \tilde{I}_3 \hat{R}_{cc}^* \tilde{I}_3\} v_c}{v_c^H \{P + \tilde{I}_3 P^* \tilde{I}_3\} v_c} = \frac{v_c^H \hat{R}_{cc}^{fb} v_c}{v_c^H P^{fb} v_c} \tag{3.34}$$

$$\text{subject to} \quad \tilde{I}_3 v_c = v_c^*$$

A proof similar to that given in Appendix A shows that each of the three generalized eigenvectors (GEVEC) of the matrix pencil $\{\hat{R}_{cc}^{fb}, P^{fb}\}$ exhibits conjugate centro-symmetry such that the minimizing v_c for (3.34) is simply taken to be the one associated with the smallest generalized eigenvalue. Denoting as $[\mu, 1, \mu^*]^T$ the optimum v_c thus found, with the middle component normalized to be unity, the two roots of $v_c(z) = \mu + z + \mu^* z^2$ are given by $\frac{-1 \pm \sqrt{1 - 4|\mu|^2}}{2\mu^*}$, leading to the following ML estimates of u_1 and u_2:

$$\hat{u}_1 = \frac{1}{j\pi} \ln\left\{\frac{-1+\sqrt{1-4|\mu|^2}}{2\mu^*}\right\} \tag{3.35a}$$

$$\hat{u}_2 = \frac{1}{j\pi} \ln\left\{\frac{-1-\sqrt{1-4|\mu|^2}}{2\mu^*}\right\} \tag{3.35b}$$

Consequently, the two signals are not resolved if $1-4|\mu|^2 > 1$, or $|\mu| < \frac{1}{2}$.

We here summarize the new BDML method for nonsymmetric multipath case.

Algorithmic Summary of Non-Symmetric BDML Method with Generalized Butler Beamformer

(1.) With $\mathbf{W}_B = \left[\mathbf{w}_1 \vdots \mathbf{w}_2 \vdots \mathbf{w}_3\right] = \mathbf{CU}$ as given by (3.14) and $\hat{\mathbf{R}}_{xx} = \frac{1}{N}\sum_{n=1}^{N} \mathbf{x}(n)\mathbf{x}^H(n)$, form $\hat{\mathbf{R}}_{bb} = \mathbf{W}_B^H \hat{\mathbf{R}}_{xx} \mathbf{W}_B$.

(2.) Form $\hat{\mathbf{R}}_{cc} = (\mathbf{U}^H)^{-1} \hat{\mathbf{R}}_{bb} \mathbf{U}^{-1}$ and $\mathbf{P} = \mathbf{C}^H\mathbf{C}$.

(3.) With $\hat{\mathbf{R}}_{cc}^{fb} = \frac{1}{2}\left\{\hat{\mathbf{R}}_{cc} + \tilde{\mathbf{I}}_3 \hat{\mathbf{R}}_{cc}^{*} \tilde{\mathbf{I}}_3\right\}$ and $\mathbf{P}^{fb} = \mathbf{P} + \tilde{\mathbf{I}}_3 \mathbf{P}^{*} \tilde{\mathbf{I}}_3$, compute $\mathbf{v}_c = [\mu\ ,\ 1\ ,\ \mu^{*}]^T$ as GEVEC of 3x3 pencil $\{\hat{\mathbf{R}}_{cc}^{fb}\ ,\ \mathbf{P}^{fb}\}$ associated with smallest GEV.

(4.) If $|\mu| < \frac{1}{2}$, multipath signals not resolved. Otherwise:

(5.) $\hat{u}_1 = \frac{1}{j\pi}\ln\left\{\frac{-1+\sqrt{1-4|\mu|^2}}{2\mu^{*}}\right\}$; $\hat{u}_2 = \frac{1}{j\pi}\ln\left\{\frac{-1-\sqrt{1-4|\mu|^2}}{2\mu^{*}}\right\}$

The above development can be easily extended to the symmetric multipath case with slight modification. To begin with, consider the quadratic polynomial $v_c(z)$ with two unit roots occurring at $z = e^{\pm j\pi u_o}$.

$$v_c(z) = (z - e^{j\pi u_o})(z - e^{-j\pi u_o}) \tag{3.36}$$

The two roots of $v_c(z)$ form complex conjugate pair, implying that each of the coefficients of $v_c(z)$ must be real, and together they must exhibit centro-symmetry property. Combining this observation with the fact that $\mathbf{x}^T\mathbf{R}\mathbf{x} = \mathbf{x}^T\mathrm{Re}\{\mathbf{R}\}\mathbf{x}$ if $\mathbf{x}$ is real and $\mathbf{R}$ is hermitian, we arrive at the following optimization problem leading to the ML angle estimates for symmetric multipath

$$\underset{\mathbf{v}_c}{\text{Minimize}} \quad \frac{\mathbf{v}_c^H\, \mathrm{Re}\{\hat{\mathbf{R}}_{cc}^{fb}\}\, \mathbf{v}_c}{\mathbf{v}_c^H\, \mathrm{Re}\{\mathbf{P}^{fb}\}\, \mathbf{v}_c} \tag{3.37}$$

$$\text{subject to } \tilde{\mathbf{I}}_3 \mathbf{v}_c = \mathbf{v}_c$$

where $\mathrm{Re}\{\hat{\mathbf{R}}_{cc}^{fb}\}$ and $\mathrm{Re}\{\mathbf{P}^{fb}\}$ satisfy

$$\mathrm{Re}\{\hat{\mathbf{R}}_{cc}^{fb}\} = \mathrm{Re}\{\hat{\mathbf{R}}_{cc}^{fb}\}^T \ ;\ \tilde{\mathbf{I}}_3 \mathrm{Re}\{\hat{\mathbf{R}}_{cc}^{fb}\}\tilde{\mathbf{I}}_3 = \mathrm{Re}\{\hat{\mathbf{R}}_{cc}^{fb}\} \tag{3.38a}$$

$$\mathrm{Re}\{\mathbf{P}^{fb}\} = \mathrm{Re}\{\mathbf{P}^{fb}\}^T \ ;\ \tilde{\mathbf{I}}_3 \mathrm{Re}\{\mathbf{P}^{fb}\}\tilde{\mathbf{I}}_3 = \mathrm{Re}\{\mathbf{P}^{fb}\} \tag{3.38b}$$

Therefore, (3.37) manifests itself as a problem identical in form to that

described by (2.32). The minimizing $\mathbf{v}_c$, then, is that centro-symmetric generalized eigenvector (CS-GEVEC) of the 3x3 matrix pencil $\{\mathrm{Re}\{\hat{\mathbf{R}}_{cc}^{fb}\}, \mathrm{Re}\{\mathbf{P}^{fb}\}\}$ associated with the smaller generalized eigenvalue. Letting $[1, \gamma, 1]$ be the optimum real, centro-symmetric vector, the two roots of the polynomial $1 + \gamma z + z^2$ form complex conjugate pair and are located on the unit circle if and only if $|\gamma| < 2$, in which case they are given by $-\frac{\gamma}{2} \pm j\frac{1}{2}\sqrt{4-\gamma^2}$. The ML estimate of the direct path angle u_o is then determined by

$$\hat{u}_o = \frac{1}{j\pi}\ln\left\{-\frac{\gamma}{2} + j\frac{1}{2}\sqrt{4-\gamma^2}\right\} \tag{3.39}$$

with $|\gamma| > 2$ serves as a flag that the algorithm failed to resolve the two signals.

We conclude this section by presenting the algorithmic summary for the symmetric BDML method when a generalized Butler beamformer is employed

Algorithmic Summary of Symmetric BDML Method
with Generalized Butler Beamformer

(1.) With $\mathbf{W} = \left[\mathbf{w}_1 \vdots \mathbf{w}_2 \vdots \mathbf{w}_3\right] = \mathbf{CU}$ as given by (3.14) and $\hat{\mathbf{R}}_{xx} = \frac{1}{N}\sum_{n=1}^{N}\mathbf{x}(n)\mathbf{x}^H(n)$, form $\hat{\mathbf{R}}_{bb} = \mathbf{W}^H\hat{\mathbf{R}}_{xx}\mathbf{W}$.

(2.) Form $\hat{\mathbf{R}}_{cc} = (\mathbf{U}^H)^{-1}\hat{\mathbf{R}}_{bb}\mathbf{U}^{-1}$ and $\mathbf{P} = \mathbf{C}^H\mathbf{C}$.

(3.) With $\hat{\mathbf{R}}_{cc}^{fb} = \frac{1}{2}\left\{\hat{\mathbf{R}}_{cc} + \tilde{\mathbf{I}}_3\hat{\mathbf{R}}_{cc}^{*}\tilde{\mathbf{I}}_3\right\}$ and $\mathbf{P}^{fb} = \frac{1}{2}\left\{\mathbf{P} + \tilde{\mathbf{I}}_3\mathbf{P}^{*}\tilde{\mathbf{I}}_3\right\}$, compute $\mathbf{v}_c = [1, \gamma, 1]^T$ as CS-EVEC of 3x3 real pencil $\left\{\mathrm{Re}\{\hat{\mathbf{R}}_{cc}^{fb}\}, \mathrm{Re}\{\mathbf{P}^{fb}\}\right\}$ assoc. with smaller EV.

(4.) If $|\gamma| > 2$, multipath signals not resolved. Otherwise:

(5.) $\hat{u}_o = \frac{1}{j\pi}\ln\left\{-\frac{\gamma}{2} + j\frac{1}{2}\sqrt{4-\gamma^2}\right\}$

3.4 Parameterization of Beamspace Manifold Vectors

As was discussed in the previous section, the generalized Butler beamformers facilitate simple, efficient BDML estimation primarily due to the fact that the Vandermonde structure of the element space manifold vector achieved with a linear uniformly-spaced array is achieved in beamspace as well. The transformation from an Mx1 element space Vandermonde manifold vector $\mathbf{a}(u)$ to a 3x1 real beamspace manifold vector $\mathbf{b}(u)$ using a beamforming matrix given in (3.14) is accomplished by a two-stage procedure. First, an Mx3 beamforming matrix $\mathbf{C}$ corresponding to three overlapping subarrays transforms $\mathbf{a}(u)$ into a 3x1 Vandermonde vector $\mathbf{c}(u)$ having the same compositional form as $\mathbf{a}(u)$. Second, $\mathbf{c}(u)$ is transformed into another 3x1 real vector $\mathbf{b}(u)$ by a 3x3 nonsingular matrix $\mathbf{U}^H$. Since the second stage involves only a nonsingular transformation, it is possible to recover the element space manifold vector from the beamspace manifold vector perfectly without loss of information by the following steps

$$\mathbf{c}(u) = \left[e^{-j\pi u} \vdots 1 \vdots e^{j\pi u} \right] = (\mathbf{U}^H)^{-1}\mathbf{b}(u)\, G^{-1}(u) \tag{3.40a}$$

$$\mathbf{a}(u) = \left[e^{-j\pi\frac{M-1}{2}u}, \ldots, e^{-2j\pi u}, e^{-j\pi u}, 1, e^{j\pi u}, e^{2j\pi u}, \ldots, e^{j\pi\frac{M-1}{2}u} \right]^T \tag{3.40b}$$

where $G(u)$ is given by (3.27). It is then clear that $\mathbf{a}(u)$ is fully recoverable from $\mathbf{b}(u)$ as long as $G(u) \neq 0$, which is true when u is not equal to any of the M-3 common nulls. Since two Vandermonde array manifold vectors are linear independent if and only if they correspond to different angles, the above observation may be alternatively interpreted as that there exists a one-to-one mapping between the element space manifold vectors and the beamspace manifold vectors except for those associated with the common nulls. This indicates that a simple parameterization of $\mathbf{b}(u)$ is possible with a generalized Butler matrix beamformer.

Consider again the equation relating $\mathbf{c}(u)$ and $\mathbf{b}(u)$ as given by (3.40a). Since we choose $\mathbf{U}$ to be such that $\tilde{\mathbf{I}}_3\mathbf{U} = \mathbf{U}^*$ and $\mathbf{b}(u)$ is real, we have

$$\tilde{\mathbf{I}}_3(\mathbf{U}^H)^{-1}\mathbf{b}(u) = (\mathbf{U}^H\tilde{\mathbf{I}}_3)^{-1}\mathbf{b}(u) = (\mathbf{U}^T)^{-1}\mathbf{b}(u) = \left[(\mathbf{U}^H)^{-1}\mathbf{b}(u)\right]^* \tag{3.41}$$

This verifies that $(\mathbf{U}^H)^{-1}\mathbf{b}(u)$ exhibits the desired conjugate centro-symmetry property as indicated by (3.40a) and is real-valued as well. Assuming $G(u) \neq 0$, (3.40a) implies that the first and second components of $(\mathbf{U}^H)^{-1}\mathbf{b}(u)$ must have the same nonzero magnitude. Thus, $|\bar{\mathbf{u}}_1^H\mathbf{b}(u)| = |\bar{\mathbf{u}}_2^H\mathbf{b}(u)|$,

where $\bar{u}_1$ and $\bar{u}_2$ denote the first and second columns of $\mathbf{U}^{-1}$, respectively. This leads to

$$\mathbf{b}^T(u)\mathrm{Re}\{V_d\}\mathbf{b}(u) = 0 \tag{3.42}$$

where

$$\left[\, \bar{u}_1 \vdots \bar{u}_2 \vdots \bar{u}_1^* \,\right] = \mathbf{U}^{-1} \tag{3.43a}$$

$$\mathbf{V}_d = \bar{u}_1\bar{u}_1^H - \bar{u}_2\bar{u}_2^T \tag{3.43b}$$

where we have used the fact that $\mathbf{b}(u)$ and $\bar{u}_2$ are real. Denoting as b_i the i-th component of $\mathbf{b}(u)$, and v_{ij} the (i,j)-th component of $\mathrm{Re}\{\mathbf{V}_d\}$, we obtain from (3.42) the following parametric equation for $\mathbf{b}(u)$

$$v_{11}b_1^2 + v_{22}b_2^2 + v_{33}b_3^2 + 2v_{12}b_1b_2 + 2v_{13}b_1b_3 + 2v_{23}b_2b_3 = 0 \tag{3.44}$$

knowing that $\mathrm{Re}\{\mathbf{V}_d\}$ is real and symmetric. (3.44) represents a quadratic surface in a three dimensional space indexed by (b_1,b_2,b_3). It is rather interesting to note that the shape of this parametric surface is completely determined by $\mathbf{V}_d$, which is in turn determined by $\mathbf{U}$. In other words, the parameterization of the beamspace manifold vectors is completely characterized by the uncommon nulls associated with the generalized Butler beamformer. It should be kept in mind, however, that the generalized Butler matrix beamformer itself is characterized not only by the uncommon nulls, but also by the common nulls.

The parametric expression described in (3.44) simplifies greatly if we substitute in the respective quantities associated with the Mx3 Butler matrix beamformer as given by (2.36). From (3.6) and (3.7), it is easily derived that the $\mathbf{U}$ matrix associated with the Mx3 Butler beamformer can be expressed as

$$\mathbf{U} = \mathbf{E} = \begin{bmatrix} e^{j\frac{\pi}{M}} & 1 & e^{-j\frac{\pi}{M}} \\ -2\cos\frac{\pi}{M} & -2\cos\frac{2\pi}{M} & -2\cos\frac{\pi}{M} \\ e^{-j\frac{\pi}{M}} & 1 & e^{j\frac{\pi}{M}} \end{bmatrix} \tag{3.45}$$

with its inverse given by

$$\mathbf{E}^{-1} = \begin{bmatrix} \xi e^{j\frac{2\pi}{M}} & \xi & \xi e^{-j\frac{2\pi}{M}} \\ \eta & \eta & \eta \\ \xi e^{-j\frac{2\pi}{M}} & \xi & \xi e^{j\frac{2\pi}{M}} \end{bmatrix} \tag{3.46}$$

where

$$\xi = \left[2\cos\frac{3\pi}{M} - 2\cos\frac{\pi}{M}\right]^{-1} \quad ; \quad \eta = \left[2 - 2\cos\frac{2\pi}{M}\right]^{-1} \tag{3.47}$$

Substitution of (3.46) and (3.47) into (3.43) accompanied by some algebraic manipulation yields the following expression for $\mathrm{Re}\{\mathbf{V}_d\}$ for the case of an Mx3 Butler beamformer:

$$\mathrm{Re}\{\mathbf{V}_{Bd}\} = \xi \begin{bmatrix} 0 & \eta(\cos\frac{2\pi}{M} - 1) & \xi(\cos\frac{4\pi}{M} - 1) \\ \eta(\cos\frac{2\pi}{M} - 1) & 0 & \eta(\cos\frac{2\pi}{M} - 1) \\ \xi(\cos\frac{4\pi}{M} - 1) & \eta(\cos\frac{2\pi}{M} - 1) & 0 \end{bmatrix} \tag{3.48}$$

It is noteworthy that $\mathrm{Re}\{\mathbf{V}_{Bd}\}$ has only three distinct components, **0**, $\xi^2(\cos\frac{4\pi}{M} - 1)$, and $\xi\eta(\cos\frac{2\pi}{M} - 1)$. Since (3.42) is invariant under scaling, we may normalize $\mathrm{Re}\{\mathbf{V}_{Bd}\}$ by its (1,2)-th component and substitute the resulting normalized quantities into (3.44). Not surprisingly, the parametric equation in this case simplies greatly to the following form

$$(b_1 + b_3)b_2 + \beta b_1 b_3 = 0 \tag{3.49}$$

where

$$\beta = \frac{\eta(\cos\frac{2\pi}{M} - 1)}{\xi(\cos\frac{4\pi}{M} - 1)} \tag{3.50}$$

As should be noted, (3.49) defines the relationship between the three components of **b**(u) only in relative terms. That is, we can multiply **b**(u) by an arbitrary scalar and still satisfy (3.49). However, since we have already shown that two beamspace manifold vectors associated with two distinct angles (except for those associated with the common nulls) are linearly independent, multiplying **b**(u) by a nonzero scalar does not cause ambiguities at all. As a

check, we consider several cases that appear to be interesting.

(1) $b_2 = 0$: This implies $b_1 b_3 = 0$. Three possible cases are:

$$b_1 = 0 \ \& \ b_3 \neq 0 \ \Rightarrow \ u = -\frac{2}{M}$$

$$b_1 \neq 0 \ \& \ b_3 = 0 \ \Rightarrow \ u = \frac{2}{M}$$

$$b_1 = 0 \ \& \ b_3 = 0 \ \Rightarrow \ u = \text{any common null}$$

(2) $b_2 \neq 0$: In this case, we can set b_2 to be unity and relate b_1 and b_3 by

$$b_3 = \frac{-b_1}{1 + b_1 \beta} \tag{3.51}$$

Some interesting cases are:

$$b_1 = 0 \ \& \ b_3 = 0 \ \Rightarrow \ u = 0$$

$$1 + b_1 \beta \rightarrow 0 \ \Rightarrow \ u \rightarrow -\frac{2}{M}$$

It is easily verified that within the interval $(-\frac{2}{M}, \frac{2}{M})$, both b_2 and $1+b_1\beta$ are nonzero such that $\mathbf{b}(u)$ can be expressed in terms of a single parameter as given by

$$\mathbf{b}(u) \equiv \mathbf{b}(t) = \begin{bmatrix} t \\ 1 \\ -\frac{t}{1 + t\beta} \end{bmatrix} \tag{3.52}$$

With this parametric expression for $\mathbf{b}(u)$, we may proceed to obtain u as a function of t. From (3.40a) and (3.43), $e^{j\pi u}$ can be written in terms of $\mathbf{b}(u)$ in the following fashion

$$e^{j\pi u} = \frac{\bar{\mathbf{u}}_3^H \mathbf{b}(u)}{\bar{\mathbf{u}}_2^H \mathbf{b}(u)} \tag{3.53}$$

which in turn leads to

$$u = \frac{1}{j\pi}\ln\left\{\frac{\bar{\mathbf{u}}_3^H \mathbf{b}(u)}{\bar{\mathbf{u}}_2^H \mathbf{b}(u)}\right\} \tag{3.54}$$

Upon substitution of (3.46) and (3.52) into (3.54), we end up with the following equation relating u and t for the Mx3 Butler matrix beamformer

$$u = \frac{1}{j\pi}\ln\left\{\frac{(\xi e^{j\frac{2\pi}{M}} t + \eta)(1 + \beta t) - \xi e^{-j\frac{2\pi}{M}} t}{(\xi t + \eta)(1 + \beta t) - \xi t}\right\} \tag{3.55}$$

The above described parameterization for $\mathbf{b}(u)$ provides an alternative approach to obtaining the BDML estimates from the optimum v vector orthogonal to both $\mathbf{b}(u_1)$ and $\mathbf{b}(u_2)$. First, substituting into $\mathbf{v}^T\mathbf{b}(u) = 0$ the parametric expression given in (3.55) yields a quadratic equation in t in the following form

$$v_2 + (v_1 - v_3 + v_2\beta)t + v_1\beta t^2 = 0 \tag{3.56}$$

which has two solutions for t given by

$$\hat{t}_{1,2} = \frac{-(v_1 - v_3 + v_2\beta) \pm \sqrt{(v_1 - v_3 + v_2\beta)^2 - 4v_1v_2}}{2v_1\beta} \tag{3.57}$$

Since t must be real, we have the following constraint on the components of v

$$(v_1 - v_3 + v_2\beta)^2 - 4v_1v_2 \geq 0 \tag{3.58}$$

which is easily shown to be equivalent to that described in Section 2.4. Therefore, a failure should be registered if v fails to satisfy (3.58). Second, with $\hat{t}_1$ and $\hat{t}_2$ available, the angle estimates $\hat{u}_1$ and $\hat{u}_2$ are simply determined by

$$\hat{u}_1 = \frac{1}{j\pi}\ln\left\{\frac{(\xi e^{j\frac{2\pi}{M}} \hat{t}_1 + \eta)(1 + \beta\hat{t}_1) - \xi e^{-j\frac{2\pi}{M}} \hat{t}_1}{(\xi\hat{t}_1 + \eta)(1 + \beta\hat{t}_1) - \xi\hat{t}_1}\right\} \tag{3.59a}$$

$$\hat{u}_2 = \frac{1}{j\pi}\ln\left\{\frac{(\xi e^{j\frac{2\pi}{M}}\hat{t}_2 + \eta)(1+\beta\hat{t}_2) - \xi e^{-j\frac{2\pi}{M}}\hat{t}_2}{(\xi\hat{t}_2 + \eta)(1+\beta\hat{t}_2) - \xi\hat{t}_2}\right\} \tag{3.59b}$$

For the special case of symmetric multipath, $v_1 = v_3$ such that (3.57) simplies to

$$\hat{t}_{1,2} = \frac{-v_2\beta \pm \sqrt{(v_2\beta)^2 - 4v_1v_2}}{2v_1\beta} \tag{3.60}$$

with $(v_2\beta)^2 - 4v_1v_2 \leq 0$ indicating failure. By direct calculation we can show that $\hat{t}_1$ and $\hat{t}_2$ are related according to

$$\hat{t}_2 = \frac{-\hat{t}_1}{1+\beta\hat{t}_1} \tag{3.61a}$$

$$\hat{t}_1 = \frac{-\hat{t}_2}{1+\beta\hat{t}_2} \tag{3.61b}$$

which implies that the two associated beamspace manifold vectors satisfy

$$\tilde{\mathbf{I}}_3\mathbf{b}(\hat{t}_1) = \mathbf{b}(\hat{t}_2) \tag{3.62}$$

From (3.59), the BDML estimate of the direct path angle is given by

$$\hat{u}_1 = \frac{1}{j\pi}\ln\left\{\frac{(\xi e^{j\frac{2\pi}{M}}\hat{t}_1 + \eta)(1+\beta\hat{t}_1) - \xi e^{-j\frac{2\pi}{M}}\hat{t}_1}{(\xi\hat{t}_1 + \eta)(1+\beta\hat{t}_1) - \xi\hat{t}_1}\right\} \tag{3.63}$$

Substituting (3.61b) into (3.63), we get, after a little manipulation, the following relation

$$\hat{u}_1 = \frac{1}{j\pi}\ln\left\{\frac{(\xi e^{-j\frac{2\pi}{M}}\hat{t}_2 + \eta)(1+\beta\hat{t}_2) - \xi e^{j\frac{2\pi}{M}}\hat{t}_2}{(\xi\hat{t}_2 + \eta)(1+\beta\hat{t}_2) - \xi\hat{t}_2}\right\}$$

$$= \frac{1}{j\pi}\ln\left\{\frac{(\xi e^{j\frac{2\pi}{M}}\hat{t}_2 + \eta)(1+\beta\hat{t}_2) - \xi e^{-j\frac{2\pi}{M}}\hat{t}_2}{(\xi\hat{t}_2 + \eta)(1+\beta\hat{t}_2) - \xi\hat{t}_2}\right\}^* \tag{3.64}$$

Since the argument of the log function in (3.64) has unity magnitude, it is

easily deduced that $\hat{u}_1 = -\hat{u}_2$ as was expected.

The BDML estimation procedures for both symmetric and nonsymmetric cases employing an Mx3 Butler matrix beamformer and the parameterization described above are summarized below. To be consistent with the notations used previously in Chapter 2, we denote as u_o and t_o the direct path angle and its associated parameter for the symmetric case.

Algorithmic Summary of Symmetric BDML Method
With Butler Beamformer and Parameterization

(0.) $\xi = \left(2\cos\frac{3\pi}{M} - 2\cos\frac{\pi}{M}\right)^{-1}$; $\eta = \left(2 - 2\cos\frac{2\pi}{M}\right)^{-1}$; $\beta = \frac{\eta(\cos\frac{2\pi}{M} - 1)}{\xi(\cos\frac{4\pi}{M} - 1)}$

(1.) With $\mathbf{S} = \left[\mathbf{a}(2/M) : \mathbf{a}(0) : \mathbf{a}(-2/M)\right]$ & $\hat{\mathbf{R}}_{xx} = \frac{1}{N}\sum_{n=1}^{N}\mathbf{x}(n)\mathbf{x}^H(n)$, form $\hat{\mathbf{R}}_{bb} = \mathbf{S}^H\hat{\mathbf{R}}_{xx}\mathbf{S}$.

(2.) Compute $\mathbf{v} = [v_1, v_2, v_1]^T$ as that CS-EVEC of $\mathrm{Re}\{\hat{\mathbf{R}}_{bb}^{fb}\} = \frac{1}{2}\mathrm{Re}\left\{\hat{\mathbf{R}}_{bb} + \tilde{\mathbf{I}}_3\hat{\mathbf{R}}_{bb}\tilde{\mathbf{I}}_3\right\}$ associated with the smaller EV.

(3.) If $(v_2\beta)^2 - 4v_1v_2 \leq 0$, signals not resolved.

(4.) Otherwise: With v_2 and v_1 determined in (2.), compute t_o according to:

$$t_o = \frac{-v_2\beta + \sqrt{(v_2\beta)^2 - 4v_1v_2}}{2v_1\beta}$$

(5.) Estimate u_o according to:

$$\hat{u}_o = \frac{1}{j\pi}\ln\left\{\frac{(\xi e^{j\frac{2\pi}{M}}\hat{t}_o + \eta)(1 + \beta\hat{t}_o) - \xi e^{-j\frac{2\pi}{M}}\hat{t}_o}{(\xi\hat{t}_o + \eta)(1 + \beta\hat{t}_o) - \xi\hat{t}_o}\right\}$$

Algorithmic Summary of Nonsymmetric BDML Method
With Butler Beamformer and Parameterization

(0.) $\xi = \left(2\cos\frac{3\pi}{M} - 2\cos\frac{\pi}{M}\right)^{-1}$; $\eta = \left(2 - 2\cos\frac{2\pi}{M}\right)^{-1}$; $\beta = \frac{\eta(\cos\frac{2\pi}{M} - 1)}{\xi(\cos\frac{4\pi}{M} - 1)}$

(1.) With $\mathbf{S}=\left[\mathbf{a}(2/M):\mathbf{a}(0):\mathbf{a}(-2/M)\right]$ & $\hat{\mathbf{R}}_{xx}=\frac{1}{N}\sum_{n=1}^{N}\mathbf{x}(n)\mathbf{x}^H(n)$, form $\hat{\mathbf{R}}_{bb}=\mathbf{S}^H\hat{\mathbf{R}}_{xx}\mathbf{S}$.

(2.) Compute $\mathbf{v}=[v_1\ ,\ v_2\ ,\ v_3]^T$ as EVEC of 3x3 matrix $\mathrm{Re}\{\hat{\mathbf{R}}_{bb}\}$ assoc. with smallest EV.

(3.) If $(v_1-v_3+v_2\beta)^2-4v_1v_2\geq 0$, signal not resolved.

(4.) Otherwise: With v_1, v_2, and v_3 determined in (2.), compute t_1 and t_2 according to:

$$\hat{t}_{1,2}=\frac{-(v_1-v_3+v_2\beta)\pm\sqrt{(v_1-v_3+v_2\beta)^2-4v_1v_2}}{2v_1\beta}$$

(5.) Estimate u_1 and u_2 according to:

$$\hat{u}_1=\frac{1}{j\pi}\ln\left\{\frac{(\xi e^{j\frac{2\pi}{M}}\hat{t}_1+\eta)(1+\beta\hat{t}_1)-\xi e^{-j\frac{2\pi}{M}}\hat{t}_1}{(\xi\hat{t}_1+\eta)(1+\beta\hat{t}_1)-\xi\hat{t}_1}\right\}$$

$$\hat{u}_2=\frac{1}{j\pi}\ln\left\{\frac{(\xi e^{j\frac{2\pi}{M}}\hat{t}_2+\eta)(1+\beta\hat{t}_2)-\xi e^{-j\frac{2\pi}{M}}\hat{t}_2}{(\xi\hat{t}_2+\eta)(1+\beta\hat{t}_2)-\xi\hat{t}_2}\right\}$$

As a final remark, we note that the above described parameterization for the beamspace manifold vectors depends only upon the uncommon nulls and can be readily extended to other generalized Butler beamformers. For the special class of beamformers whose uncommon nulls are formed in a fashion identical to that associated with the Mx3 Butler beamformer, we have exactly the same parametric equation as that described by (3.49). However, this does not mean that all Mx3 generalized Butler matrix beamformer with the same set of uncommon nulls will produce the same BDML estimates since the estimation of the optimum $\mathbf{v}$ vector in (3.56) depends upon selection of the common nulls as well. To achieve good performance, one needs to assure that selection of both the common and uncommon nulls leads to high SNR gain in the vicinity of the two targets. It should also be noted that the two alternative BDML estimation procedures summarized above are not computationally more efficient than the original ones developed in Chapter 2. Rather, the major motivation of working with the parametric expression is that it provides a simpler way of illustrating the behavior of the beamspace manifold vectors,

simpler way of illustrating the behavior of the beamspace manifold vectors, which may not have closed-form expression in terms of u in general.

CHAPTER 4
REFINEMENTS TO BEAMSPACE DOMAIN ML ESTIMATOR FOR COHERENT MULTIPATH

4.1 Introduction

We noted in Section 2.4 that the performance of the BDML estimator for both the symmetric and nonsymmetric multipath cases degrades severely in a coherent environment when the direct and specular path signals arrive at the center element of the array very nearly equal in amplitude and perfectly or very nearly 180° out of phase. In addition, the BDML Method for nonsymmetric multipath breaks down when the direct and specular path signals arrive perfectly 0° in-phase at the center element of the array as well. To overcome these problems, we propose three auxiliary algorithms for the BDML estimator. The first algorithm presented in Section 4.2 deals solely with the symmetric multipath scenario. The a-priori information about the constant complex reflection coefficient in the case of coherent multipath is incorporated in order to reduce the track breaking probability. In Section 4.3, an ad-hoc procedure is developed for converting a nonsymmetric problem into a symmetric one. Estimation of the bisector angle between the two paths is first done, followed by a secondary steering of the three beams. A novel efficient frequency diversity scheme, which is equally applicable to both the symmetric and nonsymmetric cases, is then presented in Section 4.4.

4.2 Estimation of the Reflection Coefficient

If the surface of reflection is relatively smooth, and the target is not moving too fast in relative terms, the specular multipath signal is merely a time-delayed, amplitude-attenuated replica of the direct path signal over multiple snapshots. This condition is referred to as coherent multipath. Due to the sinusoidal nature of the returning signals, the time-delay translates into a phase-shift such that $c_2(n) = \rho e^{j\Delta\Psi} c_1(n)$, where ρ is the magnitude of the surface reflection coefficient and $\Delta\Psi$ is the phase difference between the two signals measured at the center of the array.

4.2.1 Development of the Algorithm

Let $\rho_c = \rho e^{j\Delta\Psi}$ denote the complex reflection coefficient. The beamspace snapshot vector in the case of coherent symmetric multipath may be expressed in the following manner:

$$\mathbf{x}_B(n) = [\mathbf{b}(u_o) + \rho_c \mathbf{b}(-u_o)]c_1(n) + \mathbf{n}_B(n) \quad n=1,...,N \tag{4.1}$$

The fact that ρ_c is constant over the observation interval changes the complexion of the ML formulation of the problem of estimating the direct path angle. Indeed, it represents a-priori information about a coherent multipath scenario which needs to be incorporated into the ML estimation scheme. Of course, we are assuming that N, possibly one corresponding to a single snapshot, is small or the assumption of coherence may be invalidated.

We proceed motivated by the work of Ballance and Jaffer [BALL87] who incorporate multipath coherence into the ML estimator for low angle radar tracking based in element space. Ballance and Jaffer found that at the expense of increased computation, exploitation of the coherence gives rise to an element space based ML estimator exhibiting increased performance over that achieved with the ML estimator in element space which does not account for ρ_c constant. As we shall see, this is the case in beamspace as well. Of course, similar to the situation throughout, the beamspace domain based ML estimator for coherent multipath is dramatically less computationally burdensome than the counterpart procedure in element space proposed by Ballance and Jaffer. We will deal solely with the case of symmetric multipath which admits a simple iterative implementation.

As before, the practical assumption that the noise in beamspace is Gaussian distributed leads to a generalized least squares problem which with $\mathbf{x}_B(n)$ given by (2.10) is as follows:

$$\underset{(u_o,\rho_c,c_1(1),\cdots,c_1(N))}{\text{Minimize}} \quad \sum_{n=1}^{N} \| \mathbf{x}_B(n) - [\mathbf{b}(u_o) + \rho_c \mathbf{b}(-u_o)]c_1(n)\|^2_{\mathbf{Q}^{-1}} \tag{4.2}$$

$$\text{subject:} \quad |\rho_c| \leq 1$$

where $\mathbf{Q} = \mathbf{S}^H\mathbf{S}$. Note that the constraint on $|\rho_c|$ arises from the fact that the amplitude of the specular path signal is no larger than that of the direct path. Let $\mathbf{b}(u_o,\rho_c) = \mathbf{b}(u_o) + \rho_c\mathbf{b}(-u_o)$. Substituting the least square error solution for $c_1(n)$, i. e., the LS solution to the equation $\mathbf{b}(u_o,\rho_c)c_1(n) = \mathbf{x}_B(n)$, into (4.2) leads to the following optimization problem:

$$\underset{(u_o,\rho_c)}{\text{Maximize}} \sum_{n=1}^{N} \frac{\mathbf{x}_B^H(n)\,\mathbf{Q}^{-1}\mathbf{b}(u_o,\rho_c)\mathbf{b}^H(u_o,\rho_c)\mathbf{Q}^{-1}\,\mathbf{x}_B(n)}{\mathbf{b}^H(u_o,\rho_c)\mathbf{Q}^{-1}\mathbf{b}(u_o,\rho_c)}$$

$$= N\frac{\mathbf{b}^H(u_o,\rho_c)\mathbf{Q}^{-1}\hat{\mathbf{R}}_{bb}\mathbf{Q}^{-1}\mathbf{b}(u_o,\rho_c)}{\mathbf{b}^H(u_o,\rho_c)\mathbf{Q}^{-1}\mathbf{b}(u_o,\rho_c)} \tag{4.3}$$

$$\text{subject:} \quad |\rho_c| \leq 1$$

where $\hat{\mathbf{R}}_{bb}$ is as defined previously in Chapter 2. The optimization problem described by (4.3) cannot be manipulated into a closed-form expression for $\hat{u}_o$. To avoid having to search over two variables one of which is complex, we take a suboptimal approach by decomposing the problem into two single variable optimization problems which may be solved iteratively. The algorithm is as follows. Assume an initial estimate of u_o is available. Let $\mathbf{B}(u_o) = [\mathbf{b}(u_o) \vdots \mathbf{b}(-u_o)]$ and $\rho = [1,\rho_c]^T$ such that $\mathbf{b}(u_o,\rho_c) = \mathbf{B}(u_o)\rho$. An alternative expression for (3.3) is then

$$\underset{\rho}{\text{Maximize}} \frac{\rho^H\mathbf{B}^T(u_o)\mathbf{Q}^{-1}\hat{\mathbf{R}}_{bb}\mathbf{Q}^{-1}\mathbf{B}(u_o)\rho}{\rho^H\mathbf{B}^T(u_o)\mathbf{Q}^{-1}\mathbf{B}(u_o)\rho} \tag{4.4}$$

$$\text{subject:} \quad |\rho_c| \leq 1$$

where we have assumed that u_o is fixed at the initial estimate resulting in an optimization problem with respect to the single complex variable ρ_c. Since (4.4) is quadratic, the optimal ρ_c is either a solution to the corresponding unconstrained problem, or it must satisfy $|\rho_c| = 1$. As a consequence, we shall first solve the following unconstrained problem.

$$\underset{\rho}{\text{Maximize}} \frac{\rho^H\mathbf{B}^T(u_o)\mathbf{Q}^{-1}\hat{\mathbf{R}}_{bb}\mathbf{Q}^{-1}\mathbf{B}(u_o)\rho}{\rho^H\mathbf{B}^T(u_o)\mathbf{Q}^{-1}\mathbf{B}(u_o)\rho} \tag{4.5}$$

We note that the objective function in (4.5) is invariant under scaling for ρ such that the solution is to take ρ as a scalar multiple of the generalized eigenvector of the 2x2 matrix pencil $\{\, \mathbf{B}^T(u_o)\mathbf{Q}^{-1}\hat{\mathbf{R}}_{bb}\mathbf{Q}^{-1}\mathbf{B}(u_o)\,,\, \mathbf{B}^T(u_o)\mathbf{Q}^{-1}\mathbf{B}(u_o)\,\}$ associated with the larger of the two generalized eigenvalues. The optimal value of ρ_c is then the ratio of the second component of the optimal ρ to the first component.

If the optimal ρ_c thus found fail to satisfy $|\rho_c| < 1$, we instead solve the equality constrained problem given by

$$\underset{\rho_c}{\text{Maximize}} \frac{\rho^H \mathbf{B}^T(u_o)\mathbf{Q}^{-1}\hat{\mathbf{R}}_{bb}\mathbf{Q}^{-1}\mathbf{B}(u_o)\rho}{\rho^H \mathbf{B}^T(u_o)\mathbf{Q}^{-1}\mathbf{B}(u_o)\rho} \tag{4.6}$$

$$\text{subject:} \quad |\rho_c| = 1$$

Again, since the cost function is invariant under complex scaling, the problem can be equivalently stated as

$$\underset{\rho_c}{\text{Maximize}} \frac{\rho^H \mathbf{B}^T(u_o)\mathbf{Q}^{-1}\hat{\mathbf{R}}_{bb}\mathbf{Q}^{-1}\mathbf{B}(u_o)\rho}{\rho^H \mathbf{B}^T(u_o)\mathbf{Q}^{-1}\mathbf{B}(u_o)\rho} \tag{4.7}$$

$$\text{subject:} \quad \tilde{\mathbf{I}}_2\rho = \rho^*$$

without loss of generality. Following a similar argument as that made in Section 2.3 regarding Method II for symmetric BDML estimation, we easily find that the maximizing ρ is a scalar multiple of the generalized eigenvector of the pencil $\{ \mathbf{B}^T(u_o)\mathbf{Q}^{-1}\{\hat{\mathbf{R}}_{bb} + \tilde{\mathbf{I}}_3\hat{\mathbf{R}}^*_{bb}\tilde{\mathbf{I}}_3\}\mathbf{Q}^{-1}\mathbf{B}(u_o)\ ,\ \mathbf{B}^T(u_o)\mathbf{Q}^{-1}\mathbf{B}(u_o)\ \}$ corresponding the the smaller generalized eigenvalue. The optimal ρ_c is again the ratio of the second component of the optimal ρ to the first component.

Next, consider the value of ρ_c thus found to be substituted into (4.3) and the ensuing problem of finding that value of u_o which maximizes (4.3) given this ρ_c. To manipulate (4.3) into a form amenable to a closed-form solution, we invoke the relationship $\mathbf{b}(-u_o) = \tilde{\mathbf{I}}_3\mathbf{b}(u_o)$ noted previously in (2.10). Substituting $\mathbf{b}(u_o,\rho_c) = (\mathbf{I}_3 + \rho_c\tilde{\mathbf{I}}_3)\mathbf{b}(u_o)$ into (4.3) yields the following alternative expression for the objective function in (4.3):

$$\underset{\mathbf{b}(u_o)}{\text{Maximize}} \frac{\mathbf{b}^T(u_o)\ \text{Re}\{(\mathbf{I}_3 + \rho_c\tilde{\mathbf{I}}_3)^H\mathbf{Q}^{-1}\hat{\mathbf{R}}_{bb}\mathbf{Q}^{-1}(\mathbf{I}_3 + \rho_c\tilde{\mathbf{I}}_3)\}\ \mathbf{b}(u_o)}{\mathbf{b}^T(u_o)\ \{(\mathbf{I}_3 + \rho_c\tilde{\mathbf{I}}_3)^H\mathbf{Q}^{-1}(\mathbf{I}_3 + \rho_c\tilde{\mathbf{I}}_3)\}\ \mathbf{b}(u_o)} \tag{4.8}$$

where we have invoked the fact that $\mathbf{b}(u_o)$ is a real-valued vector and that $(\mathbf{I}_3 + \rho_c\tilde{\mathbf{I}}_3)^H\mathbf{Q}^{-1}\hat{\mathbf{R}}_{bb}\mathbf{Q}^{-1}(\mathbf{I}_3 + \rho_c\tilde{\mathbf{I}}_3)$ is a Hermitian matrix. Note that we have expressed the resulting optimization problem as a search over $\mathbf{b}(u_o)$ as opposed to a search over u_o itself. We do this primarily so that we may approximate the solution for u_o by taking $\mathbf{b}(u_o)$ to be the generalized eigenvector of the 3x3 real matrix pencil $\{\ \text{Re}\{(\mathbf{I}_3 + \rho_c\tilde{\mathbf{I}}_3)^H\mathbf{Q}^{-1}\hat{\mathbf{R}}_{bb}\mathbf{Q}^{-1}(\mathbf{I}_3 + \rho_c\tilde{\mathbf{I}}_3)\}\ ,\ \text{Re}\{(\mathbf{I}_3 + \rho_c\tilde{\mathbf{I}}_3)^H\mathbf{Q}^{-1}(\mathbf{I}_3 + \rho_c\tilde{\mathbf{I}}_3)\}\ \}$ associated with the largest generalized eigenvalue. At this point, the optimal $\mathbf{b}(u_o)$ thus found may be substituted back into (4.4) to obtain a new value of ρ_c corresponding to the second iteration. Likewise, the new value of ρ_c may

be subsequently substituted into (4.5) to obtain the estimate of $\mathbf{b}(u_o)$ at the second iteration. The procedure may be iterated in this fashion, alternating between the computation of the largest GEVEC of a 2x2 pencil in determining the optimum ρ at the k-th iteration, denoted ρ_k, and the computation of the largest GEVEC of a 3x3 pencil in determining the optimum vector $\mathbf{b}(u_o)$ at the k-th iteration, denoted $\mathbf{b}_k(u_o)$. Of course, $\mathbf{b}_k(u_o)$ is determined only to within an unknown scalar multiple. The procedure may be terminated when the 2-norm of the difference between $\mathbf{b}(u_o)$ and $\mathbf{b}_{k+1}(u_o)$, both normalized to have a 2-norm equal to one, is less than some pre-determined threshold ϵ. The specific steps will be delineated in algorithmic form shortly.

At the end of the iterative procedure outlined above, we have an estimate of the vector $\mathbf{b}(u_o)$ from which we desire to recover u_o. There are a number of ways we may proceed to do this. An efficient approach is compute the projection operator onto the orthogonal complement of the 1-D space spanned by $\mathbf{b}(u_o)$ as $\mathbf{P}_b^{\perp} = \mathbf{I} - \mathbf{b}(u_o)[\mathbf{b}(u_o)^T\mathbf{b}(u_o)]^{-1}\mathbf{b}^T(u_o)$ and search for that value of u such that $\mathbf{b}(u) = \mathbf{S}^H\mathbf{a}(u)$ is orthogonal to the range of $\mathbf{P}_b^{\perp}$. Note that due to additive noise, $\mathbf{P}_b^{\perp}\,\mathbf{b}(u)$ is nonzero for all u and we shall instead compute u via the following optimization problem:

$$\underset{u}{\text{Minimize}} \;\; ||\mathbf{P}_b^{\perp}\,\mathbf{b}(u)||^2 = ||\mathbf{P}_b^{\perp}\,\mathbf{S}^H\mathbf{a}(u)||^2 = \mathbf{a}(u)^H\mathbf{S}^H\mathbf{P}_b^{\perp}\,\mathbf{S}^H\mathbf{a}(u) \qquad (4.9)$$

The search may be accomplished via any of the numerical techniques such as Newton descent, Golden Section search, etc, and should be started at the most recent estimate of u_o.

4.2.2 Simplifications for Butler Matrix Beamformer

The use of the Mx3 Butler beamformer in this case leads to substantial simplifications. First, the noise covariance matrix $\mathbf{Q}$ is simply a scalar multiple of the 3x3 identify matrix. Second, the numerical search required in the final estimation of u_o can be avoided by employing the "common nulls" property described in Section 2.3.

Upon substitution of (3.7)-(3.10), the problem in (4.9) simplifies to

$$\underset{u}{\text{Minimize}} \;\; ||\mathbf{P}_b^{\perp}\,\mathbf{E}^H\mathbf{a}_3(u)||^2 = \mathbf{a}_3(u)\mathbf{E}\mathbf{P}_b^{\perp}\,\mathbf{E}^H\mathbf{a}_3(u) \qquad (4.10)$$

where $\mathbf{E}$ is given by (3.7) and $\mathbf{a}_3(u)$ is defined according to (3.25). Note that we have assumed that u is small such that G(u) in (3.10) does not vary much

within the angular region of interests. Let $\omega = e^{-j\pi u}$. Due to the Vandermonde structure of $\mathbf{a}_3(u)$, (4.10) can be formulated as a quartic equation given by

$$-2q_2^*\omega^{-2} - q_1^*\omega^{-1} + q_1\omega + 2q_2\omega^2 = 0 \qquad (4.11)$$

where $q_1 = \mathbf{P}_b^e(1,2) + \mathbf{P}_b^e(2,3)$, $q_2 = \mathbf{P}_b^e(1,3)$, and $\mathbf{P}_b^e(i,j)$ is the (i,j)-th component of $\mathbf{P}_b^e = \mathbf{E}\mathbf{P}_b^{\perp}\mathbf{E}^H\mathbf{a}_3(u)$. The quartic equation in (4.11) has at least two roots on the unit circle and the optimum solution is the one minimizing the cost function given in (4.10).

The Beamspace Domain ML algorithm utilizing the Mx3 Butler matrix beamformer modified for the case of coherent symmetric multipath is summarized in algorithmic form below.

ρ-Based BDML Method for Coherent Symmetric Multipath with Butler Matrix Beamformer

(1.) With $\mathbf{S} = \frac{1}{\sqrt{M}}\left[\mathbf{a}(2/M):\mathbf{a}(0):\mathbf{a}(-2/M)\right]$ & $\hat{\mathbf{R}}_{xx} = \frac{1}{N}\sum_{n=1}^{N}\mathbf{x}(n)\,\mathbf{x}^H(n)$, form $\hat{\mathbf{R}}_{bb} = \mathbf{S}^H\hat{\mathbf{R}}_{xx}\mathbf{S}$.

(2.) With initial estimate of u_o, form $\mathbf{b}_1(u_o)$. (k=1: first iteration.)

(3.) With $\mathbf{b}_k(u_o)$, form $\mathbf{B}_k = \left[\mathbf{b}_k(u_o) : \tilde{\mathbf{I}}_3\mathbf{b}_k(u_o)\right]$

(4.) Compute $\rho_k = [\rho_1\ ,\ \rho_2]^T$ as "largest" GEVEC of 2x2 pencil $\{\mathbf{B}_k^T\hat{\mathbf{R}}_{bb}\mathbf{B}_k,\ \mathbf{B}_k^T\mathbf{B}_k\}$.

(5.) If $|\rho_2| < |\rho_1|$, go to (6.). Otherwise:
Compute $\rho_k = [\rho_1\ ,\ \rho_2]^T$ as "largest" GEVEC of 2x2 pencil $\{\mathbf{B}_k^T\hat{\mathbf{R}}_{bb}\mathbf{B}_k + \tilde{\mathbf{I}}_2\mathbf{B}_k^T\hat{\mathbf{R}}_{bb}\mathbf{B}_k\tilde{\mathbf{I}}_2\ ,\ \mathbf{B}_k^T\mathbf{B}_k + \tilde{\mathbf{I}}_2\mathbf{B}_k^T\mathbf{B}_k\tilde{\mathbf{I}}_2\}$

(6.) With $\hat{\rho}_{c,k} = \rho_2/\rho_1$, form $\mathbf{J}_k = \mathbf{I}_3 + \hat{\rho}_{c,k}\tilde{\mathbf{I}}_3$.

(7.) Compute $\mathbf{b}_{k+1}(u_o)$ as "largest" GEVEC of 3x3 pencil $\{\mathrm{Re}\{\mathbf{J}_k^H\hat{\mathbf{R}}_{bb}\mathbf{J}_k\}\ ,\ \mathbf{J}_k^H\mathbf{J}_k\}$.

(8.) If $\left\| \frac{\mathbf{b}_{k+1}(u_o)}{\|\mathbf{b}_{k+1}(u_o)\|_2} - \frac{\mathbf{b}_k(u_o)}{\|\mathbf{b}_k(u_o)\|_2} \right\|_2 > \epsilon$ go to (3).

(9.) With $\mathbf{b}_{k+1}(u_o)$, construct: $\mathbf{P}_b^e = \mathbf{E}\left[\mathbf{I}_3 - \frac{\mathbf{b}_{k+1}\mathbf{b}_{k+1}^T}{\mathbf{b}_{k+1}^T\mathbf{b}_{k+1}}\right]\mathbf{E}^H$

(10.) Solve $-2q_2^* - q_1^* \hat{z} + q_1 \hat{z}^3 + 2q_2 \hat{z}^4 = 0$

where $q_1 = \mathbf{P}_b^e(1,2) + \mathbf{P}_b^e(2,3)$ and $q_2 = \mathbf{P}_b^e(1,3)$.

(11.) $\hat{u}_o = \frac{1}{j\pi} \ln \hat{z}$

where $\hat{z}$ is the unit root found in (10.) which minimizes the cost function in (4.10).

Simulations illustrating the improvement in performance achieved with this estimation scheme in a coherent multipath scenario over that obtained with the Butler matrix beamformer based BDML method outlined at the end of Section 2.3 will be presented in Section 4.5. In closing, we point out in the case of a single snapshot, i.e.., N=1, the two methods are the same, as one would expect. This may be easily shown but is not done so here for sake of brevity.

4.3 Bisector Angle Estimation for Nonsymmetric Multipath

We noted in Section 2.5 that the BDML method for nonsymmetric multipath breaks down when the direct and specular path signals arrive perfectly in-phase or 180° out-of-phase. On the other hand, the BDML method for symmetric multipath theorectically performs best for $\Delta\Psi = 0°$. One may thus expect to achieve significant improvement in performance at $\Delta\Psi = 0°$ provided that a procedure is available to convert a nonsymmetric problem to a symmetric one. In this section, we will develop a scheme to estimate the bisector angle between the direct and specular paths based on a characteristic property of the beamspace correlation matrix for symmetric multipath. The conversion from nonsymmetric to symmetric multipath is done with a second steering of the three beams such that the pointing angle of the center beam is the estimate of the bisector angle. For the sake of simplicity, we here restrict the beamforming matrix **S** to be the Mx3 Butler matrix beamformer.

4.3.1 Development of the Algorithm

(2.50) describes the asymptotic form of the beamspace correlation matrix under both symmetric and nonsymmetric multipath conditions. The only difference between the two is that in the case of symmetric multipath **B** satisfies the property $\tilde{\mathbf{I}}_3 \mathbf{B} \tilde{\mathbf{I}}_2 = \mathbf{B}$. It is this property which gives meaning to the forward-backward beamspace correlation matrix, $\mathbf{R}_{bb}^{fb}$, as analyzed in

(2.53) and (2.54). Indeed, the bisector angle estimator (BAE) to be developed in this section is based on the fact that the forward-backward average in beamspace described by (2.33) is meaningless in the case of nonsymmetric multipath. Denote the noiseless component of $\mathbf{R}_{bb}^{fb}$ as $\mathbf{C}_{bb}^{fb}$. More specifically, the BAE is based on the fact that under symmetric multipath conditions $\mathbf{C}_{bb}^{fb}$ is of rank two, while under nonsymmetric multipath conditions $\mathbf{C}_{bb}^{fb}$ is of full rank provided $\Delta\Psi$ is not equal to either 0° or 180°. Thus, in the former case the determinant of $\mathbf{C}_{bb}^{fb}$ is zero, while in the latter case the determinant of $\mathbf{C}_{bb}^{fb}$ is nonzero. The peculiarity occurring with either $\Delta\Psi = 0^\circ$ and $\Delta\Psi = 180^\circ$ is averted by employing the well known technique of spatial smoothing [SHAN85a], [WILL88].

Consider the signal-only component of the forward-backward averaged beamspace correlation matrix, denoted $\mathbf{C}_{bb}^{fb}$, under symmetric multipath conditions. Invocation of the property $\tilde{\mathbf{I}}_3\mathbf{B}\tilde{\mathbf{I}}_2 = \mathbf{B}$ yields

$$\mathbf{C}_{bb}^{fb} = \frac{1}{2}\left\{\mathbf{B}\mathbf{R}_{ss}\mathbf{B}^T + \tilde{\mathbf{I}}_3\mathbf{B}\mathbf{R}_{ss}\mathbf{B}^T\tilde{\mathbf{I}}_3\right\}$$

$$= \mathbf{B}\frac{1}{2}\left\{\mathbf{R}_{ss} + \tilde{\mathbf{I}}_2\mathbf{R}_{ss}\tilde{\mathbf{I}}_2\right\}\mathbf{B}^T = \mathbf{B}\mathbf{R}_{ss}^{fb}\mathbf{B}^T \qquad (4.12)$$

where $\mathbf{R}_{ss}^{fb}$ is defined by (2.54). It was observed previously that $\mathbf{R}_{ss}^{fb}$ is real-valued and of full rank equal two in the practical case where the magnitude of the reflection coefficient is less than unity. Thus, under symmetric multipath conditions $\mathbf{C}_{bb}^{fb}$ is a real-valued, symmetric 3x3 matrix of rank two. Hence, $\det\left(\mathbf{C}_{bb}^{fb}\right) = \det\left(\mathrm{Re}\{\mathbf{C}_{bb}^{fb}\}\right) = 0$ under symmetric multipath conditions regardless of the phase difference $\Delta\Psi$. For the nonsymmetric multipath case, consider the real part of the signal-only component of the forward-backward averaged beamspace correlation matrix

$$\mathrm{Re}\{\mathbf{C}_{bb}^{fb}\} = \frac{1}{2}\left\{\mathbf{B}\mathrm{Re}\{\mathbf{R}_{ss}\}\mathbf{B}^T + \tilde{\mathbf{I}}_3\mathbf{B}\mathrm{Re}\{\mathbf{R}_{ss}\}\mathbf{B}^T\tilde{\mathbf{I}}_3\right\} \qquad (4.13)$$

Under nonsymmetric multipath conditions, the relationship $\tilde{\mathbf{I}}_3\mathbf{B}\tilde{\mathbf{I}}_2 = \mathbf{B}$ does not hold such that we cannot simplify (4.13) any further. We noted previously that $\mathrm{Re}\{\mathbf{R}_{ss}\}$, defined by (2.51), is of full rank equal to two so long as $\Delta\Psi$ is not equal to either 0° or 180°. In the case of $\mathrm{Re}\{\mathbf{R}_{ss}\}$ of full rank

$$\text{range}\left\{\text{Re}\{\mathbf{C}_{bb}^{fb}\}\right\} = \text{range}\left\{\mathbf{B}\text{Re}\{\mathbf{R}_{ss}\}\mathbf{B}^T + \tilde{\mathbf{I}}_3\mathbf{B}\text{Re}\{\mathbf{R}_{ss}\}\mathbf{B}^T\tilde{\mathbf{I}}_3\right\}$$

$$= \text{span}\left\{\mathbf{b}(u_1)\,,\ \mathbf{b}(u_2)\,,\ \tilde{\mathbf{I}}_3\mathbf{b}(u_1)\,,\ \tilde{\mathbf{I}}_3\mathbf{b}(u_2)\right\}$$

$$= \text{span}\left\{\mathbf{b}(u_1)\,,\ \mathbf{b}(u_2)\,,\ \mathbf{b}(-u_1)\,,\ \mathbf{b}(-u_2)\right\} \qquad (4.14)$$

From the definition of $\mathbf{b}(u)$ in (3.8-9), it is easily proved that any three members of the set of four vectors $\{\mathbf{b}(u_1)\,,\ \mathbf{b}(u_2)\,,\ \mathbf{b}(-u_1)\,,\ \mathbf{b}(-u_2)\}$ are linearly independent provided both u_1 and u_2 lie in the range $(-\frac{2}{M}\,,\ \frac{2}{M})$ and $u_2 \neq -u_1$. This indicates that $\text{Re}\{\mathbf{C}_{bb}^{fb}\}$ is of full rank equal to 3 and, as a consequence, $\det\left\{\text{Re}\{\mathbf{C}_{bb}^{fb}\}\right\} > 0$ under nonsymmetric multipath conditions as long as $\Delta\Psi$ is not equal to either 0° or 180°. In these two cases, $\text{Re}\{\mathbf{R}_{ss}\}$ is of rank one such that $\text{range}\{\text{Re}\{\mathbf{C}_{bb}^{fb}\}\} = \text{span}\{\mathbf{b}(u_1) \pm \rho\mathbf{b}(u_2)\,,\ \tilde{\mathbf{I}}_3\{\mathbf{b}(u_1) \pm \rho\mathbf{b}(u_2)\}\}$, where the "+" is for the case $\Delta\Psi = 0^\circ$ and "−" is for the case $\Delta\Psi = 180^\circ$. Thus, when $\Delta\Psi$ is equal to either 0° or 180°, the rank of $\text{Re}\{\mathbf{C}_{bb}^{fb}\}$ is two and $\det\left\{\text{Re}\{\mathbf{C}_{bb}^{fb}\}\right\} = 0$ whether the multipath is symmetric or nonsymmetric. Since we wish to use $\det\left\{\text{Re}\{\mathbf{C}_{bb}^{fb}\}\right\}$ as a discriminator between the symmetric and nonsymmetric multipath cases, we employ spatial averaging [SHAN85a], [WILL88] as a means for averting the peculiarity occurring with $\Delta\Psi$ equal to either 0° or 180°.

Spatial smoothing is employed to insure that $\text{Re}\{\mathbf{R}_{ss}\}$ is of full rank equal to two regardless of the phase difference. In this mode of operation, the beamspace correlation matrix is spatially averaged over a number of identical, overlapping subarrays extracted from the overall array. The procedure exploits the fact that the phase difference between the direct and specular signals at the center of each subarray is different. We emphatically point out that spatial smoothing is only recommended for the purposes of estimating the bisector angle, denoted u_c, between the direct and specular paths, i. e., $u_c = \frac{1}{2}\{u_1 + u_2\}$. Once, the bisector angle is estimated, it is recommended that the BDML method for symmetric multipath outlined in Section 2.3 be employed with the modification that $\mathbf{S}_M = \left[\mathbf{a}_M(-\frac{2}{M}) \vdots \mathbf{a}_M(0) \vdots \mathbf{a}_M(\frac{2}{M})\right]$ be

replaced by $\mathbf{S}_{\wedge 1}^{c} = \left[\mathbf{a}_{\wedge 1}(\hat{u}_c - \frac{2}{M}) \vdots \mathbf{a}_{\wedge 1}(\hat{u}_c) \vdots \mathbf{a}_{\wedge 1}(\hat{u}_c + \frac{2}{M})\right]$, where $\hat{u}_c$ is the bisector angle estimate. A pejorative side effect of spatial smoothing is that the effective aperture is that of the subarray. Although the reduction in effective array aperture is not critical in the estimation of the bisector angle, the corresponding loss in resolution may prove critical in the subsequent estimation of the angles of the direct and specular paths. We will outline the overall procedure at the end of this section.

The subarrays employed in spatial smoothing are each composed of a number of contiguous elements, say L. Adjacent subarrays have all but one element in common. An M element array is composed M-L+1 such subarrays. A typical number for L is $\frac{2}{3}$M [WILL88]. The extraction of the snapshot vector for the k-th subarray, denoted $\mathbf{x}_s(n;k)$, k=1,...,M-L+1, from $\mathbf{x}(n)$, which contains the outputs of all array elements at the n-th snapshot, may be expressed mathematically as

$$\mathbf{x}_s(n;k) = \mathbf{E}_k^T \mathbf{x}(n) \qquad \text{where:} \quad \mathbf{E}_k = \begin{bmatrix} \mathbf{0} \\ \mathbf{I} \\ \mathbf{0} \end{bmatrix} \begin{matrix} (k-1)xL \\ LxL \\ (M-L-k+1)xL \end{matrix} \tag{4.15}$$

With these subarray snapshot vectors, the spatially smoothed element space correlation matrix, denoted $\tilde{\mathbf{R}}_{xx}$, is constructed as

$$\tilde{\mathbf{R}}_{xx} = \frac{1}{N(M-L+1)} \sum_{n=1}^{N} \sum_{k=1}^{M-L+1} \mathbf{x}_s(n;k)\mathbf{x}_s^H(n;k) \tag{4.16}$$

Finally, the spatially smoothed beamspace sample correlation matrix, denoted $\tilde{\mathbf{R}}_{bb}$, is constructed as

$$\tilde{\mathbf{R}}_{bb} = \mathbf{S}_L^H \tilde{\mathbf{R}}_{xx} \mathbf{S}_L \tag{4.17}$$

where

$$\mathbf{S}_L = \left[\mathbf{a}_L(-\tfrac{2}{L}) \vdots \mathbf{a}_L(0) \vdots \mathbf{a}_L(\tfrac{2}{L})\right] \tag{4.18}$$

Assume without loss of generality that L is odd, $\mathbf{a}_L(u)$ is described by (3.25) with N = L. Note that the three columns of $\mathbf{S}_L$ are mutually orthogonal such that $\mathbf{S}_L^H\mathbf{S}_L = L\mathbf{I}_3$. It can be shown [SHAN85a], [WILL88] that the signal-only (no noise) component of $\tilde{\mathbf{R}}_{bb}$, denoted $\tilde{\mathbf{C}}_{bb}$, may be expressed as

$$\tilde{\mathbf{C}}_{bb} = \mathbf{B}_s\tilde{\mathbf{R}}_{ss}\mathbf{B}_s^H \tag{4.19}$$

where

$$\mathbf{B}_s = \left[\mathbf{S}_L^H \mathbf{a}_L(u_1) \vdots \mathbf{S}_L^H \mathbf{a}_L(u_2)\right] = \left[\mathbf{b}_s(u_1) \vdots \mathbf{b}_s(u_2)\right] \tag{4.20}$$

and, more importantly,

$$\tilde{\mathbf{R}}_{ss} = \frac{1}{M-L+1} \sum_{k=1}^{M-L+1} \Phi^{k-1} \mathbf{R}_{ss} (\Phi^{k-1})^* \quad \text{where: } \Phi = \begin{bmatrix} e^{-j\pi u_1} & 0 \\ 0 & e^{-j\pi u_2} \end{bmatrix} \tag{4.21}$$

$\tilde{\mathbf{R}}_{ss}$ is the effective sampled source covariance matrix achieved with spatial smoothing. From the theory espoused in [SHAN85a], it is readily deduced that $\tilde{\mathbf{R}}_{ss}$ of full rank equal to two as long as $u_2 \neq u_1$ and M-L+1 $\geq$ 2. In the case under consideration, however, where the difference between u_1 and u_2 is quite small, $\tilde{\mathbf{R}}_{ss}$ may be ill-conditioned making $\mathrm{Re}\{\tilde{\mathbf{R}}_{ss}\}$ ill-conditioned in the case of $\Delta\Psi = 0^\circ$ and $\Delta\Psi = 180^\circ$. The choice of $L = \frac{2}{3}M$ corresponds to averaging over approximately M/3 subarrays. Simulations have indicated that this is adequate to insure that $\mathrm{Re}\{\tilde{\mathbf{R}}_{ss}\}$ is of full rank equal to two even for angular separations between the direct and specular paths as small as a tenth of a beamwidth.

Under practical conditions, it is easily argued that that $\tilde{\mathbf{R}}_{bb}$ has the following asymptotic form

$$E\{\tilde{\mathbf{R}}_{bb}\} = \mathbf{B}_s \tilde{\mathbf{R}}_{ss} \mathbf{B}_s^H + \sigma_{bn}^2 \mathbf{I}_3 \tag{4.22}$$

Since $\tilde{\mathbf{C}}_{bb}$ is positive semi-definite of rank 2, it follows that the smallest eigenvalue of $E\{\tilde{\mathbf{R}}_{bb}\}$, denoted λ_{min}^{bb}, is σ_{bn}^2. $\tilde{\mathbf{C}}_{bb}$ may thus be estimated as

$$\tilde{\mathbf{C}}_{bb} = \tilde{\mathbf{R}}_{bb} - \hat{\lambda}_{min}^{bb} \mathbf{I}_3 \tag{4.23}$$

where $\hat{\lambda}_{min}^{bb}$ is the smallest eigenvalue of $\tilde{\mathbf{R}}_{bb}$. With this estimate of the signal-only component of the spatially smoothed beamspace sample correlation matrix $\tilde{\mathbf{R}}_{bb}$, $\tilde{\mathbf{C}}_{bb}^{fb}$ is constructed according to

$$\tilde{\mathbf{C}}_{bb}^{fb} = \frac{1}{2}\{\tilde{\mathbf{C}}_{bb} + \tilde{\mathbf{I}}_3 \tilde{\mathbf{C}}_{bb} \tilde{\mathbf{I}}_3\} \tag{4.24}$$

From the arguments made previously, it follows that in the asymptotic or no noise cases, the 3x3 real matrix $\mathrm{Re}\{\tilde{\mathbf{C}}_{bb}^{fb}\}$ will have full rank in the case of nonsymmetric multipath, regardless of $\Delta\Psi$, and rank two in the case of symmetric multipath. This implies that in the asymptotic or no noise cases, $\det\left(\mathrm{Re}\{\tilde{\mathbf{C}}_{bb}^{fb}\}\right) = 0$ under symmetric multipath conditions, while under nonsymmetric multipath conditions $\det\left(\mathrm{Re}\{\tilde{\mathbf{C}}_{bb}^{fb}\}\right) > 0$. Alternatively, we can

say that $\mathrm{Re}\{\tilde{\mathbf{C}}_{bb}^{fb}\}$ is positive semi-definite under symmetric multipath conditions, while under nonsymmetric multipath conditions, $\mathrm{Re}\{\tilde{\mathbf{C}}_{bb}^{fb}\}$ is strictly positive definite. These observations prompt the following scheme for estimating the bisector angle u_c. First, in the formation of $\tilde{\mathbf{R}}_{bb}$ according to (4.16-4.18), replace $\mathbf{S}_L = \left[\mathbf{a}_L(-\frac{2}{L}) \vdots \mathbf{a}_L(0) \vdots \mathbf{a}_L(\frac{2}{L})\right]$ by $\mathbf{S}_L^c = \left[\mathbf{a}_L(u_c - \frac{2}{L}) \vdots \mathbf{a}_L(u_c) \vdots \mathbf{a}_L(u_c + \frac{2}{L})\right]$ to form $\tilde{\mathbf{R}}_{bb}(u_c)$. Second, subtract $\hat{\lambda}_{min}^{bb}\mathbf{I}_3$ from $\tilde{\mathbf{R}}_{bb}(u_c)$ to form $\tilde{\mathbf{C}}_{bb}(u_c)$. Third, form $\tilde{\mathbf{C}}_{bb}^{fb}(u_c) = \frac{1}{2}\{\tilde{\mathbf{C}}_{bb}(u_c) + \tilde{\mathbf{I}}_3\tilde{\mathbf{C}}_{bb}(u_c)\tilde{\mathbf{I}}_3\}$. Finally, estimate the bisector angle as that value of u_c in the interval $(-\frac{2}{M}, \frac{2}{M})$ for which $\det\left|\mathrm{Re}\{\tilde{\mathbf{C}}_{bb}^{fb}(u_c)\}\right|$ achieves its minimum value. We state this procedure in a more mathematically explicit manner below.

First, the two matrix beamformers $\mathbf{S}_L = \left[\mathbf{a}_L(-\frac{2}{L}) \vdots \mathbf{a}_L(0) \vdots \mathbf{a}_L(\frac{2}{L})\right]$ and $\mathbf{S}_L^c = \left[\mathbf{a}_L(u_c - \frac{2}{L}) \vdots \mathbf{a}_L(u_c) \vdots \mathbf{a}_L(u_c + \frac{2}{L})\right]$ may be related through a diagonal transformation as

$$\mathbf{S}_L^c = \mathbf{D}(u_c)\mathbf{S}_L \qquad \text{where: } \mathbf{D}(u_c) = \mathrm{diag}\{\mathbf{a}_L(u_c)\} \tag{4.25}$$

The notation $\mathrm{diag}\{\mathbf{a}_L(u_c)\}$ indicates that $\mathbf{D}(u_c)$ is a LxL diagonal matrix the ii component of which is the i-th component of the Lx1 vector $\mathbf{a}_L(u_c)$ described by (3.25) with M=L. The spatially smoothed beamspace sample correlation matrix obtained with the translated beamformer $\mathbf{S}_L^c$ may thus be expressed as

$$\tilde{\mathbf{R}}_{bb}(u_c) = \mathbf{S}_L^{cH}\tilde{\mathbf{R}}_{xx}\mathbf{S}_L^c = \mathbf{S}_L^H\mathbf{D}^*(u_c)\tilde{\mathbf{R}}_{xx}\mathbf{D}(u_c)\mathbf{S}_L \tag{4.26}$$

Note that $\mathbf{D}(u_c)$ defined above satisfies $\mathbf{D}^*(u_c)\mathbf{D}(u_c) = \mathbf{I}_3$ such that $\mathbf{S}_L^{cH}\mathbf{S}_L^c = L\mathbf{I}_L$. From this property it may be proved that the noise-only component of $E\{\tilde{\mathbf{R}}_{bb}(u_c)\}$ does not vary with u_c. Hence, the signal-only component of $\tilde{\mathbf{R}}_{bb}(u_c)$ is estimated as

$$\tilde{\mathbf{C}}_{bb}(u_c) = \mathbf{S}_L^H\mathbf{D}^*(u_c)\tilde{\mathbf{R}}_{xx}\mathbf{D}(u_c)\mathbf{S}_L - \hat{\lambda}_{min}^{bb}\mathbf{I}_3 \tag{4.27}$$

where $\hat{\lambda}_{min}^{bb}$ is the smallest eigenvalue of $\tilde{\mathbf{R}}_{bb}$. Hence, the estimate of the bisector angle, u_c, is the solution to the following optimization problem.

$$\underset{u_c}{\text{Minimize}} \det\left|\frac{1}{2}\mathrm{Re}\left\{\mathbf{S}_L^H\mathbf{D}^*(u_c)\tilde{\mathbf{R}}_{xx}\mathbf{D}(u_c)\mathbf{S}_L + \tilde{\mathbf{I}}_3\mathbf{S}_L^H\mathbf{D}^*(u_c)\tilde{\mathbf{R}}_{xx}\mathbf{D}(u_c)\mathbf{S}_L\tilde{\mathbf{I}}_3\right\} - \hat{\lambda}_{min}^{bb}\mathbf{I}_3\right|$$

$$\text{subject to } u_c \in (-\frac{2}{M}\ ,\ \frac{2}{M}) \tag{4.28}$$

where we have used the fact that $\tilde{\mathbf{I}}_3\tilde{\mathbf{I}}_3 = \mathbf{I}_3$. The interval constraint on u_c reflects the condition that the direct and specular path signals arrive within a beamwidth of broadside to the array. Ostensibly, the objective function in (4.28) is too complicated to allow a simple closed-form solution for u_c, the bisector angle estimate. Thus, it appears that a 1-D search procedure is required such as Golden Section Search, for example. However, a simple closed-form estimation procedure may in fact be achieved by exploiting the result in (3.7). Exploitation of this result allows us to formulate the search for u_c in terms of finding $\lambda_c = e^{j\pi u_c}$ as the root of a quartic equation. The appropriate development is provided below.

4.3.2 Simplifications of the Cost Function

$\mathbf{S}_L$ may be factored in a manner similar to that in (3.7) for $\mathbf{S}$:

$$\mathbf{S}_L = \mathbf{H}_L\mathbf{E}_L \tag{4.29}$$

where $\mathbf{H}_L$ is the Lx3 Toeplitz matrix

$$\mathbf{H}_L = \begin{bmatrix} \mathbf{h}_L & 0 & 0 \\ 0 & \mathbf{h}_L & 0 \\ 0 & 0 & \mathbf{h}_L \end{bmatrix} \tag{4.30}$$

$\mathbf{h}_L = [h_0\ ,\ h_1\ ,\ \cdots\ ,\ h_{L-3}]^T$ is the coefficient vector for the polynomial of order L-3 whose roots are the roots common to each of the three polynomials formed with a particular column of $\mathbf{S}_L$ as the coefficient vector.

$$h(z) = h_0 + h_1 z + h_2 z^2 + \cdots + h_{L-3} z^{L-3} = \alpha_L \prod_{m=2}^{L-2} \left(z - e^{j\frac{2\pi m}{L}} \right) \tag{4.31}$$

where α_L is defined similar to α in (3.5). $\mathbf{E}_L$ in (4.29) is 3x3 described by (3.45) with M replaced by L:

$$\mathbf{E}_L = \begin{bmatrix} -e^{-j\frac{\pi}{L}} & 1 & -e^{j\frac{\pi}{L}} \\ 2\cos(\frac{\pi}{L}) & -2\cos(\frac{2\pi}{L}) & 2\cos(\frac{\pi}{L}) \\ -e^{j\frac{\pi}{L}} & 1 & -e^{-j\frac{\pi}{L}} \end{bmatrix} \tag{4.32}$$

Note that $\mathbf{E}_L$ exhibits the following properties

$$\text{(a) } \tilde{\mathbf{I}}_3\mathbf{E}_L = \mathbf{E}_L^* \text{ ; (b) } \mathbf{E}_L\tilde{\mathbf{I}}_3 = \mathbf{E}_L^* \text{ ; (c) } \tilde{\mathbf{I}}_3\mathbf{E}_L\tilde{\mathbf{I}}_3 = \mathbf{E}_L \tag{4.33}$$

The spatially smoothed beamspace sample correlation matrix $\tilde{\mathbf{R}}_{bb}$ may be expressed in terms of $\mathbf{H}_L$ and $\mathbf{E}_L$ as

$$\tilde{\mathbf{R}}_{bb} = \mathbf{S}_L^H\tilde{\mathbf{R}}_{xx}\mathbf{S}_L = \mathbf{E}_L^H\mathbf{H}_L^H\tilde{\mathbf{R}}_{xx}\mathbf{H}_L\mathbf{E}_L = \mathbf{E}_L^H\tilde{\mathbf{R}}_{hh}\mathbf{E}_L \tag{4.34}$$

where $\tilde{\mathbf{R}}_{hh}$ is the 3x3 matrix

$$\tilde{\mathbf{R}}_{hh} = \mathbf{H}_L^H\tilde{\mathbf{R}}_{xx}\mathbf{H}_L = (\mathbf{E}_L^H)^{-1}\tilde{\mathbf{R}}_{bb}\mathbf{E}_L^{-1} \tag{4.35}$$

Invoking the result in (3.8-9), it is easily shown that the signal-only (no noise) component of $\tilde{\mathbf{R}}_{hh}$, denoted $\tilde{\mathbf{C}}_{hh}$, may be expressed as

$$\tilde{\mathbf{C}}_{hh} = \mathbf{A}_3\mathbf{G}\tilde{\mathbf{R}}_{ss}\mathbf{G}^*\mathbf{A}_3^H \tag{4.36}$$

where $\mathbf{A}_3$ is the 3x2 matrix

$$\mathbf{A}_3 = \begin{bmatrix} e^{-j\pi u_1} & e^{-j\pi u_2} \\ 1 & 1 \\ e^{j\pi u_1} & e^{j\pi u_2} \end{bmatrix} \tag{4.37}$$

and $\mathbf{G}$ is the 2x2 diagonal matrix

$$\mathbf{G} = \begin{bmatrix} \mathbf{h}_L^H\mathbf{a}_L(u_1) & 0 \\ 0 & \mathbf{h}_L^H\mathbf{a}_L(u_2) \end{bmatrix} \tag{4.38}$$

Note that (4.34) implies that $\tilde{\mathbf{C}}_{bb}$ and $\tilde{\mathbf{C}}_{hh}$ are related according to

$$\tilde{\mathbf{C}}_{bb} = \mathbf{E}_L^H\tilde{\mathbf{C}}_{hh}\mathbf{E}_L \tag{4.39}$$

Exploitation of the properties of $\mathbf{E}_L$ described by (4.33) yields the result

$$\mathrm{Re}\{\tilde{\mathbf{C}}_{bb}\} = \frac{1}{2}\left\{\mathbf{E}_L^H\tilde{\mathbf{C}}_{hh}\mathbf{E}_L + \mathbf{E}_L^T\tilde{\mathbf{C}}_{hh}^*\mathbf{E}_L^*\right\} = \frac{1}{2}\left\{\mathbf{E}_L^H\tilde{\mathbf{C}}_{hh}\mathbf{E}_L + \mathbf{E}_L^H\tilde{\mathbf{I}}_3\tilde{\mathbf{C}}_{hh}^*\tilde{\mathbf{I}}_3\mathbf{E}_L\right\}$$

$$= \mathbf{E}_L^H\frac{1}{2}\left\{\tilde{\mathbf{C}}_{hh} + \tilde{\mathbf{I}}_3\tilde{\mathbf{C}}_{hh}^*\tilde{\mathbf{I}}_3\right\}\mathbf{E}_L = \mathbf{E}_L^H\tilde{\mathbf{C}}_{hh}^{fb}\mathbf{E}_L \tag{4.40}$$

where $\tilde{\mathbf{C}}_{hh}^{fb}$ is defined as

$$\tilde{\mathbf{C}}_{hh}^{fb} = \frac{1}{2}\left\{\tilde{\mathbf{C}}_{hh} + \tilde{\mathbf{I}}_3\tilde{\mathbf{C}}_{hh}^*\tilde{\mathbf{I}}_3\right\} \tag{4.41}$$

Note that the definition of the forward-backward average of $\tilde{\mathbf{C}}_{hh}$ in (4.41) is different from that of $\hat{\mathbf{R}}_{bb}$ in (2.33) due to the conjugate on $\tilde{\mathbf{C}}_{hh}$ in the second

term within the brackets on the right hand side of (4.41). Invoking the property that $\mathbf{A}_3$ in (4.37) satisfies $\tilde{\mathbf{I}}_3\mathbf{A}_3 = \mathbf{A}_3^*$, yields the following expression for $\tilde{\mathbf{C}}_{hh}^{fb}$:

$$\tilde{\mathbf{C}}_{hh}^{fb} = \frac{1}{2}\left\{\mathbf{A}_3\mathbf{G}\tilde{\mathbf{R}}_{ss}\mathbf{G}^*\mathbf{A}_3^H + \tilde{\mathbf{I}}_3\mathbf{A}_3^*\left\{\mathbf{G}\tilde{\mathbf{R}}_{ss}\mathbf{G}^*\right\}^*\mathbf{A}_3^T\tilde{\mathbf{I}}_3\right\}$$

$$= \mathbf{A}_3\,\mathrm{Re}\{\mathbf{G}\tilde{\mathbf{R}}_{ss}\mathbf{G}^*\}\,\mathbf{A}_3^H \tag{4.42}$$

Let's consider the case of symmetric multipath wherein $u_2 = -u_1$. With $u_2 = -u_1$ in (4.37), we find that $\mathbf{A}_3$ satisfies $\mathbf{A}\tilde{\mathbf{I}}_2 = \mathbf{A}^*$. This property only holds for the symmetric multipath case. Invoking this property yields the following expression for $\mathrm{Re}\{\tilde{\mathbf{C}}_{hh}^{fb}\}$ for the case of symmetric multipath:

$$\mathrm{Re}\{\tilde{\mathbf{C}}_{hh}^{fb}\} = \frac{1}{2}\left\{\tilde{\mathbf{C}}_{hh}^{fb} + \tilde{\mathbf{C}}_{hh}^{fb*}\right\}$$

$$= \frac{1}{2}\left\{\mathbf{A}_3\mathrm{Re}\{\mathbf{G}\tilde{\mathbf{R}}_{ss}\mathbf{G}^*\}\mathbf{A}_3^H + \mathbf{A}_3\tilde{\mathbf{I}}_2\mathrm{Re}\{\mathbf{G}\tilde{\mathbf{R}}_{ss}\mathbf{G}^*\}\tilde{\mathbf{I}}_2\mathbf{A}_3^H\right\}$$

$$= \mathbf{A}_3\,\frac{1}{2}\left\{\mathrm{Re}\{\mathbf{G}\tilde{\mathbf{R}}_{ss}\mathbf{G}^*\} + \tilde{\mathbf{I}}_2\mathrm{Re}\{\mathbf{G}\tilde{\mathbf{R}}_{ss}\mathbf{G}^*\}\tilde{\mathbf{I}}_2\right\}\mathbf{A}_3^H \tag{4.43}$$

We observe that $\mathrm{Re}\{\tilde{\mathbf{C}}_{hh}^{fb}\}$, a 3x3 matrix, is of rank 2 in the asymptotic and no noise cases under symmetric multipath conditions. It is easily shown that under nonsymmetric multipath conditions, $\mathrm{Re}\{\tilde{\mathbf{C}}_{hh}^{fb}\}$ is of full rank equal to 3. Similar to the preceding, we can emulate symmetric multipath conditions by operating on $\mathbf{A}_3$ in (4.37) by the matrix

$$\mathbf{W}(u_c) = \begin{bmatrix} e^{-j\pi u_c} & 0 & 0 \\ 0 & 1 & 0 \\ 0 & 0 & e^{j\pi u_c} \end{bmatrix} \tag{4.44}$$

with $u_c = \frac{1}{2}\{u_1 + u_2\}$.

From these observations, it follows that the bisector angle estimation procedure in (4.28) may be equivalently formulated in terms of $\mathrm{Re}\{\tilde{\mathbf{C}}_{hh}^{fb}\}$ as

$$\underset{u_c}{\text{Minimize}}\ \det\left(\mathrm{Re}\{\mathbf{W}^*(u_c)\tilde{\mathbf{C}}_{hh}^{fb}\mathbf{W}(u_c)\}\right) \tag{4.45}$$

$$\text{subject to } u_c \in (-\frac{2}{M}, \frac{2}{M})$$

where $\tilde{\mathbf{C}}_{hh}^{fb}$ is determined from $\mathrm{Re}\{\tilde{\mathbf{C}}_{bb}^{fb}\}$ as

$$\tilde{\mathbf{C}}_{hh}^{fb} = \mathbf{E}_{\ell}^{H\,-1}\mathrm{Re}\{\tilde{\mathbf{C}}_{bb}^{fb}\}\mathbf{E}_{\ell}^{-1} \tag{4.46}$$

This relationship is deduced from (4.40). Note that $\mathbf{E}_{\ell}$ is constructed according to (4.32) and is easily inverted. More importantly, note that whereas $\mathbf{D}(u_c)$ in (4.28) is LxL, where L is the number of elements in each subarray employed in the process of spatial smoothing, $\mathbf{W}(u_c)$ in (4.45) is only 3x3. As a consequence, the optimization problem posed in (4.45) is much easier to solve than the equivalent one posed in (4.28). In fact, it is shown in Appendix A that the solution procedure is tantamount to solving for the roots of a quartic equation. Let $\hat{\lambda}_c = e^{j2\pi\hat{u}_c}$. It is shown in Appendix A that $\hat{\lambda}_c$ is a root of the polynomial

$$p(\lambda) = -2p_o^* - p_1^*\lambda + p_1\lambda^3 + 2p_0\lambda^4 = 0 \tag{4.47}$$

where the coefficients p_o and p_1 are a function of the components of $\tilde{\mathbf{C}}_{hh}^{fb}$, denoted $\left(\tilde{\mathbf{C}}_{hh}^{fb}\right)_{ij}$, i,j=1,2,3.

$$p_o = \left(\tilde{\mathbf{C}}_{hh}^{fb}\right)_{12}^2\left(\tilde{\mathbf{C}}_{hh}^{fb}\right)_{13} - \left(\tilde{\mathbf{C}}_{hh}^{fb}\right)_{22}\left(\tilde{\mathbf{C}}_{hh}^{fb}\right)_{13}^2 \tag{4.48}$$

$$p_1 = 2\left|\left(\tilde{\mathbf{C}}_{hh}^{fb}\right)_{12}\right|^2\left(\tilde{\mathbf{C}}_{hh}^{fb}\right)_{13} - 2\left(\tilde{\mathbf{C}}_{hh}^{fb}\right)_{11}\left(\tilde{\mathbf{C}}_{hh}^{fb}\right)_{12}^2 \tag{4.49}$$

It is easily shown that at least two of the roots of $p(\lambda)$ in (4.47) lie on the unit circle. Thus, $\hat{\lambda}_c = e^{j2\pi\hat{u}_c}$ is that root lying on the unit circle which minimizes the objective function in (4.45).

Once, the bisector angle is estimated, it is recommended that the BDML method for symmetric multipath outlined in Section II be employed with the modification that $\mathbf{S}_M = \left[\mathbf{a}_M(-\frac{2}{M}) : \mathbf{a}_M(0) : \mathbf{a}_M(\frac{2}{M})\right]$ be replaced by $\mathbf{S}_M^c = \left[\mathbf{a}_M(\hat{u}_c - \frac{2}{M}) : \mathbf{a}_M(\hat{u}_c) : \mathbf{a}_M(\hat{u}_c + \frac{2}{M})\right]$. A summary of the symmetrized BDML method is delineated below.

Algorithmic Summary of Symmetrized BDML Method

(1.) With $L=\frac{2}{3}M$, $S_L = \left[\mathbf{a}_L(-\frac{2}{L}) : \mathbf{a}_L(0) : \mathbf{a}_L(\frac{2}{L})\right]$, and N snapshots $\mathbf{x}(n)$, $n=1,...,N$, form

$$\mathbf{x}_B(n;k) = \mathbf{S}_L^H \mathbf{E}_k^T \mathbf{x}(n) \quad \text{where: } \mathbf{E}_k = \begin{bmatrix} \mathbf{0} \\ \mathbf{I} \\ \mathbf{0} \end{bmatrix} \begin{matrix} (k-1)xL \\ LxL \\ (M-L-k+1)xL \end{matrix}$$

$k=1,...,M-L+1$; $n=1,...,N$

(2.) Construct $\tilde{\mathbf{R}}_{bb} = \frac{1}{N(M-L+1)} \sum_{n=1}^{N} \sum_{k=1}^{M-L+1} \mathbf{x}_B(n;k)\mathbf{x}_B^H(n;k)$

(3.) compute $\hat{\lambda}_{min}^{bb}$ as the smallest eigenvalue of $\tilde{\mathbf{R}}_{bb}$ and form

$$\tilde{\mathbf{C}}_{bb}^{fb} = \frac{1}{2}\left\{\tilde{\mathbf{R}}_{bb} + \tilde{\mathbf{I}}_3 \tilde{\mathbf{R}}_{bb} \tilde{\mathbf{I}}_3\right\} - \hat{\lambda}_{min}^{bb} \mathbf{I}_3$$

(4.) form $\tilde{\mathbf{C}}_{hh}^{fb} = \mathbf{E}_L^{H\,-1} \mathrm{Re}\{\tilde{\mathbf{C}}_{bb}^{fb}\} \mathbf{E}_L^{-1}$ where $\mathbf{E}_L$ is given by (4.32).

(5.) Compute roots of $p(\lambda) = -2p_o^* - p_1^*\lambda + p_1\lambda^3 + 2p_0\lambda^4 = 0$ where

$$p_o = \left(\tilde{\mathbf{C}}_{hh}^{fb}\right)_{12}^2 \left(\tilde{\mathbf{C}}_{hh}^{fb}\right)_{13} - \left(\tilde{\mathbf{C}}_{hh}^{fb}\right)_{22} \left(\tilde{\mathbf{C}}_{hh}^{fb}\right)_{13}^2$$

$$p_1 = 2\left|\left(\tilde{\mathbf{C}}_{hh}^{fb}\right)_{12}\right|^2 \left(\tilde{\mathbf{C}}_{hh}^{fb}\right)_{13} - 2\left(\tilde{\mathbf{C}}_{hh}^{fb}\right)_{11} \left(\tilde{\mathbf{C}}_{hh}^{fb}\right)_{12}^2$$

(6.) $\hat{u}_c = \frac{1}{j2\pi}\ln(\hat{\lambda}_c)$, where $\hat{\lambda}_c$ equal to that root of $p(\lambda)$ having unity magnitude for which $\det\left(\mathrm{Re}\{\mathbf{W}^*(\lambda_c)\tilde{\mathbf{C}}_{hh}^{fb}\mathbf{W}(\lambda_c)\}\right)$ is minimum where

$$\mathbf{W}(\lambda_c) = \begin{bmatrix} \lambda_c^* & 0 & 0 \\ 0 & 1 & 0 \\ 0 & 0 & \lambda_c \end{bmatrix}$$

(7.) With $\mathbf{S}_M^c = \left[\mathbf{a}_M(\hat{u}_c - \frac{2}{M}) : \mathbf{a}_M(\hat{u}_c) : \mathbf{a}_M(\hat{u}_c + \frac{2}{M})\right]$, form

$$\hat{\mathbf{R}}_{bb} = \frac{1}{N}\sum_{n=1}^{N} \mathbf{x}_B(n)\mathbf{x}_B^H(n) \quad \text{where: } \mathbf{x}_B(n) = \mathbf{S}_M^H \mathbf{x}(n)$$

(8.) Compute $\mathbf{v} = [v_1, v_2, v_1]^T$ as that centro-symmetric eigenvector of $\mathrm{Re}\{\hat{\mathbf{R}}_{bb}^{fb}\} = \frac{1}{2}\mathrm{Re}\left\{\hat{\mathbf{R}}_{bb} + \tilde{\mathbf{I}}_3\hat{\mathbf{R}}_{bb}\tilde{\mathbf{I}}_3\right\}$ associated with the smaller eigenvalue.

(9.) estimate u_o according to

$$\hat{u}_o = \frac{1}{\pi}\tan^{-1}\left\{\left[\left\{\frac{v_o - 2v_1\cos(\frac{\pi}{M})}{v_0\cos(\frac{2\pi}{M}) - 2v_1\cos(\frac{\pi}{M})}\right\}^2 - 1\right]^{\frac{1}{2}}\right\}$$

(10.) finally: $\hat{u}_1 = \hat{u}_o + \hat{u}_c \;\; ; \;\; \hat{u}_2 = -\hat{u}_o + \hat{u}_c$

4.4 Performance Improvement Via the Use of Frequency Diversity

We noted in the previous section that the performance of the BDML estimator for both the symmetric and nonsymmetric multipath cases degrades severely in a coherent environment when the direct and specular path signals arrive at the center element of the array very nearly equal in amplitude and perfectly or very nearly 180° out of phase. In addition, the BDML Method for nonsymmetric multipath breaks down when the direct and specular path signals arrive perfectly in-phase at the center element of the array as well. Provided the appropriate hardware is available, one of the obvious ways to avoid having the track broken under either of these conditions is to employ frequency diversity [KEZY88], [SKOL80]. In this case, the radar transmitter emits multiple narrowband signals spaced in frequency with the frequency spacings judiciously chosen so that the phase difference occurring at the center of the array at each transmission frequency is significantly different from frequency bin to frequency bin. Depending on the system hardware, the pulses at the various frequencies may be transmitted simultaneously and/or in rapid succession corresponding to frequency hopping. An example of a real radar system where frequency diversity is employed is the Multi-parameter Adaptive Radar System (MARS) described by V. Kezys and S. Haykin [KEZY88]. This experimental bistatic radar array consists of a 32-element, horizontally polarized linear array operating coherently over the band 8.05 to 12.34 GHz. Each antenna element is followed by two receiver channels allowing for simultaneous reception on two separate frequencies: one fixed at 10.2 GHz and the other agile over the band 8.05 to 12.34 GHz in 30 MHz steps. Many defense radar systems employ frequency diversity in some manner as well.

Let f_0 denote the frequency for which the M elements of the array are spaced by a half-wavelength; f_0 will be referred to as the reference frequency. Consider J-1 additional frequencies denoted f_i, i=1,...,J-1, employed such that for a given observation interval a total of J distinct frequencies are transmitted. We are here assuming that the same M element array described in Sect. II is employed for all frequencies. This, of course, has practical implications with regard to the range over which the frequencies may vary. We simply note here as an example the parameters of the MARS system cited above. We will assume that during the observation interval, N_i snapshot vectors for the transmission frequency f_i, denoted $\mathbf{x}(n\,;f_i)$, are collected. Again, N_i, i=0,..,J-1, may be as small as one in some practical situations. Now, for the sake of generality, consider the nonsymmetric multipath scenario. Similar to before, our goal is to compute the ML estimates of u_1 and u_2 given as data the beamspace snapshot vectors $\mathbf{x}_B(n\,;f_i) = \mathbf{S}^H(f_i)\mathbf{x}(n\,;f_i)$, i=0,...,J-1, n =1,...,$N_i$, where $\mathbf{S}(f_i)$ is an Mx3 beamforming matrix which, as implied, may be different for each frequency. To this end, let $\mathbf{a}(u\,;f_i)$ denote the element space manifold vector associated with the frequency f_i, i=0,...,J-1. The element space manifold vector for the reference frequency, f_0, is described by (2.2). $\mathbf{a}(u)$ in (2.2), now denoted $\mathbf{a}(u\,;f_0)$, may be easily generalized for frequency values other than f_0. The result for f_i, i=0,...,J-1, is as follows:

$$\mathbf{a}(u;f_i)=\left[e^{-jL\pi\frac{f_i}{f_0}u},\cdots,e^{-j2\pi\frac{f_i}{f_0}u},e^{-j\pi\frac{f_i}{f_0}u},1,e^{j\pi\frac{f_i}{f_0}u},e^{j2\pi\frac{f_i}{f_0}u},\cdots,e^{jL\pi\frac{f_i}{f_0}u}\right]^T \quad (4.50)$$

Note that the difference between $\mathbf{a}(u\,;f_i)$ and $\mathbf{a}(u\,;f_0)$ is simply a scaling of the argument which is illustrated by observing that $\mathbf{a}(\frac{f_0}{f_i}u\,;f_i) = \mathbf{a}(u;f_0)$. Now, given $\mathbf{S}(f_i)$ the beamspace manifold vector associated with frequency f_i is simply $\mathbf{b}(u\,;f_i) = \mathbf{S}^H(f_i)\mathbf{a}(u\,;f_i)$ with $\mathbf{a}(u\,;f_i)$ given by (4.50). A development similar to that which lead from (2.22) to (2.24) leads to the result that the BDML estimates of u_1 and u_2 may be found as the solution to the following optimization problem:

$$\underset{u_1,\,u_2}{\text{Minimize}} \sum_{i=0}^{J-1}\sum_{n=1}^{N_i}\mathbf{x}_B^H(n;f_i)\,\mathbf{Q}^{-1/2}(f_i)\mathbf{P}^{\perp}_{\mathbf{B}_w}(u_1,u_2;f_i)\mathbf{Q}^{-1/2}(f_i)\mathbf{x}_B(n;f_i) \quad (4.51)$$

where $\mathbf{Q}(f_i) = \mathbf{S}^H(f_i)\mathbf{S}(f_i)$ and $\mathbf{P}^{\perp}_{\mathbf{B}_w}(u_1,u_2\,;f_i)$ is the projection operator onto the orthogonal complement of the span of $\mathbf{Q}^{-1/2}(f_i)\mathbf{b}(u_1;f_i)$ and $\mathbf{Q}^{-1/2}(f_i)\mathbf{b}(u_2\,;f_i)$. Due to the dependence of $\mathbf{P}^{\perp}_{\mathbf{B}_w}(u_1,u_2\,;f_i)$ on the index i, i. e., on the value of f_i, we cannot formulate a closed-form procedure for the

BDML estimates of u_1 and u_2, the solution to (4.51), similar to the BDML Method outlined in Section III. The best we can do is to convert the objective function in (4.51) to a sum of ratios of two quadratic forms of the type in (2.45) giving rise to a set of coupled optimization problems. It is our goal here to retain the computational simplicity of the BDML estimation schemes outlined previously while still incorporating in a coherent manner the additional data provided by the use of the auxiliary frequencies. In particular, we would like to achieve simple, closed-form expressions similar to those obtained previously in the case where the beamforming matrix is of the Butler type in (2.36). To do so, we invoke the coherent signal subspace concept developed by Wang and Kaveh in their extension of the MUSIC algorithm for wideband sources [WANG85], [HUNG88].

4.4.1 Coherent Signal Subspace Processing

In a nutshell, the basic idea behind coherent signal subspace processing applied here is to apply a matrix transformation $\mathbf{T}_i$ to $\mathbf{x_B}(n\,;f_i)$ such that if $\mathbf{x_B}(n\,;f_i) = c_1(n\,;f_i)\mathbf{b}(u_1\,;f_i) + c_2(n\,;f_i)\mathbf{b}(u_2\,;f_i) + \nu(n\,;f_i)$ then $\mathbf{T}_i\mathbf{x_B}(n\,;f_i) = c_1(n\,;f_i)\mathbf{b}(u_1\,;f_0) + c_2(n\,;f_i)\mathbf{b}(u_2\,;f_0) + \mathbf{T}_i\nu(n\,;f_i)$. That is, we attempt to translate the signal information at each of the auxiliary frequencies f_i, i=1,...J-1, to the reference frequency f_0 where it may be coherently combined. It is apparent that the matrix $\mathbf{T}_i$ must satisfy the following relationships.

$$\mathbf{T}_i\mathbf{b}(u_1;f_i) = \mathbf{b}(u_1;f_0) \text{ and } \mathbf{T}_i\mathbf{b}(u_2;f_i) = \mathbf{b}(u_2;f_0) \quad i=1,\ldots,J-1 \tag{4.52}$$

A matrix satisfying (4.52) is referred to as a focusing matrix. With $\mathbf{B}_i = \left[\mathbf{b}(u_1\,;f_i) : \mathbf{b}(u_2\,;f_i)\right]$, i=0,...,J-1, one possible choice for for the focusing matrix is

$$\mathbf{T}_i = \mathbf{B}_0\left(\mathbf{B}_i^T\mathbf{B}_i\right)^{-1}\mathbf{B}_i^T \qquad i=1,\ldots,J-1 \tag{4.53}$$

Note that $\mathbf{T}_i$ in (4.53) is a real 3x3 matrix. Now, the cumulative effect of the coherent signal subspace transformations applied to each of the beamspace snapshot vectors may be equivalently implemented as a transformation on the beamspace correlation matrices. The end result is that the BDML Method for nonsymmetric multipath outlined in Sect. III is executed with the coherently combined beamspace correlation matrix $\bar{\mathbf{R}}_{bb} = \frac{1}{J}\sum_{i=0}^{J-1}\mathbf{T}_i\hat{\mathbf{R}}_{bb}(f_i)\mathbf{T}_i^T$, where $\hat{\mathbf{R}}_{bb}(f_i) = \mathbf{S}^H(f_i)\,\hat{\mathbf{R}}_{xx}(f_i)\,\mathbf{S}(f_i)$, i=0,...,J-1, as opposed to being executed with

the beamspace correlation matrix at a single frequency. Note that in this formulation $\mathbf{T}_0 = \mathbf{I}$.

To briefly illustrate the efficacy of the coherent signal subspace approach, consider the asymptotic form of $\hat{\mathbf{R}}_{bb}(f_i)$ which, based on (2.50), may be expressed as

$$\mathbf{R}_{bb}(f_i) = \mathbf{B}(f_i)\mathbf{R}_{ss}(f_i)\mathbf{B}^T(f_i) + \sigma^2_{n,i}\mathbf{S}^H(f_i)\mathbf{S}(f_i) \tag{4.54}$$

where $\mathbf{B}(f_i) = \left[\mathbf{b}(u_1;f_i) \vdots \mathbf{b}(u_2;f_i)\right]$, i=0,...,J-1. Employing the ideal focusing matrices in (4.53), we find that $\bar{\mathbf{R}}_{bb}$ has the following asymptotic form:

$$\begin{aligned}
\bar{\mathbf{R}}_{bb} &= \frac{1}{J}\sum_{i=0}^{J-1} \mathbf{T}_i\mathbf{R}_{bb}(f_i)\mathbf{T}_i^T \\
&= \frac{1}{J}\sum_{i=0}^{J-1}\mathbf{T}_i\mathbf{B}(f_i)\mathbf{R}_{ss}(f_i)\mathbf{B}^T(f_i)\mathbf{T}_i^T + \frac{1}{J}\sum_{i=0}^{J-1}\sigma^2_{n,i}\mathbf{T}_i\mathbf{S}^H(f_i)\mathbf{S}(f_i)\mathbf{T}_i^T \\
&= \mathbf{B}(f_0)\left\{\frac{1}{J}\sum_{i=0}^{J-1}\mathbf{R}_{ss}(f_i)\right\}\mathbf{B}^T(f_0) + \frac{1}{J}\sum_{i=0}^{J-1}\sigma^2_{n,i}\mathbf{T}_i\mathbf{Q}(f_i)\mathbf{T}_i^T \\
&= \mathbf{B}(f_0)\bar{\mathbf{R}}_{ss}\mathbf{B}^T(f_0) + \bar{\mathbf{Q}}
\end{aligned} \tag{4.55}$$

where, as implied, $\bar{\mathbf{R}}_{ss}$ is the algebraic average of the source covariance matrices $\mathbf{R}_{ss}(f_i)$ associated with each of the frequencies f_i, i=0,...,J-1. (4.55) implies that $\bar{\mathbf{R}}_{ss}$ is the effective source covariance matrix achieved with coherent signal subspace processing. For a single frequency $\mathbf{R}_{ss}(f_i)$ is of the form in (2.49) with $\Delta\Psi$ replaced by $\Delta\Psi_i$, the phase difference occurring at the center of the array at frequency f_i, i=0,...,J-1. The success of this frequency diversity scheme in combating the rank deficiency problems occurring with the BDML estimator for nonsymmetric, coherent multipath hinges on $\Delta\Psi_i$ being different for each transmitted frequency. If this is the case, $\bar{\mathbf{R}}_{ss}$ will be of full rank equal to 2, as will it's real part, as long as at least one additional frequency is employed. With $\bar{\mathbf{R}}_{ss}$ of full rank, the aforementioned problems are avoided in accordance with arguments provided in Section 2.5. Furthermore, an argument may be provided similar to that for spatial smoothing in [SHAN85], [EVAN82] that as the number of frequencies J increases, $\bar{\mathbf{R}}_{ss}$ approaches the highly desirable diagonal form, provided the frequencies are chosen judiciously. As far as combating signal cancellation is concerned, it is, of course, highly desirable that the frequencies be chosen such the probability of $\Delta\Psi_i$ being approximately equal to 180° at more than one

frequency is quite low.

A point glossed over earlier is that construction of $\mathbf{T}_i$ according to (4.53) requires knowledge of the angles which we are trying to estimate. This suggests an iterative procedure wherein we begin by constructing an initial set of focusing matrices based on some coarse estimates of the angles. Proceeding with the initial set of focusing matrices yields estimates of the angles corresponding to the first iteration. The new pair of angles are used to construct an updated set of focusing matrices which, in turn, yield the estimates of the angles at the second iteration. The procedure is then iterated until the absolute value of the difference between respective angle estimates obtained at the (k+1)-th and k-th iterations is less than some threshold for both the direct and specular paths. As the angles of interest in the low-angle tracking problem are within a beamwidth of broadside, the initial estimates of u_1 and u_2, denoted u_1^0 and u_2^0, respectively, may be taken to be zero. With $u_1^0 = u_2^0 = 0$, the initial set of focusing matrices must satisfy $\mathbf{T}_i\mathbf{b}(0;f_i) = \mathbf{b}(0;f_0)$, i=1,...,J-1. At this point, let us specialize and consider only the case where the Butler matrix beamformer is applied at each frequency. To this end, let u_{B_i} denote the angle of the upper auxiliary beam formed at frequency f_i such that

$$\mathbf{S}(f_i) = \left[\mathbf{a}(u_{B_i}\,;\,f_i) \vdots \mathbf{a}(0\,;\,f_i) \vdots \mathbf{a}(-u_{B_i}\,;\,f_i) \right] \qquad i=0,\ldots,J-1 \qquad (4.56)$$

Invoking the previously cited property that $\mathbf{a}(u\,;\,f_i)$ in (4.50) satisfies $\mathbf{a}(\frac{f_0}{f_i}u\,;\,f_i) = \mathbf{a}(u\,;\,f_0)$,a it follows that a Butler matrix is achieved for each frequency if $u_{B_i} = \frac{f_0}{f_i}\frac{2}{M}$, i=0,...,J-1. In this case, the columns of $\mathbf{S}(f_i)$ are orthogonal for each f_i such that $\mathbf{Q}(f_i) = \mathbf{S}^H(f_i)\mathbf{S}(f_i) = M\mathbf{I}$. Furthermore, with this selection of u_{B_i}, it follows that $\mathbf{S}(f_i) = \mathbf{S}(f_0)$, i=0,...,J-1. We will invoke this property in the outline to be presented shortly. Another consequence of this choice of beamforming matrices is that $\mathbf{b}(0;f_i) = \mathbf{b}(0;f_0)$ for all i such that the initial focusing matrix for each frequency may be taken to the identity matrix, i. e., $\mathbf{T}_i = \mathbf{I}$, i=0,...,J-1, at the first iteration. Finally, the use of the Butler matrix beamformer at the reference frequency, f_0, allows us to solve for the estimates of u_1 and u_2 at each iteration via the roots of a quadratic equation according to the BDML method for nonsymmetric multipath outlined in Section 2.4. An outline of the coherent signal subspace modified BDML Method for nonsymmetric multipath employing frequency diversity and a Butler matrix beamformer at each frequency is delineated below.

Coherent Signal Subspace Modified BDML for Nonsymmetric Multipath with Frequency Diversity and Butler Beamformer

Initialization:

(1.) With $\mathbf{S} = [\mathbf{a}(\frac{2}{M}\,;\,f_0) \vdots \mathbf{a}(0\,;\,f_0) \vdots \mathbf{a}(-\frac{2}{M}\,;\,f_0)]$ and

$$\hat{\mathbf{R}}_{xx}(f_i) = \frac{1}{N_i}\sum_{n=1}^{N_i}\mathbf{x}(n\,;\,f_i)\,\mathbf{x}^H(n\,;\,f_i),\ \text{construct:}$$

$$\hat{\mathbf{R}}_{bb}(f_i) = \mathbf{S}^H\hat{\mathbf{R}}_{xx}(f_i)\,\mathbf{S},\quad i=0,\ldots,J-1.$$

(2.) (a.) $k=0$. (b.) $u_1^0 = u_2^0 = 0$. (c.) Construct $\overline{\mathbf{R}}_{bb} = \frac{1}{J}\sum_{i=0}^{J-1}\hat{\mathbf{R}}_{bb}(f_i)$ and assign $\overline{\mathbf{Q}} = \mathbf{I}$.

Iteration:

(3.) $k=k+1$, compute $\mathbf{v} = [v_1\ ,\ v_2\ ,\ v_3]^T$ as GEVEC of pencil $\{\mathrm{Re}\{\overline{\mathbf{R}}_{bb}\}, \overline{\mathbf{Q}}\}$ assoc. with smallest GEV.

(4.) $\alpha = \dfrac{q_o}{q_1}$ where:

$$q_0 = -v_1\,e^{-j\frac{\pi}{M}} + v_2 - v_3\,e^{j\frac{\pi}{M}}\ \ \&\ \ q_1 = 2(v_1+v_3)\cos(\frac{\pi}{M}) - 2v_2\cos(\frac{2\pi}{M}).$$

(5.) $\hat{z}_1 = \dfrac{-1+j\sqrt{4\,|\,\alpha\,|^2-1}}{2\alpha}$ ☞ $\hat{u}_1 = \dfrac{1}{j\pi}\ln\{\hat{z}_1\}$;

$\hat{z}_2 = \dfrac{-1-j\sqrt{4\,|\,\alpha\,|^2-1}}{2\alpha}$ ☞ $\hat{u}_2 = \dfrac{1}{j\pi}\ln\{\hat{z}_2\}$

(6.) If $\left|u_1^k - u_1^{k-1}\right| < \epsilon$ and $\left|u_2^k - u_2^{k-1}\right| < \epsilon$, then $\hat{u}_1 = u_1^k$ and $\hat{u}_2 = u_2^k$. **STOP!**

(7.) With $\mathbf{B}_i = \left[\mathbf{b}(u_1^k\,;\,f_i) \vdots \mathbf{b}(u_2^k\,;\,f_i)\right]$, i=0,...,J-1, construct the focusing matrices $\mathbf{T}_i = \mathbf{B}_0\left(\mathbf{B}_i^T\mathbf{B}_i\right)^{-1}\mathbf{B}_i^T$.

(8.) With $\mathbf{T}_0 = \mathbf{I}$, construct $\overline{\mathbf{R}}_{bb} = \frac{1}{J}\sum_{i=0}^{J-1}\mathbf{T}_i\hat{\mathbf{R}}_{bb}(f_i)\mathbf{T}_i^T$ and $\overline{\mathbf{Q}} = \frac{1}{J}\sum_{i=0}^{J-1}\mathbf{T}_i\mathbf{T}_i^T$. **GO TO (3.).**

Note that the construction of $\overline{\mathbf{Q}}$ in (8.) assumes that the expected power of the noise is the same for all frequencies, i. e., $\sigma^2_{n,0}=\sigma^2_{n,1}=\ldots=\sigma^2_{n,J-1}$. If this is not the case, two modifications to the above algorithm should be incorporated.

First, the initialization process should include an extra step in in which $\sigma^2_{n,i}$ is estimated as the smallest eigenvalue (EV) of $\hat{\mathbf{R}}_{bb}(f_i)$, i=0,...,J-1. $\overline{\mathbf{Q}}$ in (8.) should then be computed as $\overline{\mathbf{Q}} = \frac{1}{J}\sum_{i=0}^{J-1} \sigma^2_{n,i}\mathbf{T}_i\mathbf{T}_i^T$. As a side note on this matter, we point out that Hung and Kaveh have proposed unitary focusing matrices in [28]. If we could restrict $\mathbf{T}_i$, i=1,...,J, to be unitary here, equality of $\sigma^2_{n,i}$ for all i would not be required for the algorithm above to work properly as $\overline{\mathbf{Q}} = \frac{1}{J}\sum_{i=0}^{J-1} M\sigma^2_{n,i}\mathbf{T}_i\mathbf{T}_i^T = \left\{\frac{M}{J}\sum_{i=0}^{J-1}\sigma^2_{n,i}\right\}\mathbf{I}$ such that $\overline{\mathbf{Q}}$ may be normalized to be equal to $\mathbf{I}$ at each iteration. However, the 2-norm of $\mathbf{b}(u_1 ; f_i)$ varies with f_i such that finding a unitary matrix $\mathbf{T}_i$ which satisfies $\mathbf{T}_i\mathbf{b}(u_1 ; f_i) = \mathbf{b}(u_1 ; f_0)$ is, in general, not possible. Recall that the 2-norm of a vector obtained by pre-multiplying another vector by a unitary matrix is the same as that of the original vector.

Summarizing at this point, we note that the benefits reaped from the utilization of the coherent signal subspace concept in the case of low angle radar tracking with frequency diversity are two-fold. First, the frequency diversity facilitates diversity in the phase difference occurring at the center of the array which, when exploited by the coherent signal subspace processing, serves to lessen the probability of track breaking. Correspondingly, the focusing matrices serve to coherently combine the signal energy contained in the various frequencies while, at the same time, the noise energy in the different frequency bands is combined in an incoherent fashion. The second beneficial aspect of coherent signal subspace processing is that it expedites computational simplicity. The only growth in computation with respect to single frequency operation is the computation and implementation of the focusing matrices. This claim is somewhat tempered by the fact that the focusing matrices are not known a-priori which gives rise to an iterative procedure and, hence, additional computation. However, similar to observations made by Wang and Kaveh in the case of coherent signal subspace processing applied to passive MUSIC for wideband sources, we find that the estimates converge in just a few iterations. Along the lines of computational complexity, we should point out the dramatic advantage of working in beamspace as opposed to working in element space. If we were to employ frequency diversity and coherent signal subspace processing in element space, the focusing matrices would be MxM and complex whereas in beamspace they are real and 3x3, regardless of the number of elements. Also, with Butler matrix beamforming, the angle estimates obtained at each iteration are simply

computed via the roots of a quadratic equation as in steps (4) and (5) in the algorithmic summary above. As pointed out previously, a closed-form solution for the ML estimates in the case of element space processing is not possible even if the IQML algorithm is employed.

4.4.2 Beamspace Manifold Invariance Technique

At this point, we introduce an intriguing variation of the frequency diversity scheme outlined above in which we choose the auxiliary frequencies in a judicious fashion so as to effectively force the focusing transformations necessary for coherently combining the signal information at the reference frequency to be exactly equal to a known scalar multiple of the identity matrix for all J-1 auxiliary frequencies, i. e., $\mathbf{T}_i = w_i\mathbf{I}$, i=1,...,J-1, where w_i is known. With the focusing transformations known a-priori there is no need to iterate as in the procedure outlined above, i. e., perfect "focusing" is achieved at the outset such that the computational complexity is the same as that for single frequency operation. In addition, if the respective Butler matrix beamformer is employed at each frequency, the problem of estimating the noise power at each frequency is avoided as well. This follows from the following argument. With $\mathbf{T}_i = w_i\mathbf{I}$, i=1,...,J-1, and $\mathbf{Q}(f_i) = \mathbf{S}^H(f_i)\mathbf{S}(f_i) = M_i\mathbf{I}$, i=1,...,J-1, then

$$\overline{\mathbf{Q}} = \frac{1}{J}\sum_{i=0}^{J-1} \sigma_{n,i}^2 \mathbf{T}_i \mathbf{Q}(f_i)\mathbf{T}_i^T = \left\{\frac{1}{J}\sum_{i=0}^{J-1} w_i M_i \sigma_{n,i}^2\right\}\mathbf{I} \qquad (4.57)$$

such that $\overline{\mathbf{Q}}$ may be normalized to be equal to the identity matrix. Thus, the new procedure has some very attractive advantages over the frequency diversity scheme employing coherent signal subspace processing developed above. However, there is a trade-off for achieving computational simplicity: the choice of frequencies with the new scheme is limited to those frequencies which satisfy $f_i = \frac{M}{M_i} f_0$ where M_i is an integer less than M, the total number of array elements. For example, with a M=15 element array, the auxiliary frequencies would be limited to $1.0714f_0$, $1.154f_0$, $1.25f_0$, $1.364f_0$, and $1.5f_0$, $1.667f_0$, etc. In the former method, the choice of the values of the auxiliary frequencies was only limited by the capabilities of the hardware not the algorithm itself. The reason for the restriction on the frequency values imposed with the new scheme is due to the fact that it is based on keeping the shape of the array patterns associated with each of the three beamforming weight vectors at each frequency *the same for each frequency,* to within a

scalar multiple, in the general vicinity of broadside. Along these lines, we present the following argument.

Consider a beam steered to broadside at the reference frequency with rectangular weighting. Recall that the reference frequency f_0 is that frequency for which the M elements of the array are spaced by a half-wavelength. The nulls of the associated array pattern are located at $u = \pm m\frac{2}{M}$, $m=1,...,\frac{M-1}{2}$. If the frequency is increased with all other parameters fixed, the array pattern becomes "narrower". The nulls of the array pattern associated with frequency f_i are located at $u = \pm m\frac{f_0}{f_i}\frac{2}{M}$, $m=1,...,\frac{M-1}{2}$. However, if we operate at f_i but only employ a subarray of M_i contiguous elements, where, of course, $M_i < M$, the nulls of the associated array pattern are located at $u = \pm m\frac{f_0}{f_i}\frac{2}{M_i}$, $m=1,...,\frac{M_i-1}{2}$. Thus, if we wish to keep the location of the nulls occurring with frequency f_i the same as those occurring with f_0 and an M element array, we may employ a subarray of length M_i and choose $f_i = \frac{M}{M_i}f_0$. We now illustrate the advantage of doing such with regard to coherent signal subspace processing.

Let the element space manifold vector associated with frequency f_i and a subarray of M_i contiguous elements be denoted $\mathbf{a}(u;f_i,M_i)$. $\mathbf{a}(u;f_i)$ in (4.50), now denoted $\mathbf{a}(u\,;f_i,M)$, is easily generalized for subarrays of length M_i as follows:

$$\mathbf{a}(u;f_i,M_i) = \left[e^{-j\pi\frac{M_i-1}{2}\frac{f_i}{f_0}u}, e^{-j\pi\frac{M_i-3}{2}\frac{f_i}{f_0}u}, ..., 1, ..., e^{j\pi\frac{M_i-3}{2}\frac{f_i}{f_0}u}, e^{j\pi\frac{M_i-1}{2}\frac{f_i}{f_0}u}\right]^T$$

if M_i is odd

$$\mathbf{a}(u;f_i,M_i) = \left[e^{-j\pi\frac{M_i}{2}\frac{f_i}{f_0}u}, ..., e^{-j\pi\frac{f_i}{2f_0}u}, e^{j\pi\frac{f_i}{2f_0}u}, ..., e^{j\pi\frac{M_i}{2}\frac{f_i}{f_0}u}\right]^T \quad (4.58)$$

if M_i is even.

Further, let $\mathbf{S}(f_i,M_i)$ denote an M_ix3 beamforming matrix to be applied to a subarray of length M_i at frequency f_i. With rectangular weighting, the general form of $\mathbf{S}(f_i,M_i)$ is as follows:

$$\mathbf{S}(f_i,M_i) = \left[\mathbf{a}(u_{B_i};f_i,M_i) \vdots \mathbf{a}(0;f_i,M_i) \vdots \mathbf{a}(-u_{B_i};f_i,M_i)\right] \quad i=0,...,J-1. \quad (4.59)$$

The attendant beamspace manifold vector $\mathbf{b}(u;f_i) = \mathbf{S}^H(f_i,M_i)\mathbf{a}(u;f_i,M_i)$ for

i=0,...,J-1, may be expressed in the following form:

$$\mathbf{b}(u;f_i) = \left[\frac{\sin\left(M_i \frac{\pi}{2}\frac{f_i}{f_0}(u-u_{B_i})\right)}{\sin\left(\frac{\pi}{2}\frac{f_i}{f_0}(u-u_{B_i})\right)}, \frac{\sin\left(M_i \frac{\pi}{2}\frac{f_i}{f_0}u\right)}{\sin\left(\frac{\pi}{2}\frac{f_i}{f_0}u\right)}, \frac{\sin\left(M_i \frac{\pi}{2}\frac{f_i}{f_0}(u+u_{B_i})\right)}{\sin\left(\frac{\pi}{2}\frac{f_i}{f_0}(u+u_{B_i})\right)} \right]^T \tag{4.60}$$

where M_0 is simply M, the number of elements in the entire array. Now, in the low-angle radar tracking scenario, u and u_{B_i} are quite small such that we may invoke the approximation $\sin(x) \simeq x$ for $x \ll 1$ in the denominator of each the three components of $\mathbf{b}(u;f_i)$ in (4.60). This approximation is tantamount to approximating the respective array patterns associated with each of the weight vectors $\mathbf{a}(u_{B_i};f_i,M_i)$, $\mathbf{a}(0;f_i,M_i)$, and $\mathbf{a}(-u_{B_i};f_i,M_i)$as a sinc function for small values of u, i. e., in the vicinity of the mainlobe and first sidelobes. Thus, $\mathbf{b}(u;f_i)$, i=0,...,J-1, in (4.60) may be approximated in the following fashion:

$$\mathbf{b}(u;f_i) \simeq \frac{f_0}{f_i}\left[\frac{\sin\left(M_i \frac{\pi}{2}\frac{f_i}{f_0}(u-u_{B_i})\right)}{\frac{\pi}{2}(u-u_{B_i})}, \frac{\sin\left(M_i \frac{\pi}{2}\frac{f_i}{f_0}u\right)}{\frac{\pi}{2}u}, \frac{\sin\left(M_i \frac{\pi}{2}\frac{f_i}{f_0}(u+u_{B_i})\right)}{\frac{\pi}{2}(u+u_{B_i})} \right]^T \tag{4.61}$$

Note that in making this approximation we have assumed that $\frac{f_i}{f_0}$ is on the order of unity as dictated by practical considerations. Observing (4.60), we note that if u_{B_i} is chosen to be the same angle for each frequency and f_i and M_i satisfy $M_i f_i = M f_0$, i=1,...,J-1, $\mathbf{b}(u;f_i)$ will be identical for all J frequencies to within a known scalar multiple, i. e., $\mathbf{b}(u;f_0) = \frac{f_i}{f_0}\mathbf{b}(u;f_i)$ for i=1,...,J-1. Hence, the appropriate focusing matrices to achieve coherent combining of the signal information at the reference frequency are $\mathbf{T}_i = \frac{f_i}{f_0}\mathbf{I}$, i=0,...,J-1, such that the coherently combined beamspace correlation matrix is simply computed as

$$\bar{\mathbf{R}}_{bb} = \frac{1}{J}\sum_{i=0}^{J-1}\left(\frac{f_i}{f_0}\right)^2 \hat{\mathbf{R}}_{bb}(f_i)$$

$$= \frac{1}{J}\sum_{i=0}^{J-1}\left(\frac{f_i}{f_0}\right)^2 \mathbf{S}^H(f_i,M_i)\,\hat{\mathbf{R}}_{xx}(f_i,M_i)\,\mathbf{S}(f_i,M_i) \tag{4.62}$$

where $\hat{\mathbf{R}}_{xx}(f_i,M_i)$ is the sample correlation matrix formed from the outputs of

a subarray of M_i contiguous elements. Note that an M element uniformly-spaced array is inherently composed of $M-M_i+1$ identical subarrays of M_i contiguous elements. It would, of course, be nonsensical to utilize just one of these. To remedy this apparent dilemma, we recommend that spatial smoothing be performed over the $M-M_i+1$ subarrays of length M_i and that the resulting spatially smoothed correlation matrix denoted $\tilde{\mathbf{R}}_{xx}(f_i,M_i)$ and defined by

$$\tilde{\mathbf{R}}_{xx}(f_i,M_i) = \frac{1}{M-M_i+1} \sum_{k=1}^{M-M_i+1} \mathbf{E}_k^T \hat{\mathbf{R}}_{xx}(f_i,M)\mathbf{E}_k \qquad (4.63)$$

$$\text{where: } \mathbf{E}_k = \begin{bmatrix} \mathbf{0} & (k-1)xM_i \\ \mathbf{I} & M_i xM_i \\ \mathbf{0} & (M-M_i-k+1)xM_i \end{bmatrix}$$

replace $\hat{\mathbf{R}}_{xx}(f_i,M_i)$ in (4.62). Note that $\hat{\mathbf{R}}_{xx}(f_i,M)$ in (4.63) is the the sample correlation matrix formed from the outputs of all M elements of the array at frequency f_i.

Now, one of the stipulations in the above development is that u_{B_i} be the same for all frequencies. If we choose $u_{B_i} = \frac{2}{M}$, then a Butler matrix beamformer is achieved at the reference frequency such that u_1 and u_2 may be simply determined from the roots of a quadratic equation. Furthermore, in turns out that with $u_{B_i} = \frac{2}{M}$ substituted in (4.59) for i=0,...,J-1, we find that a Butler matrix beamformer is achieved at each of the auxiliary frequencies $f_i = \frac{M}{M_i} f_0$. This follows from the fact that $\mathbf{a}(u\ ;\ f_i,M_i)$ as defined by (4.58) satisfies $\mathbf{a}(u\ ;\ f_i\ ,\ M_i) = \mathbf{a}(\frac{f_i}{f_0}u\ ;\ f_0\ ,\ M_i)$ such that

$$\mathbf{a}(\pm\tfrac{2}{M}\ ;\ f_i\ ,\ M_i) = \mathbf{a}(\pm\tfrac{f_i}{f_0}\tfrac{2}{M}\ ;\ f_0\ ,\ M_i) = \mathbf{a}(\pm\tfrac{2}{M_i}\ ;\ f_0\ ,\ M_i) \qquad (4.64)$$

where in the far right side we have used the fact that $f_0M = f_iM_i$. For M_i elements uniformly-spaced by a half-wavelength corresponding to the reference frequency f_0, it follows from previous arguments that the vectors $\mathbf{a}(\frac{2}{M_i}\ ;\ f_0,M_i)$, $\mathbf{a}(0\ ;\ f_0,M_i)$ and $\mathbf{a}(-\frac{2}{M_i}\ ;\ f_0,M_i)$ are mutually orthogonal and the polynomials formed from them have M_i-3 roots in common. As a consequence, $\mathbf{Q}(f_i) = \mathbf{S}^H(f_i,M_i)\mathbf{S}(f_i,M_i)$, where $\mathbf{S}(f_i,M_i)$ is defined by (4.59)

with $u_{B_i} = \frac{2}{M}$, is identically equal to the identity matrix for each of the auxiliary frequencies. Thus, $\overline{\mathbf{Q}}$ may be taken to be the identity matrix in accordance with the result in (4.57).

The development above leads us to the following simplified version of the previously outlined algorithm employing coherent signal subspace processing in conjunction with frequency diversity when the auxiliary frequencies chosen satisfy $f_i = \frac{M}{M_i} f_0$ where M_i is some integer less than M.

Beam Invariant, Coherent Signal Subspace Modified BDML for Nonsymmetric Multipath with Frequency Diversity

(1.) Select integer $M_i < M$ and compute corresponding $f_i = \frac{M}{M_i} f_0$, $i=1,\ldots,J\text{-}1$, and construct:

$$\mathbf{S}(f_i,M_i) = \left[\mathbf{a}(\tfrac{2}{M};f_i,M_i) \vdots \mathbf{a}(0;f_i,M_i) \vdots \mathbf{a}(-\tfrac{2}{M};f_i,M_i)\right]$$

$$\text{and } \hat{\mathbf{R}}_{xx}(f_i,M) = \frac{1}{N_i} \sum_{n=1}^{N_i} \mathbf{x}(n;f_i)\,\mathbf{x}^H(n;f_i)$$

(2.) $\tilde{\mathbf{R}}_{xx}(f_i,M_i) = \frac{1}{M-M_i+1} \sum_{k=1}^{M-M_i+1} \mathbf{E}_k^T \hat{\mathbf{R}}_{xx}(f_i,M)\mathbf{E}_k$ where

$$\mathbf{E}_k = \begin{bmatrix} \mathbf{0} & (k-1)xM_i \\ \mathbf{I} & M_i x M_i \\ \mathbf{0} & (M-M_i-k+1)xM_i \end{bmatrix}, \quad i=0,\ldots,J-1.$$

(3.) With $\hat{\mathbf{R}}_{bb}(f_i) = \mathbf{S}^H(f_i,M_i)\,\tilde{\mathbf{R}}_{xx}(f_i,M_i)\,\mathbf{S}(f_i,M_i)$, $i=0,\ldots,J\text{-}1$, constructs:

$$\overline{\mathbf{R}}_{bb} = \frac{1}{J} \sum_{i=0}^{J-1} \left(\frac{f_i}{f_0}\right)^2 \mathbf{R}_{bb}(f_i)\,.$$

(4.) Compute $\mathbf{v} = [v_1\ ,\ v_2\ ,\ v_3]^T$ as EVEC of 3x3 matrix $\mathrm{Re}\{\overline{\mathbf{R}}_{bb}\}$ assoc. with smallest EV.

(5.) $\alpha = \frac{q_o}{q_1}$ where:

$$q_0 = -v_1\, e^{-j\frac{\pi}{M}} + v_2 - v_3\, e^{j\frac{\pi}{M}} \;\&\; q_1 = 2(v_1+v_3)\cos(\tfrac{\pi}{M}) - 2v_2\cos(\tfrac{2\pi}{M}).$$

$$(6.)\ \hat{z}_{1,2} = \frac{-1 \pm j\sqrt{4\,|\,\alpha\,|^2 - 1}}{2\alpha} \ \Rightarrow\ \hat{u}_{1,2} = \frac{1}{j\pi}\ln\{\hat{z}_{1,2}\}$$

4.5 Computer Simulations

Computer simulations were conducted to demonstrate the performance of each of the three auxiliary procedures proposed in this section. The array employed was linear with M=15 identical elements uniformly-spaced by a half-wavelength. Each execution of the BDML algorithm was conducted with N snapshots collected over an interval in which the complex reflection coefficient, ρ_c, was constant corresponding to a coherent multipath case. In the simulation model, $\rho = |\,\rho_c\,|$ was assumed to be 0.9. A 15x3 Butler beamformer of the form (2.36) was used to transform the 15x1 element space snapshot vectors to 3x1 beamspace snapshot vectors. Finally, the additive noise was modeled to be spatially white Gaussian and uncorrelated with the received signal echoes.

4.5.1 Simulations for $\hat{\rho}$-based BDML Scheme

This simulation demonstrates the improvement in performance attributed to the auxiliary process of estimating the reflection coefficient. The target elevation was 2° or 0.26 beamwidths, the SNR was fixed at 5 dB, and N = 10. In each of the 100 independent trials, five iterations were performed to obtain the estimate of the beamspace DOA vector $\hat{\mathbf{b}}(u_1)$. The means and standard deviations of the resulting estimates are listed in Table 4.1 for six different phase differences. For each of the six cases, we find that both the bias and the deviation decrease with the $\hat{\rho}$-based estimator relative to the original one. The disparity is greatest for $\Delta\psi$=180° and is negligible for $\Delta\psi$ close to 0°. This clarifies our earlier statement that the $\hat{\rho}$-based method is best for $\Delta\psi$ close to 180°. Notice that in addition to the reduction of bias and variance, the number of outliers reduces for $\Delta\psi$=157.5° and 180°. An outlier is registered whenever the angle estimate is greater than 7.64°. In other words, the resolution capability has been improved and the probability of loss of track has been reduced to a great extent. Note that in this case, the number of failures does not reduce. This may be attributed to the fact that for $\hat{u}$=0, the ρ-based BDML estimator cannot not distinguish between single path and multipath cases.

Table 4.1 Comparison of the performance of the original and the $\hat{\rho}$-based BDML methods for symmetric multipath with M = 15, N = 10, SNR = 5 dB, and θ_0=2°. $\bar{\theta}$ and $\hat{\sigma}$ represent the sample mean and sample standard deviation in degrees of the estimates from 100 independent trials. For each trial, five iterations were executed to get the estimate of b(u).

$\Delta\phi$	Without $\hat{\rho}$			With $\hat{\rho}$		
	$\bar{\theta}$	$\hat{\sigma}$	# outliers	$\bar{\theta}$	$\hat{\sigma}$	# outliers
0°	2.0014	0.1748	0	2.0014	0.1748	0
45°	1.9942	0.1959	0	1.9942	0.1958	0
90°	1.9744	0.2668	0	1.9745	0.2666	0
135°	1.8816	0.5858	0	1.8821	0.5833	0
157.5°	1.7197	1.0355	1	1.7203	1.0216	0
180°	3.5874	4.6536	10	1.8044	1.8018	0

4.5.2 Simulations for Symmetrized BDML Scheme

The next set of simulation results demonstrate the performance of the symmetrized BDML (S-BDML) scheme in a low-angle radar tracking scenario. The target angle, θ_1, was 2° and the specular path angle, θ_2, was $-1°$ such that the actual bisector angle, θ_c, was $\sin^{-1}(\frac{1}{2}\{\sin\theta_1 + \sin\theta_2\}) = 0.4998°$. Note that the bisector angle is defined in terms of the reduced angle $u = \sin\theta$. A subarray size, $M_s = 11$, was chosen in order to perform spatial smoothing.

The first simulation results compare the performance of the original version of BDML with the symmetrized version for various combinations of direct path SNR and phase difference $\Delta\Psi$. For each particular combination of SNR and $\Delta\Psi$, sample means and sample standard deviations of the respective estimates of θ_1 and θ_2 obtained from either BDML or S-BDML were computed from the results of 100 independent trials. The results achieved with BDML and S-BDML are presented in Figures 4.1 and 4.2, respectively. In addition, the sample means and sample standard deviations of the corresponding estimates of θ_c computed in the case of the S-BDML method are plotted in Figure 4.3. The aforementioned breakdown of the BDML methodin the respective cases of $\Delta\Psi = 0°$ and $\Delta\Psi = 180°$ is apparent in Figure 4.1. The BDML estimator simply does not provide reliable angle estimates under either of these two conditions regardless of the SNR. The substantial improvement in performance achieved with the S-BDML estimator in the case of $\Delta\Psi = 0°$ is exhibited in Figure 4.2. The trade-off for this improvement, of course, is the extra computation involvedin computing the bisector angle estimate. The improvement in performance achieved with S-BDML in the case of $\Delta\Psi = 90°$ is rather modest as this value of $\Delta\Psi$ is that for which BDML performs best. Although S-BDML did not perform much better than BDML in the case of $\Delta\Psi = 180°$ for SNR's below 15 dB, reliable estimates were obtained with an SNR of 20 dB.

As indicated previously, Figure 4.3 exhibits the performance of the bisector angle estimator (BAE) employed in the S-BDML procedure. Interestingly, he sample mean approaches the true bisector angle as $\Delta\Psi$ increases from 0° to 180° with 180° giving rise to the smallest bias for all SNR values except 0 dB. A significant bias, on the order of half a degree, is observed with $\Delta\Psi = 0°$ even at the relatively high SNR of 20 dB. On the other hand, Figure 4.2 indicates that the sample standard deviation of the corresponding S-BDML estimates of θ_1 and θ_2 were smallest in the case of $\Delta\Psi = 0°$. In fact, although the respective Cramer Rao Lower Bound (CRLB)

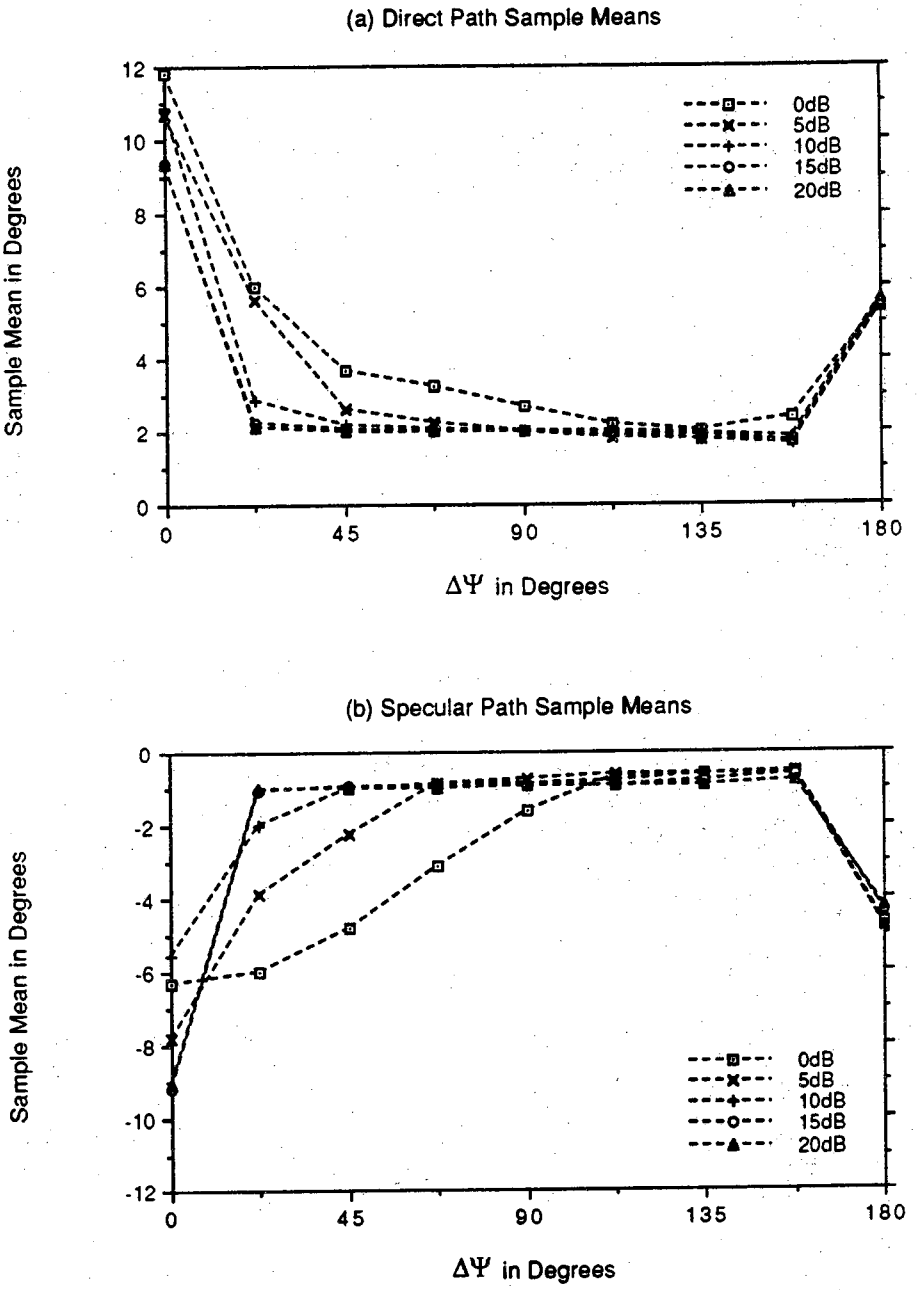

Figure 4.1 Performance of the BDML estimator in a nonsymmetric multipath scenario for five different direct path SNR values with target angle $\theta_1=2^\circ$, specular path angle $\theta_2=-1^\circ$, M=15, N=5, and $\rho=0.9$. Sample mean and sample standard deviation were computed from 100 independent trials.

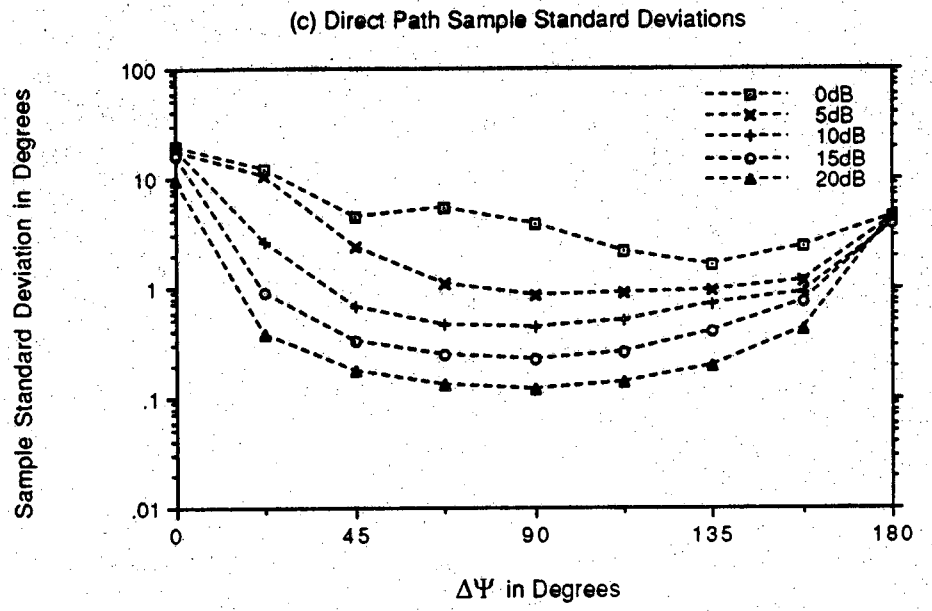

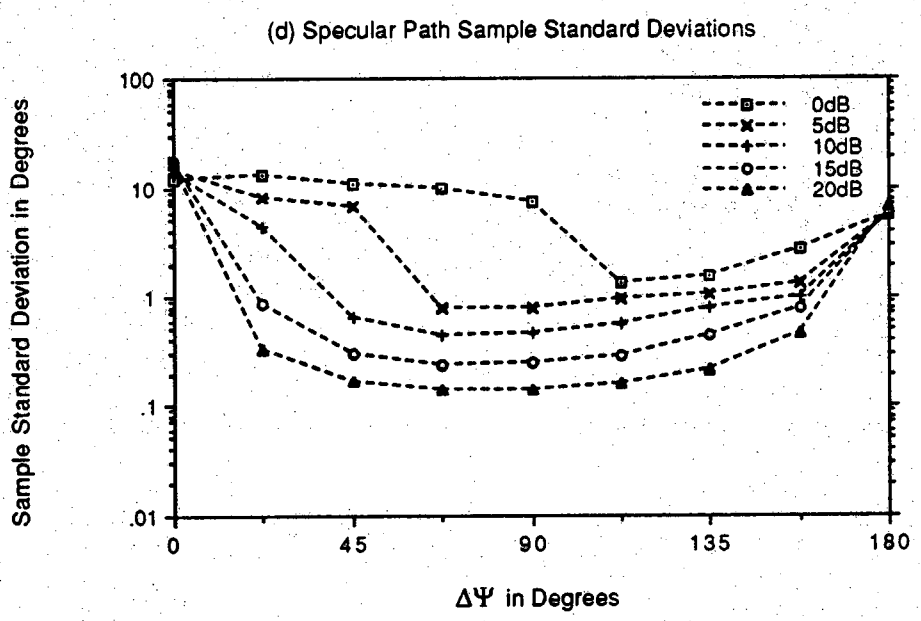

Figure 4.1, continued.

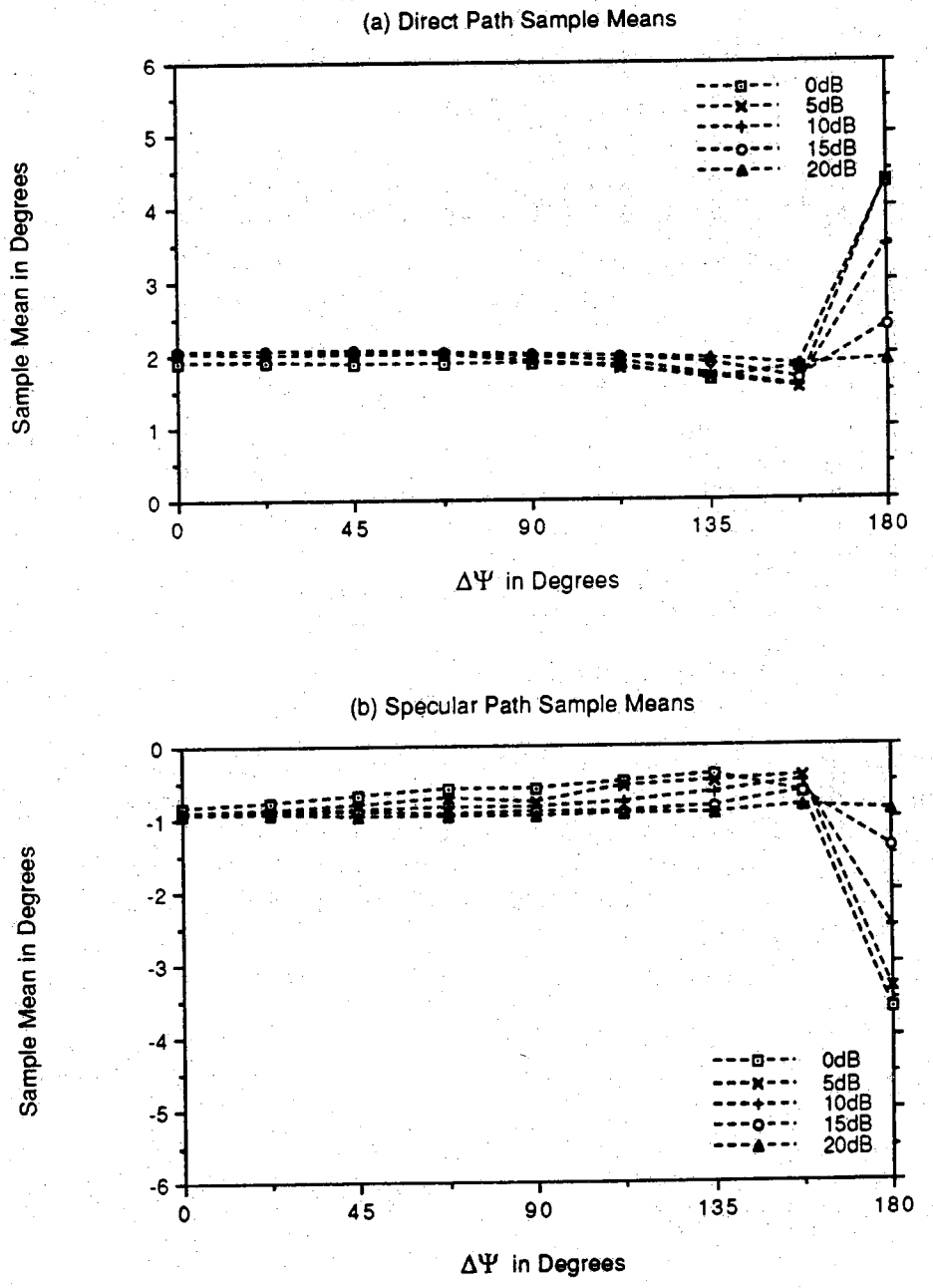

Figure 4.2 Performance of the S-BDML estimator in a nonsymmetric multipath scenario for five different direct path SNR values with target angle θ_1=2°, specular path angle θ_2=−1°, M=15, N=5, and ρ=0.9. Sample mean and sample standard deviation were computed from 100 independent trials.

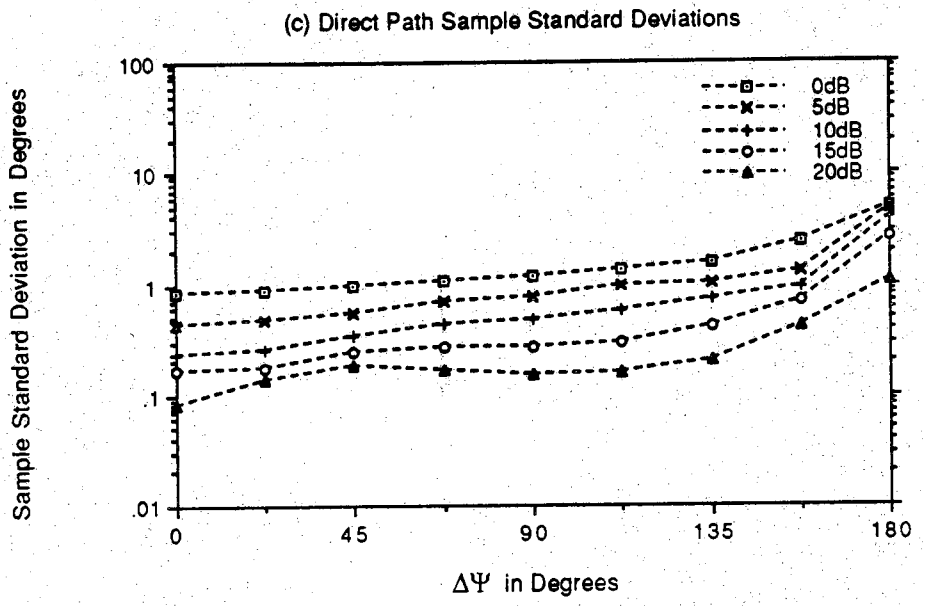

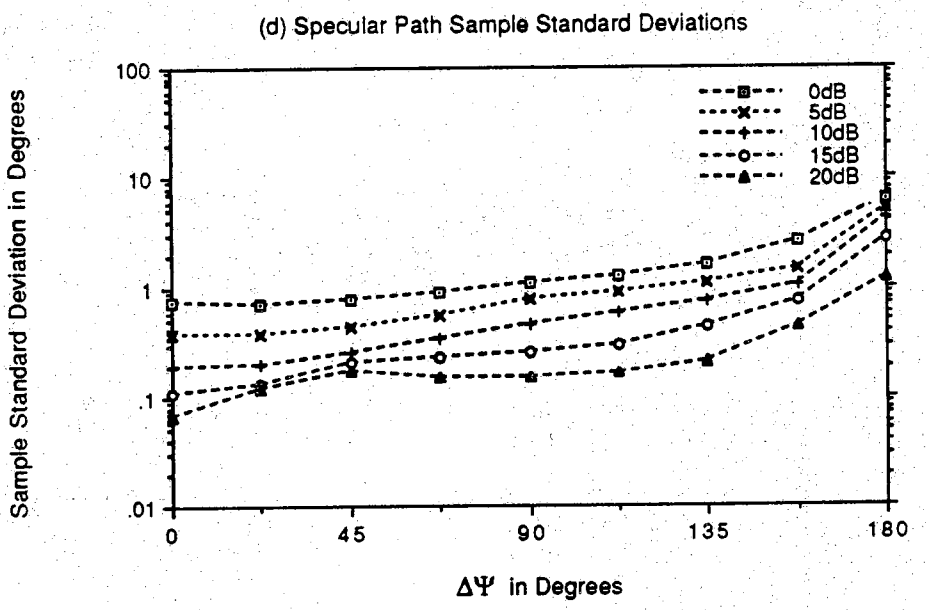

Figure 4.2, continued.

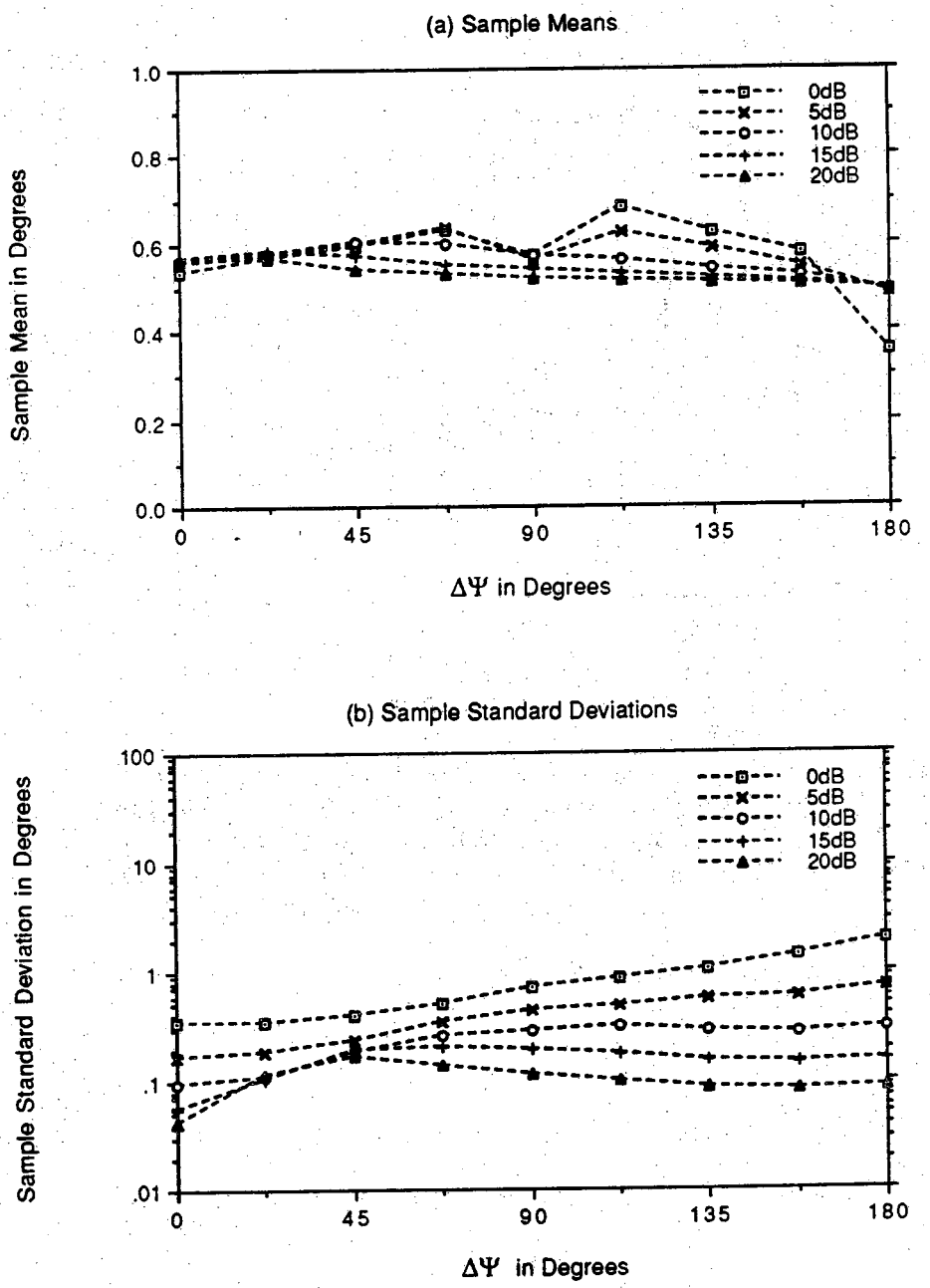

Figure 4.3 Performance of the bisector angle estimator in a nonsymmetric multipath scenario for five different direct path SNR values with target angle θ_1=2°, specular path angle θ_2=−1°, M=15, N=5, and ρ=0.9. Sample mean and sample standard deviation were computed from 100 independent trials.

is not plotted in Figure 4.2(c), the sample standard deviation of the S-BDML estimates of θ_1 for $\Delta\Psi = 0^\circ$ is significantly below the CRLB. The same is true with regard to the S-BDML estimates of θ_2. (A comparison between the CRLB and the sample standard deviations obtained from S-BDML estimates is made in the discussion accompanying the simulations presented in Figure 4.4.) This observation is, of course, not contradictory since the CRLB only holds for unbiased estimators. Further, this observation substantiates the conjecture made by Cantrell et. al. in [CANT81] that a biased estimator must exist for which the performance in the case of $\Delta\Psi = 0^\circ$ is significantly better than that dictated by the CRLB.

The second set of simulation results compare the performance and computational load of the S-BDML method with that of the improved three subaperture (3-APE) method of Gordon [GORD83] and the IQML method of Bresler and Macovski [BRES86]. The 3-APE method is a variation of an earlier version of the three subaperture method of Cantrell, Gordon, and Trunk [CANT81], which incorporates the practical constraint that ρ, the magnitude of the reflection coefficient, is less than one. The IQML algorithm is a computationally efficient implementation of the element space based ML estimation scheme. All simulation parameters were the same as in the first set of simulations discussed above except that the direct path SNR was fixed at 20 dB and each of the algorithms was executed given only a single snapshot, i. e., N=1. The performance of the three algorithms was examined as the phase difference $\Delta\Psi$ varied between 0° and 180° in increments of 22.5°. In each case, sample means and sample standard deviations were computed from the execution of a 100 independent trials. Sample means computed from estimates of the direct and specular path angles are plotted in Figures 4.4(a) and 4.4(b), respectively. The corresponding sample standard deviations are plotted in Figures 4.4(c) and 4.4(d) along with the respective Cramer-Rao Lower Bounds (CRLB's). The CRLB's were computed based on formulas provided by Stoica and Nehorai in [STOI89].

The most important observation gleaned from Figure 4.4 is that the symmetrized BDML method significantly outperforms both the 3-APE and IQML methods in the case of $\Delta\Psi = 0^\circ$, and in the case of $\Delta\Psi = 22.5^\circ$ as well. For example, in Figure 4.4(d) it is observed that the sample standard deviation (sample standard deviation) of the estimates of the specular path signal obtained from S-BDML for $\Delta\Psi = 0^\circ$ is approximately two orders of magnitude less than that obtained with either 3-APE or IQML. Observing the corresponding sample means plotted in Figure 4.4(b) for $\Delta\Psi = 0^\circ$, it is

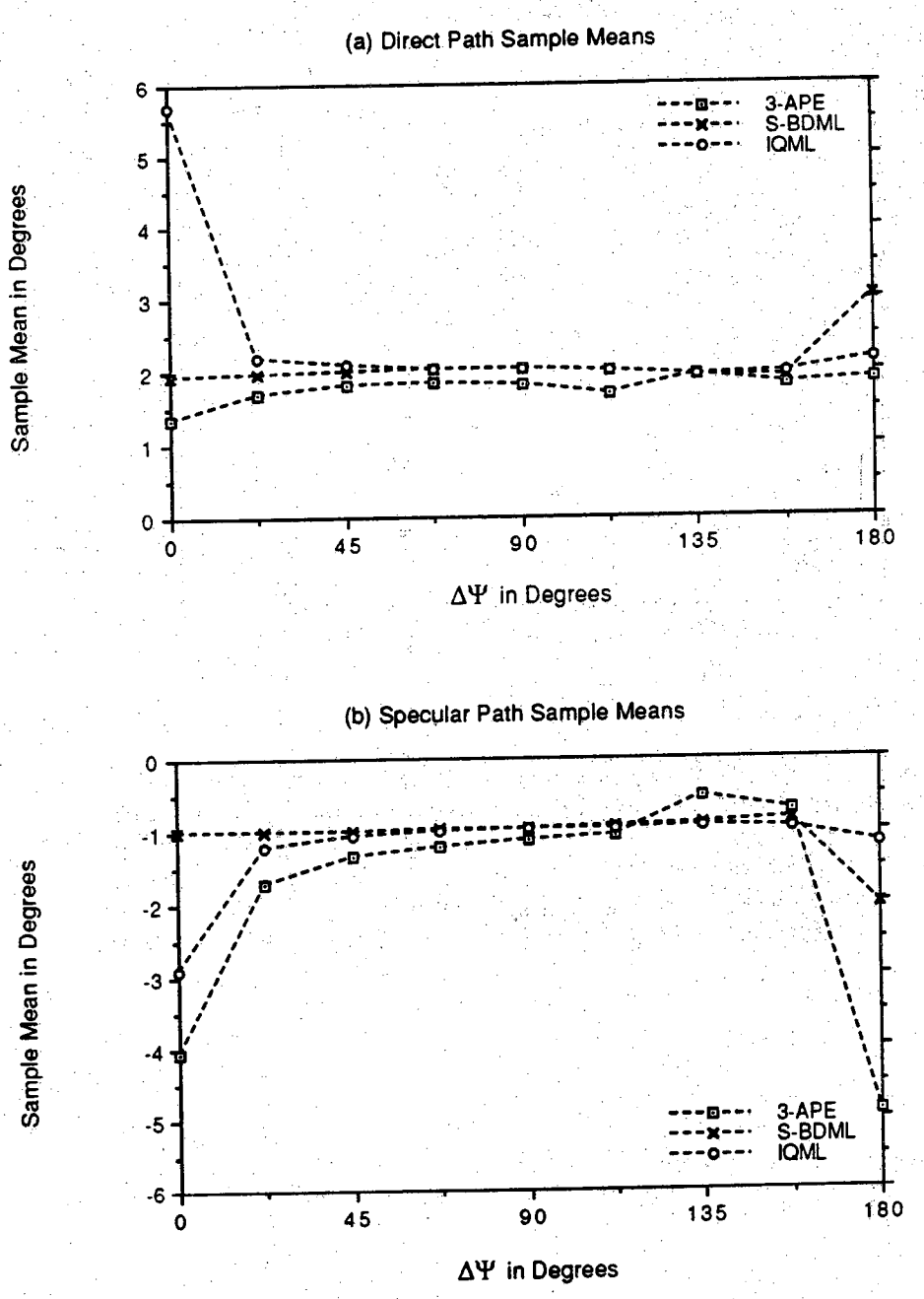

Figure 4.4 Comparison of the performance of the S-BDML method with that of the three aperture method and the IQML algorithm in a nonsymmetric multipath scenario with target angle θ_1=2°, specular path angle θ_2=−1°, M=15, N=1, SNR=20 dB for direct path, and ρ=0.9. Sample mean and sample standard deviation were computed from 100 independent trials.

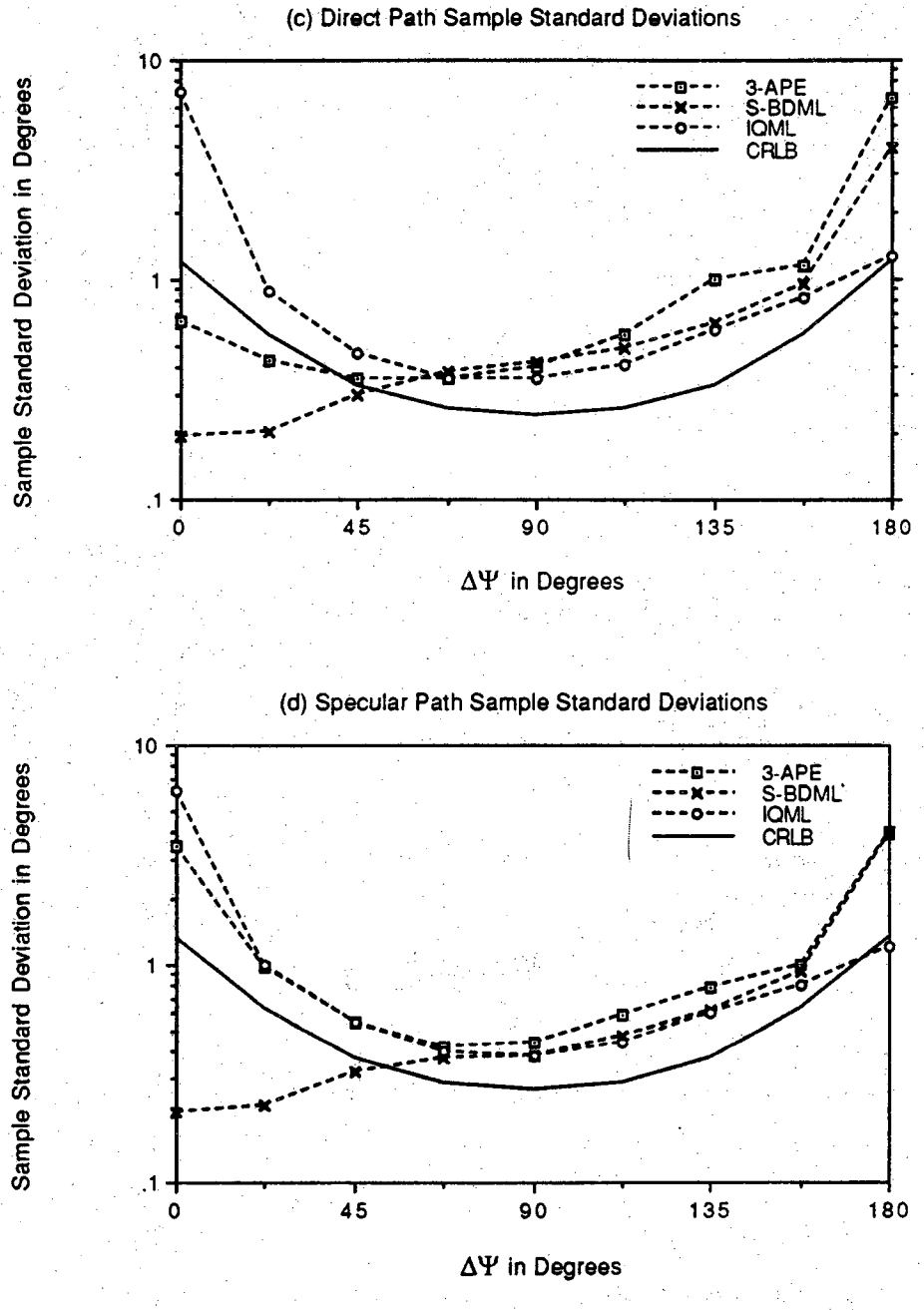

Figure 4.4, continued.

apparent that the 3-APE and IQML methods simply provide unreliable estimates of the specular path angle for small values of $\Delta\Psi$. It should be noted, though, that the angle of interest is actually that of the direct path signal. The performance of the 3-APE method is much better in this regard; the sample standard deviation of the 3-APE estimates of the direct path angle for $\Delta\Psi = 0^\circ$ is below that dictated by the CRLB. The corresponding bias, however, is rather high approximately equal to -0.6°. On the other hand, it is observed that the sample standard deviation of the S-BDML estimates of the direct path angle for $\Delta\Psi = 0^\circ$ is below the CRLB by roughly an order of magnitude, while the bias is rather small, on the order of a tenth of a degree! The IQML method provides totally unreliable estimates of both angles in the case of $\Delta\Psi = 0^\circ$. On the other hand, the IQML method significantly outperforms both the S-BDML and3-APE methods in the case of $\Delta\Psi = 180^\circ$.

To assess the trade-off between performance and computational load among the three algorithms,the number of floating point operations (flops) per execution was examined. This number was determined using the PRO-MATLAB software package for each of the three algorithms under the conditions specified above; it did not include the initial computation involved in setting up the data. The numbers are listed below.

3-APERTURE : $3.8\text{x}10^3$ avg. # flops/execution

S-BDML : $7.4\text{x}10^4$ # flops/execution

IQML : $6.5\text{x}10^5$ avg. # flops/execution

As indicated, the number of flops required for both the IQML and 3-APE methods is the respective average obtained over all 900 trial runs (100 independent trials for each of nine different phase differences). In contrast to S-BDML, each of these two methods is iterative in nature, i. e., not closed-form. The actual number of flops for a given execution can vary rather significantly depending on the SNR and phase difference $\Delta\Psi$.Notwithstanding, we note that the 3-APE method is the least burdensome with an average computational load approximately one-twentieth that of S-BDML and two orders of magnitude lower than that of IQML. The increased computational load of S-BDML relative to 3-APE is a trade-off for the significant improvement in performance observed at the smaller values of $\Delta\Psi$. The algorithms perform similarly for phase differences greater than 22.5°, although the sample standard deviation of the S-BDML estimates was always lower than the corresponding sample standard deviation of the 3-APE

method. Finally, we point out that the computational load of S-BDML is roughly an order of magnitudelower than that of IQML. Although IQML performed quite well for $\Delta\Psi = 180^\circ$, achieving the CRLB, it performed quite poorly for $\Delta\Psi = 0^\circ$.

4.5.3 Simulations for Multi-Frequency BDML Scheme

The final set of simulation results illustrate the power of using frequency diversity to overcome the aforementioned problems of signal cancellation and rank deficiency encountered with the BDML estimator when the phase difference between the direct and specular path signals at the center of the array at the reference frequency is either 180° or 0°. The statistics compiled in Table 4.2 compare the performance of the BDML estimation scheme employing a single frequency with that employing coherent signal subspace processing in conjunction with spatial smoothing for four frequencies satisfying $f_i = \frac{M}{M_i} f_0$, i=0,1,2,3, where M = 15. Here, f_0 was chosen to be that frequency for which the elements are spaced by a half-wavelength. The four values of M_i chosen were $M_0 = 15$, $M_1 = 13$, $M_2 = 11$, and $M_3 = 9$ corresponding to the frequencies f_0, $f_1 = 1.154f_0$, $f_2 = 1.364f_0$, and $f_3 = 1.667f_0$. Let $\Delta\Psi_i$, i=0,...,3, denote the phase difference occurring at the center of the array, modulo 360°, at the respective frequency f_i. Further, let $\Delta\Psi_{0,T}$ denote the total phase difference between the direct and specular path signals at the center of the array at the reference frequency counting integer number of wavelengths delays, i. e., without the modulo by 360° operation. The values of $\Delta\Psi_i$, i=1,2,3, were determined from $\Delta\Psi_{0,T}$ according to

$$\Delta\Psi_i = \left\{ \frac{f_i}{f_0} \{\Delta\Psi_{0,T} - 180^\circ\} + 180^\circ \ , \ \mathrm{mod}(360^\circ) \right\} \quad i=1,2,3 \quad (4.65)$$

in accordance with the model of the low-angle radar tracking scenario described by Skolnik [SKOL80]. Note that this formula accounts for a 180° phase shift occurring at the surface of reflection, a phenomenon discussed by Skolnik [SKOL80] and Barton [BART74]. Also, this formula holds regardless of whether the multipath is symmetric or not. In the symmetric multipath example, the target elevation angle was θ=1°, the direct path SNR was 5 dB, and $\Delta\Psi_{0,T}$ was 540°. Hence, $\Delta\Psi_0 = \{540 \ , \ \mathrm{mod}(360^\circ)\} = 180^\circ$ yielding maximum signal cancellation at the reference frequency. With $\Delta\Psi_{0,T}$=540° and the frequency values chosen, (4.65) dictates that

Table 4.2 Comparison of the performance of the single frequency-based BDML method and the multiple frequencies-based BDML method with M = 15, N = 10, SNR = 5 dB, and θ as given below. The four values of M_i used were M_o=15, M_1=13, M_2=11, and M_3=9 leading to the frequencies f_o, $1.154f_o$, $1.364f_o$, and $1.667f_o$, with f_o corresponding to half-wavelength spacings. $\bar{\theta}$ and $\hat{\sigma}$ represent the sample mean and sample standard deviation in degrees of the estimates from 100 independent trials.

	$\Delta\psi$		Single Frequency	Multiple Frequencies
Symmetric Multipath	180°	$\bar{\theta}$	3.2218	0.9754
		$\hat{\sigma}$	4.8142	0.1606
		# failures	42	0
Nonsymmetric Multipath	0°	$\bar{\theta}_1$	7.1861	1.9891
		$\hat{\sigma}_1$	14.2476	0.1743
		$\bar{\theta}_2$	-8.9785	-0.9932
		$\hat{\sigma}_2$	16.0743	0.2038
		# failures	0	0
	180°	$\bar{\theta}_1$	5.7616	2.0010
		$\hat{\sigma}_1$	8.1700	0.2286
		$\bar{\theta}_2$	-4.0492	-1.0269
		$\hat{\sigma}_2$	6.3873	0.2100
		# failures	28	0

$\Delta\Psi_1 = 235°$, $\Delta\Psi_2 = 310°$, and $\Delta\Psi_3 = 60°$. The statistics listed under the single frequency column were those obtained with the symmetric BDML estimator applied to N=10 snapshots of data obtained at the reference frequency. We note that the estimates are totally unreliable. A drastic improvement in performance is obtained when frequency diversity is employed as indicated by the statistics listed under the multiple frequency column. In this case, the coherent signal subspace modified BDML estimator outlined at the end of Section 4.4 was executed with N=10 snapshots of data from each of the four frequency bins. Here, $\mathbf{T}_i = \frac{f_i}{f_0}\mathbf{I}$, i=0,...,3, were used as the appropriate beamspace domain based focusing matrices. In this case, the BDML estimator is rather accurate. An improvement in performance of the same proportions is obtained in a nonsymmetric multipath scenario for the two problem cases of $\Delta\Psi_0 = 0°$ and $\Delta\Psi_0 = 180°$. For both nonsymmetric multipath examples, the target elevation angle was $\theta_1 = 2°$, the specular path angle was $\theta_2 = -1°$, and the direct path SNR was 5 dB. In the first example, $\Delta\Psi_{0,T}$ was chosen to be $360°$ giving $\Delta\Psi_0 = 0°$. As expected, the nonsymmetric BDML estimator performs miserably when applied to N=10 snapshots of data obtained at the reference frequency. In the case of multiple frequency operation, note that with $\Delta\Psi_{0,T}=360°$ and the frequency values indicated previously, (4.65) dictates that $\Delta\Psi_1 = 27°$, $\Delta\Psi_2 = 66°$, and $\Delta\Psi_3 = 120°$. Again using the coherent signal subspace modified BDML estimator outlined at the end of Sect. V with $\mathbf{T}_i = \frac{f_i}{f_0}\mathbf{I}$, i=0,...,3, we find that fairly accurate estimates are obtained. A similar improvement in performance is obtained for the case $\Delta\Psi_{0,T}=540°$ corresponding to $\Delta\Psi_0 = 180°$. Again, single frequency operation at the reference frequency provides useless results while multiple frequency operation provides rather accurate estimates.

As a final note, we note that in the simulation examples described above involving multiple frequency operation, the BDML estimator effectively worked with forty snapshots while it had to work with only ten snapshots in the case of single frequency operation. We remark that an increase in the number of snapshots at the reference frequency by a factor of four in the case of single frequency operation would not serve to increase the performance of the nonsymmetric BDML estimator by any degree in the case of either $\Delta\Psi_0 = 0°$ or $\Delta\Psi_0 = 180°$. As discussed in Section 2.5, for these two phase differences, the nonsymmetric BDML estimator breaks down even in the case of an infinite number of snapshots.

CHAPTER 5
ADAPTIVE BEAMFORMING FOR INTERFERENCE CANCELLATION

5.1 Introduction

Adaptive beamforming plays an important role in enhancing the performance of antenna arrays working in the presence of strong interferers or jammers. Beam patterns are formed by weighting and summing the array outputs to pass the desired signals distortionlessly and at the same time suppress the noise and interfering sources. Many beamforming schemes have been proposed for the application of Direction-of-Arrival Estimation [MONZ80], [BYRN87], [BRES88], [FORS87], [FRIE89], [FROS76], [GRIF87], [HAUP84], [MAYH87], [STEY86], [VAN89]. In general, they can be classified in two categories: the open loop beamformers and the closed loop beamformers [FRIE89]. In the open loop schemes, the DOA's of the desired and/or interfering sources need to be estimated first, usually done with some element space direction finding techniques such as MUSIC and ESPRIT [ROY89]. A procedure then follows to synthesize the desired beam patterns based on the estimated interference DOA's. The procedure usually involves a constrained optimization problem which leads to a solution for the optimum beamforming weight vectors. Several optimization criteria that are often used are the Minimum Variance Distortionless Response (MVDR) criterion [CAPO69], the Maximum Output Signal-to-Interference Ratio criterion [MONZ80], and the Minimum Mean-Square Error (MMSE) criterion [MONZ80]. It was shown that these methods differ only by virtue of some scalar processing that follows a common matrix filter and combiner operator [MONZ80]. In the close loop techniques, however, the weight vectors are adjusted automatically according to the variation in the output data form the combiner. An error criterion is usually set up to determine how to update the weights. Some examples of the closed loop beamformer can be found in [MONZ80], [HUDS81], [STEI76], [WIDR85], [APPL76], [RIEG67], [FROS76]. Some aspects of both the open and closed loop approaches were addressed in the paper of Griffiths and Buckley [GRIF87], and that of Friedlander and

Porat [FRIE89]. The main point is that the close loop beamformers are potentially more robust than the open loop ones since they are able to adjust themselves to uncertainties in the array and outside environment. However, in the case where the interferences are fully correlated with the desired signals, it has been shown that the closed loop schemes fail to work properly [WIDR85]. As a consequence, we shall concern ourselves with the open loop approach for the low-angle radar tracking problem. In particular, we will concentrate on the MVDR type of beamformers.

Since the pioneer work of Capon [CAPO69], the MVDR beamforming technique has received a great deal of attention in the areas of sonar, radar, and spectrum estimation. Some tutorial work can be found in the papers of Cox [COX73], Gabriel [GABR84], Frost [FROS76], and Johnson [JOHN82], the books by Monzingo and Miller [MONZ80] and Hudson [HUDS81]. Recent work on the performance analysis of the MVDR beamformer applied in various signal environments includes the papers of Reddy et. al. [REDD87], Shan et. al. [SHAN85], Zoltowski [ZOLT88b], and Van Veen [VAN89]. Their work was based on the assumption that no a-priori knowledge about the interfering sources is available. Under such condition, it is well known that the MVDR beamformer suffers severe performance degradation if the interfering sources are highly correalted with the desired signals. Not only does the beamformer fail to form deep nulls in the directions of the interferences, the desired signals may be cancelled partially or completely as well. In this regrad, Reddy et. al. [REDD87] incorporated spatial smoothing in their development of optimum beamformers. Bresler et. al. [BRES88] recommended the use of IQML algorithm as a means of obtaining the polynomial whose roots correspond to the DOA's of the interferences. The coefficients of the polynomial are then used to construct the optimum beamforming weight vector. The advantages to their approach are that the problem associated with signal coherence can be avoided and the actual DOA estimates of the interferences need not be computed.

In conventional adaptive beamforming, beampatterns are synthesized by weighting and linearly combining the outputs from the array elements. Interference cancellation is accomplished by judiciously choosing the weight vector so as to put nulls in the interfering directions and pass the desired sources without distortion. Inherent in this approach, however, is the assumption that there exists only one desired source within the mainlobe region. As an example, consider adaptive monopulse radar tracking [GABR84] wherein two beams, referred to as the left and right beams, are formed in the

vicinity of a detected target to accurately determine its angular location. The estimation problem of determining the angle of a single target given two beamformer outputs as encountered in monopulse radar tracking is a "two element - one source" array signal processing problem. Adaptive monopulse operation assumes that there is only one target within the field of view of the two beams and treats other sources as undesired interferences. The two beams are then designed to produce a null in the direction of each undesired source. This is accomplished, however, under the premise that the estimates of the locations of the interferences are available. In the case where two targets are located within a beamwidth of each other, as occurring in low-angle radar tracking, the beamformer, in an attempt to form a null in the direction of one of the targets, inevitably loses SNR gain for the other target. As a result, neither of the targets is accurately located. Motivated by the sub-beamwidth resolution capability exhibited by the BDML methods, we recommend the use of adaptively formed three beams in combating this problem. In this case, we assume that the two targets are located within the field of view of the three beams.

In this chapter, we present several novel MVDR-based beamforming techniques for the three-beam, two-target scenario. We will do so according to a two-stage algorithm wherein a polynomial whose roots correspond to the DOA's of the interferences is first estimated, and then an optimization problem is solved to obtain the weight vectors of the three beams for the BDML estimator. Motivated by the simplifications in computation achieved with the Mx3 Butler matrix beamformer, the three beams are formed in such a fashion so as to have M-3 nulls in common and that each beamforming vector has a null in the direction of each interfering source. An extra constraint is imposed in order to retain complex conjugate symmetry of the beamforming vectors employed in the BDML schemes. We will also present a least squares (LS) based technique for designing an orthogonal beamforming matrix. We accomplish so by finding a set of three mutually orthogonal beamforming weight vectors, with nulls in prescribed directions, which are closest to a set of "reference" weight vectors in a least squares sense. The problem can be formulated as a generalized Procruste problem and a closed-form solution is easily obtained via a 3x3 singular value decomposition. Other types of beamformers using different optimality criteria are achieved with certain modifications. Simulation results demonstrating the performance of the new beamforming techniques will be presented.

5.2 Problem Description

In the development of the BDML estimation schemes for low-angle tracking, we have assumed that the interfering sources are not too strong so that they can be filtered out by the beamforming operation. However, this is not always reliable as in some cases, strong interferers or smart jammers may be deliberately introduced and cause the track to break. A general result is that the DOA estimates tend to be "pushed" toward the interfering direction if the latter dominate the former in power. This is mainly due to the fact that we have underestimated the number of sources such that the sources become "fused". One possible remedy for this is to form D+1 beams, where D is the total number of sources, to simultaneously estimate the D DOA's. By doing so, it is very likely to degrade the performance of the estimator to a great extent, especially when D is large compared to the number of elements M. In addition, the computational load involved in this mode of operation will increase as D becomes large. An alternative approach, however, is to instead cancell those undesired sources by judiciously placing nulls in specified directions.

We consider here the low-angle radar tracking scenario in which echoes return from u_1 and u_2 via a direct path and a specular path, respectively, and K interfering sources from u_{Ik}, k=1,...,K, arrive outside the mainlobe region of the three beams. Assuming a uniformly-spaced linear array with half-wavelength spacings composed of M elements, the n-th array output snapshot vector can be expressed as

$$\mathbf{x} = \mathbf{A}_d\mathbf{s}_d + \mathbf{A}_I\mathbf{s}_I + \mathbf{n} \tag{5.1}$$

where $\mathbf{A}_d$ and $\mathbf{A}_I$ denote the Mx2 and MxK DOA matrices associated with the target echoes and the interferences, respectively. $\mathbf{s}_d$ and $\mathbf{s}_I$ are the corresponding complex signal vectors received at the array. The target echoes may be partially correlated or even coherent with the interferers. When the three beams method is employed, the Mx1 element space snapshot vector transforms into a 3x1 vector given by

$$\begin{aligned} \mathbf{x}_B &= \mathbf{W}^H\mathbf{x} \\ &= \mathbf{W}^H\mathbf{A}_d\mathbf{s}_d + \mathbf{W}^H\mathbf{A}_I\mathbf{s}_I + \mathbf{W}^H\mathbf{n} \\ &= \mathbf{B}_d\mathbf{s}_d + \mathbf{B}_I\mathbf{s}_I + \mathbf{n}_B \end{aligned} \tag{5.2}$$

where $\mathbf{W} = [\, \mathbf{w}_l \vdots \mathbf{w}_c \vdots \mathbf{w}_u \,]$ is an Mx3 beamforming matrix. If one applies the BDML estimation procedure developed previously to the beamspace

snapshot vector given by (5.2), the resulting estimates are usually unreliable primarily due to the fact that the Gaussian noise assumption is no longer valid and the least squares solution does not yield the ML estimates. In fact, one may consider the last two terms on the right hand side of (5.2) as the effective noise vector and proceed to solve an ML problem. However, doing so requires the knowledge about the interference correlation matrix, which requires an infinite number of snapshots. The correlation between the target echoes and the interferences further complicates the problem. In addition, the interferers could vary their power such that the problem of nonstationarity may arise. These make a direct ML approach infeasible. Motivated by the adaptive monopulse tracking technique developed by Davis et. al. [DAVI76], we recommend that the three beams should be formed in a fashion so as to filter out the outputs from the undesired interferences, i. e., the second term on the RHS of (5.2). Mathematically, this translates into a matrix equation described by

$$\mathbf{W}^H \mathbf{A}_I = \mathbf{0} \tag{5.3}$$

In terms of beamforming, this states that the three beampatterns should have K common nulls in the directions of the K interferers, or equivalently, the polynomials constructed with the three columns of $\mathbf{W}$ according to (5.1) must have K roots at $e^{j\pi u_{Ik}}$, k=1,...,K. We assume that the estimates $\hat{u}_{Ik}$, k=1,...K, are available, or more specifically, the polynomial, denoted as I(z), having as roots $e^{j\pi \hat{u}_{Ik}}$, k=1,...,K, is available. For the latter case, several element space based direction finding schemes such as IQML [BRES86], FBLP [TUFT82] and PRO-ESPRIT [ZOLT89a] are applicable as in these algorithms, the DOA estimates are obtained by finding unit roots of a judiciously constructed polynomial. For the sake of brevity, we invoke the notation defined in Section 3.1, i. e., we denote as $\mathbf{h}$ the coefficient vector associated with an an (N-1)-th order polynomial h(z) given by

$$h(z) = h_o + h_1 z + \cdots + h_{N-1} z^{N-1} \tag{5.4a}$$

$$\mathbf{h} = [\, h_o \; h_1 \; \cdots \; h_{N-1} \,]^T \tag{5.4b}$$

A polynomial representation for each of the three columns of $\mathbf{W}$ is then given by

$$w_l(z) = I(z)\, r_l(z) \tag{5.5a}$$

$$w_c(z) = l(z)\, r_c(z) \tag{5.5b}$$

$$w_u(z) = l(z)\, r_u(z) \tag{5.5c}$$

where $r_l(z)$, $r_c(z)$, and $r_u(z)$, are (M-K-1)-th order polynomials. In addition to the constraints on the null locations, it is often necessary to specify the beamforming SNR gain in the directions of the desired signals such that they can be passed with minimum distortion while rejecting the contribution of the noise. One commonly used criterion for this purpose is the MVDR criterion proposed by Capon. In the MVDR method, the beamforming weight vector is chosen so as to minimize to array output expected power while at the same time maintaining unit gain in the desired direction, i. e., the direction of look, and is computed as the solution to the following constrained optimization problem

$$\underset{\mathbf{w}}{\text{Minimize}}\ E\{\ |\mathbf{w}^H\mathbf{x}|^2\ \} = \mathbf{w}^H\mathbf{R}_{xx}\mathbf{w} \tag{5.6}$$

$$\text{subject to} \quad \mathbf{w}^H\mathbf{a}(u_d) = 1$$

where $\mathbf{w}$ is the beamforming weight vector and u_d denotes the direction of look, usually chosen to be the desired source angle. The linear constraint is set up to ensure that the desired signal is passed without distortion. It is well known that if the interferences are not fully correlated with the desired signal, the MVDR beamformer obtained via (5.6) is capable of cancelling the interferences by forming nulls in the interfering directions. However, in low-angle radar tracking, coherent interferences may be present, either generated by multipath propagation or by smart jammers. In this case, the MVDR beamformer may not only fail to form nulls in the interfering directions, but may also tend to cancel the desired signal. Due to this phenomenon, it is necessary to modify the conventional MVDR method for the low-angle radar tracking scenario.

5.3 Modified MVDR Beamformer for BDML Estimator

One way to remedy the signal cancellation problem occurring with the conventional MVDR beamformer when interfering sources completely correlated with the desired signal exist is to incorporate a-priori knowledge about the interfering directions, if available. In addition, when the beamformer operates in the presence of spatially white noise, it is usually desirous to minimize the expected output noise power, which yields the so-

called quiescent beam patterns, instead of the expected output signal variance. This is mainly due to the following facts. First, in low-angle radar tracking, the number of snapshots available for each tracking update is typically small such that using the sample correlation matrix $\hat{\mathbf{R}}_{xx}$ in (5.6), in general, does not yield a weight vector with satisfactory performance. Second, in the case of coherent multipath, the conventional MVDR beamformer may totally break down as the specular path signal appears as a coherent interfering source to the beamformer. Third, the quiescent beamformer is completely determined by the constraint equations, which makes the characterization of its SNR gain performance an easy task.

In order to remove the contribution of the interferences, we need to set up multiple constraints which ensure cancellation in the interfering directions. Letting u_{Ik}, k=1,...,K, denote the DOA's of the K interfering sources and u_d the desired direction of look, the minimum noise power (MNP) beamforming weight vector is determined via the following constrained optimization problem

$$\underset{\mathbf{w}}{\text{Minimize}}\ E\{\,|\mathbf{w}^H\mathbf{n}|^2\,\} = \mathbf{w}^H\mathbf{R}_{nn}\mathbf{w} \tag{5.7}$$

$$\text{subject to} \quad \mathbf{C}^H\mathbf{w} = \mathbf{f}$$

where $\mathbf{n}$ is the noise vector present at the array output as defined in (2.1) and $\mathbf{R}_{nn} = E\{\mathbf{n}\mathbf{n}^H\}$ is its associated correaltion matrix. In the case of spatially white noise, $\mathbf{R}_{nn}$ is simply a scalar multiple of the MxM identity matrix. The constraints are defined as follows: $\mathbf{C}$ is an Mx(K+1) matrix constructed according to

$$\mathbf{C} = \left[\mathbf{a}(u_d) \vdots \mathbf{a}(u_{I1}) \vdots \cdots \vdots \mathbf{a}(u_{IK})\right] \tag{5.8}$$

and $\mathbf{f}$ is a (K+1)x1 unit vector defined by

$$\mathbf{f} = \left[\,1\,,\,0\,,\,\ldots\,,\,0\,\right]^T \tag{5.9}$$

The multiple constraints ensure that the beamformer produces unit gain in the desired look direction u_d and zero gain in the interfering directions. The solution to (5.7) is

$$\mathbf{w}_{opt} = \mathbf{R}_{nn}^{-1}\mathbf{C}(\mathbf{C}^H\mathbf{R}_{nn}^{-1}\mathbf{C})^{-1}\mathbf{f} \tag{5.10}$$

which simplifies to $\mathbf{C}(\mathbf{C}^H\mathbf{C})^{-1}\mathbf{f}$ for the case of spatially white noise. In some applications, it is also necessary to control the beamwidth of the optimum

beamformer in order to improve resolution performance. In this case, we need two extra constraints to specify the location of the first null on either side of the mainlobe associated with the beamformer. This is easily incorporated into (5.7) by redefining **C** and **f** according to

$$\mathbf{C}' = \left[\mathbf{a}(u_d) \vdots \mathbf{a}(u_l^\circ) \vdots \mathbf{a}(u_u^\circ) \vdots \mathbf{a}(u_{l1}) \vdots \cdots \vdots \mathbf{a}(u_{lK}) \right] \tag{5.11a}$$

$$\mathbf{f}' = \left[1 , 0 , \ldots , 0 \right]^T \tag{5.11b}$$

where u_l° denotes the location of the first null on the lower side of the mainlobe and u_u° is defined likewise for the upper side null. Note that $\mathbf{C}'$ and $\mathbf{f}'$ are Mx(K+3) and (K+3)x1, respectively.

Before closing this section, we would like to investigate the behavior of the optimum beamformer in a benign environment, i. e., in the presence of spatially white noise only. Upon substitution of $\mathbf{R}_{nn} \propto \mathbf{I}_M$, $\mathbf{C} = \mathbf{a}(u_d)$ and $\mathbf{f} = 1$ into (5.10), we get

$$\mathbf{w}_{opt} = \frac{1}{M} \mathbf{a}(u_d) \tag{5.12}$$

Not surprisingly, we end up with a Fourier beamformer steered to the desired angle u_d. This agrees with our earlier observation in Section 2.2 that the Fourier beamformer provides optimum SNR gain under the spatially white noise assumption.

5.3.1 Application of MVDR Criterion to Three Beams Case

Now consider the case of the BDML estimation in which three beams are formed in different look directions and each beam has K nulls in K prescribed interfering directions. This leads to three separate MNP beamforming problems described by

$$\underset{\mathbf{w}_l}{\text{Minimize}} \ \mathbf{w}_l^H \mathbf{R}_{nn} \mathbf{w}_l \tag{5.13a}$$

$$\text{subject to} \quad \mathbf{C}_l^H \mathbf{w}_l = \mathbf{f}$$

$$\underset{\mathbf{w}_c}{\text{Minimize}} \ \mathbf{w}_c^H \mathbf{R}_{nn} \mathbf{w}_c \tag{5.13b}$$

$$\text{subject to} \quad \mathbf{C}_c^H \mathbf{w}_c = \mathbf{f}$$

$$\underset{\mathbf{w}_u}{\text{Minimize}} \ \mathbf{w}_u^H \mathbf{R}_{nn} \mathbf{w}_u \tag{5.13c}$$

$$\text{subject to} \quad \mathbf{C}_u^H \mathbf{w}_u = \mathbf{f}$$

where $\mathbf{w}_l$, $\mathbf{w}_c$, and $\mathbf{w}_u$ denote the optimum weight vector for the lower, center, and upper beams, respectively. The matrices involved in the constraint equations are defined as follows

$$\mathbf{C}_l = \left[\mathbf{a}(-u_B) \vdots \mathbf{a}(u_{I1}) \vdots \cdots \vdots \mathbf{a}(u_{IK})\right] \tag{5.14a}$$

$$\mathbf{C}_c = \left[\mathbf{a}(0) \vdots \mathbf{a}(u_{I1}) \vdots \cdots \vdots \mathbf{a}(u_{IK})\right] \tag{5.14b}$$

$$\mathbf{C}_u = \left[\mathbf{a}(u_B) \vdots \mathbf{a}(u_{I1}) \vdots \cdots \vdots \mathbf{a}(u_{IK})\right] \tag{5.14c}$$

$$\mathbf{f} = \left[1 \ , \ 0 \ , \ \ldots \ , \ , \ 0\right]^T \tag{5.14d}$$

where u_B is the look direction of the upper beam as defined in Section 2.2, and $\mathbf{f}$ is (K+1)x1. From (5.10), the solution to each of the individual constrained problems in (5.13) is given by

$$\mathbf{w}_l = \mathbf{R}_{nn}^{-1} \mathbf{C}_l (\mathbf{C}_l^H \mathbf{R}_{nn}^{-1} \mathbf{C}_l)^{-1} \mathbf{f} \tag{5.15a}$$

$$\mathbf{w}_c = \mathbf{R}_{nn}^{-1} \mathbf{C}_c (\mathbf{C}_c^H \mathbf{R}_{nn}^{-1} \mathbf{C}_c)^{-1} \mathbf{f} \tag{5.15b}$$

$$\mathbf{w}_u = \mathbf{R}_{nn}^{-1} \mathbf{C}_u (\mathbf{C}_u^H \mathbf{R}_{nn}^{-1} \mathbf{C}_u)^{-1} \mathbf{f} \tag{5.15c}$$

The three beamforming weight vectors thus obtained have look directions at $u = -u_B$, 0, and u_B, respectively. In some applications, it might be necessary to specify the beamwidth associated with the three beams. To accomplish so, we need to impose two extra constraints in each of the three optimization problems in (5.13). For example, we may form extra nulls at $u = -u_B \pm \delta$ for the lower beam, $\pm\delta$ for the center beam, and $u_B \pm \delta$ for the upper beam such that each one has a 3-dB beamwidth approximately equal to δ. u_B and δ thus represent design parameters which need to be determined a-priori. A reasonable choice for δ is $\frac{2}{M}$, which corresponds to the case of uniform weighting.

The optimum weight vectors computed via (5.13) do not necessary exhibit conjugate centro-symmetry (CCS) as is essential in our development of the BDML method. To ensure that, we need to impose one more constraint, i. e., $\tilde{\mathbf{I}}_M \mathbf{w} = \mathbf{w}^*$, for each of the three optimization problem in (5.11). The optimization problems, defined in accordance with these auxiliary constraints, are given by

$$\underset{\mathbf{w}_l}{\text{Minimize}} \quad \mathbf{w}_l^H \mathbf{R}_{nn} \mathbf{w}_l \tag{5.16a}$$

$$\text{subject to} \quad \mathbf{C}_l^H \mathbf{w}_l = \mathbf{f} \; ; \; \tilde{\mathbf{I}}_M \mathbf{w}_l = \mathbf{w}_l^*$$

$$\underset{\mathbf{w}_c}{\text{Minimize}} \quad \mathbf{w}_c^H \mathbf{R}_{xx} \mathbf{w}_c \tag{5.16b}$$

$$\text{subject to} \quad \mathbf{C}_c^H \mathbf{w}_c = \mathbf{f} \; ; \; \tilde{\mathbf{I}}_M \mathbf{w}_c = \mathbf{w}_c^*$$

$$\underset{\mathbf{w}_u}{\text{Minimize}} \quad \mathbf{w}_u^H \mathbf{R}_{nn} \mathbf{w}_u \tag{5.16c}$$

$$\text{subject to} \quad \mathbf{C}_u^H \mathbf{w}_u = \mathbf{f} \; ; \; \tilde{\mathbf{I}}_M \mathbf{w}_u = \mathbf{w}_u^*$$

Invoking the technique for solving (2.32), we rewrite (5.16) in the following fashion:

$$\underset{\mathbf{w}_l}{\text{Minimize}} \quad \mathbf{w}_l^H \mathbf{R}_{nn}^{fb} \mathbf{w}_l \tag{5.17a}$$

$$\text{subject to} \quad \mathbf{C}_l^H \mathbf{w}_l = \mathbf{f} \; ; \; \tilde{\mathbf{I}}_M \mathbf{w}_l = \mathbf{w}_l{}^*$$

$$\underset{\mathbf{w}_c}{\text{Minimize}} \quad \mathbf{w}_c^H \mathbf{R}_{nn}^{fb} \mathbf{w}_c \tag{5.17b}$$

$$\text{subject to} \quad \mathbf{C}_c^H \mathbf{w}_c = \mathbf{f} \; ; \; \tilde{\mathbf{I}}_M \mathbf{w}_c = \mathbf{w}_c{}^*$$

$$\underset{\mathbf{w}_u}{\text{Minimize}} \quad \mathbf{w}_u^H \mathbf{R}_{nn}^{fb} \mathbf{w}_u \tag{5.17c}$$

$$\text{subject to} \quad \mathbf{C}_u^H \mathbf{w}_u = \mathbf{f} \; ; \; \tilde{\mathbf{I}}_M \mathbf{w}_u = \mathbf{w}_u{}^*$$

where

$$\mathbf{R}_{nn}^{fb} = \frac{1}{2}\left\{\mathbf{R}_{nn} + \tilde{\mathbf{I}}_M \mathbf{R}_{nn}^{*} \tilde{\mathbf{I}}_M\right\} \tag{5.18}$$

The linear constraints in (5.15) remain unchanged since all the columns of $\mathbf{C}_l$, $\mathbf{C}_c$, and $\mathbf{C}_u$ are conjugate centro-symmetric as can be seen according to (2.1). If we ignore the second constraint in each of the optimization problems in (5.17) (we will show that this does not affect the problem later), the optimum weight vectors are simply given by (5.15) with $\mathbf{R}_{nn}$ replaced by $\mathbf{R}_{nn}^{fb}$, which leads to

$$\mathbf{w}_l = \mathbf{R}_{nn}^{fb\,-1}\mathbf{C}_l(\mathbf{C}_l^H\mathbf{R}_{nn}^{fb\,-1}\mathbf{C}_l)^{-1}\mathbf{f} \tag{5.19a}$$

$$\mathbf{w}_c = \mathbf{R}_{nn}^{fb\,-1}\mathbf{C}_c(\mathbf{C}_c^H\mathbf{R}_{nn}^{fb\,-1}\mathbf{C}_c)^{-1}\mathbf{f} \tag{5.19b}$$

$$\mathbf{w}_u = \mathbf{R}_{nn}^{fb\,-1}\mathbf{C}_u(\mathbf{C}_u^H\mathbf{R}_{nn}^{fb\,-1}\mathbf{C}_u)^{-1}\mathbf{f} \tag{5.19c}$$

Incorporating the facts that $\tilde{\mathbf{I}}_M\mathbf{R}_{nn}^{fb}\tilde{\mathbf{I}}_M = \mathbf{R}_{nn}^{fb\,*}$ and that $\tilde{\mathbf{I}}_M\mathbf{a}(u) = \mathbf{a}^*(u)$, we can easily verify the following relation:

$$\begin{aligned}\tilde{\mathbf{I}}_M\mathbf{w}_l &= \tilde{\mathbf{I}}_M\mathbf{R}_{nn}^{fb\,-1}\tilde{\mathbf{I}}_M\tilde{\mathbf{I}}_M\mathbf{C}_l(\mathbf{C}_l^H\tilde{\mathbf{I}}_M\tilde{\mathbf{I}}_M\mathbf{R}_{nn}^{fb\,-1}\tilde{\mathbf{I}}_M\tilde{\mathbf{I}}_M\mathbf{C}_l)^{-1}\mathbf{f} \\ &= (\mathbf{R}_{nn}^{fb\,-1})^*\mathbf{C}_l^*(\mathbf{C}_l^T(\mathbf{R}_{nn}^{fb\,-1})^*\mathbf{C}_l^*)^{-1}\mathbf{f} = \mathbf{w}_l^*\end{aligned} \tag{5.20}$$

It can be shown that $\mathbf{w}_c$ and $\mathbf{w}_u$ exhibit conjugate centro-symmetry as well. Therefore, the optimum weight vectors obtained in (5.19) are indeed the solutions to the corresponding problems described in (5.16). With these weight vectors constructed, we may then proceed to obtain the BDML estimates of u_1 and u_2 using the procedures developed in Chapter two. It is worth noting that, in general, the beamforming matrix consisting of the three vectors obtained in (5.19) does not produce beamspace manifold vectors satisfying (2.17), i. e., $\tilde{\mathbf{I}}_3\mathbf{b}(u_1) = \mathbf{b}(u_2)$ when the multipath is symmetric such that $u_2 = -u_1$. This results in loss of a-priori information in the development of the symmetric BDML method. As can be seen from the analysis presented in Section 2.4, the BDML estimator with the modified MNP beamforming matrix can no longer handle 0° phase difference for the symmetric multipath case. A remedy for this is to employ the alternative BDML procedure for generalized Butler matrix beamformers developed in Section 3.3.2. In the presence of interferences, however, some modifications are necessary. In short, the three beamforming weight vectors must have M-3 nulls in common in order to facilitate a simple closed-form solution for the BDML estimator.

5.3.2 MNP Based Generalized Butler Beamformers

Before beginning this section, we review some of the relevant work on the generalized Butler matrix beamformers presented in Chapter 3. As defined in Section 3.3.1, an Mx3 generalized Butler matrix beamformer $\mathbf{W}$ is a matrix having the following factorization

$$\mathbf{W} = \left[\mathbf{w}_1 \vdots \mathbf{w}_2 \vdots \mathbf{w}_3 \right] = \mathbf{CU} \tag{5.21}$$

where $\mathbf{C}$ is an Mx3 banded, Toeplitz matrix given by

$$\mathbf{C} = \begin{bmatrix} \mathbf{c} & 0 & 0 \\ 0 & \mathbf{c} & 0 \\ 0 & 0 & \mathbf{c} \end{bmatrix} \tag{5.22}$$

and $\mathbf{U} = [\, \mathbf{u}_1 \vdots \mathbf{u}_2 \vdots \mathbf{u}_3 \,]$ is 3x3. By using the following relations

$$p(z) = q(z)r(z) \;\; \text{☞} \;\; \mathbf{p} = \begin{bmatrix} \mathbf{q} & 0 & 0 \\ 0 & \mathbf{q} & 0 \\ 0 & 0 & \mathbf{q} \end{bmatrix} \mathbf{r} = \begin{bmatrix} \mathbf{r} & 0 & 0 \\ 0 & \mathbf{r} & 0 \\ 0 & 0 & \mathbf{r} \end{bmatrix} \mathbf{q} \tag{5.23}$$

we may express (5.21) in terms of polynomials in a fashion given below

$$w_1(z) = c(z)u_1(z) \tag{5.24a}$$

$$w_2(z) = c(z)u_2(z) \tag{5.24b}$$

$$w_3(z) = c(z)u_3(z) \tag{5.24c}$$

which accounts for the M-3 common nulls associated with the three beams. The above equivalence between matrix and polynomial representations will be exploited shortly in the development of the MNP-based generalized Butler beamformers.

For the application of BDML estimation, three different types of criteria are considered: 1) minimum total noise power criterion; 2) minimum individual noise power criterion; 3) mutual orthogonality criterion. It is worth noting that in the ideal case of no interferences and spatially white noise, they should all correspond to the Mx3 Butler beamformer defined in (2.36).

(1) Minimum Total Noise Power (MTNP):
The minimum total noise power beamformer minimizes the total noise output power from the three beamspace ports and is determined as the solution to the following optimization problem

$$\underset{\mathbf{w}_l\,\mathbf{w}_c\,\mathbf{w}_u}{\text{Minimize}} \quad E\{\,|\mathbf{w}_l^H\mathbf{n}|^2 + |\mathbf{w}_c^H\mathbf{n}|^2 + |\mathbf{w}_u^H\mathbf{n}|^2\,\} \tag{5.25}$$

$$\text{subject to} \quad \mathbf{w}_l^H\mathbf{a}(-u_B) = \mathbf{w}_c^H\mathbf{a}(0) = \mathbf{w}_u^H\mathbf{a}(u_B) = 1$$

$$\text{subject to} \quad \mathbf{w}_l^H\mathbf{a}(u_{Ik}) = \mathbf{w}_c^H\mathbf{a}(u_{Ik}) = \mathbf{w}_u^H\mathbf{a}(u_{Ik}) = 0 \quad k = 1,\ldots,K$$

$$\text{subject to} \quad \tilde{\mathbf{I}}_M\mathbf{w}_l = \mathbf{w}_l^* \;;\; \tilde{\mathbf{I}}_M\mathbf{w}_c = \mathbf{w}_c^* \;;\; \tilde{\mathbf{I}}_M\mathbf{w}_u = \mathbf{w}_u^*$$

$$\text{subject to} \quad w_l(z)\,,\; w_c(z)\,,\text{ and } w_u(z) \text{ have M-3 roots in common}$$

where u_B, u_{Ik}, k=1,...,K, and $\mathbf{n}$ are as defined previously. The minimum total noise power beamformer minimizes the total noise power at the three beamspace ports when the respective nulls associated with the three beamforming weight vectors are formed in such a fashion so as to maintain M-3 nulls in common. The remaining degrees of freedom in (5.25) can be used to determine the uncommon nulls as well as control the beamwidth of the three beams.

(2) Minimum Individual Noise Power (MINP):
A suboptimal but efficient alternative to the MTNP scheme is to minimize the noise power individually rather than totally. This leads to a set of three coupled optimization problems defined as follows

$$\underset{\mathbf{w}_l}{\text{Minimize}} \quad E\{\,|\mathbf{w}_l^H\mathbf{n}|^2\,\} \tag{5.26a}$$

$$\text{subject to} \quad \mathbf{w}_l^H\mathbf{a}(-u_B) = 1$$

$$\text{subject to} \quad \mathbf{w}_l^H\mathbf{a}(u_{Ik}) = 0 \quad k = 1,\ldots,K$$

$$\text{subject to} \quad \tilde{\mathbf{I}}_M\mathbf{w}_l = \mathbf{w}_l^*$$

$$\underset{\mathbf{w}_c}{\text{Minimize}} \quad E\{\,|\mathbf{w}_c^H\mathbf{n}|^2\,\} \tag{5.26b}$$

$$\text{subject to} \quad \mathbf{w}_c^H\mathbf{a}(0) = 1$$

$$\text{subject to} \quad \mathbf{w}_c^H\mathbf{a}(u_{Ik}) = 0 \quad k = 1,\ldots,K$$

$$\text{subject to} \quad \tilde{\mathbf{I}}_M\mathbf{w}_c = \mathbf{w}_c^*$$

$$\underset{\mathbf{w}_u}{\text{Minimize}}\ E\{\,|\mathbf{w}_u^H\mathbf{n}|^2\,\} \tag{5.26c}$$

$$\text{subject to}\quad \mathbf{w}_u^H\mathbf{a}(u_B) = 1$$

$$\text{subject to}\quad \mathbf{w}_u^H\mathbf{a}(u_{Ik}) = 0 \quad k = 1,\ldots,K$$

$$\text{subject to}\quad \tilde{\mathbf{I}}_M\mathbf{w}_u = \mathbf{w}_u^*$$

subject to $w_l(z)$, $w_c(z)$, and $w_u(z)$ have M-3 roots in common

It turns out that the three problems are coupled. This is solely due to the of M-3 common roots constraint. To facilitate a simple closed-form solution for each problem, it is desirous to develop a procedure which circumvents this constraint.

(3) Mutual Orthogonality (MO):
There are two advantages to working with mutual orthogonal beamforming weight vectors. First, if the noise in element space is uncorrelated from element to element, the noise in bemspace will also be mutually uncorrelated. Second, if the noise in element space is saptially white, the weight vectors may be normalized such that the beamspace noise correlation matrix is simply a scalar multiple of the 3x3 identity matrix leading to simplifications for the BDML scheme. The mutually orthogonal beamformer is constructed in accordance with

$$\underset{\mathbf{w}_l\,\mathbf{w}_c\,\mathbf{w}_u}{\text{Minimize}}\ \|\mathbf{w}_l^\circ - \mathbf{w}_l\|^2 + \|\mathbf{w}_c^\circ - \mathbf{w}_c\|^2 + \|\mathbf{w}_u^\circ - \mathbf{w}_u\|^2 \tag{5.27}$$

$$\text{subject to}\quad \mathbf{w}_l^H\mathbf{w}_c = \mathbf{w}_c^H\mathbf{w}_u = \mathbf{w}_u^H\mathbf{w}_l = 0$$

$$\text{subject to}\quad \mathbf{w}_l^H\mathbf{a}(u_{Ik}) = \mathbf{w}_c^H\mathbf{a}(u_{Ik}) = \mathbf{w}_u^H\mathbf{a}(u_{Ik}) = 0 \quad k=1,\ldots,K$$

$$\text{subject to}\quad \tilde{\mathbf{I}}_M\mathbf{w}_l = \mathbf{w}_l^* \ ;\ \tilde{\mathbf{I}}_M\mathbf{w}_c = \mathbf{w}_c^* \ ;\ \tilde{\mathbf{I}}_M\mathbf{w}_u = \mathbf{w}_u^*$$

subject to $w_l(z)$, $w_c(z)$, and $w_u(z)$ have M-3 roots in common

where $\mathbf{w}_l^\circ$, $\mathbf{w}_c^\circ$, and $\mathbf{w}_u^\circ$ are the three columns of a "reference" beamforming matrix. For the application of BDML estimation in a spatially white noise environment, we recommend the use of the Mx3 Butler beamformer as the reference beamformer since it exhibits optimum SNR gain performance, and more importantly, its three columns are mutually *orthonormal.*

With the above problem formulation and the relations given in (5.23), we now proceed to describe the procedures for constructing the optimum weight vectors for each of the three types of beamformers. For simplicity, we here assume spatially white noise, i. e., $\mathbf{R}_{nn} \propto \mathbf{I}_M$. Motivated by the "good" performance achieved with the Mx3 Butler beamformer for the BDML estimators, we choose $u_B = \frac{2}{M}$ such that the the directions of look associated with the lower, center, and upper beams are $-\frac{2}{M}$, 0, and $\frac{2}{M}$, respectively. In addition, we select the uncommon nulls associated with the three beams for the MTNP beamformer in accordance with:

$$\text{upper beam}: \quad u = -\frac{2}{M} \text{ and } u = 0$$

$$\text{center beam}: \quad u = -\frac{2}{M} \text{ and } u = \frac{2}{M}$$

$$\text{lower beam}: \quad u = \frac{2}{M} \text{ and } u = 0$$

5.3.2.1 Generalized MTNP Butler Beamformer

The three beams have M-3 nulls in common, K of which are known as they correspond to the K interfering directions. Each beam has two uncommon nulls, which are prescribed a-priori as above. Employing polynomial notation, we obtain the following expressions for the three beams

$$w_l(z) = c(z)u_l(z) \tag{5.28a}$$

$$w_c(z) = c(z)u_c(z) \tag{5.28b}$$

$$w_u(z) = c(z)u_u(z) \tag{5.28c}$$

where $c(z)$ denotes the polynomial associated with the unknown common nulls and $u_l(z)$, $u_c(z)$, and $u_u(z)$ are the polynomials associated with the known nulls, including common and uncommon ones, for the lower, center, and upper beams, respectively. With the above selection of uncommon nulls, we have the following polynomial factorizations

$$u_l(z) = \kappa_l(z - e^{j\pi\frac{2}{M}})(z-1)\prod_{k=1}^{K}(z - e^{j\pi u_{lk}}) \tag{5.29a}$$

$$u_c(z) = \kappa_c(z - e^{j\pi\frac{2}{M}})(z - e^{-j\pi\frac{2}{M}})\prod_{k=1}^{K}(z - e^{j\pi u_{lk}}) \tag{5.29b}$$

$$u_u(z) = \kappa_u(z - e^{-j\pi\frac{2}{M}})(z-1)\prod_{k=1}^{K}(z - e^{j\pi u_{lk}}) \tag{5.29c}$$

where κ_l, κ_c, and κ_u are complex scalars ensuring that each polynomial has a set of conjugate centro-symmetric coefficients with the leading coefficient having unity magnitude. Note that the coefficients for each of the polynomials $u_l(z)$, $u_c(z)$, and $u_u(z)$ form a conjugate centro-symmetric vector due to the following lemma.

Lemma: If all the roots of a polynomial $p(z)$ lie on the unit circle, then the vector $\mathbf{p}$ composed of its coefficients may be normalized to exhibit conjugate centro-symmetry.

The leading coefficient of each polynomial is set to have unity magnitude so that under no interference condition, the optimum MTNP beamformer is just the Mx3 Butler beamformer. Substitution of the matrix representations of (5.28) into (5.25) yields, after some manipulation, the following matrix optimization problem

$$\underset{\mathbf{c}}{\text{Minimize}}\ \mathbf{c}^H\mathbf{U}_l^H\mathbf{U}_l\mathbf{c} + \mathbf{c}^H\mathbf{U}_c^H\mathbf{U}_c\mathbf{c} + \mathbf{c}^H\mathbf{U}_u^H\mathbf{U}_u\mathbf{c} \tag{5.30}$$

$$\text{subject to}\quad \mathbf{c}^H\mathbf{U}_l^H\mathbf{a}(-\frac{2}{M}) = 1$$

$$\text{subject to}\quad \mathbf{c}^H\mathbf{U}_c^H\mathbf{a}(0) = 1$$

$$\text{subject to}\quad \mathbf{c}^H\mathbf{U}_u^H\mathbf{a}(\frac{2}{M}) = 1$$

$$\text{subject to}\quad \tilde{\mathbf{I}}_{M-K-3}\mathbf{c} = \mathbf{c}^*$$

where we haved invoked the assumption that $E\{\mathbf{n}\mathbf{n}^H\} \propto \mathbf{I}_M$ and the fact that conjugate centro-symmetry of $\mathbf{c}$, $\mathbf{u}_l$, $\mathbf{u}_c$, and $\mathbf{u}_u$ implies conjugate centro-symmetry of $\mathbf{w}_l$, $\mathbf{w}_c$, and $\mathbf{w}_u$. The Mx(M-K-3) matrices $\mathbf{U}_l$, $\mathbf{U}_c$, and $\mathbf{U}_u$ are banded, toeplitz as given by

$$\mathbf{U}_l = \begin{bmatrix} \mathbf{u}_l & 0 & 0 & 0 \\ 0 & \mathbf{u}_l & 0 & 0 \\ \vdots & \vdots & \vdots & \vdots \\ 0 & 0 & \mathbf{u}_l & 0 \\ 0 & 0 & 0 & \mathbf{u}_l \end{bmatrix} \tag{5.31a}$$

$$\mathbf{U}_c = \begin{bmatrix} \mathbf{u}_c & 0 & 0 & 0 \\ 0 & \mathbf{u}_c & 0 & 0 \\ \vdots & \vdots & \vdots & \vdots \\ 0 & 0 & \mathbf{u}_c & 0 \\ 0 & 0 & 0 & \mathbf{u}_c \end{bmatrix} \tag{5.31b}$$

$$\mathbf{U}_u = \begin{bmatrix} \mathbf{u}_u & 0 & 0 & 0 \\ 0 & \mathbf{u}_u & 0 & 0 \\ \vdots & \vdots & \vdots & \vdots \\ 0 & 0 & \mathbf{u}_u & 0 \\ 0 & 0 & 0 & \mathbf{u}_u \end{bmatrix} \tag{5.31c}$$

Note that $\mathbf{u}_l$, $\mathbf{u}_c$, and $\mathbf{u}_u$ are conjugate centro-symmetric such that

$$\tilde{\mathbf{I}}_M \mathbf{U}_l \tilde{\mathbf{I}}_{M-K-3} = \mathbf{U}_l^* \tag{5.32a}$$

$$\tilde{\mathbf{I}}_M \mathbf{U}_c \tilde{\mathbf{I}}_{M-K-3} = \mathbf{U}_c^* \tag{5.32b}$$

$$\tilde{\mathbf{I}}_M \mathbf{U}_u \tilde{\mathbf{I}}_{M-K-3} = \mathbf{U}_u^* \tag{5.32c}$$

Rewriting (5.28) and letting m = M-K-3, we have

$$\underset{\mathbf{c}}{\text{Minimize}} \quad \mathbf{c}^H \mathbf{U} \mathbf{c} \tag{5.33}$$

$$\text{subject to} \quad \mathbf{T}^H \mathbf{c} = \mathbf{1}_3 \;\; ; \;\; \tilde{\mathbf{I}}_m \mathbf{c} = \mathbf{c}^*$$

where

$$\mathbf{U} = \mathbf{U}_l^H \mathbf{U}_l + \mathbf{U}_c^H \mathbf{U}_c + \mathbf{U}_u^H \mathbf{U}_u \tag{5.34a}$$

$$\mathbf{T} = \left[\mathbf{U}_l^H \mathbf{a}(-\frac{2}{M}) \vdots \mathbf{U}_c^H \mathbf{a}(0) \vdots \mathbf{U}_u^H \mathbf{a}(\frac{2}{M}) \right] \tag{5.34b}$$

and $\mathbf{1}_3$ is a 3x1 all-one vector given by

$$\mathbf{1}_3 = \begin{bmatrix} 1 , 1 , 1 \end{bmatrix}^T \tag{5.35}$$

Employing the technique for solving (2.32), we formulate the problem in (5.30) in the following alternative form

$$\underset{\mathbf{c}}{\text{Minimize}} \quad \mathbf{c}^H \frac{1}{2}\left\{\mathbf{U} + \tilde{\mathbf{I}}_m \mathbf{U}^* \tilde{\mathbf{I}}_m\right\}\mathbf{c} = \mathbf{c}^H \mathbf{U}_{fb}\mathbf{c} \tag{5.36}$$

$$\text{subject to} \quad \frac{1}{2}\left\{\mathbf{T} + \tilde{\mathbf{I}}_m \mathbf{T}^*\right\}^H \mathbf{c} = \mathbf{T}_{fb}^H \mathbf{c} = \mathbf{1}_3$$

$$\tilde{\mathbf{I}}_m \mathbf{c} = \mathbf{c}^*$$

where we have incorporated the fact that both $\mathbf{c}^H\mathbf{U}_l\mathbf{c}$ and $\mathbf{T}^H\mathbf{c}$ are real. From (5.32), it is easily deduced that $\mathbf{U}_{fb} = \mathbf{U}$ and $\mathbf{T}_{fb} = \mathbf{T}$ such that aside from the conjugate centro-symmetry constraint, the solution to (5.36) is given by

$$\mathbf{c}_{opt} = \mathbf{U}^{-1}\mathbf{T}(\mathbf{T}^H\mathbf{U}^{-1}\mathbf{T})^{-1}\mathbf{1}_3 \tag{5.37}$$

Observing that $\tilde{\mathbf{I}}_M\mathbf{U}\tilde{\mathbf{I}}_m = \mathbf{U}^*$ and $\tilde{\mathbf{I}}_m\mathbf{T} = \mathbf{T}^*$, we can readily verify that $\tilde{\mathbf{I}}_m\mathbf{c}_{opt} = \mathbf{c}_{opt}^*$ such that $\mathbf{c}_{opt}$ described by (5.37) is indeed the solution to (5.36). With $\mathbf{c}_{opt}$ available, the optimum weight vectors are constructed according to

$$\mathbf{w}_l = \mathbf{C}\mathbf{u}_l \tag{5.38a}$$

$$\mathbf{w}_c = \mathbf{C}\mathbf{u}_c \tag{5.38b}$$

$$\mathbf{w}_u = \mathbf{C}\mathbf{u}_u \tag{5.38c}$$

where $\mathbf{C}$ is the Toeplitz representation of $\mathbf{c}_{opt}$ defined by

$$\mathbf{C} = \begin{bmatrix} \mathbf{c}_{opt} & 0 & 0 \\ 0 & \mathbf{c}_{opt} & 0 \\ 0 & 0 & \mathbf{c}_{opt} \end{bmatrix} \tag{5.39}$$

and $\mathbf{u}_l$, $\mathbf{u}_c$, and $\mathbf{u}_u$, are as given by (5.29).

The three weight vectors $\mathbf{w}_l$, $\mathbf{w}_c$, and $\mathbf{w}_u$, obtained in (5.38) are conjugate centro-symmetric as proved below

$$\tilde{\mathbf{I}}_M\mathbf{w}_l = \tilde{\mathbf{I}}_M\mathbf{C}\tilde{\mathbf{I}}_{K+3}\tilde{\mathbf{I}}_{K+3}\mathbf{u}_l = \mathbf{C}^*\mathbf{u}_l^* = \mathbf{w}_l^* \tag{5.40a}$$

$$\tilde{\mathbf{I}}_M \mathbf{w}_c = \tilde{\mathbf{I}}_M \mathbf{C} \tilde{\mathbf{I}}_{K+3} \tilde{\mathbf{I}}_{K+3} \mathbf{u}_c = \mathbf{C}^* \mathbf{u}_c^* = \mathbf{w}_c^* \tag{5.40b}$$

$$\tilde{\mathbf{I}}_M \mathbf{w}_u = \tilde{\mathbf{I}}_M \mathbf{C} \tilde{\mathbf{I}}_{K+3} \tilde{\mathbf{I}}_{K+3} \mathbf{u}_u = \mathbf{C}^* \mathbf{u}_u^* = \mathbf{w}_u^* \tag{5.40c}$$

Finally, the Mx3 MTNP matrix beamformer consisting of these three weight vectors is simply given by

$$\mathbf{W}_{mt} = \left[\mathbf{w}_l \vdots \mathbf{w}_c \vdots \mathbf{w}_u \right] = \mathbf{C} \left[\mathbf{u}_l \vdots \mathbf{u}_c \vdots \mathbf{u}_u \right] \tag{5.41}$$

5.3.2.2 Generalized MINP Butler Beamformer

In order to remove the last constraint in (5.26), a polynomial whose roots correspond to the M-3 common nulls of the three beams is first determined. There are many ways to accomplish so, and for simplicity. For the sake of simplicity, we here take a suboptimal approach in which the center beam is constructed first in accordance with the minimum noise power criterion. The common polynomial may be obtained by taking out the first null on either side of the mainlobe associated with the resulting weight vector. However, doing so requires rooting an (M-1)-th order polynomial, which might be extremely computationally expensive for large M. In order to facilitate a simple procedure for constructing the lower and upper beams, we form two "hard nulls" for the center beam at $u = \frac{2}{M}$ and $u = -\frac{2}{M}$ corresponding to the first lower and upper nulls, respectively, for the case of Fourier beamforming steered to $u = 0$. Denote as $d(z)$ and $k(z)$ the polynomial associated with the unknown nulls and known nulls of the center beam , and $\mathbf{d}$ and $\mathbf{k}$ their corresponding vector representations, respectively. In this case, $k(z)$ is simply identical to $u_c(z)$ described by (5.29b):

$$k(z) = \kappa_c (z - e^{j\pi\frac{2}{M}})(z - e^{-j\pi\frac{2}{M}}) \prod_{k=1}^{K} (z - e^{j\pi u_k}) \tag{5.42}$$

Employing the MNP criterion, we have the following minimization problem

$$\underset{\mathbf{d}}{\text{Minimize}} \ \mathbf{d}^H \mathbf{K}^H \mathbf{K} \mathbf{d} \tag{5.43}$$

$$\text{subject to} \quad \mathbf{a}^H(0)\mathbf{K}\mathbf{d} = 1 \ ; \ \tilde{\mathbf{I}}_m \mathbf{d} = \mathbf{d}^*$$

where

$$\mathbf{K} = \begin{bmatrix} \mathbf{k} & 0 & 0 \\ 0 & \mathbf{k} & 0 \\ 0 & 0 & \mathbf{k} \end{bmatrix} \tag{5.44a}$$

is the Toeplitz representation for $\mathbf{k}$ and m = M-K-3. Comparing (5.43) with (5.33) and using the result given by (5.37), the solution to (5.43) is easily seen to be

$$\mathbf{d} = \frac{1}{\mathbf{a}(0)^H \mathbf{K}\mathbf{K}^+ \mathbf{a}(0)} \mathbf{K}^+ \mathbf{a}(0) \tag{5.45}$$

where $\mathbf{K}^+ = (\mathbf{K}^H\mathbf{K})^{-1}\mathbf{K}^H$ is the pseudo-inverse of $\mathbf{K}$. which can be readily verified to exhibit conjugate centro-symmetry. The Mx1 vector $\mathbf{w} = \mathbf{K}\mathbf{d}$ then represents the desired beamforming weight vector. In order to obtain an (M-3)-th order polynomial with roots corresponding to the M-3 common nulls, we simply divide out the two roots at $e^{\pm j2\pi/M}$ from w(z) as described mathematically below:

$$\begin{aligned} p(z) &= d(z) \frac{k(z)}{\varsigma (z - e^{j\pi\frac{2}{M}})(z - e^{-j\pi\frac{2}{M}})} \\ &= \frac{\kappa_c d(z)(z - e^{j\pi\frac{2}{M}})(z - e^{-j\pi\frac{2}{M}}) \prod_{k=1}^{K} (z - e^{j\pi u_{1k}})}{\varsigma (z - e^{j\pi\frac{2}{M}})(z - e^{-j\pi\frac{2}{M}})} \\ &= \frac{\kappa_c}{\varsigma} d(z) \prod_{k=1}^{K} (z - e^{j\pi u_{1k}}) \end{aligned} \tag{5.46}$$

where ς is a normalizing complex scalar ensuring that the coefficients of p(z) are conjugate centro-symmetric. With the (M-3)-th order common polynomial p(z), or $\mathbf{p}$, the (M-2)x1 vector representation for p(z), available, the beamforming weight vectors $\mathbf{w}_l$, $\mathbf{w}_c$, and $\mathbf{w}_u$ associated with the three beams may be determined by multiplying p(z) with three quadratic polynomials, $r_l(z)$, $r_c(z)$, and $r_u(z)$, respectively. In terms of matrix notations, this translates into

$$\mathbf{w}_l = \mathbf{P}\mathbf{r}_l \tag{5.47a}$$

$$\mathbf{w}_c = \mathbf{P}\mathbf{r}_c \tag{5.47b}$$

$$\mathbf{w}_u = \mathbf{P}\mathbf{r}_u \tag{5.47c}$$

where

$$\mathbf{P} = \begin{bmatrix} \mathbf{p} & 0 & 0 \\ 0 & \mathbf{p} & 0 \\ 0 & 0 & \mathbf{p} \end{bmatrix} \tag{5.48}$$

and $\mathbf{r}_l$, $\mathbf{r}_c$, and $\mathbf{r}_u$ are the vector representations for $r_l(z)$, $r_c(z)$, and $r_u(z)$, respectively and are determined individually in accordance with the MNP criterion as described by the following three optimization problems.

$$\underset{\mathbf{r}_l}{\text{Minimize}} \quad \mathbf{r}_l^H \mathbf{P}^H \mathbf{P} \mathbf{r}_l \tag{5.49a}$$

$$\text{subject to} \quad \mathbf{a}^H(-\frac{2}{M})\mathbf{P}\mathbf{r}_l = 1 \;\; ; \;\; \tilde{\mathbf{I}}_3 \mathbf{r}_l = \mathbf{r}_l^*$$

$$\underset{\mathbf{r}_c}{\text{Minimize}} \quad \mathbf{r}_c^H \mathbf{P}^H \mathbf{P} \mathbf{r}_c \tag{5.49b}$$

$$\text{subject to} \quad \mathbf{a}^H(0)\mathbf{P}\mathbf{r}_c = 1 \;\; ; \;\; \tilde{\mathbf{I}}_3 \mathbf{r}_c = \mathbf{r}_c^*$$

$$\underset{\mathbf{r}_u}{\text{Minimize}} \quad \mathbf{r}_u^H \mathbf{P}^H \mathbf{P} \mathbf{r}_u \tag{5.49c}$$

$$\text{subject to} \quad \mathbf{a}^H(\frac{2}{M})\mathbf{P}\mathbf{r}_u = 1 \;\; ; \;\; \tilde{\mathbf{I}}_3 \mathbf{r}_c = \mathbf{r}_u^*$$

Following the (5.43)-(5.45), we have

$$\mathbf{r}_l = \frac{1}{\mathbf{a}^H(-\frac{2}{M})\mathbf{P}\mathbf{P}^+\mathbf{a}(-\frac{2}{M})}\mathbf{P}^+\mathbf{a}(-\frac{2}{M}) \tag{5.50a}$$

$$\mathbf{r}_c = \frac{1}{\mathbf{a}(0)^H\mathbf{P}\mathbf{P}^+\mathbf{a}(0)}\mathbf{P}^+\mathbf{a}(0) \tag{5.50b}$$

$$\mathbf{r}_u = \frac{1}{\mathbf{a}^H(\frac{2}{M})\mathbf{P}\mathbf{P}^+\mathbf{a}(\frac{2}{M})}\mathbf{P}^+\mathbf{a}(\frac{2}{M}) \tag{5.50c}$$

where $\mathbf{P}^+ = (\mathbf{P}^H\mathbf{P})^{-1}\mathbf{P}^H$ is the pseudo-inverse of $\mathbf{P}$. With $\mathbf{P}$ and $\mathbf{r}_l$, $\mathbf{r}_c$, and $\mathbf{r}_u$ obtained from (5.50), the MINP beamforming matrix can then be constructed in accordance with (5.47) as follows

$$\mathbf{W}_{mi} = \left[\mathbf{w}_l \vdots \mathbf{w}_c \vdots \mathbf{w}_u \right] = \mathbf{P} \left[\mathbf{r}_l \vdots \mathbf{r}_c \vdots \mathbf{r}_u \right] \tag{5.51}$$

Note that each of the three columns of $\mathbf{W}_{mi}$ is conjugate centro-symmetric since $\mathbf{r}_l$, $\mathbf{r}_c$, $\mathbf{r}_u$, and $\mathbf{p}$ are all conjugate centro-symmetric.

The MINP beamformer exhibits more flexibility than the MTNP beamformer as no restrictions on the locations of the uncommon nulls are made.

5.3.2.3 Generalized MO Butler Beamformer

The problem described by (5.27) is too complicated to admit closed-form solutions for $\mathbf{w}_l$, $\mathbf{w}_c$, and $\mathbf{w}_u$. A simpler alternative is to again first remove the common roots constraint by obtaining a (M-3)-th order polynomial associated with the M-3 common roots. Following the procedure delineated in the preceding subsection, we find the "common" polynomial p(z) and its associated Toeplitz representation $\mathbf{P}$ as given by (5.48). Substituting the expressions for the weight vectors given in (5.47) into (5.27) and rewritting the constraint equations, we end up with the following optimization problem

$$\underset{\mathbf{r}_l \mathbf{r}_c \mathbf{r}_u}{\text{Minimize}} \; \| \mathbf{w}_l^o - \mathbf{P}\mathbf{r}_l \|^2 + \| \mathbf{w}_c^o - \mathbf{P}\mathbf{r}_c \|^2 + \| \mathbf{w}_u^o - \mathbf{P}\mathbf{r}_u \|^2 \tag{5.52}$$

$$\text{subject to} \quad \mathbf{r}_l^H \mathbf{P}^H \mathbf{P} \mathbf{r}_c = \mathbf{r}_c^H \mathbf{P}^H \mathbf{P} \mathbf{r}_u = \mathbf{r}_u^H \mathbf{P}^H \mathbf{P} \mathbf{r}_l = 0$$

$$\tilde{\mathbf{I}}_3 \mathbf{r}_l = \mathbf{r}_l^* \; ; \; \tilde{\mathbf{I}}_3 \mathbf{r}_c = \mathbf{r}_c^* \; ; \; \tilde{\mathbf{I}}_3 \mathbf{r}_u = \mathbf{r}_u^*$$

where $\mathbf{r}_l$, $\mathbf{r}_c$, and $\mathbf{r}_u$ are all 3x1. To further simplify the problem, we can, without loss of generality, assume that the three weight vectors are mutually "orthonormal", i. e., they are mutually orthogonal unit length vectors. Rearranging (5.52) in matrix form, we have

$$\underset{\mathbf{R}}{\text{Minimize}} \; \| \mathbf{W}^o - \mathbf{P}\mathbf{R} \|_F^2 \tag{5.53}$$

$$\text{subject to} \quad \mathbf{R}^H \mathbf{P}^H \mathbf{P} \mathbf{R} = \mathbf{I}_3 \; ; \; \tilde{\mathbf{I}}_3 \mathbf{R} = \mathbf{R}^*$$

where

$$\mathbf{W}^o = \left[\mathbf{w}_l^o \vdots \mathbf{w}_c^o \vdots \mathbf{w}_u^o \right] \tag{5.54a}$$

$$\mathbf{R} = \left[\mathbf{r}_l \vdots \mathbf{r}_c \vdots \mathbf{r}_u \right] \tag{5.54b}$$

We here choose the reference beamformer to be the Mx3 Butler beamformer scaled by $\frac{1}{\sqrt{M}}$ such that

$$\mathbf{w}_l^o = \frac{1}{\sqrt{M}}\mathbf{a}(-\frac{2}{M}) \;\; ; \;\; \mathbf{w}_c^o = \frac{1}{\sqrt{M}}\mathbf{a}(0) \;\; ; \;\; \mathbf{w}_u^o = \frac{1}{\sqrt{M}}\mathbf{a}(\frac{2}{M}) \tag{5.55a}$$

$$\mathbf{W}^o = \frac{1}{\sqrt{M}}\mathbf{S} \tag{5.55b}$$

Note that the scaling factor $\frac{1}{\sqrt{M}}$ insures that the three columns of $\mathbf{W}^o$ are mutually orthonormal. With $\mathbf{G} = \mathbf{G}^H = (\mathbf{P}^H\mathbf{P})^{1/2}$, (5.53) can be rewritten as

$$\underset{\mathbf{R}}{\text{Minimize}} \;\; \| \frac{1}{\sqrt{M}}\mathbf{S} - \mathbf{P}\mathbf{G}^{-1}\mathbf{T} \|_F^2 \tag{5.56}$$

$$\text{subject to} \;\; \mathbf{T}^H\mathbf{T} = \mathbf{I}_3 \;\; ; \;\; \tilde{\mathbf{I}}_3\mathbf{G}^{-1}\mathbf{T} = (\mathbf{G}^{-1}\mathbf{T})^*$$

where $\mathbf{T} = \mathbf{GR}$. Leaving out the second constraint in (5.56), we find that the resulting optimization problem as given by

$$\underset{\mathbf{R}}{\text{Minimize}} \;\; \| \frac{1}{\sqrt{M}}\mathbf{S} - \mathbf{P}\mathbf{G}^{-1}\mathbf{T} \|_F^2 \tag{5.57}$$

$$\text{subject to} \;\; \mathbf{T}^H\mathbf{T} = \mathbf{I}_3$$

is simply a generalized version of the Procruste rotation problem [GOLU84]. Geometrically speaking, we rotate the subspace spanned by the three columns of $\mathbf{PG}^{-1}$ via a unitary transformation $\mathbf{T}$ until it is best approximated by the subspace spanned by the three columns of $\mathbf{S}$ in a minimum Frobenius norm sense. It is a well known result that $\mathbf{T}$ is obtained by taking the singular value decomposition (SVD) of $\mathbf{G}^{-1}\mathbf{P}^H\mathbf{S}$, and forcing all the singular values to be unity. Mathematically, if $\mathbf{G}^{-1}\mathbf{P}^H\mathbf{S} = \mathbf{U}\Sigma\mathbf{V}^H$ is the SVD, then $\mathbf{T} = \mathbf{UV}^H$ is the unitary matrix that minimizes the cost function in (5.57). Leaving out the constraint on conjugate centro-symmetry for the moment, we have from $\mathbf{T} = \mathbf{UV}^H$ the optimum $\mathbf{R}$ matrix for (5.53) given by

$$\mathbf{R}_{opt} = \mathbf{G}^{-1}\mathbf{UV}^H \tag{5.58}$$

In Appendix D, we prove that the $\mathbf{R}_{opt}$ matrix thus obtained satisfies $\tilde{\mathbf{I}}_3\mathbf{R}_{opt} = \mathbf{R}_{opt}^*$. Therefore, $\mathbf{R}_{opt}$ is indeed the optimum solution to (5.53) and

the Mx3 matrix constructed according to

$$\mathbf{W}_{mo} = \mathbf{P}\mathbf{R}_{opt} \tag{5.59}$$

is the corresponding optimum mutually "orthonormal" matrix beamformer. Note that the optimum MO matrix beamformer does not necessarily produced maximum SNR gain at the look directions $u = -\frac{2}{M}$, $u = 0$, and $u = \frac{2}{M}$ since no constraints were imposed to guarantee that. However, as long as the interfering directions are not close to the broadside of the array, we should expect the maximum SNR gain to occur at angles close to $u = -\frac{2}{M}$, 0, and $\frac{2}{M}$, respectively, for the three beams.

In conclusion, we present the algorithmic summary of the BDML method for nonsymmetric multipath using an adaptively formed beamforming matrix.

BDML Method for Nonsymmetric Multipath
with Adaptive Matrix Beamformer

(1.) With $\mathbf{W}$ constructed according to (5.41), (5.51), or (5.59) and $\hat{\mathbf{R}}_{xx} = \frac{1}{N}\sum_{n=1}^{N} \mathbf{x}(n)\mathbf{x}^H(n)$, form $\hat{\mathbf{R}}_{bb} = \mathbf{W}^H\hat{\mathbf{R}}_{xx}\mathbf{W}$. Also, let $\mathbf{p}$ denotes the (M-2)x1 vector associated with the M-3 common nulls.

(2.) With $\hat{\mathbf{R}}_{bb}$ and $\mathbf{W}$ from (1.), compute $\mathbf{v} = [v_1 , v_2 , v_3]^T$ as GEVEC of 3x3 real matrix pencil $\{ \mathrm{Re}\{\hat{\mathbf{R}}_{bb}\} , \mathbf{W}^H\mathbf{W} \}$ assoc. with smallest GEV.

(3.) With v_i, i=1,2,3, from (2.), form $\mathbf{e} = \mathbf{W}\mathbf{v}$ and $q(z) = q_0 + q_1 z + q_0^* z^2$ where:

$$q_0 = \frac{e_0}{p_0} \; ; \; q_1 = \frac{e_1 - q_0 p_1}{p_0} \; ; \; q_2 = \frac{e_{M-1}}{p_{M-3}}$$

where p_i and e_i are the (i+1)-th component of $\mathbf{p}$ and $\mathbf{e}$, respectively.

(4.) Let $\alpha = \frac{q_0}{q_1}$. If $|\alpha| < \frac{1}{2}$, multipath signals not resolved. Otherwise:

(5.) $\hat{z}_{1,2} = \frac{-1 \pm j\sqrt{4|\alpha|^2 - 1}}{2\alpha}$ ☞ $\hat{u}_{1,2} = \frac{1}{j\pi}\ln\{z_{1,2}\}$

5.4 Computer Simulations

In this section, we present computer simulation results to illustrate the behavior of the three adaptive generalized Butler beamformers developed in the preceding section. The array employed was linear consisting of M=15 sensor elements equally spaced by a half-wavelength. The interference environment involved two interferers located at 17° and 30°, respectively. Spatially white noise was assumed as well. For the sake of brevity, we assumed exact knowledge about the interfering directions and hence did not concern ourselves with any particular estimation problem. The optimum beamforming weight vectors were computed using the formulae given in (5.41), (5.51), and (5.59), respectively. Figure 5.1 depicts the respective beam patterns associated with the MTNP, MINP, and MO matrix beamformers, as well as that associated with the Mx3 Butler beamformer. Each pattern was normalized such that the maximum response was one. It is interesting to observe that in order to form nulls in the interfering directions and retain M-3 nulls in common, all three adaptive beamformers inevitably produce higher sidelobe level than that associated with the Mx3 Butler beamformer in certain angular regions. The MTNP array pattern exhibits relatively high first sidelobe in the lower beam but fairly low sidelobes near the two interferers while the MINP and MO beamformers produce smoother sidelobe patterns. The beam pattern associated with the MO beamformer appears to be very similar to that associated with the MINP beamformer as can be expected since they share the same set of common nulls. All three adaptive beamformers behave quite similarly to the Mx3 Butler beamformer within the mainlobe region.

To compare their noise suppression capability, the SNR gain produced at the three directions of look, i. e., $u = 0$ and $\pm\frac{2}{M}$, respectively, by the lower, center, and upper beams of each of the above four beamformers are shown in Table 5.1. Undoubtfully, the Butler beamformer produces the highest SNR gain for all three beams as it should be. The SNR gain achieved with the MINP beamforming is nearly identical to that that achieved with the MO beamforming, both being close to the ideal case of Butler beamforming. Surprisingly, the MTNP beamformer produced the lowest SNR gain among the four for all cases. This may be attributed to the restriction imposed upon the locations of the uncommon nulls in the design of the MTNP beamformer. For the other two beamformers, however, no such restriction was made.

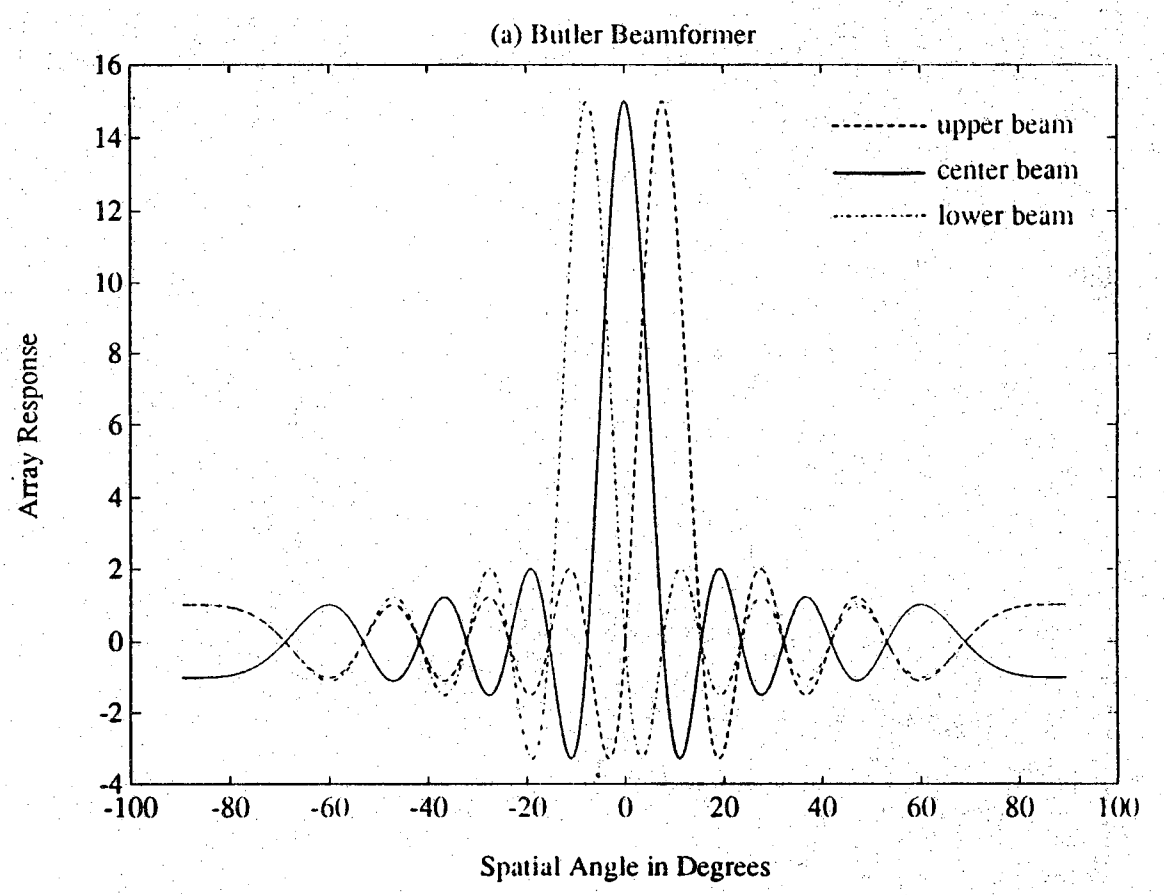

Figure 5.1 The respective array patterns associated with the Butler beamformer and the three adaptively constructed beamformers for the case of M=15 element uniformly-spaced linear array and two interferers present at 17° and 30°. (a) Butler beamformer (b) MTNP beamformer (c) MINP beamformer (d) MO beamformer. In each case, the three adaptive beam patterns have 12 nulls in common, including those corresponding to the two interferers.

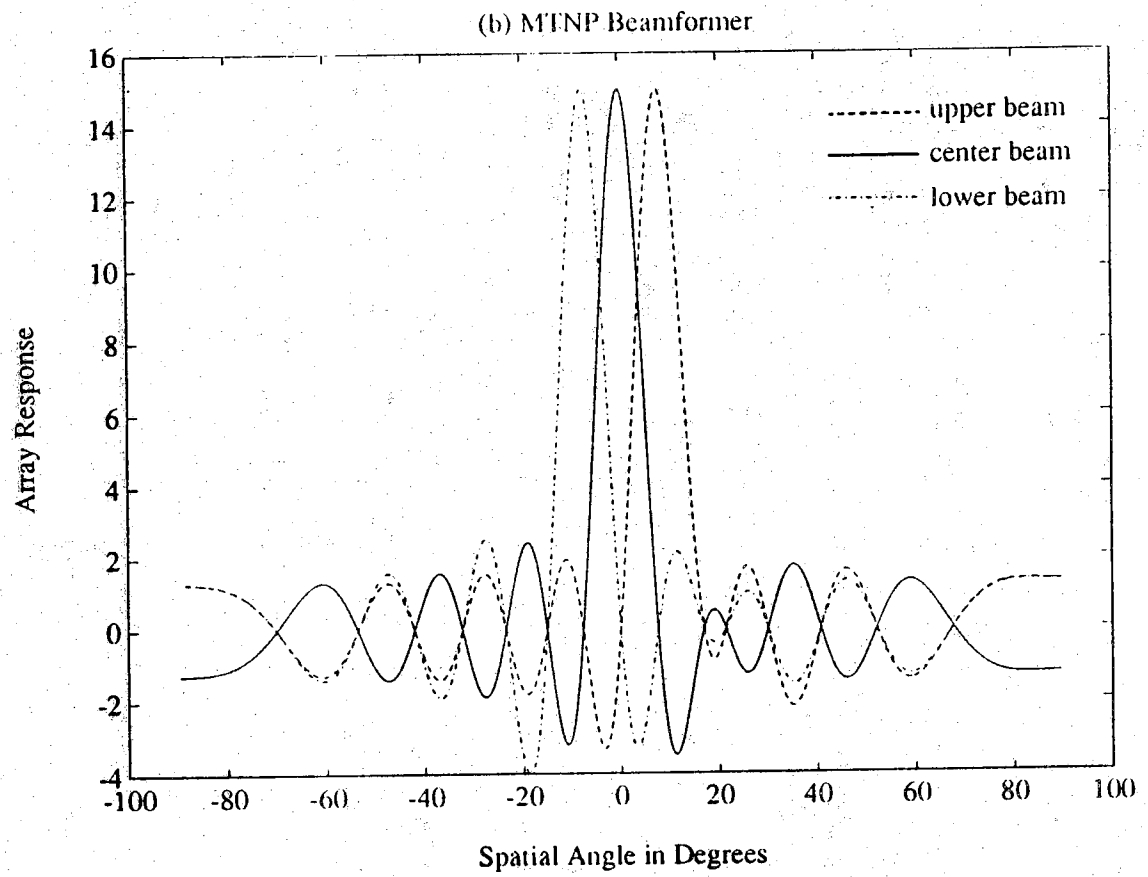

Figure 5.1, continued.

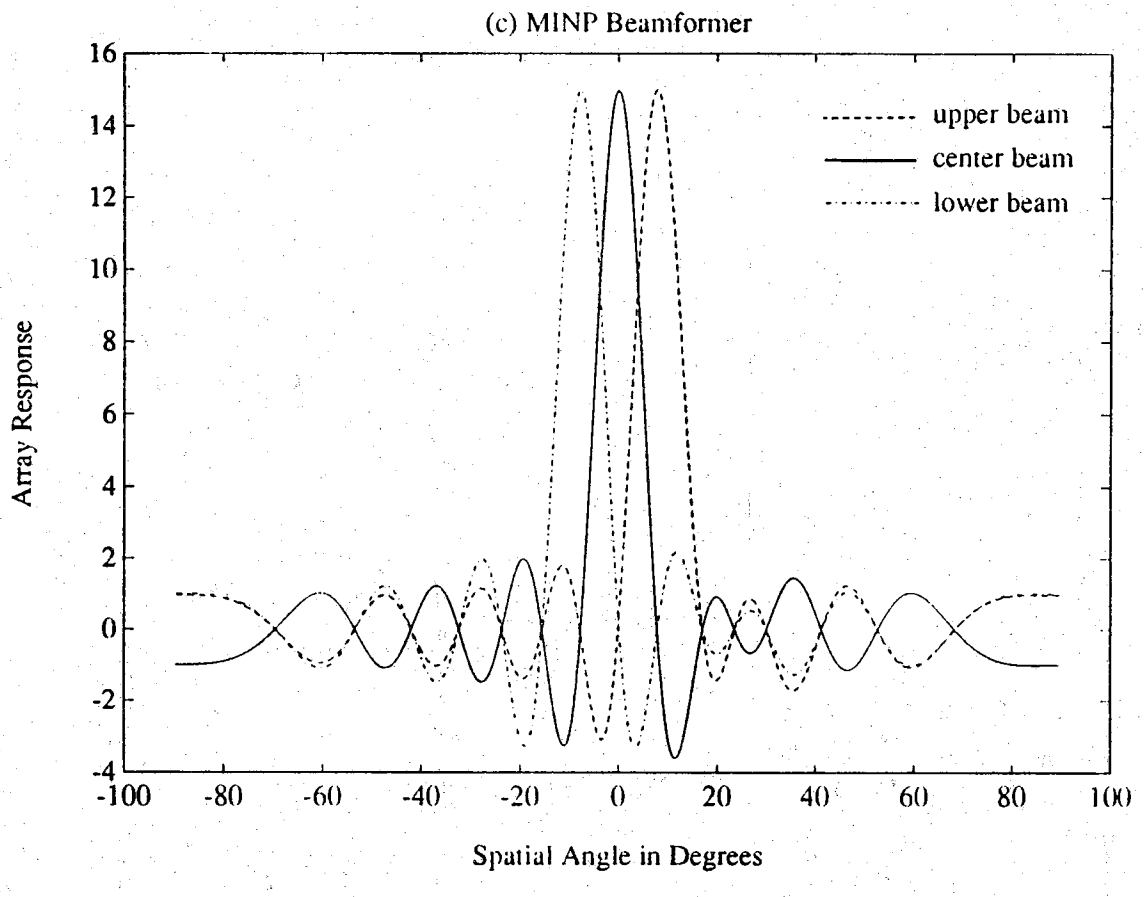

Figure 5.1, continued.

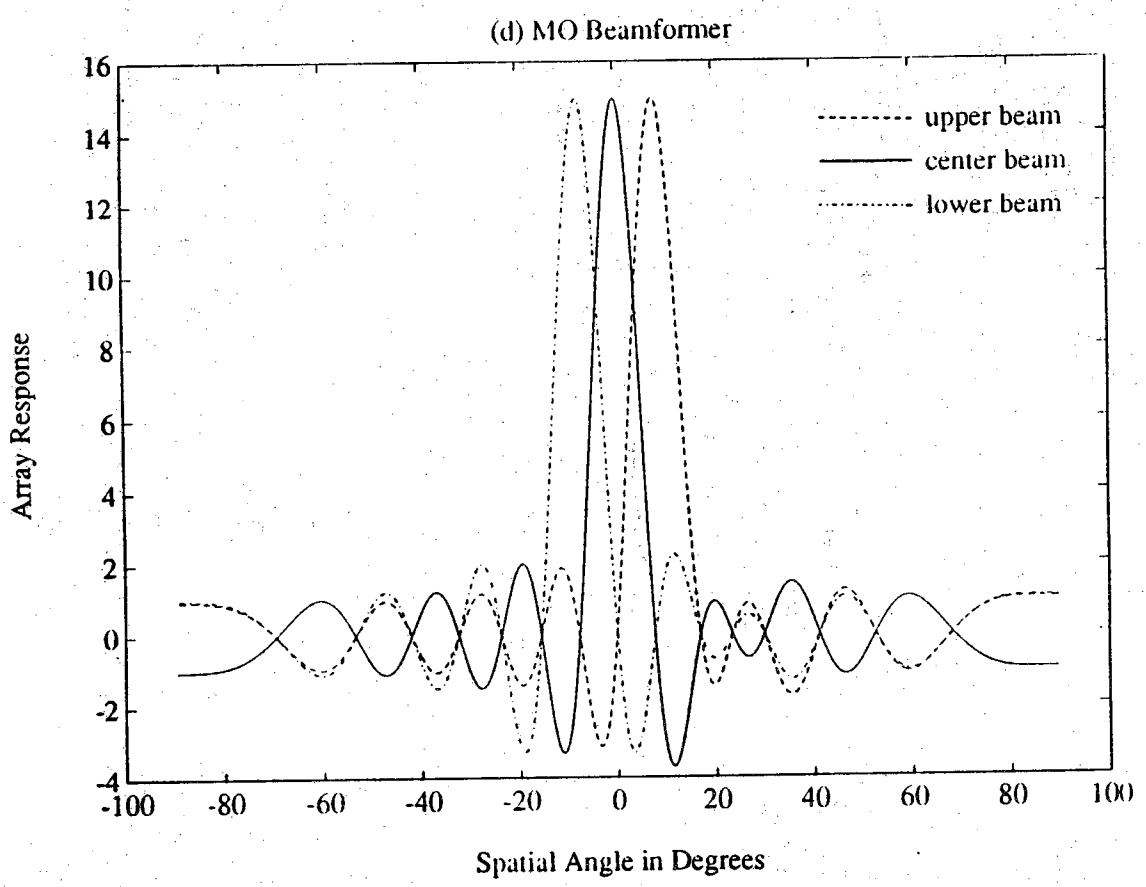

Figure 5.1, continued.

In the final simulation, interference rejection performance was evaluated by introducing a 0.5° error in both the estimates of the interfering directions such that while constructing the polynomials $u_l(z)$, $u_c(z)$, and $u_u(z)$ in (5.29) and $k(z)$ in (5.42), $\theta_{I1}=17.5°$ and $\theta_{I2}=29.5°$. The optimum beamforming weight vectors were computed and the resulting SNR gain in the two true interfering directions produced by the three beams are listed in Table 5.2. It is shown that the MTNP beamformer performs fairly well with SNR gain 16 dB and 12 dB lower than that achieved with the Butler beamformer at $\theta=17°$ and 30°, respectively. The MINP and MO beamformers again yield comparable results due to their similarity in beam pattern. The MTNP beamformer performs better for the interference at 17° than that at 30° while the MINP and MO beamformers, on the contrary, produce lower SNR gain at 30° than at 17°. Huristically speaking, the interference at 17° is more detrimental than the one at 30° in the case of low angle radar tracking and therefore should be suppressed to the greatest extent. The Butler beamformer performs rather poorly in this case as it does not account for any interference cancellation.

Table 5.1 Comparison of the noise suppression performance of the Butler beamformer with that of the three adaptive beamformers for the case of M=15 element uniformly-spaced linear array and two interferers present at 17° and 30°. The SNR gain was computed for u=0 for the center beam, $u=-\frac{2}{M}$ for the lower beam, and $u=\frac{2}{M}$ for the upper beam, respectively.

Type of Beamformer →	Butler	MTNP	MINP	MO
Lower Beam	15.0000	14.8129	14.9121	14.9156
Center Beam	15.0000	14.7700	14.8522	14.8511
Upper Beam	15.0000	14.5017	14.5939	14.5925

Table 5.2 Comparison of the interference rejection performance of the Butler beamformer with that of the three adaptive beamformers for the case of M=15 element uniformly-spaced linear array and two interferers present at 17° and 30°. In forming the three adaptive beamformers, the interfering directions used were 17.5° and 29.5°. The SNR gain in dB was computed for θ_I=17° and 30°.

θ_I	Type of Beamformer →	Butler	MTNP	MINP	MO
17°	Lower Beam	-12.5013	-28.3071	-25.8181	-25.5633
	Center Beam	-9.5876	-25.4089	-22.7055	-22.4931
	Upper Beam	-4.5159	-20.4451	-17.8982	-17.8055
30°	Lower Beam	-13.2430	-25.0188	-28.8969	-28.7267
	Center Beam	-11.7609	-23.5522	-27.2956	-27.1275
	Upper Beam	-9.4934	-21.3926	-25.4676	-25.3303

CHAPTER 6
CONCLUSIONS, FINAL COMMENTS, AND FUTURE RESEARCH

6.1 Conclusion

We have developed a system of estimation schemes for low-angle radar tracking. The goals of the research pursued herein were to 1) document and model the classical low-angle radar tracking problem from a statistical perspective; 2) develop an efficient estimator for a sub-beamwidth multipath scenario; 3) develop auxiliary procedures capable of overcoming difficulties occurring in coherent multipath propagation; 4) extend the results to a more general interferences environment.

Chapter 1 described some related work in the area of low-angle radar tracking. An overview of the Maximum Likelihood (ML) method was presented. It was argued that beamspace processing in contrast to element space processing becomes attractive in light of its low computational load. The ML method was recommended due to its ability to handle the single snapshot case and fully correlated (coherent) sources. Although some efficient beamspace domain ML estimators have been proposed, they nevertheless lack the ability to handle coherent multipath under some extreme conditions such as 180° phase difference. The contradictory phenomenon occurring at 0° phase difference for nonsymmetric multipath is well documented in the literature. However, an effective solution to that problem has not been proposed before.

Chapter 2 developed simple, close-form ML estimators for both the symmetric and nonsymmetric multipath cases. They were derived based on the 3-beam scheme of Haykin and the IQML algorithm of Bresler. It was shown that under certain conditions, Haykin's method corresponds nearly to the beamspace domain ML (BDML) estimator. Performance analysis for coherent multipath revealed that the BDML method for symmetric case is theoretically capable of handling any phase differences so long as the magnitude of the reflection coefficient is not exactly equal to one. For nonsymmetric case, the only conditions for which breakdown occurs are those extreme cases where the direct and specular path signals are perfectly in-phase

or 180° out-of-phase at the center of the array. This analysis provided insight into the behavior of the Cramer-Rao Lower Bound (CRLB) for two arbitrary closely-spaced coherent sources. In particular, it accounted for the poor performance associated with 0° phase difference for nonsymmetric multipath. Simulation results showed that the BDML method performed comparably to the element space based IQML method under moderate conditions while the computational load for BDML was much lower than that for IQML. The major advantage to employing the Butler matrix beamformer is that the angle estimates may be simply determined from the roots of a quadratic equation. In addition, the computational complexity of BDML remains essentially the same as the number of array elements increases. In contrast, the computational complexity of IQML increases greatly as the number of elements increases. Other simulation studies involving various combinations of angles, SNR values, and phase differences demonstrated the agreement between theoretical analysis and pratical results.

Chapter 3 investigated the structure of the Butler matrix beamformer and developed several generalized versions of it. In particular, we considered an alternative interpretation for beamforming in terms of polynomials and sequences. It was shown that the Butler beamformer can be decomposed as a product of two matrices, with one corresponding to the common nulls, and the other corresponding to the uncommon nulls. The matrix associated with the common nulls exhibits a banded, Toeplitz structure such that we may consider it as associated with three overlapping subarrays, each one having all but one sensor in common with an adjacent subarray. The matrix associated with the uncommon nulls was chosen to be nonsingular so as to facilitate a one-to-one mapping between the element space and beamspace manifold vectors. A class of generalized Butler beamformers was constructed by appropriately choosing the common and uncommon nulls in accordance with a set of constraints. An alternative BDML estimation scheme applicable to both symmetric and nonsymmetric cases was developed based on the generalized Butler beamformers. It appeared to be more flexible than the BDML methods described in Chapter 2, especially when the uncommon nulls were formed in a nonsymmetric fashion. A simple parameterization of the beamspace manifold vectors was made possible with the use of a Butler beamformer. For angles near broadside, a beamspace manifold vector may be expressed in terms of a single parameter t accounting for the relationship between its three components. An equation relating t and u was derived subsequently, allowing one to obtain an angle estimate $\hat{u}$ directly from an estimate of t. Although the

new method does not help to ease computational burden, it does provide insight into the behavior of the beamspace manifold vectors, which may be difficult to deal with in the u domain. The correctness of this parameterization was verified by considering several special cases.

Chapter 4 presented three auxiliary procedures for the refinement to the BDML method under coherent multipath conditions. The ρ-based BDML estimation scheme was shown to provide a simple, iterative procedure for simultaneously estimating the direct path angle and the complex reflection coefficient for symmetric multipath. Each execution of the algorithm only involved either a 2x2 complex generalized eigenvalue decomposition or a 3x3 real generalized eigenvalue decomposition. Simulations showed that substantial improvement in performance was achieved when the phase difference was close to 180°. The conversion of a nonsymmetric problem into a symmetric one was accomplished based on the distinctive rank property associated with the beamspace forward-backward averaged correlation matrix in the symmetric case. The bisector angle between the two paths was first estimated, then followed by a second steering of the three beams. The bisector angle estimate was computed via the solution of a judiciously constructed quartic equation. Significant improvement in accuracy with the symmetrized BDML method over the original BDML method was observed when the two signals were nearly in-phase. Frequency diversity was incorporated mainly as a remedy for severe fading occurring in the 180° out-of-phase case. The coherent signal subspace concept of Wang and Kaveh was invoked for retaining the computational simplicity of the BDML method developed for single frequency operation. It was shown that if the frequencies f_i were chosen such that $f_i = \frac{M}{M_i} f_o$, and spatial smoothing was conducted in a judicious fashion, perfect focusing may be achieved without iterating. The only condition required was that both the direct and specular path angles are small enough such that the approximation $\sin\theta \simeq \theta$ is valid. Simulations indicated that the multi-frequency BDML scheme is so far the most reliable estimation procedure for low-angle radar tracking involving coherent multipath. It becomes particularly advantageous as the size of the array or the number of snapshots increases. Provided that the appropriate hardware is available, it is strongly recommended.

Chapter 5 developed a novel adaptive beamforming technique for interference cancellation when the BDML scheme is employed in low-angle radar tracking. The algorithm described was a null synthesis scheme rather

than a closed loop adaptive algorithm. The a-priori information about the interferences was incorporated in the form of a polynomial whose roots correspond to the interfering directions. The idea of common nulls associated with the Mx3 Butler beamformer was incorporated into the synthesis procedure so as to formulate the BDML estimation problem as that associated with a 3x3 generalized eigenvalue decomposition and a quadratic equation. Three different beamformers were developed based on different optimality criteria. The MTNP beamformer minimizes the total output noise power from the three beam ports and usually exhibits patterns similar to that associated with the quiescent beamformer. The MINP beamformer minimizes output noise power from the three beams individually and therefore manifests itself as more flexible than the MTNP beamformer. For most cases, these two beamformers performed fairly well in terms of SNR gain and sidelobe levels. The MO beamformer was constructed based on the least squares criterion and mutual orthonormality constraint. The optimum LS fit was defined in terms of a reference beamforming matrix having certain desired properties. The three mutually orthonormal beamforming weight vectors produce a beamspace noise correlation matrix proportional to the identity matrix and, as a result, simplifies the computation involved in the BDML estimation procedures. Although the beam patterns were not guaranteed to exhibit maxima exactly at the desired directions of look, simulation results showed that the MO beamformer did indeed produce maximum SNR gain at angles close to the look directions determined by the reference beamformer.

6.2 Final Comments

Some final comments are in order. They are made primarily to extend the areas of applications for the BDML estimation schemes developed so far.

6.2.1 Target Tracking in Freespace

First, the BDML estimation schemes presented here were developed for the cases of two targets located in the general vicinity of broadside. For more general phased array radar scenarios, one would simply steer the three beams, keeping their relative angular positions fixed, to other directions of look. From the outputs of the three beams, one would have to determine whether there were one or two targets in the direction of look using such criteria as Akaike Information Criteria (AIC) [AKAI74] or Minimum Description Length (MDL)

[SCHW78], for example. In the event that two targets are detected, the BDML estimation scheme may be employed to estimate the angular positions of the two targets relative to the pointing angle of the center or reference beam. In this mode, the nonsymmetric BDML estimator is more generally applicable than the symmetric one. In light of the problem of the nonsymmetric BDML estimator in the 0° phase difference case, however, it is desirable to convert a nonsymmetric problem to a symmetric one using the ad-hoc procedure developed in Section 4.3. In this case, the entire array is "electronically" steered to the desired direction of look and the correlation matrix to be worked with is the one formed with the steered array.

6.2.2 Multiple Targets Case

Third, the BDML estimation schemes developed are not restricted to two-target cases. It can theoretically handle D targets with D+1 beams provided that $D+1<M$. The premise, however, is that one needs to know where to form the beams, i. e., one needs to determine the directions of look so as to produce high SNR gain in the target directions. In the case of tracking, the look directions can be taken as the most recent estimates of the target angles. Motivated by the computational simplicity attained with the Butler matrix beamformer, it is desirable to employ a set of beamforming vectors having M-D-1 nulls in common. In this case, the BDML angle estimates can be simply determined from the roots of a D-th order polynomial equation.

6.2.3 Frequency Diversity for General Scenarios

To incorporate frequency diversity for more general scenarios, it is necessary to judiciously design the beam patterns so as to retain the perfect focusing achieved with uniform weighting. For example, when two sources are separated by more than two beamwidths, the small angle approximation invoked in Section 3.4 is no longer valid. In this case, the Kaiser weighting [HARR78] is more appropriate since its spectrum depends on u thru the product Mu only ($u = \sin\theta$ and M is the number of elements). Other possible candidates are those whose spectra are invariant under scaling operation, i. e., $P(ku) \propto P(u)$, where P(u) denotes a spatial spectrum. The frequency diversity scheme is equally applicable to the wideband case. The idea is to partition the entire frequency band into J subbands centered at f_i, i=0,...,J-1, in such a

fashion so as to retain the relationship $Mf_o = M_i f_i$, i=1,...J-1, as described in Section 4.4. Note that this scheme works best for large M as the number of frequencies satisfying $Mf_o = M_i f_i$ is proportional to M.

6.2.4 Efficient BDML-Based Interference Cancellation

In Chapter 5, the beamforming techniques were developed based on the assumption that a polynomial associated with the interfering directions is available via certain direction finding algorithms such as IQML and ESPRIT. We point out, however, that it is possible to achieve so relying solely upon the BDML methods. The idea is to alternately estimate the target and interference directions in an adaptive fashion. The algorithm is a two-step procedure: I) form K+1 beams in the K (estimated) interfering directions and a reference direction, each beam having a null in each of the (estimated) target directions, and apply the BDML method to the resulting K+1 dimensional beamspace snapshot data. In the end, we obtain a K-th order polynomial whose roots correspond to the K interfering directions.; II) with the k-th order polynomial obtained in I), we proceed to estimate the target angles using one of the matrix beamformers constructed in Section 5.3. The algorithm is performed adaptively in the sense that the estimates of both the target and interference directions obtained most recently are incorporated in phase I to form the desired K+1 beams. Of course, we may form the K+1 beams according to one of the three criteria described in 5.3.

6.3 Future Research

The following suggestions are made to inspire further interests in the area of low-angle radar tracking.

6.3.1 Analysis of Resolution Capability

Analysis of resolution capability has attracted the interests of many researchers in the area of spectrum estimation and array signal processing [COX73], [OWSL84], [KAVE86], [WANG86], [JEFF85], [PORA88], [OTTE89]. Recently the resolution threshold for some eigen-assisted methods (e. g. MUSIC and Minimum-Norm) has been quantitatively analyzed in several papers [KAVE86], [WANG86], [JEFF85], [PORA88] for both element space and beamspace domain applications. Their approach was to compute the first

and second moments of the null spectrum and then determine the probability of resolution via certain ad-hoc criterion. These analysis procedures can be readily applied to the BDML estimators as the latter is in fact an eigen-assisted method resembling MUSIC. One major drawback of the above mentioned methods is that exact expressions for the moments of the null spectrum is difficult to obtain and barely manageable. In addition, the criterion for discriminating resolved and unresolved cases is ambiguous in nature. The BDML method, on the other hand, provides a quantitative description of the condition of resolution, as can be seen in Section 2.3. The criterion was simply an inequality involving three real components of v and the probability of resolution is exactly the probability of that the inequality holds. This suggests that a closed-form expression for v, the "smallest" eigenvector of $\mathbf{R}_{bb}$ should be derived and a statistical perturbation analysis for that be conducted. The procedure should be simple due to the low dimensionality associated with beamspace domain processing.

6.3.2 Diffuse Multipath

The classical specular-reflection model for surface reflections has been modified to account for surface roughness [BART74], [BART79], [SMIT79]. These modifications describe several effects: 1) the reduction in magnitude of the specular component with increased roughness; 2) the spreading of angle of arrival of reflected components surrounding the specular image. This phenomenon is referred to as diffuse multipath propagation. The problem of low-angle radar tracking involving diffuse multipath is complicated by the fact that prediction of spatial distributions of diffuse multipath is a complex process for which no rigorous theory exists. Actual sea and ground surfaces are difficult to characterize analytically. A popular model for diffuse multipath is the "glistening surface" model proposed by Beckmann and Spizzichino [BECK63] and Barton [BART74]. The model states that most of the diffuse power from a normally distributed surface will reach the radar from the region within the glistening surface. Namely, the diffuse power will concentrate over certain region surrounding the specular image in the spatial spectrum. Therefore, it can be treated as a noise-like interference superimposed upon the specular return. To employ ML method in this case, one needs to characterize the correlation matrix of the diffuse return, which often involves a complex estimation procedure. Under this circumstance, beamspace domain processing is more advantageous as the spatial passband

associated with the beamformer is usually narrow such that it is adequate to model the diffuse return as spatial white noise in beamspace. This facilitates a simpler way of estimating the beamspace noise (including diffuse return) correlation matrix. In addition, the small dimensionality involved in beamspace domain processing makes some iterative correlation matrix estimation schemes [LECA89] realizable.

6.3.3 Two Dimensional Beamspace Domain Processing

Although the BDML estimation schemes presented here were developed for the case of multiple snapshots, they are applicable in the case of a single snapshot as well, as would be the case with monopulse radar tracking. Judging from the performance obtained with N=0 snapshots in the case of a M=15 element array, a much larger number of elements would be required for adequate performance in the single snapshot case. We remark that each radar system comprising the PAVE-PAWS phased array network has two janus faces composed of 1,792 transmit-receive antenna elements each; the COBRA DANE phased array radar system is composed of 15,360 such elements. Along these lines, we note that actual phased array such as those comprising the AEGIS and PAVE-PAWS series, as well as the mammoth COBRA DANE phased array, are planar with the elements uniformly-spaced on a rectangular grid. For the sake of simplicity, we here considered only the case of a linear array. The BDML estimation schemes developed within may be easily extended for the case of a 2-D grid array with uniform spacing along both axes. In this case, the array may be viewed as a collection of uniformly-spaced, linear arrays in parallel. If we apply the same weight vector to each linear array in parallel, to look at a specific azimuthal angle, for example, we obtain a collection of what are referred to as super-element outputs. We could then apply three different beamforming vectors, pointed to three closely-spaced elevation angles, for example, to the collection of super-element outputs. The final beamspace outputs may then be supplied to the BDML estimator to produce estimates of the elevation angles of two closely-spaced targets. Azimuthal angles may be estimated in a similar fashion.

LIST OF REFERENCES

LIST OF REFERENCES

[AKAI74] Akaike, H., "A New Look at the Statistical Model Identification," *IEEE Trans. Auto. Control,* vol. AC-19, no. 12, pp. 716-723, Dec. 1974.

[APPL76] Applebaum, S. P., "Adaptive Arrays," *IEEE Trans. Antennas Propagation,* vol. AP-24, pp. 585-598, Sept. 1976.

[BALL87] Ballance, W. P. and Jaffer, A. G., "Low Angle Direction Finding Based on Maximum Likelihood: A Unification," *Conference Record of the 21st Asilomar Conference on Signals, Systems, and Computers,* pp. 119-124, Nov. 1987.

[BART74] Barton, D. K., "Low Angle Radar Tracking," *Proc. IEEE,* vol. 62, pp. 687-704, June 1974.

[BART79] Barton, D. K., "Multipath Fluctuation Effects in Track-While-Scan Radar," *IEEE Trans. Aerospace and Electronic Systems,* vol. AES-15, no. 6, pp. 754-763, Nov. 1979.

[BECK63] Beckmann, P. and Spizzichino, A., **The Scattering of EM Waves from Rough Surfaces,** Pergamon, New York, NY., 1963.

[BRES86] Bresler, Y. and Macovski, A., "Exact Maximum Likelihood Parameter Estimation of Superimposed Exponential Signals in Noise," *IEEE Trans. Acoustics, Speech, and Signal Processing,* vol. ASSP-34, no. 5, pp. 1081-1089, Oct. 1986.

[BRES88] Bresler, Y., Reddy, V. U., and Kailath, T., "Optimum Beamforming for Coherent Signal and Interferences," *IEEE Trans. Acoustics, Speech, and Signal Processing,* vol. ASSP-36, no. 6, pp. 833-843, June 1988.

[BUCK88] Buckley, K. M. and Xu, X. L., "Broad-Band, Beam-Space, Signal-Subspace Source Localization," *IEEE 1988 Antennas and Propagation International Symposium Digest,* Quebec, Canada, pp. 246-249, June 1988.

[BYRN87] Byrne, C. L. and Steele, A. K., "Sector-Focused Stability for High-Resolution Array Processing," *Proceedings of 1987 IEEE Int'l Conference on Acoustic, Speech, and Signal Processing,* pp. 2340-2343, April 1987.

[CANT80] Cantoni, A. and Godera, L. C., "Resolving the Directions of Sources in a Correlated Field Incident on an Array," *J. Acoust. Soc. Amer.*, vol. 67, no. 4, pp. 1247-1255, April 1980.

[CANT81] Cantrell, B. H., Gordon, W. B., and Trunk, G. V., "Maximum Likelihood Elevation Angle Estimation of Radar Targets Using Subapertures," *IEEE Trans. Aerospace and Electronic systems,* vol. AES-17, no. 3, pp. 213-221, March 1981.

[CAPO69] Capon, J., "High-Resolution Frequency-Wavenumber Spectrum Analysis," *Proc. IEEE,* vol. 57, pp. 1408-1418, Aug. 1969.

[COX73] Cox, H., "Resolving Power and Sensitivity to Mismatch of Optimum Array Processing," *J. Acoust. Soc. Amer.*, vol. 54, no. 3, pp. 771-785, 1973.

[DAVI76] Davis, R. C., Brennan, L. E., and Reed, L. S., "Angle Estimation with Adaptive Arrays in External Noise Fields," *IEEE Trans. Aerospace and Electronic Systems,* vol. AES-12, no. 3, pp. 179-186, Mar. 1976.

[EVAN82] Evans, J. E., Johnson, J. R., and Sun, D. F., "Application of Advanced Signal Processing Techniques To Angle-of-Arrival Estimation in ATC Navigation and Surveillance Systems," *M.I.T. Lincoln Lab., Tech. Report* no. 582, 23 June 1982.

[FORS87] Forster, P. and Vezzosi, G., "Application of Spheroidal Sequences to Array Processing," *Proceedings of 1987 IEEE Int'l Conference on Acoustic, Speech, and Signal Processing,* pp. 2267-2271, April 1987.

[FROS76] Frost, O. L., "An Algorithm for Linearly Constrained Adaptive Array Processing," *Proc. IEEE,* vol. 60, no. 9, pp. 670-684, September, 1976.

[GABR84] Gabriel, W. F., "A High-Resolution Target-Tracking Concept Using Spectral Techniques," *NRL Report 6109,* May 1984.

[GABR88] Gabriel, W. F., "Large-Aperture Sparse Array Antenna Systems of Moderate Bandwidth for Multiple Emitter Location," *Proc. Fourth Workshop on Spectrum Estimation and Modeling,* pp. 7-12, August 1988.

[GABR80] Gabriel, W. F., "Spectral Analysis and Adaptive Array Superresolution Techniques," *Proc. IEEE,* vol. 68, no. 6, pp. 654-666, June 1980.

[GOLU80] Golub, G. H. and Van Loan, C. F., "An Analysis of the Total Least Squares Problem," *SIAM J. Numer. Anal.*, vol. 17, no. 6, pp. 883-893, Dec. 1980.

[GOLU84] Golub, G. H. and Van Loan, C. F., **Matrix Computations,** Johns Hopkins University Press, Baltimore, MD., 1984.

[GORD83] Gordon, W. B., "Improved Three Subaperture Method for Elevation Angle Estimation," *IEEE Trans. Aerospace and Electronics Systems,* vol. AES-19, no. 1, pp. 114-122, January, 1983.

[GRIF87] Griffiths, L. J. and Buckley, K. M., "Quiescent Pattern Control in Linearly Constrained Adaptive Arrays," *IEEE Trans. Acoustics, Speech, and Signal Processing,* vol. ASSP-35, no. 7, pp. 917-926, July 1987.

[HARR78] Harris, S., "Use of Windows for Harmonic Analysis," *Proc. IEEE,* vol. 66, no. 1, pp. 49-69, January, 1978.

[HAUP84] Haupt, R. L., "Simultaneous Nulling in the Sum and Difference Patterns of a Monopulse Antenna," *IEEE Trans. Antennas and Propagation,* vol. AP-32, no. 5, pp. 486-493, May, 1984.

[HAYK83] Haykin, S. and Kesler, J., "Adaptive Canceler for Elevation Angle Estimation in the Presence of Multipath," *Proc. IEE,* vol. 130, pp. 303-308, June 1983.

[HAYK84] Haykin, S., "Least Squares Adaptive Antenna for Angle of Arrival Estimation," *Proc. IEEE,* vol. 72, no. 4, pp. 528-530, April 1984.

[HAYK85] Haykin, S., "Radar Array Processing for Angle of Arrival Estimation," *Array Signal Processing,* Prentice-Hall, Englewood Cliffs, NJ, Chap. 4, 1985.

[HUDS81] Hudson, J. E., **Principles of Adaptive Arrays,** Peter Peregrinus, Stevenage, U.K., 1981.

[HUNG88] Hung, H. and Kaveh, M., "Focusing Matrices for Coherent Single-Subspace Processing," *IEEE Trans. Acoust., Speech, Signal Process.,* vol. ASSP-36, no. 8, p. 1272-1281, August 1988.

[JEFF85] Jeffries, D. J. and Farrier, D. R., "Asymptotic Results for Eigenvector Methods," *IEE Proc.,* vol. 132, no. 7, pp. 589-594, Dec. 1985.

[JOHN82] Johnson, D. H. and DeGraaf, S. R., "Improving the Resolution of Bearing in Passive Sonar Arrays by Eigenvalue Analysis," *IEEE Trans. Acoustic, Speech, and Signal Processing,* vol. 30, no. 4, pp. 638-647, August, 1982.

[KAVE86] Kaveh, M. and Barabell, A. J., "The Statistical Performance of the MUSIC and the Minimum-Norm Algorithms in Resolving Waves in Noise," *IEEE Trans. Acoustics, Speech, and Signal Processing,* vol. ASSP-34, pp. 331-341, April 1986.

[KESL80] Kesler, V. and Haykin, S., "A New Adaptive Antenna for Elevation Angle Estimation in the Presence of Multipath," *IEEE 1980 Antenna and Propagation International Symposium Digest,* (Quebec, Canada), pp. 130-133, June 1980.

[KEZY88] Kezys, V. and Haykin, S., "Multifrequency Angle-of-Arrival Estimation: An Experimental Evaluation," *SPIE Int'l. Symposium, Advanced Algorithms and Architectures for Signal Processing III,* August 1988, SPIE Vol. 975, pp. 98-106.

[KSIE68] Ksieski, A. A. and McGhee, R. B., Jr., "A Decision Theoretic Approach to the Angular Resolution and Parameter Estimation Problem for Multiple Targets," *IEEE Trans. Aerospace and Electronic Systems,* vol. AES-4, pp. 443-445, May 1968.

[LECA89] Le Cadre, J. P., "Parametric Methods for Spatial Signal Processing in the Presence of Unknown Colored Noise Fields," *IEEE Trans. Acoustic, Speech, and Signal Processing,* vol. 37, no. 7, pp. 965-983, July 1989.

[LEE89] Lee, T. S. and Zoltowski, M., "Beamspace Domain ML Based Low Angle Radar Tracking with an Array of Antennas," *IEEE Antennas and Propagation Symposium Digest,* San Jose, CA, June 1989.

[MAYH87] Mayhan, J. T. and Niro, L., "Spatial Spectrum Estimation Using Multiple Beam Antennas," *IEEE Trans. Antennas Propagation,* vol. AP-35, no. 8, pp. 897-906, Aug. 1987.

[MONZ80] Monzingo, R. A. and Miller, T. W., **Intro. to Adaptive Arrays,** Wiley & Sons, New York, NY, 1980

[OTTE89] Ottersten, B. and Ljung, L., "Asymptotic Results for Sensor Array Processing," *Proc. ICASSP 89 conf.* Glasgow, Scotland, May 1989.

[OWSL84] Owsley, N. L., "High Resolution Spectrum Analysis by Dominant Mode Enhancement," in **VLSI and Modern Signal Processing,** S. Y. Kung, H. H. Whitehouse, and T. Kailath, Eds., Prentice-Hall, Englewood Cliffs, NJ, 1984.

[PORA88] Porat, B. and Friedlander, B., "Analysis of the Asymptotic Relative Efficiency of the MUSIC Algorithm," *IEEE Trans. Acoustic, Speech, and Signal Processing,* vol. 36, no. 4, pp. 532-543, April, 1988.

[FRIE89] Friedlander, B. and Porat, B., "Performance Analysis of a Null-Steering Algorithm Based on Direction-of-Arrival Estimation," *IEEE Trans. Acoustic, Speech, and Signal Processing,* vol. 37, no. 4, pp. 461-466, April, 1989.

[REDD87] Reddy, V. U., Paulraj, A., and Kailath, T., "Performance Analysis of the Optimum Beamformer in the Presence of Correlated Sources and its Behavior under Spatial Smoothing," *IEEE Trans. Acoustics, Speech, and Signal Processing,* vol. ASSP-35, pp. 927-936, July 1987.

[RIEG73] Riegler, R. L. and Compton, R. T., Jr., "An Adaptive Array for Interference Rejection," *Proc. IEEE,* vol. 61, pp. 748-758, June 1973.

[ROY89] Roy, R. and Kailath, T., "ESPRIT - Estimation of Signal Parameters via Rotational Invariance Techniques," *IEEE Trans. Acoustics, Speech, and Signal Processing,* vol. 37, no. 7, pp. 984-995, July 1989.

[SCHM79] Schmidt, R. O., "Multiple Emitter Location and Signal Parameter Estimation," in *Proc. RADC Spectral Estimation Workshop,* Rome, NY, pp. 243-256, 1979.

[SCHW78] Schwartz, G., "Estimating the Dimension of a Model," *Ann. of Stat.,* vol. 6, pp. 461-464, 1978.

[SHAN85a] Shan, T. J., Wax, M., and Kailath, T., "On Spatial Smoothing for Direction-of-Arrival Estimation of Coherent Signals," *IEEE Trans. Acoustics, Speech, and Signal Processing,* vol. 33, pp. 806-811, Aug. 1985.

[SHAN85b] Shan, T. J., and Kailath, T., "Adaptive Beamforming for Coherent Signals and Interference," *IEEE Trans. Acoustics, Speech, and Signal Processing,* vol. ASSP-33, pp. 527-536, June 1985.

[SKOL80] Skolnik, M. I., **Introduction to Radar Systems,** McGraw-Hill, New York, 1980, pp. 442-446.

[SMIT79] Smith, P. G. and Mrstik, A. V., "Multipath Tracking Errors in Elevation-Scanning and Monopulse Radars," *IEEE Trans. Aerospace and Electronic Systems,* vol. AES-15, no. 6, pp. 765-775, Nov. 1979.

[STEI76] Steinberg, B. D., **Principle of Aperture & Array System Design,** John Wiley & Sons, New York, 1976, Chaps. 5-6.

[STEY86] Steyskal, H., Shore, R. A., and Haupt, R. L., "Methods for Null Control and Their Effects on the Radiation Pattern," *IEEE Trans. Antennas and Propagation,* vol. AP-34, no. 3, pp. 404-409, March, 1986.

[STOI88] Stoica, P. and Nehorai, A., "MUSIC, Maximum Likelihood and Cramer-Rao Bound," *Proc. ICASSP 88 Conf.,* New York, pp. 2296-2299, April 1988.

[STOI89] Stoica, P. and Nehorai, A., "MUSIC, Maximum Likelihood and Cramer-Rao Bound," *IEEE Trans. Acoustics, Speech, and Signal Processing,* vol. 37, no. 5, pp. 720-741, May 1989.

[TRUN79a] Trunk, G. V., Cantrell, B. H., and Gordon, W. B., "Probability Density of the Maximum Likelihood Elevation Estimation of Radar Targets," *IEEE Trans. Aerospace and Electronics Systems,* vol. AES-15, no. 2, pp. 288-290, March 1979.

[TRUN79b] Trunk, G. V., Cantrell, B. H., and Gordon, W. B., "Bounds on Elevation Error Estimates of a Target in Multipath," *IEEE Trans. Aerospace and Electronics Systems,* vol. AES-15, no. 6, pp. 883-887, Nov. 1979.

[TUFT82] Tufts, D. W. and Kumaresan, R., "Frequency Estimation of Multiple Sinusoids: Making Linear Prediction Like Maximum Likelihood," *Proc. IEEE,* vol. 70, pp. 975-990, Sept. 1982.

[VAN84] Golub, G. H. and Van Loan, C. F., **Matrix Computations,** Johns Hopkins University Press, Baltimore, MD., 1984.

[VAN68] Van Tree, H. L., **Detection, Estimation, and Modulation Theory,** Wiley, New York, NY., 1968.

[VAN88] Van Veen, B. and Williams, B., "Structured Covariance Matrices and Dimensionality Reduction in Array Processing," *Proc. Fourth Workshop on Spectrum Estimation and Modeling,* pp. 168-171, Aug. 1988.

[VAN89] Van Veen, B. D., "An Analysis of Several Partially Adaptive Beamformer Designs," *IEEE Trans. Acoustic, Speech, and Signal Processing,* vol. 37, no. 2, pp. 192-203, Feb. 1989.

[WANG85] Wang, H. and Kaveh, M., "Coherent Single-Subspace Averaging for the Detection and Estimation of Angles of Arrival of Multiple Wide-Band Sources," *IEEE Trans. Acoustics, Speech, and Signal Processing,* vol. ASSP-33, no. 4, p. 823-831, Aug. 1985.

[WANG86] Wang, H. and Kaveh, M., "On the Performance of Signal-Subspace Processing, Part I: Narrow-Band System," *IEEE Trans. Acoustics, Speech, and Signal Processing,* vol. ASSP-34, pp. 1201-1209, Oct. 1986.

[WHIT74] White, W. D., "Low-angle Radar Tracking in the Presence of Multipath," *IEEE Trans. Aerospace and Electronic Systems,* vol. AES-10, pp. 835-853, Nov. 1974.

[WIDR67] Widrow, B. et al., "Adaptive Antenna Systems," *Proc. IEEE,* vol. 55, pp. 2143-2159, Dec. 1967.

[WIDR85] Widrow, B. and Stearns, S. D., **Adaptive Signal Processing,** Prentice-Hall, Englewood Cliffs, NJ, 1985.

[WILL88] Williams, R. T., Prasad, S., Mahalanabis, A. K., and Sibula, L. H., "An Improved Spatial Smoothing Technique for Bearing Estimation in a Multipath Environment," *IEEE Trans. Acoustics, Speech, and Signal Processing,* vol. 36, pp. 425-432, April 1988.

[XU88] Xu, X. L. and Buckley, K. M., "Reduced-Dimension Beam-Space Broad-Band Localization: Preprocessor Design and Evaluation," *Proc. Fourth Workshop on Spectrum Estimation and Modeling,* pp. 22-26, Aug. 1988.

[ZISK88] Ziskand, I. and Wax, M., "Maximum Likelihood Localization of Multiple sources by Alternating Projection," *IEEE Trans. Acoustics, Speech, Signal Processing,* vol. ASSP-36, no. 10, p. 1553-1560, Oct. 1988.

[ZOLT88a] Zoltowski, M., "High Resolution Sensor Array Signal Processing in the Beamspace Domain: Novel Techniques Based on the Poor Resolution of Fourier Beamforming," *Proc. Fourth ASSP Workshop on Spectrum Estimation and Modeling,* pp. 350-335, August 1988.

[ZOLT88b] Zoltowski, M., "On the Performance Analysis of the MVDR Beamformer in the Presence of Correlated Interference," *IEEE Trans. Acoustics, Speech, and Signal Processing,* vol. 36, no. 6, pp. 945-947, June 1988.

[ZOLT89a] Zoltowski M. and Stavrinides D., "Sensor Array Signal Processing via a Procrustes Based Eigenanalysis of the ESPRIT Data Pencil," *IEEE Trans. Acoustics, Speech, and Signal Processing,* vol. 37, no. 6, pp. 832-861, June 1989.

[ZOLT89b] Zoltowski, M. and Lee, T. S., "Maximum Likelihood Based Sensor Array Signal Processing in the Beamspace Domain for Low-angle Radar Tracking," in review, *IEEE Trans. Acoustics, Speech, and Signal Processing.*

[ZOLT89c] Zoltowski, M. and Lee, T. S., "Bearing Estimation in Beamspace Employing Frequency Diversity," *SPIE Int'l Symposium, Advanced Algorithms and Architectures for Signal Processing IV,* SPIE vol. 1152, Aug. 1989.

[ZOLT89d] Zoltowski, M. and Lee, T. S., "ML Based Monopulse Bearing Estimation for Adaptive Phased Array Radar," *Conference Record of the 23rd Asilomar Conference on Signal, Systems and Computers,* Nov. 1989.

[ZOLT89e] Zoltowski, M. and Lee, T. S., "Bisector Angle Estimation for Nonsymmetric Multipath," in review *IEEE Trans. Aerospace and Electronics Systems.*

APPENDICES

Appendix A
Properties of the Eigenvectors of a Real Matrix Exhibiting Both Symmetry and Per-Symmetry

In this Appendix, we prove a theorem describing some properties of the eigenvectors of a real matrix, $\mathbf{A}$, of dimension mxm, say, which is both symmetric, $\mathbf{A}^T = \mathbf{A}$, and per-symmetric (symmetric about the cross-diagonal), $\tilde{\mathbf{I}}_m \mathbf{A} \tilde{\mathbf{I}}_m = \mathbf{A}^T$, such that the matrix satisfies the following two properties.

$$\text{(a) } \mathbf{A}^T = \mathbf{A} \qquad \text{(b) } \tilde{\mathbf{I}}_m \mathbf{A} \tilde{\mathbf{I}}_m = \mathbf{A} \tag{A.1}$$

where $\tilde{\mathbf{I}}_m$ is a reverse permutation matrix of dimension m as defined in Sect. II by (2.6).

Theorem:

Each eigenvector, $\mathbf{e}_i$, i=1,...,m, of a real matrix $\mathbf{A}$ which is both symmetric and per-symmetric (satisfies (A.1) above) and has m distinct eigenvalues satisfies the relationship $\tilde{\mathbf{I}}_m \mathbf{e}_i = \pm \mathbf{e}_i$, i. e., exhibits either centro-symmetry, $\tilde{\mathbf{I}}_m \mathbf{e}_i = \mathbf{e}_i$, or centro-anti-symmetry, $\tilde{\mathbf{I}}_m \mathbf{e}_i = -\mathbf{e}_i$. Moreover, if m is such that m=2k, k or half of the eigenvectors exhibit centro-symmetry while the remaining k exhibit centro-anti-symmetry. If m is odd such that m=2k+1, k+1 of the eigenvectors exhibit centro-symmetry while the remaining k exhibit centro-anti-symmetry.

Proof:

Let λ_i be the eigenvalue of $\mathbf{A}$ associated with the i-th eigenvector $\mathbf{e}_i$ such that

$$\mathbf{A}\mathbf{e}_i = \lambda_i \mathbf{e}_i \tag{A.2}$$

Since $\tilde{\mathbf{I}}_m \mathbf{A} \tilde{\mathbf{I}}_m = \mathbf{A}$, $\{\lambda_i, \mathbf{e}_i\}$ is also an eigenvalue-eigenvector pair of $\tilde{\mathbf{I}}_m \mathbf{A} \tilde{\mathbf{I}}_m$ as well:

$$\tilde{\mathbf{I}}_m \mathbf{A} \tilde{\mathbf{I}}_m \mathbf{e}_i = \lambda_i \mathbf{e}_i \tag{A.3}$$

Pre-multiplying both sides of (A.3) by $\tilde{\mathbf{I}}_m$ gives

$$\mathbf{A} \tilde{\mathbf{I}}_m \mathbf{e}_i = \lambda_i \tilde{\mathbf{I}}_m \mathbf{e}_i \tag{A.4}$$

where we have exploited the fact that $\tilde{\mathbf{I}}_m \tilde{\mathbf{I}}_m = \mathbf{I}_m$. (A.4) implies that $\tilde{\mathbf{I}}_m \mathbf{e}_i$ is also an eigenvector of $\mathbf{A}$ associated with the eigenvalue λ_i. Since we have assumed that the eigenvalues of $\mathbf{A}$ are distinct, it follows that the eigenvector

associated with each eigenvalue is unique to within a scalar multiple such that $\tilde{\mathbf{I}}_m \mathbf{e}_i$ must be a real scalar multiple of $\mathbf{e}_i$, i. e.,

$$\tilde{\mathbf{I}}_m \mathbf{e}_i = \gamma_i \mathbf{e}_i \tag{A.5}$$

Pre-multiplying both sides of (A.5) by $\tilde{\mathbf{I}}_m$ gives

$$\mathbf{e}_i = \gamma_i \tilde{\mathbf{I}}_m \mathbf{e}_i \tag{A.6}$$

Note that the $\mathbf{e}_i$ are real since $\mathbf{A}$ is real and symmetric. Finally, substituting (A.5) into (A.6) gives $\mathbf{e}_i = \gamma_i^2 \mathbf{e}_i$ which indicates that γ_i is either +1 or -1 which when substituted in (A.5) gives the desired result $\tilde{\mathbf{I}}_m \mathbf{e}_i = \pm \mathbf{e}_i$. This proves the first part of the theorem that the eigenvectors under scrutiny exhibit either centro-symmetry or centro-anti-symmetry.

To complete the proof, consider the case of m even such that m=2k, where k is a positive integer. Further, consider the span of a set of k+1 centro-symmetric vectors, $\mathbf{e}_i$, i=1,...,k+1, of dimension 2kx1. Such a set of vectors may be expressed in the following form

$$\mathbf{e}_1 = \begin{bmatrix} \mathbf{f}_1 \\ \cdots \\ \tilde{\mathbf{I}}_k \mathbf{f}_1 \end{bmatrix} \quad ; \quad \mathbf{e}_2 = \begin{bmatrix} \mathbf{f}_2 \\ \cdots \\ \tilde{\mathbf{I}}_k \mathbf{f}_2 \end{bmatrix} \quad ; \quad \cdots\cdots \quad ; \quad \mathbf{e}_{k+1} = \begin{bmatrix} \mathbf{f}_{k+1} \\ \cdots \\ \tilde{\mathbf{I}}_k \mathbf{f}_{k+1} \end{bmatrix} \tag{A.7}$$

where the k+1 vectors $\mathbf{f}_i$, i=1,..., k+1, lie in $\mathcal{R}^k$, k-dimensional real space, and, as a consequence, are linearly dependent. Thus, we can always find a set of coefficients, c_i, i=1,...,k+1, satisfying

$$c_1 \mathbf{f}_1 + c_2 \mathbf{f}_2 + \cdots + c_{k+1} \mathbf{f}_{k+1} = \mathbf{0} \tag{A.8}$$

The same set of coefficients may be applied to the vectors $\tilde{\mathbf{I}}_k \mathbf{f}_i$, i=1,..., k+1, to obtain the zero vector as well as a consequence of the following observation

$$c_1 \tilde{\mathbf{I}}_k \mathbf{f}_1 + c_2 \tilde{\mathbf{I}}_k \mathbf{f}_2 + \cdots + c_{k+1} \tilde{\mathbf{I}}_k \mathbf{f}_{k+1}$$

$$= \tilde{\mathbf{I}}_k \left\{ c_1 \mathbf{f}_1 + c_2 \mathbf{f}_2 + \cdots + c_{k+1} \mathbf{f}_{k+1} \right\} = \mathbf{0} \tag{A.9}$$

which follows from (A.8). (A.9) combined with (A.8) further implies that the same set of coefficients, c_i, i=1,...,k+1, may be applied to the vectors $\mathbf{e}_i$, i=1,..., k+1, defined in (A.7) to obtain the zero vector, i. e.,

$$c_1 \mathbf{e}_1 + c_2 \mathbf{e}_2 + \cdots + c_{k+1} \mathbf{e}_{k+1} = \mathbf{0} \tag{A.10}$$

The conclusion is that the largest dimension of space spanned by a set of 2kx1

centro-symmetric vectors is k. A similar argument can be made to prove that the largest dimension of space spanned by a set of 2kx1 centro-anti-symmetric vectors is k as well. Now, since **A** is symmetric, its eigenvectors are mutually orthogonal and, hence, linearly independent. The cumulative result of all these observations is that for **A** a real, symmetric, and per-symmetric matrix of dimension mxm where m is even, m/2 or half of its eigenvectors exhibit centro-symmetry and the remaining m/2 eigenvectors exhibit centro-anti-symmetry. Similar arguments hold for the case of m odd such that m=2k+1. The primary difference between the two cases lies in the fact the center or k-th element of a (2k+1)x1 centro-anti-symmetric vector is 0. As a consequence, the largest dimension of space spanned by a set of (2k+1)x1 centro-anti-symmetric vectors is k. It is also easy to argue the largest dimension of space spanned by a set of (2k+1)x1 centro-symmetric vectors is k+1. Thus, if **A** is of dimension (2k+1)x(2k+1), k+1 of the eigenvectors exhibit centro-symmetry while the remaining k exhibit centro-anti-symmetry. This completes the proof.

Note that the theorem also holds if **A** has repeated eigenvalues yet satisfies (A.1). For sake of brevity, we do not supply the appropriate proof here.

Appendix B
Reduction of a Linear Combination of Three Butler Beam Based Polynomials to a Second Order Polynomial

In this appendix, we consider an m-th order polynomial known to have m-2 roots equally-spaced on the unit circle at known locations. We develop simple expressions for the coefficients of the residual second order polynomial obtained by dividing each of the m-2 known roots out of the original m-th order polynomial.

Consider the Mx3 Butler matrix beamformer, **S**, defined as

$$\mathbf{S} = \left[\mathbf{a}(2/M) \vdots \mathbf{a}(0) \vdots \mathbf{a}(-2/M)\right] \tag{B.1}$$

where $\mathbf{a}(u)$ is defined as follows.

$$\mathbf{a}(u) = \left[e^{-j\pi Lu}, \cdots, e^{-j2\pi u}, e^{-j\pi u}, 1, e^{j\pi u}, e^{j2\pi u}, \cdots, e^{j\pi Lu}\right]^T \tag{B.2}$$

Here M=2L+1 such that L=(M-1)/2. Let **z** be a Vandermonde vector defined as

$$\mathbf{z} = [1 \;\; z \;\; z^2 \;\; z^3 \;\; ..... \;\; z^{M-1}]^T \tag{B.3}$$

such that the inner product of any Mx1 vector with **z** is a polynomial of order M-1. Now, consider the roots of each of the three polynomials formed, respectively, with each of the three columns of **S** defined in (B.1). The middle column, $\mathbf{a}(0)$, is simply a vector composed of all ones corresponding to rectangular weighting with a beam steered to broadside, i. e., u=0. When viewed as a weight vector, $\mathbf{a}(0)$ sets up an array pattern $\mathbf{a}^H(0)\mathbf{a}(u) = \dfrac{\sin(\frac{M}{2}\pi u)}{\sin(\frac{\pi}{2}u)}$ which exhibits M-1 nulls at $u = \pm m\frac{2}{M}$, m=1,...,L. This translates into a statement that the polynomial $\mathbf{a}^H(0)\mathbf{z}$ has M-1 roots on the unit circle at the values $z = e^{j\frac{2\pi m}{M}}$, m=1,...,M-1. The situation is depicted in Figure B(b). The vector $\mathbf{a}(2/M)$, which produces the upper auxiliary beam, sets up an array pattern which is merely the pattern produced by the weight vector $\mathbf{a}(0)$ shifted to the right by the amount $\frac{2}{M}$; its peak occurs at the first null on the upper side of the reference beam. The net effect with regard to the roots is a counter-clockwise, circular shift by the amount

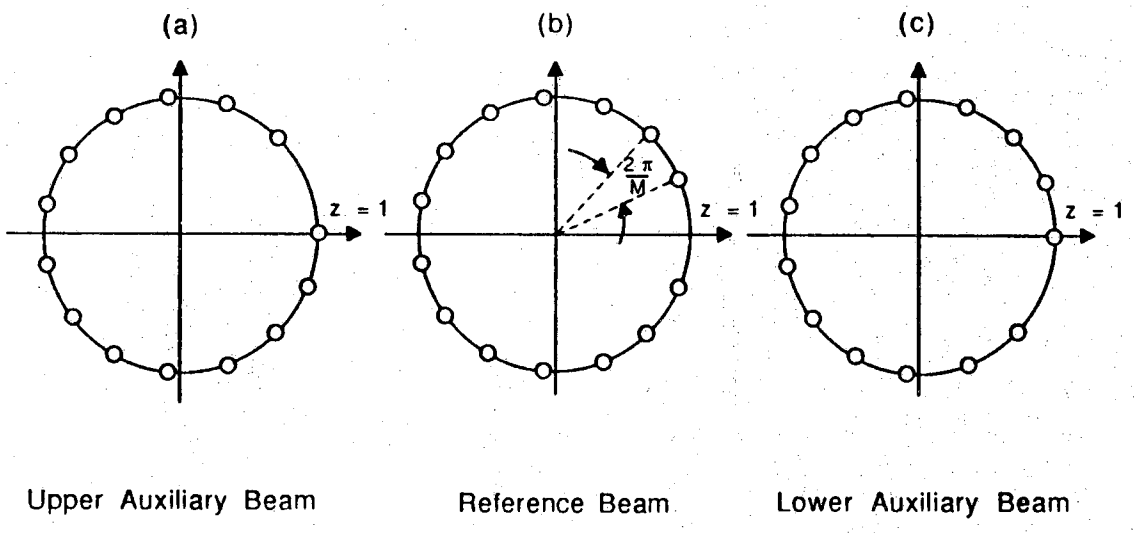

Figure B.1 Location of the respective roots of each of the three polynomials formed with a coefficient vector equal to the (a) first (b) second, and (c) third column of an Mx3 Butler matrix beamformer (M=15). All of the roots lie on the unit circle; the polynomials have M-3=12 roots in common.

$\frac{2\pi}{M}$ as depicted in Figure B(a). That is, $\frac{2\pi}{M}$ is added to the argument of each root of the "reference" polynomial $\mathbf{a}^H(0)\mathbf{z}$. Thus, the M-1 roots of the polynomial $\mathbf{a}^H(2/M)\mathbf{z}$ occur at $z = e^{j\frac{2\pi m}{M}}$, m=2,...,M. Arguing along similar lines, we find that the roots of the polynomial $\mathbf{a}^H(-2/M)\mathbf{z}$ are those of the "reference" polynomial circularly shifted clockwise by the amount $\frac{2\pi}{M}$ as depicted in Figure B(c). That is, the roots of $\mathbf{a}^H(-2/M)\mathbf{z}$ occur at $z = e^{j\frac{2\pi m}{M}}$, m=0,...,M-2. Superimposing the respective M-1 roots of each of these three polynomials, we find M-3 roots in common; the common roots are $z = e^{j\frac{2\pi m}{M}}$, m=2,...,M-2. We will make use of this observation shortly. Note that this observation implies that the respective beam patterns set up by the weight vectors $\mathbf{a}(2/M)$, $\mathbf{a}(0)$, and $\mathbf{a}(-2/M)$ have M-3 nulls in common.

Now, consider the coefficient vector $\mathbf{e} = \mathbf{S}\mathbf{v}$, where $\mathbf{v} = [v_1, v_2, v_3]^T$ and the v_i, i=1,2,3, are real-valued. The (M-1)-th order polynomial $e(z) = (\mathbf{S}\mathbf{v})^H\mathbf{z}$ may be expressed as a linear combination of the reference and two auxiliary polynomials defined above as follows:

$$e(z) = (\mathbf{S}\mathbf{v})^H\mathbf{z} = v_1\,\mathbf{a}^H(2/M)\mathbf{z} + v_2\,\mathbf{a}^H(0)\mathbf{z} + v_3\mathbf{a}^H(-2/M)\mathbf{z} \qquad \text{(B.4)}$$

It follows trivially that any root common to all three polynomials will be a root of any linear combination of the three polynomials. As a consequence of the above observations, therefore, it is apparent that regardless of the values of v_i, i=1,2,3, M-3 roots of the polynomial $(\mathbf{S}\mathbf{v})^H\mathbf{z}$ occur at $z = e^{j\frac{2\pi m}{M}}$, m=2,...,M-2. Note that this statement involves no approximation whatsoever. Thus, the roots of interest are those of a quadratic equation obtained via the following polynomial division:

$$q(z) = q_0 + q_1 z + q_2 z^2 = \frac{(\mathbf{S}\mathbf{v})^H\mathbf{z}}{\prod_{m=2}^{M-2}(z - e^{j\frac{2\pi m}{M}})} \qquad \text{(B.5)}$$

This polynomial division indicated above may be accomplished via a deconvolution of the respective coefficients of the numerator and denominator polynomials. We proceed along these lines in accordance with the following development.

Let d(z) denote the (M-3)-th order polynomial in the denominator of (B.5) with coefficients denoted d_i, i=0,...,M-3, as follows

$$d(z) = \prod_{m=2}^{M-2} (z - e^{j\frac{2\pi m}{M}}) = d_0 + d_1 z + \cdots + d_{M-3} z^{M-3} \qquad (B.6)$$

As indicated above, the (M-1)-th order polynomial in the numerator is denoted $e(z)$; the coefficients of $e(z)$ are denoted e_i, i=0,...,M-1, as follows

$$e(z) = (Sv)^H z = e_0 + e_1 z + \cdots + e_{M-1} z^{M-1} \qquad (B.7)$$

(B.5) trivially implies that $d(z)\, q(z) = e(z)$ which when expanded as follows

$$(d_0 + d_1 z + \cdots + d_{M-3} z^{M-3})(q_0 + q_1 z + q_2 z^2)$$

$$= e_0 + e_1 z + \cdots + e_{M-1} z^{M-1} \qquad (B.8)$$

allows us to determine q_0 , q_1 , and q_2 in terms of d_0 , d_1 , and d_{M-3} and e_0 , e_1 , and e_{M-1} in accordance with the following recursive relationships:

$$d_0 q_0 = e_0 \quad \Rightarrow \quad q_0 = \frac{e_0}{d_0} \qquad (B.9a)$$

$$d_0 q_1 + q_0 d_1 = e_1 \quad \Rightarrow \quad q_1 = \frac{e_1 - q_0 d_1}{d_0} \qquad (B.9b)$$

$$d_{M-3} q_2 = e_{M-1} \quad \Rightarrow \quad q_2 = \frac{e_{M-1}}{d_{M-3}} \qquad (B.9c)$$

At this point, we need to determine d_0 , d_1 , and d_{M-3} and e_0 , e_1 , and e_{M-1} in terms of known parameters and the elements of the vector $\mathbf{v}$: v_i, i=1,2,3. Let us concern ourselves with d_0 , d_1 , and d_{M-3} first. From (B.6), we immediately note that the coefficient associated with the highest order power z^{M-3} is unity, i. e., $d_{M-3} = 1$. To determine d_0 and d_1, we note that with the coefficient of the highest order power equal to unity, i. e., $d_{M-3} = 1$, d_0 is equal to the product of the roots of $d(z)$ while d_1 is equal to the negative of the sum of the roots of $d(z)$. Since the roots of $d(z)$ occur in complex conjugate pairs, as signified by the relationship $\left\{e^{j\frac{2\pi m}{M}}\right\}^* = e^{j\frac{-2\pi m}{M}} = e^{j\frac{2\pi(M-m)}{M}}$, m=2,...,M-2, it immediately follows d_o is equal to one, i. e., $d_o = \prod_{m=2}^{M-2} e^{j\frac{2\pi m}{M}} = 1$. In determining d_1 as the negative of the sum of the roots of $d(z)$, we make the observation that since $z = e^{j\frac{2\pi}{M}}$ is a root of the polynomial $\mathbf{a}^H(0)\mathbf{z} = \sum_{m=0}^{M-1} z^m$, as discussed above, we have that $\sum_{m=0}^{M-1} e^{j\frac{2\pi m}{M}} = 0$

such that

$$d_1 = -\sum_{m=2}^{M-2} e^{j\frac{2\pi m}{M}} = 1 + 2\cos(\frac{2\pi}{M}) \tag{B.10}$$

Next, we turn our attention to the numerator polynomial e(z) defined by (B.4) and (B.7). Returning to the definition of $\mathbf{a}(u)$ in (B.2), we find that

$$e_0 = v_1 e^{j\frac{2\pi L}{M}} + v_2 - v_3 e^{-j\frac{2\pi L}{M}}$$

$$= -v_1 e^{-j\frac{\pi}{M}} + v_2 + v_3 e^{j\frac{\pi}{M}} = e^*_{M-1} \tag{B.11a}$$

$$e_1 = v_1 e^{j\frac{2\pi(L-1)}{M}} + v_2 + v_3 e^{-j\frac{2\pi(L-1)}{M}}$$

$$= -v_1 e^{-j\frac{3\pi}{M}} + v_2 - v_3 e^{j\frac{3\pi}{M}} \tag{B.11b}$$

where we have used the fact that L=(M-1)/2 and the fact that $\mathbf{Sv}$, is hermitian centro-symmetric, i. e., $\tilde{\mathbf{I}}_M \mathbf{Sv} = (\mathbf{Sv})^*$. (v must be real-valued for this to hold.) We now have all the quantities necessary for substitution in (B.9a), (B.9b), and (B.9c) to determine q_0 , q_1 , and q_2 in terms of d_0 , d_1 , d_{M-3}, e_0 , e_1 , e_{M-1}, v_1 , v_2 , and v_3. After some trivial algebraic manipulation, we arrive at the following expressions for the coefficients of q(z):

$$q_0 = -v_1 e^{-j\frac{\pi}{M}} + v_2 - v_3 e^{j\frac{\pi}{M}} = q_2^* \tag{B.12a}$$

$$q_1 = 2(v_1 + v_3)\cos(\frac{\pi}{M}) - 2v_2\cos(\frac{2\pi}{M}) \tag{B.12b}$$

Thus, $q(z) = q_0 + q_1 z + q_o^* z^2$ where the center coefficient, q_1, is real. (B.12a) and (B.12b) constitute the main result of this Appendix invoked in Section III.

Consideration of the symmetric multipath problem as done in Section II leads to a consideration of the special case where $\mathbf{v}$ is centro-symmetric, $\tilde{\mathbf{I}}_3 \mathbf{v} = \mathbf{v}$. In this case, we express $\mathbf{v}$ as $\mathbf{v} = [v_1 , v_0 , v_1]^T$, where we have chosen to put a subscript 0 on the center element in keeping with the notation in Section II. This, of course, leads to certain simplifications with regard to the coefficients of $\mathbf{v}$ which are indicated below:

$$q_0 = v_0 - 2v_1\cos(\frac{\pi}{M}) = q_2 \quad ; \quad q_1 = 4v_1\cos(\frac{\pi}{M}) - 2v_0\cos(\frac{2\pi}{M}) \qquad \text{(B.13)}$$

In this case, all the coefficients of q(z) are real implying that its roots are either real or form a complex conjugate pair.

Appendix C

Simplification of the Cost Function for Bisector Angle Estimation

In this Appendix, we show that the cost function in (4.45) can be expressed in the form of a fourth order polynomial and the minimizing $\hat{u}_c$ can be determined by rooting a quartic equation. We begin the derivation by substituting (4.44) into the matrix $\mathbf{W}^*(u_c)\tilde{\mathbf{C}}_{hh}^{fb}\mathbf{W}(u_c)$ in (4.45). Letting c_{ij} denotes the ij-th component of $\tilde{\mathbf{C}}_{hh}^{fb}$, i. e., $c_{ij} = \left(\tilde{\mathbf{C}}_{hh}^{fb}\right)_{ij}$, we have

$$\mathbf{W}^*(u_c)\tilde{\mathbf{C}}_{hh}^{fb}\mathbf{W}(u_c) = \begin{bmatrix} e^{j\pi u_c} & 0 & 0 \\ 0 & 1 & 0 \\ 0 & 0 & e^{-j\pi u_c} \end{bmatrix} \begin{bmatrix} c_{11} & c_{12} & c_{13} \\ c_{12}^* & c_{22} & c_{12} \\ c_{13}^* & c_{12}^* & c_{11} \end{bmatrix} \begin{bmatrix} e^{-j\pi u_c} & 0 & 0 \\ 0 & 1 & 0 \\ 0 & 0 & e^{j\pi u_c} \end{bmatrix}$$

$$= \begin{bmatrix} c_{11} & c_{12}e^{j\pi u_c} & c_{13}e^{2j\pi u_c} \\ c_{12}^*e^{-j\pi u_c} & c_{22} & c_{12}e^{j\pi u_c} \\ c_{13}^*e^{-2j\pi u_c} & c_{12}^*e^{-j\pi u_c} & c_{11} \end{bmatrix} \qquad \text{(C.1)}$$

Note that we have invoked the property $\tilde{\mathbf{I}}_3\tilde{\mathbf{C}}_{hh}^{fb}\tilde{\mathbf{I}}_3 = \tilde{\mathbf{C}}_{hh}^{fb\,*}$. The real part of (C.1) is

$$\mathrm{Re}\{\mathbf{W}(u_c)^*\tilde{\mathbf{C}}_{hh}^{fb}\mathbf{W}(u_c)\}$$

$$= \frac{1}{2}\begin{bmatrix} 2c_{11} & c_{12}e^{j\pi u_c}+c_{12}^*e^{-j\pi u_c} & c_{13}e^{2j\pi u_c}+c_{13}^*e^{-2j\pi u_c} \\ c_{12}e^{j\pi u_c}+c_{12}^*e^{-j\pi u_c} & 2c_{22} & c_{12}e^{j\pi u_c}+c_{12}^*e^{-j\pi u_c} \\ c_{13}e^{2j\pi u_c}+c_{13}^*e^{-2j\pi u_c} & c_{12}e^{j\pi u_c}+c_{12}^*e^{-j\pi u_c} & 2c_{11} \end{bmatrix} \qquad \text{(C.2)}$$

With some algebraic manipulation, we have

$$\det\left(\mathrm{Re}\{\mathbf{W}(u_c)^*\tilde{\mathbf{C}}_{hh}^{fb}\mathbf{W}(u_c)\}\right)$$

$$= \frac{1}{4}\left(p_o^*e^{-4j\pi u_c} + p_1^*e^{-2j\pi u_c} + p_2 + p_1e^{2j\pi u_c} + p_oe^{4j\pi u_c}\right) \qquad \text{(C.3)}$$

$$\text{where : } p_o = c_{12}^2c_{13} - c_{22}c_{13}^2 \;\; ; \;\; p_1 = 2\,|\,c_{12}\,|^2c_{13} - 2c_{11}c_{12}^2$$

$$p_2 = 4c_{11}^2 c_{22} + c_{12}^{*2} c_{13} + c_{12}^2 c_{13}^* - 4c_{11} |c_{12}|^2 - 2c_{22} |c_{13}|^2$$

Differentiating (C.3) with respect to u and set to zero, we get

$$-2p_o^* e^{-4j\pi u_c} - p_1^* e^{-2j\pi u_c} + p_1 e^{2j\pi u_c} + 2p_o e^{4j\pi u_c} = 0 \qquad \text{(C.4)}$$

This suggests that the solution for u_c can be obtained by solving the following quartic equation

$$-2p_o^* \lambda^{-2} - p_1^* \lambda^{-1} + p_1 \lambda + 2p_o \lambda^2 = 0 \qquad \text{(C.5)}$$

for a unit root λ_c, where $\lambda_c = e^{2j\pi u_c}$.

Appendix D
Proof of Conjugate Centro-Symmetry of the Columns of $\mathbf{R}_{opt}$

In this appendix, we prove that the 3x3 matrix $\mathbf{R}_{opt}$ obtained in (5.58) satisfied $\tilde{\mathbf{I}}_3\mathbf{R}_{opt} = \mathbf{R}_{opt}^*$. We do so by first investigating some properties associated with the SVD of $\mathbf{G}^{-1}\mathbf{P}^H\mathbf{W}^o$. From (5.48), it is easily deduced that $\mathbf{P}$ satisfies

$$\tilde{\mathbf{I}}_M\mathbf{P}\tilde{\mathbf{I}}_3 = \mathbf{P}^* \tag{D.1a}$$

and so does $\mathbf{G}^{-1}$ as shown below

$$\tilde{\mathbf{I}}_3\mathbf{G}^{-1}\tilde{\mathbf{I}}_3 = (\tilde{\mathbf{I}}_3\mathbf{G}\tilde{\mathbf{I}}_3)^{-1} = (\tilde{\mathbf{I}}_3\mathbf{P}^H\mathbf{P}\tilde{\mathbf{I}}_3)^{-\frac{1}{2}}$$

$$= (\mathbf{P}^H\mathbf{P}^*)^{-\frac{1}{2}} = (\mathbf{G}^{-1})^* \tag{D.1b}$$

$\mathbf{W}^o$ is the Mx3 Butler beamforming matrix such that

$$\tilde{\mathbf{I}}_M\mathbf{W}^o = (\mathbf{W}^o)^* \tag{D.2}$$

Combining (D.1) and (D.2), we have

$$\tilde{\mathbf{I}}_3\mathbf{G}^{-1}\mathbf{P}^H\mathbf{W}^o = \tilde{\mathbf{I}}_3\mathbf{G}^{-1}\tilde{\mathbf{I}}_3\tilde{\mathbf{I}}_3\mathbf{P}^H\tilde{\mathbf{I}}_3\tilde{\mathbf{I}}_3\mathbf{W}^o$$

$$= (\mathbf{G}^{-1}\mathbf{P}^H\mathbf{W}^o)^* \tag{D.3}$$

which gives rise to the following results

$$\tilde{\mathbf{I}}_3\mathbf{G}^{-1}\mathbf{P}^H\mathbf{W}^o\mathbf{W}^{oH}\mathbf{P}(\mathbf{G}^{-1})^H\tilde{\mathbf{I}}_3 = (\mathbf{G}^{-1}\mathbf{P}^H\mathbf{W}^o\mathbf{W}^{oH}\mathbf{P}(\mathbf{G}^{-1})^H)^* \tag{D.4a}$$

$$\mathbf{W}^{oH}\mathbf{P}(\mathbf{G}^{-1})^H\mathbf{G}^{-1}\mathbf{P}^H\mathbf{W}^o = \mathbf{W}^{oH}\mathbf{P}(\mathbf{G}^{-1})^H\tilde{\mathbf{I}}_3\tilde{\mathbf{I}}_3\mathbf{G}^{-1}\mathbf{P}^H\mathbf{W}^o$$

$$= (\mathbf{W}^{oH}\mathbf{P}(\mathbf{G}^{-1})^H\mathbf{G}^{-1}\mathbf{P}^H\mathbf{W}^o)^* \tag{D.4b}$$

(D.4) states that $\mathbf{G}^{-1}\mathbf{P}^H\mathbf{W}^o\mathbf{W}^{oH}\mathbf{P}(\mathbf{G}^{-1})^H$ is both hermitian and per-hermitian while $\mathbf{W}^{oH}\mathbf{P}(\mathbf{G}^{-1})^H\mathbf{G}^{-1}\mathbf{P}^H\mathbf{W}^o$ is real. It is well known that if $\mathbf{G}^{-1}\mathbf{P}^H\mathbf{W}^o = \mathbf{U}\Sigma\mathbf{V}^H$ is the SVD, then

$$\mathbf{G}^{-1}\mathbf{P}^H\mathbf{W}^o\mathbf{W}^{oH}\mathbf{P}(\mathbf{G}^{-1})^H = \mathbf{U}\Sigma\mathbf{V}^H\mathbf{V}\Sigma\mathbf{U}^H = \mathbf{U}\Sigma^2\mathbf{U}^H \tag{D.5a}$$

and

$$\mathbf{W}^{oH}\mathbf{P}(\mathbf{G}^{-1})^H\mathbf{G}^{-1}\mathbf{P}^H\mathbf{W}^o = \mathbf{V}\Sigma\mathbf{U}^H\mathbf{U}\Sigma\mathbf{V}^H = \mathbf{V}\Sigma^2\mathbf{V}^H \tag{D.5b}$$

are the EVD's for $\mathbf{G}^{-1}\mathbf{P}^H\mathbf{W}^o\mathbf{W}^{oH}\mathbf{P}(\mathbf{G}^{-1})^H$ and $\mathbf{W}^{oH}\mathbf{P}(\mathbf{G}^{-1})^H\mathbf{G}^{-1}\mathbf{P}^H\mathbf{W}^o$, respectively. These indicate that $\mathbf{U}$ consists of the eigenvectors associated

with a hermitian-per-hermitian matrix while $\mathbf{V}$ consists of the eigenvectors of a real symmetric matrix. Exploiting the fact that eigenvectors of a hermitian-per-hermitian matrix are conjugate centro-symmetric and that eigenvectors of a real symmetric matrix are real, we have

$$\tilde{\mathbf{I}}_3\mathbf{U} = \mathrm{U}^* \tag{D.6a}$$

$$\mathbf{V} = \mathbf{V}^* \tag{D.6b}$$

which yields immediately

$$\begin{aligned}\tilde{\mathbf{I}}_3\mathbf{R}_{\mathrm{opt}} &= \tilde{\mathbf{I}}_3\mathbf{G}^{-1}\mathbf{U}\mathbf{V}^{\mathrm{H}} = \tilde{\mathbf{I}}_3\mathbf{G}^{-1}\tilde{\mathbf{I}}_3\tilde{\mathbf{I}}_3\mathbf{U}\mathbf{V}^{\mathrm{H}} \\ &= (\mathbf{G}^{-1})^*\mathbf{U}^*\mathbf{V}^{\mathrm{T}} = \mathbf{R}_{\mathrm{opt}}^*\end{aligned} \tag{D.7}$$

This concludes the proof.